DESIGN OF MOMENT END-PLATE CONNECTIONS FOR SEISMIC LOADING

by

Ronald L. Meng

Dissertation submitted to the Faculty of the

Virginia Polytechnic Institute and State University

in partial fulfillment of the requirements for the degree of

DOCTOR OF PHILOSOPHY

IN

CIVIL ENGINEERING

APPROVED:

T. M. Murray, Chair

Richard M. Barker

W. Samuel Easterling

Siegfried M. Holzer

Raymond H. Plaut

Mahendra P. Singh

April 22, 1996

Blacksburg, Virginia

Keywords: End-plate, Connection, Seismic, Bolted, Full-Scale

DESIGN OF MOMENT END-PLATE CONNECTIONS FOR SEISMIC LOADING

by

Ronald L. Meng

Thomas M. Murray, Chairman
Civil Engineering

(ABSTRACT)

Analytical and experimental research into the seismic response of four-bolt extended moment end-plate connections was conducted. Full-scale connections, ranging in size from moderate to large, were designed, fabricated and tested under cyclic loading until connection failure was observed. The design procedures for minimum end-plate thickness were developed from yield-line theory with prying forces included in the bolt tension forces. Stiffened end-plates, four-bolt wide connections and shimmed end-plate connections were variations of the four-bolt connection tested. A325 and A490 bolts with internal strain gauges were employed to record and analyze bolt tension forces.

Test results demonstrate that the design approach is satisfactory, but several aspects of connection response not previously observed nor reported were encountered. When weld access holes were present in an extended end-plate connection, excessive 3-D stresses developed in the hole region, causing a brittle fracture of the beam flange. In the absence of weld access holes, ductile failure occurred, evidenced by local buckling of the beam flanges and plastic hinge formation. These two responses or failures were exhibited by all connection sizes. The use of end-plate stiffeners appeared to provide sufficient stress reduction, as ductile failures were observed in all stiffened, extended end-plate connection tests with weld access holes.

Grade 50 steel, four-bolt end-plate connections with built-up beam sections were also tested and demonstrated that inadequate weld strength exists in the beam web-to-

flange welds. Prior to fracture in these welds, the connections responded in a ductile manner with local beam flange buckling.

In conjunction with the full-scale testing, finite element models were created for several connection sizes. When actual material properties of the steel and bolts were modeled, an excellent correlation of test data and the model was noted. When weld access holes were introduced in the models, an increase of flange strain in the hole region was noted.

Although not conclusive nor comprehensive for every connection configuration, the four-bolt design appears satisfactory to survive seismic activity. Further research should provide answers to other configurations and eventually provide an acceptable alternative beam-to-column connection for high seismic areas.

ACKNOWLEDGMENTS

Several organizations and corporations deserve special recognition for their financial and material support. This research was funded in part by the National Science Foundation, Arlington, Virginia, Grant No. CMS-9416171. Appreciation is extended to Nucor-Yamato Steel Company, Butler Research, Star Building Systems, and Lincoln Arc Welding for the test materials, support and other donated efforts. Appreciation is also extended to Hirschfield Steel for their donation of labor for the connection fabrication.

I would like to express special gratitude to Dr. Thomas M. Murray for his jovial guidance and direction in this research and the personal support he provided throughout my pursuit of a Doctoral degree. His ever present willingness to answer questions was a help through many challenging times. I wish to thank Dr. Richard M. Barker, Dr. W. Samuel Easterling, Dr. Siegfried M. Holzer, Dr. Raymond H. Plaut and Dr. Mahendra P. Singh for their advice and guidance during the final stages of research and analysis.

An extra special appreciation and personal thanks to Dennis Hoffman and Brett Farmer for their many hours of assistance at the lab and for the memories of the many bolts we tightened together. Thanks to all the lab "rats" without whose assistance none of the testing could have been accomplished, especially Emmett Sumner and Jeff Borgsmiller who showed me the secrets of bolt testing. I wish to thank Ann Crate for the many tasks she guided me through and for keeping the paperwork straight. Also a word of thanks to Mary Dugan for reading the drafts and correcting my use of the English language.

Finally, I wish to thank my wife Sherry and our children for their understanding, encouragement and patience throughout the countless months of study and research and the seemingly endless hours of study at home. Their assistance and support provided often needed enthusiasm to see me through the hard times.

TABLE OF CONTENTS

LIST OF FIGURES

LIST OF TABLES

CHAPTER I

INTRODUCTION AND LITERATURE REVIEW

1.1 INTRODUCTION

The moment end-plate connection is one of three fully restrained moment connections, as defined by the American Institute of Steel Construction (AISC) Manual of Steel Construction, Load & Resistance Factor Design (LRFD) 1994, that are used for beam-to-column connections. The moment end-plate connection has become increasingly popular in use, particularly by the metal building industry, because of its ease of erection in the field; yet it has comparable properties to both the flange-plate and directly welded flange connections.

The beam-to-column moment end-plate connection is composed of a steel plate welded to the end of a wide flange beam. The plate is attached to the column using various rows of fully tensioned high-strength bolts. The connection is normally shop welded and field erected. Several classifications of end-plates exist and are dependent on their detailing and arrangement of bolt patterns. An extended end-plate is one which extends beyond the flanges of the beam to allow placement of bolts outside the beam flanges. Stiffeners may be added to the extended end-plate outside the beam flange in the plane of the beam web. This configuration produces a stiffer connection and therefore allows the use of thinner end-plates in some applications. Figure 1.1 shows several commonly used extended end-plate configurations. Other classifications of end-plates do exist, e.g. flush end-plates; however, this research is limited to extended end-plates because of their use in beam-to-column connections.

Currently, moment end-plate connections are limited in structural steel building design and construction, as outlined in the Manual for Steel Construction (LRFD 1994), to "statically loaded applications ... because adequate research has not been conducted on their low cycle

fatigue strength." Previous, yet limited, research has indicated that the moment end-plate connection can safely withstand seismic loading without failure of the connection, but insufficient data and research exist to substantiate and quantify needed changes to existing design models.

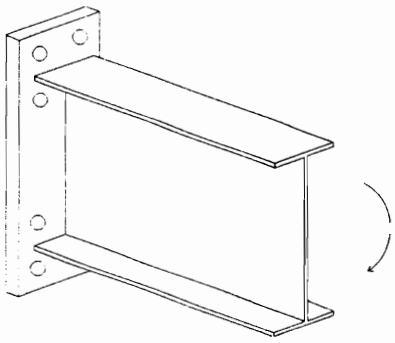

(a) Unstiffened 4-Bolt

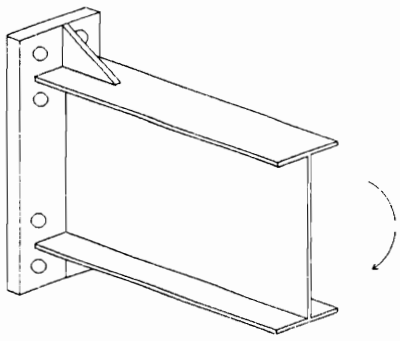

(b) Stiffened 4-Bolt

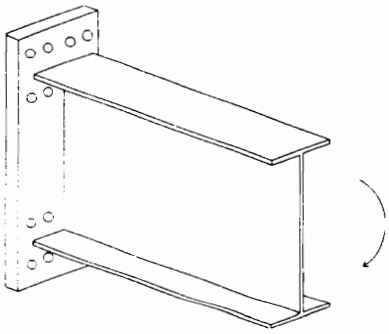

(c) 4 Bolt Wide

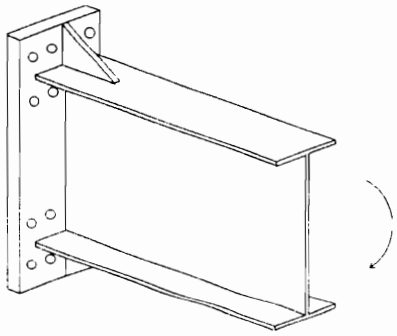

(d) Stiffened 4 Bolt Wide

FIGURE 1.1 Extended End-Plate Configurations

During the 1994 Northridge, California earthquake, directly welded flange connection failures emphasized and accentuated the need for seismically safe, yet efficient, moment resistant connections. AISC Technical Bulletin No. 2 (1994) outlines some of the failures that occurred and design and material problems associated with the flange welded connection. To

avoid future reoccurrence of similar weld failures, an alternate Type FR connection must be investigated.

For two reasons, to expand the AISC approved use of moment end-plate connections and to avoid welded connection failures, this research and study provides additional information to aid in the end-plate connection's use and acceptance to include seismic areas. Through both analytical and experimental research, design procedures for a 4-bolt unstiffened end-plate moment connection, Figure 1.1a, for use in high seismic areas are developed, analyzed and tested. Several tests were also conducted to project the design methodology to 4-bolt wide unstiffened end-plate moment connections, Figure 1.1c. Stiffened, extended end-plate connection tests, both four-bolt and four-bolt wide, Figures 1.1b and 1.1c, were also conducted to investigate the design philosophy's application to these types of end-plate moment connections and the designs' applicability to future testing.

1.2 LITERATURE REVIEW

1.2.1 Moment End-Plates

The end-plate moment connection saw its first application in the 1960's, stemming from its research and design in the 50's. The connection was not a new concept but more of an evolution of the much used split tee connection. The early designs usually resulted in thick end-plates and large bolt diameters due mainly to simplified designs and analysis of the connection. The connection slowly gained acceptance and was included in the 7th Edition, AISC Manual of Steel Construction in 1970 due in large part to the efforts of Douty and McGuire (1965). Their methods used assumptions of bolt forces due to prying action and simple statics resulting from earlier tee-stub analysis. As discussed by Griffiths (1980), this first attempt to standardize the design resulted in a very conservative connection. It did spur further interest as seen by various studies in the early 1970's. Kato and McGuire (1973) and Nair *et al.* (1974) continued the 'tee-stub' concept to account for prying action and sizing of bolts and

thickness of the end-plate. As before, the procedures continued to produce a design with thick plates and large bolt diameters. Based on this research and that of Agreshov (1976,1977), Granstron (1980) continued with a simple design of tee-hangers. His resulting design produced thinner plates and bolts than before, but he did not consider the effects of prying action.

Packer and Morris (1977) were among the first to use yield-line analysis. Using the tee-stub model for the end-plate, they developed a yield line analysis of the column flanges. Mann and Morris (1979) extended these initial efforts in the use of yield line analysis. From review of previous research, they surmised that the end-plate must exhibit plastic deformation and the formation of yield lines at its upper capacity. Their proposed design procedures determined plate thickness and bolt diameter as well as adequacy checks of the supporting column.

Krishnamurthy (1978) broke from the traditional analysis and derived empirical relationships based on statistical analysis of finite element results. Formulas derived for end-plate thickness provided thinner plates than previously obtained. He explained the prying force as a pressure bulb formed under the bolt head due to the tensioning of the bolts. The location of the pressure bulb varied, depending on the level of the flange force in the beam. As the force increases, the pressure bulb shifts towards the edge of the plate. The design procedures in the current editions of the AISC Manual of Steel Construction are in part based on his basic work

Kennedy *et al.* (1981) continued the tee-stub analogy to predict prying forces and the formation of plastic hinges and yield lines. They categorized the end-plate's behavior on three levels. First, at low loads there is the absence of any hinge formation in the plates; the plate is said to be "thick," with no prying action present. Second, upon the formation of a hinge caused by yielding of the end-plate at the beam flange, the plate is said to be "intermediate." Some prying action during the intermediate case is realized and adds to the bolt forces. The third stage, "thin," is determined when the second plastic hinge forms about the bolts. At this time, the prying action is considered to be at its maximum. Their design methods were applied

only to two tee-stub tests and were not conclusive to validate their methods, but the results did correlate well with their predictions.

Morrison (1985) and Abel (1993) have modified the Kennedy *et al.* approach for four-bolt stiffened and unstiffened extended end-plates, respectively. Each conducted analytical and experimental research that verified their prediction equations and procedures and the previous work conducted by Kennedy *et al.*

A historic outlook of the advancement and the development of end-plate moment connection design is presented in greater detail by Murray (1988).

1.2.2 Cyclic Testing of Moment End-Plates

All of the above discussed research was conducted with static (monotonic) bending or shear loading. This research has indicated that under monotonic loading, end-plate connections can indeed provide comparable strength, stiffness and ductility to the welded flange connection, a fact confirmed by several researchers (Murray 1988; Popov and Tsai 1989). Research on end-plate moment connections subjected to cyclic or seismic loading has been extremely limited, as stated by Popov and Tsai (1989) and Korol *et al.* (1991). Ghobarah *et al.* (1990) also states that the understanding of the behavior of the individual components under cyclic loading is extremely lacking; in fact, to date, literature reports only two teams have conducted any substantial full scale cyclic loading research of end-plate moment connections: Popov and Tsai (1990), and Ghobarah *et al.* (1990, 1992).

Initial experimental investigations into the cyclic performance of end-plate moment connections is limited to small beam sections with unstiffened end-plates (Sanapaolesi *et al.* 1981; Ballio *et al.* 1987). These tests were conducted utilizing specific loading sequence procedures widely adopted by European researchers. In these tests, pinching and shifting of the hysteretic loops occurred mainly due to bolt slippage between the end-plate and the column flange and yielding of the bolts and end-plate, thereby reducing the connection stiffness and its energy dissipation capacity. One probable cause of the end-plate slippage in these tests was the lack of sufficient tensioning of the bolts. To achieve maximum strength and stiffness of the

connection, the bolts must be fully tensioned. Therefore, these early seismic tests are inconclusive as to connection behavior for steel structures.

Popov and Tsai (1989) performed their initial cyclic loading research for several moment connections. Types of beam-to-column connections varied from fully welded connections to bolted end-plate connections. The objective was to investigate realistic member size and the extent of cyclic ductility with emphasis on LRFD and plastic capability in design. Their initial results produced generalities of beam-column connections and their interactions and confirmed bolt slippage as experienced by other research, causing data scatter. In later tests by Tsai and Popov (1990), cyclic behavior of end-plate connections was specifically investigated. They investigated the cause of inner bolt premature failure by variation of stiffened and unstiffened end-plates. The results of this testing indicated the need for modification of bolt design, end-plate thickness to correspond to connection strength, and end-plate stiffener recommendations. At the completion of their research, they concluded that there is still a need for further research of end-plate connections under cyclic loading.

Ghobarah *et al.* (1990) also noted the lack of information about distribution of stresses and forces in end-plate connections under cyclic loading. The objective of several of their tests was to examine the behavior of individual components within the connections. Their testing included extended end-plate element responses with stiffened and unstiffened connections. During testing, the columns were axially loaded for some of the tests and unloaded for others. Column flange and end-plate stiffeners as well as end-plate thickness were varied also. In general, they found that end-plate connections are able to dissipate energy induced in the connection from cyclic loading without loss of strength. Stiffness of the joint was reduced due mostly to bolt tension losses. They concluded that sufficient energy dissipation capability without a substantial loss of strength can be obtained by the proper proportioning of the connection. Valuable as the research of Popov and Tsai and Ghobarah *et al.* is, it has not provided design standards nor acceptable guidelines for seismic end-plate connection design.

1.2.3 Finite Element Analysis of Moment End-Plates

Research of moment end-plate connections utilizing finite element modeling has gained recent momentum from early, limited attempts. Krishnamurthy and Graddy (1976) attempted to calculate end-plate deformation/displacement for extended 4-bolt connections, but computer size and speed limited the extent and mesh complexity of the early attempts of computer modeling of bolted connections. This research and that of Kukreti *et al.* (1987) made comparisons of 2D and 3D analysis for complexity and accuracy of representation. They concluded that, at the time, 2D analysis provided adequate reliable modeling of moment end-plate connections. Ahuja (1982) used finite element analysis to investigate the elastic properties of 8-bolt stiffened connections. The programming contained both 2D and 3D modeling elements for the connection. Ghassemieh (1983) continued the investigation of Ahuja to include non-linear behavior of the end-plate and bolts. Kukreti *et al.* (1990) continued finite element modeling for an 8-bolt connection and, as with previous research, conducted parametric studies to predict end-plate displacement and inner bolt forces. These predictions were compared to actual research data for correlation, and regression analysis of the data was conducted to provide empirical equations for design of moment end-plates under monotonic loads.

Use of the finite element code ABAQUS by Bursi and Leonelli (1994) aided in prediction of end-plate deformation and displacement for extended end-plates. The finite element code ANSYS has successfully been utilized by Bahaari and Sherbourne (1993) to model extended end-plates. Both codes have successfully produced three dimensional modeling of the end-plates and provided valid predictions and analysis of plate (both thick and thin) behavior and deformation. Most finite element models of moment end-plate connections have analyzed monotonic loading.

Current finite element research of moment end-plates continues as evidenced by numerous theses and reports produced by numerous universities and research firms in the United States and Canada. Recent research reports and studies are use 3D non-linear modeling

to simulate hysteresis loop behavior and response due to varied loading. These responses are then used to predict component failure within the end-plate connection.

1.3 Objective and Scope of Research

The presence of only limited full scale and finite element research into cyclic loading of moment end-plates indicates that the moment end-plate connection design has not yet fully evolved. The relationship of the elements and their behavior is fairly well understood, but no design proportions or guidelines are available for the structural designer. AISC publications provide current design methods, but for static loading only. The next logical step is to develop, test and implement design procedures for seismic loading of the moment end-plate connection.

The objective of this research is to develop design procedures from existing knowledge and past research techniques. These designs are tested with full scale connection members and finite element modeling. The ultimate objective of this research is to present an acceptable seismic end-plate connection design procedure.

The 4-bolt extended moment end-plate connection is the emphasis of this research. The effort includes the complete design, analysis and testing of full-scale specimens. Sufficient specimens are utilized to provide adequate data to allow valid conclusions to be drawn from the testing. In addition, several designs and tests include other end-plate configurations. They are not as in-depth as the 4-bolt extended moment end-plate connection and are only intended to investigate the applicability of the end-plate connection design concepts.

CHAPTER II

THEORY AND ANALYSIS BACKGROUND

2.1 INTRODUCTION

This chapter provides background material and theoretical development needed to understand procedures used in the design, testing and analysis of the end-plate moment connection. All background material is collectively located in this chapter for ease of reading and future referencing. Theory and background presented in this chapter will be referenced in sections throughout the dissertation as may be deemed appropriate.

2.2 YIELD-LINE THEORY

Yield-line theory is a simple yet powerful method of estimating loads at which a flexural failure mechanism will form in a flat plate. It is based on the physical concept that flexural failure will not occur until flexural yielding of a plate has extended over a large enough region so that the failure mechanism can form. Yield-line analysis is based on the moment relationship within the plate and is a comparison of internal and external work performed due to a given loading. Although developed and used mainly for reinforced concrete slab design and analysis, it probably has a more valid application to a steel plate. In this work, yield-line analysis is used for calculation of the end-plate thickness.

There are two solution methods available for yield-line analysis, the energy-mechanism approach and the equilibrium method. As discussed by Ferguson (1965), "the equilibrium method gives a lower bound for a given pattern of yield lines, but does not serve to compare possible different patterns." The energy-mechanism approach is a limit design method and provides an upper bound solution. Therefore, care must be taken to

ensure that another possible mechanism does not exist. The energy-mechanism is utilized in this research as the method of yield-line analysis; it compares the plates resistant internal energy to the external energy of the load. Ferguson (1965) further states:

> *... if a slab has been reduced to a mechanism by yield lines acting as hinges, a known additional deflection of any specific point in the mechanism (by geometry) establishes the additional deflections at all points, along with the additional angle changes at the yield lines or hinges. For such a slab deflection, the loads also deflect and thereby contribute energy to the mechanism, whereas the hinges resist movement and absorb energy from the system. Thus, for a given mechanism, a given loading imparts enough energy to develop specific yield moments in the hinges. No smaller yield moment will be adequate to resist these loads. Some other mechanism may represent a more probable failure pattern; if so, it demands a larger yield moment to balance the given loading. Thus the worst mechanism, and the real mechanism which actually forms, is the one which requires the largest resisting yield moment. Any trial mechanism or yield-line pattern establishes a lower bound or lower limit on the required yield moment.*
>
> *The same procedure can be used with given yield moments to establish the ultimate load. Any given mechanism establishes an upper bound or upper limit on the collapse load. The real collapse load is the smallest that can be found from all possible mechanisms.*

Previous research by Srouji *et al.* (1983) and Abel and Murray (1992) has investigated numerous arbitrary yield-line patterns for moment end-plate connections. The pattern which provides the lowest failure loading for the four-bolt extended unstiffened moment end-plate is presented as Figure 2.1. The figure shows the controlling yield-line pattern and the yield-line mechanism used to determine the required end-plate thickness for the 4-bolt specimens designed and tested in this research.

The external work was taken as

$$W_e = M_u\theta = M_u\left(1/h\right) \tag{2.1}$$

where M_u is the ultimate beam moment at the end-plate and θ is the virtual rotation of the connection, equal to 1/h, where h is the total depth of the beam section.

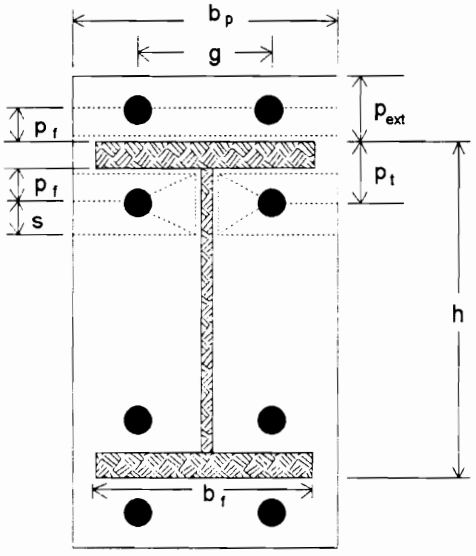

Figure 2.1 Yield-Line Mechanism
(after Srouji et al., 1983)

The internal work stored in the yield-line mechanism is then:

$$W_i = \frac{4m_p}{h}\left[\left(\frac{b_p}{2}\left(\frac{1}{p_f}+\frac{1}{s}\right)+(p_f+s)\left(\frac{2}{g}\right)\right)(h-p_f)+\frac{b_p}{2}\left(\frac{h}{p_f}+\frac{1}{2}\right)\right] \tag{2.2}$$

where the geometric parameters are shown in Figure 2.1 and

$$m_p = F_{py} t_p^2 / 4 \tag{2.3}$$

where F_{py} is the yield stress of the end-plate material and t_p is the end-plate thickness. The required end-plate thickness is found by equating Equations 2.1 and 2.2 and solving for t_p:

$$t_p = \left[\frac{M_u / F_{py}}{\left(\frac{b_p}{2}\left(\frac{1}{p_f} + \frac{1}{s} \right) + (p_f + s)\left(\frac{2}{g} \right) \right)(h - p_t) + \frac{b_p}{2}\left(\frac{h}{p_f} + \frac{1}{2} \right)} \right]^{1/2} \tag{2.4}$$

The unknown dimension, s, in Figure 2.1 is found by differentiating the internal work expression with respect to s and equating to zero, resulting in

$$s = \sqrt{b_p g} / 2 \tag{2.5}$$

2.3 BOLT FORCE PREDICTION

Kennedy *et al.* (1981) proposed a method for predicting bolt forces with prying action in split-tee connections. The Kennedy split-tee analogy consists of a flange bolted to a rigid support with two bolts, Figure 2.2. The total force at a bolt, B, is then one-half of the applied force, 2F, plus the prying force per bolt, Q. The distance "a" between the point of prying force application and the centerline of the bolt was suggested by several researchers, Mann and Morris (1978) and Nair *et al.* (1974), to be related to bolt diameter or plate thickness respectively. Hendrick *et al.* (1985) empirically determined "a" to be a function of both bolt diameter and plate thickness:

$$a = 3.682 \left(t_p / d_b \right)^3 - 0.085 \tag{2.6}$$

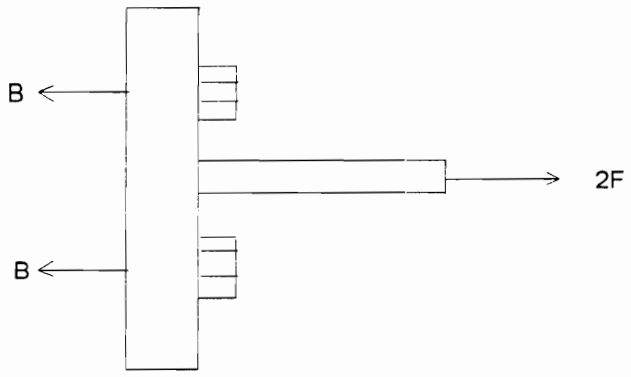

Figure 2.3 (a) Thick Plate Behavior

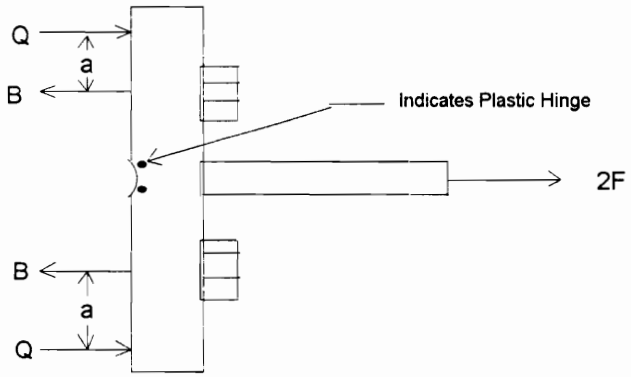

Figure 2.3 (b) Intermediate Plate Behavior

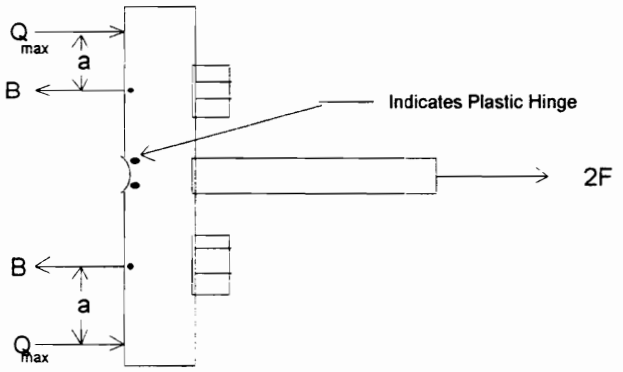

Figure 2.3 (c) Thin Plate Behavior

Figure 2.3 Kennedy Method Split-Tee Behavior
(after Morrison *et al.* (1985))

Kennedy *et al.* determined that the thick plate behavior approximation is limited to:

$$t_1 = \sqrt{2.11 p_f t_f \frac{b_f}{b_p} \frac{F_{fy}}{F_{py}}} \tag{2.7}$$

Therefore, if $t_p > t_1$, the end-plate behavior is considered to be thick. Similarly, the limit of a thin plate was determined to be approximately:

$$t_{11} = \sqrt{\frac{\left(b_f t_f F_{fy} p_f - \frac{\pi}{8} d_b^3 F_{yb}\right)}{F_{yp}\left(0.425 b_p + 0.80 w'\right)}} \tag{2.8}$$

If $t_p \leq t_{11}$, then the end-plate behavior is considered to be thin. More accurate solutions for t_1 and t_{11} can be determined once the approximations of Equations 2.7 and 2.8 are calculated. Iteration of the exact equations found in Kennedy *et al.* (1981) converge rapidly for final values.

Srouji *et al.* (1983) and Abel and Murray (1992) modified the Kennedy procedure for the four-bolt extended unstiffened moment end-plate connection. The connection was idealized into two parts: the 'outer end-plate' and the 'inner end-plate,' Figure 2.4. The outer end-plate consists of the end-plate extension outside the beam tension flange and a portion of the beam tension flange. The inner end-plate consists of the end-plate within the beam flanges and the remaining portion of the beam tension flange. Additionally, two factors, α and β, were introduced. These factors proportion the tension flange force to the outer end-plate and the inner end-plate, respectively. These factors were determined experimentally and for this configuration were found to be equal and their sum to equal unity. Therefore, $\alpha = \beta = 0.5$.

To determine the magnitude of the prying force and, hence, the inner and outer end-plate bolt forces, B_I and B_E, the stages of inner and outer end-plate behavior must first

be ascertained. The end-plate behavior is established by comparing the end-plate force with the thick plate limit force, F_1, and the thin plate limit force, F_{11}. The thick plate limit force, F_1, is:

$$F_1 = \frac{b_p t_p^2 F_{py}}{8p_f \sqrt{1 + \left(3t_p^2 / 16p_f^2 \right)}} \tag{2.9}$$

The thin plate limit force, F_{11}, is:

$$F_{11} = \frac{t_p^2 F_{py} \left[0.85 \left(b_f / 2 \right) + 0.80w' \right] + \left[\left(\pi d_b^3 F_{yb} \right) / 8 \right]}{2p_f} \tag{2.10}$$

Equations (2.9) and (2.10) are from Kennedy *et al.* (1981).

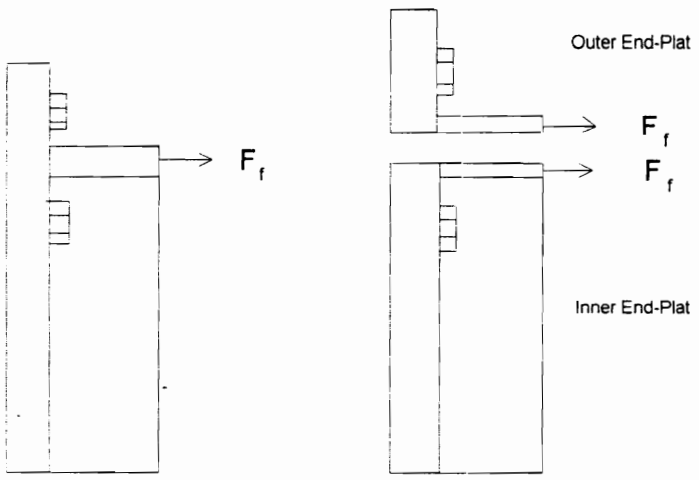

Figure 2.4 Modified Kennedy Method Idealized Model

If the inner or the outer end-plate force, βF_f or αF_f, is less than the thick plate limit force, F_1, the respective portion of the end-plate behaves as a thick plate and the prying force in that portion is zero. Hence, the bolt forces, B_I and B_E, for thick plate behavior are βF_f or αF_f divided by the number of bolts in that portion of the end-plate, two for this configuration:

$$B_I = \beta F_f/2 \quad \text{if} \quad \beta F_f < F_1$$
$$B_E = \alpha F_f/2 \quad \text{if} \quad \alpha F_f < F_1 \tag{2.11}$$

If the inner or outer end-plate force, βF_f or αF_f, is greater than or equal to the thick plate limit force, F_1, and less than or equal to the thin plate limit force, F_{11}, the end-plate behavior is intermediate and the prying force, Q, from Kennedy *et al.* (1981) is:

$$Q = \frac{\gamma F_f p_f}{2a} - \frac{\pi d_b^3 F_{yb}}{32a} - \frac{b_f t_p^2}{8a}\sqrt{F_{py}^2 - 3\left(\gamma F_f / b_f t_p\right)^2} \tag{2.12}$$

where $\gamma = \alpha$ or β depending on which portion of the end-plate is being analyzed. If Q is negative, no prying action is added to the bolt force. The bolt forces B_I and B_E for intermediate end-plate behavior are βF_f or αF_f divided by the number of bolts at that portion of the end-plate, two, plus the prying force, Q:

$$B_I = \beta F_f/2 + Q \quad \text{when} \quad F_1 \le \beta F_f \le F_{11}$$
$$B_E = \alpha F_f/2 + Q \quad \text{when} \quad F_1 \le \alpha F_f \le F_{11} \tag{2.13}$$

Finally, if the inner or outer end-plate force, βF_f or αF_f, is greater than the thin plate limit force, F_{11}, the end-plate behavior is thin and the prying force is at a maximum. The maximum prying force, Q_{max}, from Kennedy *et al.* (1981) is:

$$Q_{max} = \frac{w' t_p^2}{4a} \sqrt{F_{py}^2 - 3\left(F'/w' t_p\right)^2} \tag{2.14}$$

where F' = $F_{11}/2$ and w' = end-plate width per bolt hole less the bolt hole diameter. Hence, the bolt forces B_I and B_E for thin end-plate behavior are βF_f or αF_f, divided by the number of bolts at the portion of the end-plate, two, plus the maximum prying force, Q_{max}:

$$\begin{aligned} B_I &= \beta F_f/2 + Q_{max} \qquad \text{when} \quad \beta F_f > F_{11} \\ B_E &= \alpha F_f/2 + Q_{max} \qquad \text{when} \quad \alpha F_f > F_{11} \end{aligned} \tag{2.15}$$

The reader is cautioned that the quantities under the radicals in Equations 2.12 and 2.14 can be negative. A negative value for these terms indicates that the end-plate yielded locally in shear before the bolt prying action force could be developed; thus, the connection is not adequate for the applied loading. Equations 2.7 and 2.8 can be used as a check for the end-plate behavior to compare with plate limit force values.

2.4 CONNECTIONS WITH SHIMS

Bolt prying force prediction for moment end-plate connections has been a controversial and recurring topic of research and discussion. As reviewed in Chapter I, numerous researchers have investigated and theorized this behavior. A technique that theoretically eliminates bolt prying forces completely is the use of shims, first investigated

by Bouwman (1981) and later by Piraprez (1993). Their efforts were to eliminate low-cycle fatigue failure of bolts which underwent constantly changing tension forces.

The research of Bouwman (1981) was initially conducted with T-sections. Figure 2.5(a) shows the basic test configuration, and a free-body-diagram of the upper portion of the connection is diagrammed in Figure 2.5(b). The bolts are tensioned during set-up and create a contact force, F_c, equal to the total bolt force, F_B, the sum of all of the individual bolt forces, F_b.

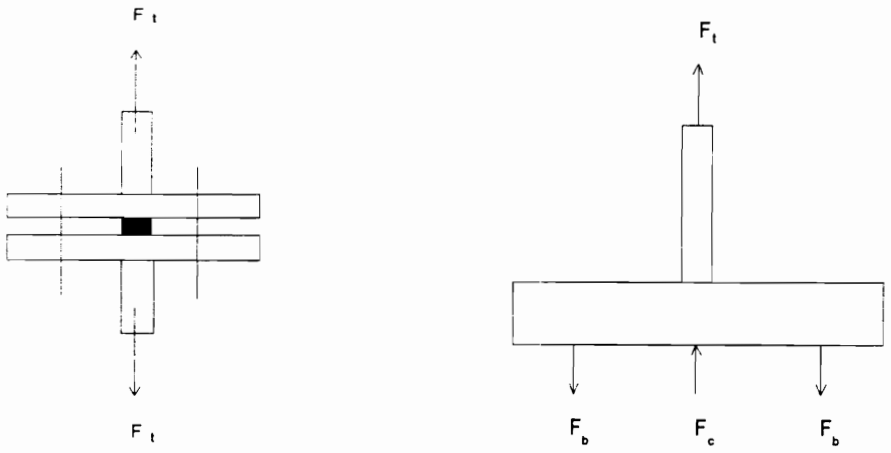

(a) T-Connections (b) Free- body-Diagram

Figure 2.5 Shimmed T-Sections

If the shim is placed as shown in Figure 2.5(a), the force transfer is from the bolts to the contact force as per the research of Bouwman (1981). Then by static analysis, when the T-section is loaded in tension, F_t, the bolt forces will not change until F_t exceeds F_c because the total bolt force, F_B, remains constant.

$$F_B = F_c + F_t \tag{2.16}$$

As the T-section is loaded (increase of F_t), F_c will decrease in magnitude until it becomes zero, at which time $F_B = F_t$. At this point, if F_t is increased, separation of the shim will occur and the bolt force will increase equal to the load. A proper design would ensure that the tension load remains below the bolt force or a desirable failure mode has occurred elsewhere before the loading force, F_t, exceeds the initial bolt tension force, F_B. Thus, the connection is in effect load tested at the time of bolt installation. Bouwman (1981) provides test results that verify the static analysis and force transfer phenomena of the shimmed T-section.

As a means to eliminate the controversy and existence of prying forces, the shimmed connection concept of Bouwman was extended to the moment end-plate connection with the use of steel shims between the end-plate and column as shown in Figure 2.6(b). With the shims placed as shown, prying forces, caused by the interaction between end-plate and column flange, cannot occur as the two members are not in physical contact. Sufficient deformation of the end-plate may eventually allow end-plate to column contact, but adequate design would delay this to well beyond beam failure. The basic design model is for the connection end-plate to respond similarly to the "thick" plate as defined by Kennedy *et al.* (1981). The limit of the "thick" plate behavior is determined by the formation of a plastic hinge in the extended portion of the end-plate near the outer edge of the tension flange weld fillet. This hinge would form during tensioning of high strength bolts, thereby load testing the connection during its erection. The end-plate thickness is determined assuming the required plate bending moment at the hinge line is equal to the effect of the tensioned bolt forces acting on the end of a cantilever of length p_f. Equating the required moment to the plate plastic moment strength, $(F_{yp} b_p t_p^2)/4$, the required end-plate thickness is:

$$t_p = \sqrt{8 B_t p_f / (F_{yp} b_p)} \tag{2.17}$$

where B_t is the specified per bolt tension force. This method of design does produce a thicker than normal end-plate.

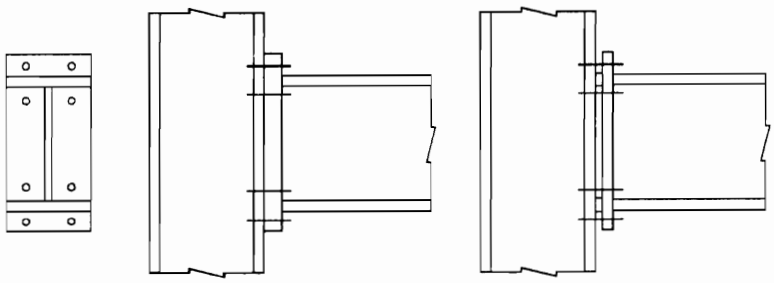

(a) Conventional (b) With Shims

Figure 2.6 End-Plate Configurations

The bolt diameter for the shimmed end-plate connection is determined by the required bolt tension force, B_t, where B_t is selected from the AISC Specification for Structural Steel Buildings, Table J3.1, Manual of Steel Construction (LRFD, 1994) and n is the number of bolts in tension; hence,

$$B_t \geq F = M_u / (d - t_f)n \qquad (2.18)$$

Because a prying force theoretically does not exist in the connections with shims, the bolt force simply becomes the pretension force, B_t.

2.5 EXTENDED, STIFFENED END-PLATE

As developed in the previous section, the end-plate thickness is determined assuming the required plate bending moment at the hinge line is equal to the effect of the tensioned bolt forces acting on the end of a cantilever of length p_f. In an attempt to reduce the excessive thickness of the shimmed connection's end-plate resulting from this design, an extended, stiffened end-plate was investigated. With the use of an end-plate thinner than determined by Equation 2.17, the stiffener provides the added bending resistance needed to prevent the formation of a plastic hinge at the outer edge of the tension flange. The length of the stiffener, as seen in Figure 2.7, and its thickness can be

adjusted until the resisting moment of the end-plate and stiffener is greater than the bolt force bending moment.

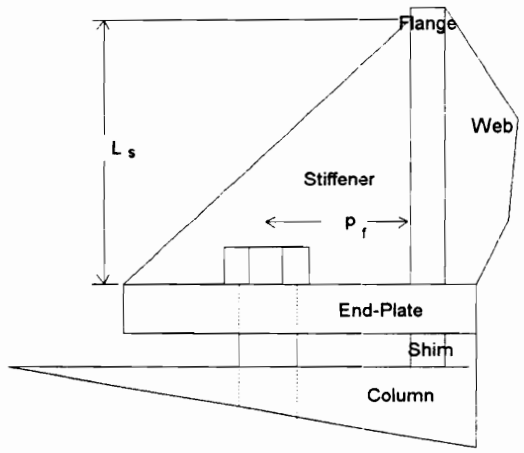

Figure 2.7 End-Plate Stiffener Geometry

The extended, stiffened end-plate design is yield strength based rather than plastic strength as with the unstiffened end-plate. Hence, at the face of the tension flange:

$$M_y = B_t * p_f \qquad \text{for the bending moment} \qquad (2.19)$$

and $$M_y = F_y I_X / y \qquad \text{for the resisting moment} \qquad (2.20)$$

where I_X - moment of inertia of plate and stiffener

and y - distance to maximum stress

Therefore, a design where

$$I_X / y > B_t p_f / F_y \qquad (2.21)$$

provides a greater resisting moment than bending moment. The relationship of I_X/y can be calculated and tabulated for varying stiffener thickness and length until sufficient resisting moment is obtained.

As the stiffener length decreases towards the end of the end-plate, so does the bending moment of the bolt. However, the contribution to the resisting moment reduces at a lesser rate than the moment caused by the bolt tension. This situation ensures that the critical moment is located at the design point, the face of the tension flange.

2.6 CYCLIC TESTING

All cyclic loading tests were designed and conducted in compliance with the procedures as outlined in ATC-24, *Guidelines for Cyclic Seismic Testing of Components of Steel Structures* (1992). The procedures are specifically written for testing with slow cyclic load application which is less than the real-time frequency of an earthquake. This method of testing is cost effective and allows the tester control of force and deformation histories, allowing visual observation of damage to the structural components as they occur. A major limitation of this testing methodology is that it severely distorts time and its material property effects. As stated in ATC-24 (1992):

> *... slow cyclic loading implies that time is distorted and strain-rate effects may alter the load-deformation response of a specimen compared to dynamic loading. Reported evidence points to the conclusion that slow cyclic testing, compared to dynamic testing, results in a small decrease in strength and increase in the rate of deterioration (Krawinkler 1988). Thus, the results from these tests can be considered as conservative for the purpose of performance assessment.*

Although this may appear to limit the value of results obtained, slow cyclic testing does provide valuable data for connection performance, stiffness and its overall strength.

Additional methods of testing can be utilized if more detailed and frequency related data is required, e.g. shaker table testing.

The following definitions from ATC-24 are provided to assist in better understanding cyclic testing and its terminology.

Cycle - a load or deformation history unit consisting of two sequential excursions, one in the positive and one in the negative loading direction.

Deformation - a generic quantity, δ, including strains, angles of shear distortion, rotations, axial deformations and displacements.

Ductility ratio - the ratio of peak deformation over yield deformation.

Excursion - a load or deformation history unit that starts and finishes at zero load, and contains a loading and unloading branch.

Force - a generic quantity, Q, including internal forces and externally applied loads.

Hysteretic area - the area enclosed by a force-deformation diagram.

Load or deformation step - a load history unit consisting of a series of cycles with constant peak load or deformation.

Peak deformation - the deformation at a load reversal point.

Total deformation range - the total deformation between the peak of an excursion and the peak of the preceding opposite excursion.

Yield force of deformation - the predicted or measured force or deformation at which significant yielding occurs.

Two methods of loading control are utilized during each specimen test, force and deformation. As their names imply, the control of loading by the tester is either by the force applied to the specimen or by the measured deformation of the specimen. For this specific research, the force control method obtains its input from the test actuator force, and the deformation method references the loading point deflection. The force control

method is utilized during cycles in the elastic region of the testing, and the deformation control method is used beyond yielding of the beam. The changeover from force to deformation control is at the calculated yield "deformation" point. This deflection value, δy, is calculated as follows:

1) Load the connection with force Q:

$$Q = .75\ Q_y \tag{2.22}$$

where

Q - "force" quantity, measured loading applied by actuator, and

Q_y - estimated load value which will cause specimen yielding. This value is based on the results of previous component testing and/or by analytical methods.

2) Average the deflections obtained during all cycles at loading Q (positive and negative) to obtain δ^*, where $\delta^* = \Sigma\ |\delta n|$

3) Calculate δy:

$$\delta y = 1.33\ \delta^* \tag{2.23}$$

Elastic stiffness of the connection may also be estimated by:

$$K_e = Q_y / \delta y \tag{2.24}$$

The recommended loading history as set forth by ATC-24 is provided as Figure 2.8. More specific information and details of recommended number of cycles for each

load step are provided within the guidelines. For the end-plate connection testing conducted for this research, each load step consisted of three complete cycles. The first two load steps (6 cycles total) were with a peak deformation less than δy. The third load step was at the estimated yield deformation, δy. The fourth and subsequent steps, deformation controlled, were at succeeding increments of δy, i.e.

4th Load Cycle	-	2 δy
5th Load Cycle	-	3 δy
6th Load Cycle	-	4 δy
7th Load Cycle	-	5 δy

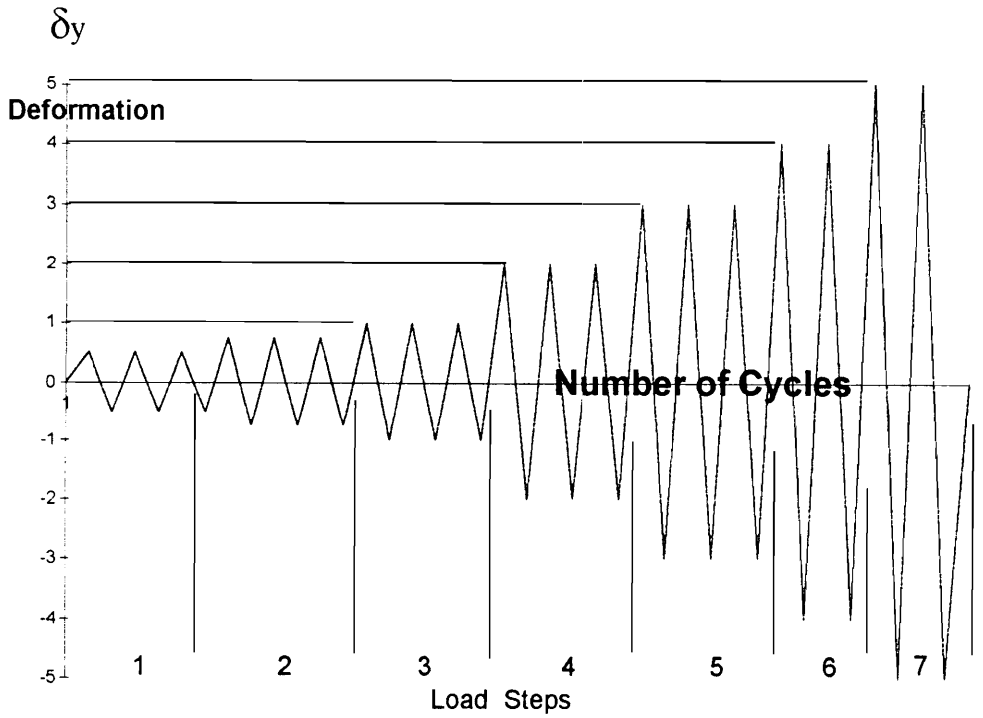

Figure 2.8 ATC-24 Load History

2.7 Reduced Beam Section

The design goal of any moment rigid frame connection is for the connection to be stronger than the connected beam and have local yielding occur within the beam prior to obtaining ultimate design strength within the connection. A recent addition to the difficulty of design of connections is the strength of steel specimens to be tested or utilized in construction of buildings versus their assumed design strength. The steel designation of A36 is based on the minimum tensile yield strength of the steel to be greater than 36 ksi. If the designer of A36 steel uses this value for many steel applications, the calculations may provide erroneous answers. Recent literature reviewed indicates that 48 to 49 ksi is a realistic yield stress for current hot-rolled A36 steel wide flange sections. Although a "stronger" beam may sometimes be satisfactory, a higher yield strength steel may dramatically change failure modes and location of the failure from that calculated during design.

To help lessen or eliminate the difference of design versus actual beam strength, a method to reduce actual beam strength to near design strength was desired. A method, patented by the steel producer ARBED, was found and studied for applicability. (The commercial royalty rights have been waived for its public use, and the method was adopted for design and testing.) The design and use of this concept does not cause any additional loading demands on the connection, supporting column or other parts of the overall rigid frame system above those of the original member size. The concept, which requires actual beam yield strength for the calculations, basically removes flange material to reduce the actual beam's cross-section and plastic moduli to those used as design assumptions.

Specific detailing or design code criteria for this method have not been published; therefore other reliable references were sought. A draft of preliminary guidelines for the use and effects of reduced beam sections was received from Nestor Iwankiw (1995) and used as a guideline for specimen preparation. The following discussion is extracted from that paper and is in part reproduced due to lack of wide dissemination of this technique.

Figure 2.9 illustrates the "Dog Bone" pattern to reduce beam section properties. Use of this beam section reduction not only allows the designer to ensure similarity of design and actual strength, but also forces inelastic behavior of the beam during seismic activity away from the end-plate connection.

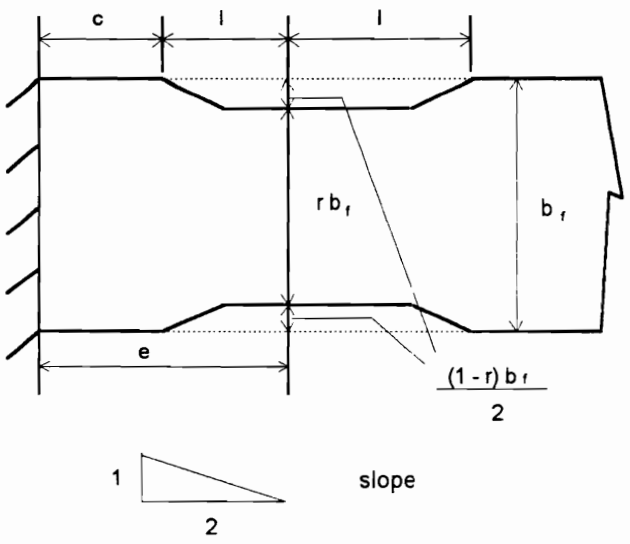

Figure 2.9 "Dog Bone" Geometry

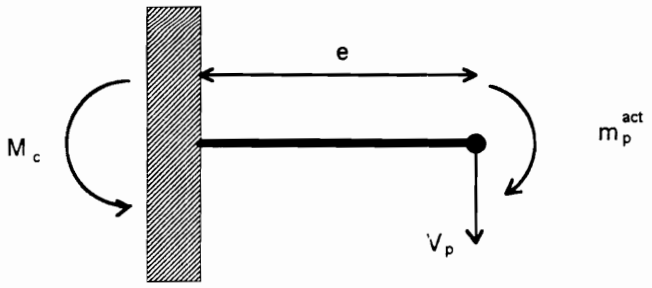

Figure 2.10 Beam Bending Moment

From Figure 2.10, the bending equilibrium requirement is as follows:

$$M_c = m_p^{act} + V_p e \qquad (2.25)$$

where

m_p^{act} = actual plastic moment capacity at min. reduced beam section = $F_y^{act} z$

z = reduced plastic section modulus of the beam

β = material strain hardening factor ($1 \leq \beta \leq 1.1$ for $Fy \geq 50$ ksi)

e = offset of plastic hinge from beam end (assume $3d/4 \leq e \leq d$)

F_y^{act} = actual yield strength of beam

V_p = beam shear due to reverse curvature bending that results in m_p^{act} limit state

M_c = moment delivered to supporting column face

$V_p e$ = moment transfer (amplification) due to shear force eccentricity from beam support

(Note: The reduced plastic moment m_p^{act} includes a steel strain hardening factor, β, which for Grade 50 and stronger shapes can be approximated by 1.1.)

To protect the beam-to-column connection itself, the maximum beam end moment delivered to the column is limited to first yield:

$$M_c = M_y^{act} \qquad (2.26)$$

where M_y^{act} = actual yield moment capacity at beam end = $F_y^{act} S$

S = elastic section modulus of steel beam

The additional moment transfer (magnification) from the reduced section to the beam end Ve can be approximated by the following simple fixed-end model subjected to only primary lateral frame loading (see Figure 2.11). (Bending due to gravity load effects are assumed to be secondary.)

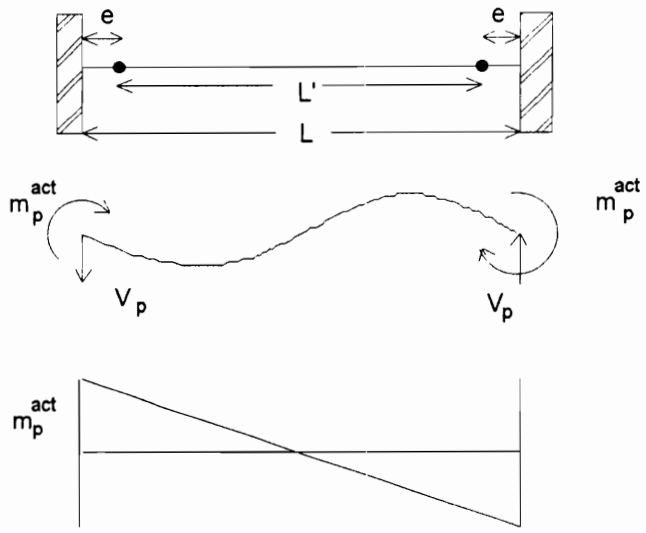

Figure 2.11 Fixed-Fixed Beam Geometry

L = clear beam span between columns

L' = reduced span between interior plastic hinges

from statics $$V_p = 2\frac{m_p^{act}}{L'} \qquad (2.27)$$

Analysis will depend on actual beam L/d (span to depth) ratio. For a general solution, using the actual beam L/d ratio, M_c can be computed from Equation (2.25) as

$$L' = L - 2e \qquad (2.28)$$

$$Ve = 2\frac{m_p^{act} e}{(L - 2e)} = 2\frac{m_p^{act}\left(e/d\right)}{\left(L/d - 2\,e/d\right)}$$

(e/d) = normalized eccentricity of interior plastic hinge (assume $3/4 \leq e/d \leq 1$)

$$M_c = m_p^{act} + \frac{2m_p^{act}\left(\frac{e}{d}\right)}{\left(\frac{L}{d} - 2\left(\frac{e}{d}\right)\right)} \quad \text{or} \quad M_c = m_p^{act}\left[1 + \frac{2\left(\frac{e}{d}\right)}{\left(\frac{L}{d} - 2\left(\frac{e}{d}\right)\right)}\right] \quad (2.29)$$

The minimum section necessary to maintain nominal elastic response at the beam end is provided by:

$$M_c \leq M_y^{act} \quad \text{or} \quad \beta F_y^{act} z\left[1 + \frac{2\frac{e}{d}}{\left(\frac{L}{d} - 2\left(\frac{e}{d}\right)\right)}\right] = F_y^{act} S$$

The average shape factor Z/S for strong axis bending of wide-flanges is 1.1, or S = 0.91Z. Therefore, dividing by Z and re-arranging,

$$\frac{z}{Z} \leq \frac{1}{\beta\left[1 + \frac{2\left(\frac{e}{d}\right)}{\left(\frac{L}{d} - 2\left(\frac{e}{d}\right)\right)}\right]\left(\frac{Z}{S}\right)} \quad , \; L/d > 2(e/d) \quad (2.30)$$

Z = plastic section modulus of the beam

resulting in the following ratios independent of F_y, for assumed values of e/d = 1 and Z/S = 1.1 (average shape factor for strong axis bending of wide flanges is 1.1 and $\beta = 1$):

(L / d)	(z / Z)
25 (flexible)	0.84
20 (stiff)	0.82
15	0.79
10 (very stiff)	0.73
7.5	0.67

A serviceability check for L/d = 20 is discussed in the 1989 AISC-ASD commentary, Sect. L3.2, as one means to minimize perceptible floor vibrations. Drift limits for regions of high seismicity require increased stiffness and tend to reduce this L/d by about 50% to the 10 or so range. Note that the stiffer low L/d beams result in a steeper moment gradient, hence increased section reduction sizes. Larger e/d is also undesirable for the same reason and vice versa. Since the modified section is accomplished only through beam flange reduction, the required reduced plastic section modulus "z" for the remaining cross-section must be related to this change in the flanges only. Equal (symmetrical) reductions in both flanges of the I-shape are assumed.

For the full original shape,

$$Z_f + Z_w = Z \tag{2.31}$$

where

Z_f = plastic section modulus of the beam flanges = $b_f t_f (d - z_f)$

Z_w = plastic section modulus of the beam web = $Z - Z_f$

b_f , t_f = flange width and thickness, respectively

Similarly, for the reduced section

$$z_f + Z_w = z \tag{2.32}$$

where z_f = plastic section modulus of the reduced flanges or, after nondimensionalizing by division by Z,

$$\frac{z_f}{Z} + \frac{Z_w}{Z} = \frac{z}{Z}$$

z/Z is the required reduced plastic section modulus reduction defined previously as a function of L/d , e/d , and Z/S in Equation (2.30).

Z_w/Z is a given I-shape geometric property; z_f can also be conveniently expressed as

$$z_f = rb_f t_f (d - t_f) = rZ_f$$

where r = reduced flange width coefficient ≤ 1.0

rb_f = reduced flange width

Consequently

$$r\left(\frac{Z_f}{Z}\right) + \left(\frac{Z_w}{Z}\right) = \left(\frac{z}{Z}\right) \quad \text{or} \quad r = \frac{\left(\frac{z}{Z}\right) - \left(\frac{Z_w}{Z}\right)}{\left(\frac{Z_f}{Z}\right)} \tag{2.33}$$

gives the purely geometrical relationship for the reduced flange width coefficient "r" based on z/Z from Equation (2.30). The flange width reduction factor is simply 1 - r, which equals

$$1 - r = 1 - \left[\frac{\left(\frac{z}{Z}\right) - \left(\frac{Z_w}{Z}\right)}{\left(\frac{Z_f}{Z}\right)}\right] = \frac{1 - \left(\frac{z}{Z}\right)}{\left(\frac{Z_f}{Z}\right)} \tag{2.34}$$

(Equations (2.33) and (2.34) can be easily tabulated for several reasonable r, Z_f/Z, and Z_w/Z values for the usual wide-flange proportions.)

Notice that, from Equation (2.33), for the resulting "r" to be meaningful (positive), z/Z must exceed Z_w/Z, i.e. the residual plastic modulus "z" cannot be less than Z_w since it is assumed that only the flanges are trimmed, which provides a lower bound limit on L/d.

$$\left(\frac{L}{d}\right)\min = \frac{2\left(\frac{e}{d}\right)}{\left[\left(\frac{Z_w}{Z}\right)\left(\frac{Z}{S}\right)\beta - 1\right]} + 2\left(\frac{e}{d}\right) \tag{2.35}$$

Equation (2.35) results in a minimum L/d of about 2 - 4, thereby mathematically confirming that this lower L/d extreme is to be avoided to maintain the usual beam flexure conditions.

The ratios Z_w / Z and Z / S were left in this common form to enable either general tabulations or charts based on a range of expected values as well as specific calculations for individual shapes. As cautious interim limits, the reduced beam section should be used only for L/d > 5 and 1 - r < 0.50 with standard wide-flange sections ($Z_f / Z \geq 0.5$).

2.8 THREE DIMENSIONAL FLANGE STRESSES

During testing of several connection specimens, abrupt and total fracture of the beam flange occurred in the area of the weld access holes. An investigation was conducted to determine the cause of these sudden fractures. The following analysis and discussion of 3-D stress in welded steel will be used later as reference to the explanation of the fractures. It is provided here as background reference and information.

Material behavior is often discussed, visualized and analyzed as one dimensional. As the length to width ratio becomes small, two dimensional analysis is applied for more accurate results and understanding of the material behavior. But far too often, the analysis is not extended to full 3-D study for several reasons: one or two dimensional

approximation is accurate enough; three dimensional behavior is more difficult to analyze and visualize; or there is ignorance of the interaction of the three dimensional stresses with material behavior. Blodgett (1992) describes the problems that may be encountered if 3-D stresses are unintentionally overlooked.

Often the ductile behavior of steel is visualized as the behavior of a typical tensile coupon specimen, one dimensional. The tensile specimen is restrained only in the axis of tension and displays normal ductile behavior. The ductility occurs because shear stresses exceed their critical yield values. Figure 2.12 shows the Mohr's Circle representation of a tensile specimen. It can be seen that $\tau_{1\text{-}3}$ and $\tau_{2\text{-}3}$ have exceeded their yield values. (From Mohr's Circle, $\tau_{cr} = 1/2\ \sigma_y$). As Blodgett (1992) explains, "if the specimen is pulled to failure, σ_y will reach its critical value, or tensile strength. By this time the two shear stresses are above the critical value and plastic strain or movement will take place." Therefore, the specimen displays ductile behavior.

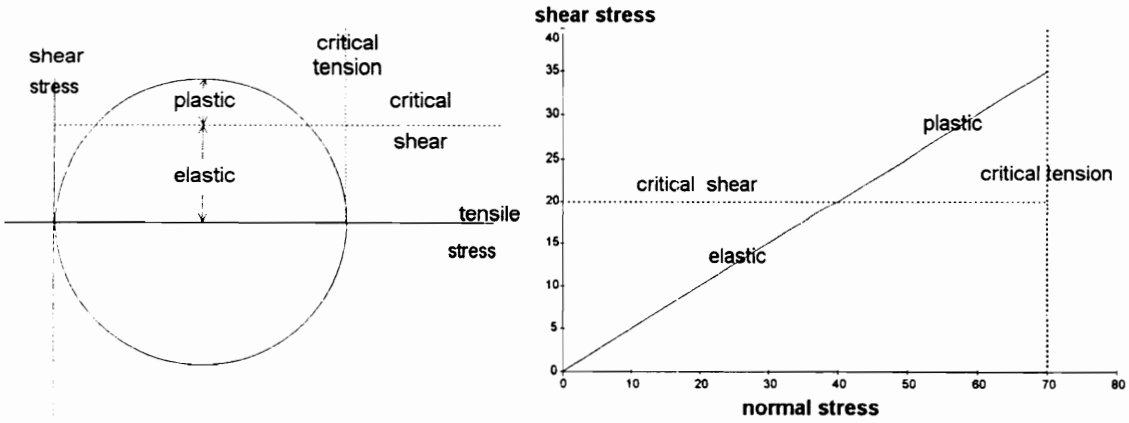

Figure 2.12 Mohr's Circle for a Tensile Coupon

The flange of a beam near the end-plate is not able to respond as does a simple tensile specimen. The flange, due to restraint near the end-plate, is subject to triaxial

stress. Any strain transverse to the flange is resisted by the weld to the end-plate and the through flange strain is resisted by the web. Therefore, as flange forces are increased due to increased bending moments, the longitudinal stress in the flange will increase (positive stress). Because the flange is restrained along the other two axes, tensile stress will be developed in those directions as well. The situation as described by Blodgett (1992) is now realized: all triaxial stresses are tensile and the steel behavior at failure is brittle rather than ductile. Figure 2.13 displays why the behavior of the steel is brittle. σ_3 reaches its critical value before either shear stress, $\tau_{2\text{-}3}$ or $\tau_{1\text{-}3}$, have been able to undergo plastic strain or ductile movement. To avoid this situation, the weld access hole return must provide sufficient flange area between it and the end-plate. The extra area would reduce the through stress component to zero, and a more favorable situation would exist. This would allow ductile behavior due to shear stresses at or exceeding their critical values before the normal stress, σ_3, reaches its critical value.

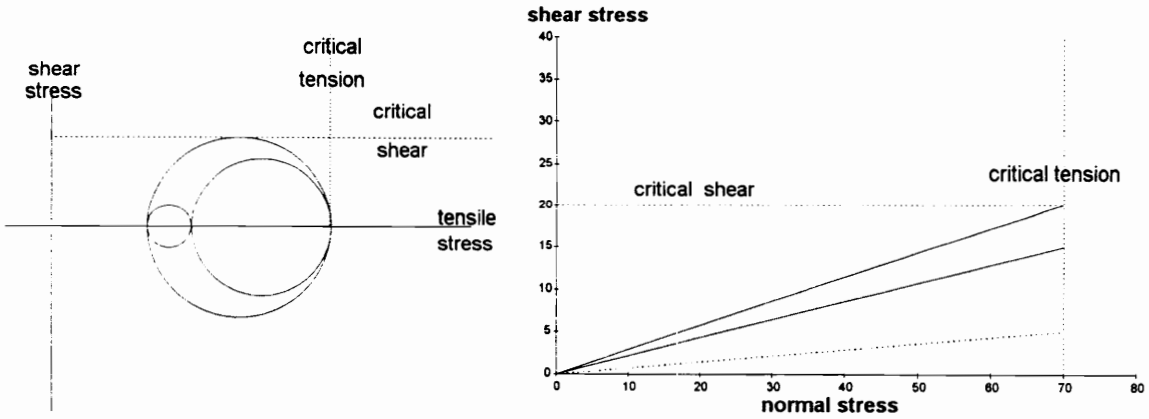

Figure 2.13 Mohr's Circle for Brittle Behavior

2.9 SUMMATION

The initial concepts discussed above are expanded and/or applied directly to develop design procedures for the moment end-plate connections in the next chapter. The cyclic testing concept is utilized for conduct of the testing and the use of the beam reduction method is applied to the W 24x76 beam size connection. The final discussion of the three dimensional stresses is a reference and basis for the probable cause of flange fracture during several tests.

CHAPTER III

MOMENT END-PLATE CONNECTION DESIGN PROCEDURES

3.1 INTRODUCTION

An LRFD based design procedure for moment end-plate connections under seismic loading is developed and tested as part of this research. This chapter presents the design procedures used for the fabrication of several types of extended moment end-plate connections. The background theory and equations for these designs as presented in Chapter 2 will be referenced and expanded as appropriate. The first design presented is for the four-bolt extended moment end-plate connection. The other sections present design procedures for shimmed four-bolt connections, 8-bolt connections (four-bolt wide) and the stiffener used in stiffened, extended end-plate connections, four-bolt or 8-bolt. Because seismic loading implies reversal of loading, all connections are designed with symmetric end-plates. Example calculations for each design are found in Appendix B.

3.2 FOUR-BOLT EXTENDED MOMENT END-PLATE CONNECTION

3.2.1 Beam Selection

These procedures and research do not address current design and selection methods of the supported beam. Any design criterion, specification or code that is used to determine the adequate or acceptable beam section is sufficient. The design procedure for the connection begins with the assumption that an adequate beam section has already been determined.

3.2.2 Type and Preliminary Size of Bolts

The following six steps determine the design strength of the connection and a preliminary bolt type and size adequate for the four-bolt extended moment end-plate connection. (Figure 3.1)

Step 1: Calculate the plastic moment strength of the beam.

$$M_p = F_y * Z_x \tag{3.1}$$

Step 2: Calculate the required moment strength of the connection. (Because the plastic hinge forms at approximately d/2 inboard from the connection and not at the connection, an additional 10% connection strength above the plastic moment strength of the beam is used for the design.)

$$M_c = 1.10\ M_p \tag{3.2}$$

Step 3: Calculate the flange force for the required connection moment strength, M_c.

$$F_f = M_c / (d - t_f) \tag{3.3}$$

Step 4: Divide the flange force by the number of tension side bolts, 4 for this design.

$$T_b = F_f / 4 \tag{3.4}$$

Step 5: Select a bolt type (A325 or A490) and diameter from Table J3.2 of the AISC Specification (Load 1993) which has greater design strength than the required bolt force, T_b, determined in Step 4.

Step 6: Calculate the moment design strength of the connection using selected type and size bolts.

$$M_{con} = 4\ \phi T_n\ (d - t_f) \geq M_c \qquad (3.5)$$

where ϕT_n is the value obtained from Table J3.2 of the AISC Specification (Load 1993).

3.2.3 End-Plate Thickness

The following eleven steps determine the geometric configuration and thickness of the moment end-plate as shown in Figure 3.1. The preliminary bolt type and size selected in the previous section are checked for prying force action and determined if adequate. If the bolts are not adequate, a larger bolt size must be selected and this design section repeated until the bolts are satisfactory.

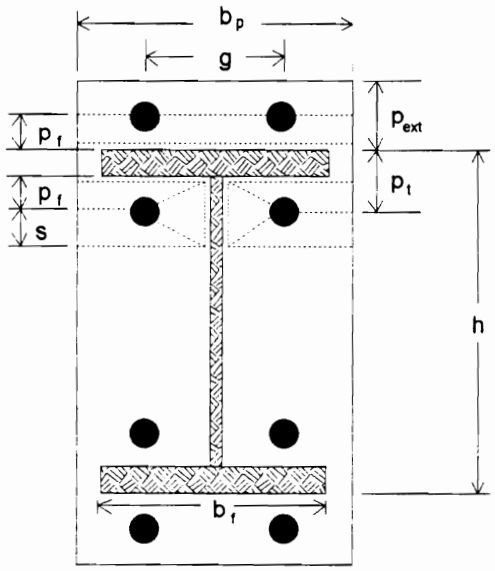

Figure 3.1 End-Plate Geometry

Step 1: Establish values to define end-plate geometry (Figure 3.1).

b_p - end-plate width, which should not be greater than beam flange width plus 1 in. for the end-plate to remain fully effective (Murray, 1990)

g - gage, greater than the minimum distance determined by wrench clearance with respect to column web thickness; the maximum gage width should not be greater than the beam flange width

p_f - pitch or distance from beam flange face to bolt centerline, should be as small as possible, determined by wrench clearance; rule of thumb is bolt diameter plus 1/2 inch

Step 2: Calculate distance from inner bolt to the innermost yield-line (Figure 3.1).

$$s = \sqrt{b_p g}/2 \tag{2.5}$$

Step 3: Calculate required end-plate thickness using Equation 2.4 with $M_u = M_{con}$,

$$t_p = \left[\frac{M_u / F_{py}}{\left(\frac{b_p}{2}\left(\frac{1}{p_f} + \frac{1}{s} \right) + (p_f + s)\left(\frac{2}{g} \right) \right)(h - p_t) + \frac{b_p}{2}\left(\frac{h}{p_f} + \frac{1}{2} \right)} \right]^{1/2} \tag{2.4}$$

and select a standard thickness greater than t_p.

Step 4: Calculate the nominal strength of the end-plate with the selected thickness determined in Step 3.

$$M_{plate} = F_{py} t_p^2 \left[\left(\frac{b_p}{2}\left(\frac{1}{p_f} + \frac{1}{s} \right) + (p_f + s)\left(\frac{2}{g} \right) \right)(h - p_t) + \frac{b_p}{2}\left(\frac{1}{2} + \frac{h}{p_f} \right) \right] \tag{3.6}$$

Step 5: Determine behavior category (thin, intermediate, or thick) of the selected end-plate by first calculating the thick and thin approximation thicknesses.

$$t_1 = \sqrt{2.11 p_f t_f \frac{b_f}{b_p} \frac{F_{fy}}{F_{py}}} \tag{2.7}$$

$$t_{11} = \sqrt{\frac{\left(b_f t_f F_{fy} p_f - \frac{\pi}{8} d_b^3 F_{yb} \right)}{F_{yp}\left(0.425 b_p + 0.80 w'\right)}} \tag{2.8}$$

if $t_p > t_1$, end-plate exhibits thick plate behavior

if $t_p \leq t_{11}$, end-plate exhibits thin plate behavior

if $t_{11} \leq t_p \leq t_1$, end-plate exhibits intermediate plate behavior

Note: The approximate values determined by Kennedy *et al.* (1981), Equations 2.7 and 2.8, are often within the round-off for standard size steel plates and the exact solutions are seldom required.

Step 6: Calculate Inner and Outer Bolt Forces.

If <u>thick</u> plate behavior,

$$B_I = \beta F_f / 2$$

$$B_E = \alpha F_f / 2 \tag{3.7}$$

and since, $\alpha = \beta = 0.5$,

$$B_I = B_E = F_f / 4 \tag{3.8}$$

If <u>thin</u> plate behavior,

$$B_I = \beta F_f / 2 + Q_{max} = F_f / 4 + Q_{max} \tag{3.9}$$

$$B_E = \alpha F_f / 2 + Q_{max} = F_f / 4 + Q_{max}$$

where $$Q_{max} = \frac{w' t_p^2}{4a}\sqrt{F_{py}^2 - 3\left(F'/w' t_p\right)^2} \qquad (2.14)$$

$$a = 3.682\left(t_p/d_b\right)^3 - 0.085 \quad ; \quad [a \le (p_{ext} - p_f) \text{ for } B_E] \qquad (2.6)$$

and $$F' = F_{11}/2 = \frac{t_p^2 F_{py}\left[0.85(b_f/2) + 0.80w'\right] + \left[\left(\pi d_b^3 F_{yb}\right)/8\right]}{4p_f} \qquad (3.10)$$

If <u>intermediate</u> plate behavior,

$$B_I = \beta F_f / 2 + Q = F_f / 4 + Q$$
$$B_E = \alpha F_f / 2 + Q = F_f / 4 + Q \qquad (3.11)$$

where $$Q = \frac{\gamma F_f p_f}{2a} - \frac{\pi d_b^3 F_{yb}}{32a} - \frac{b_f t_p^2}{8a}\sqrt{F_{FY}^2 - 3\left(\gamma F_f / b_f t_p\right)^2} \qquad (2.12)$$

$$a = 3.682\left(t_p/d_b\right)^3 - 0.085; \quad [a \le (p_{ext} - p_f) \text{ for } B_E] \qquad (2.6)$$

and $$\gamma = \alpha = \beta = 0.5$$

Step 7: Determine if selected bolt size and type are sufficient for loading.

$$B_I < 4/3\, T_b \qquad \text{and} \qquad B_E < 4/3\, T_b \qquad (3.12)$$

If B_I or B_E are greater than $4/3\, T_b$, larger sized bolts are required.

Note: The 4/3 factor used in Equation 3.12 eliminates the ϕ factor in the calculation of bolt tension and utilizes the unfactored nominal strength of the bolts. T_b is the factored bolt strength from Table J3.2 AISC Specification (Load 1993).

Step 8: Determine Length of the End-Plate (Figure 3.1).

$$L_p = h + 2\, p_{ext} \tag{3.13}$$

Step 9: Check Bolt Shear.

$$\phi R_n = \phi F_n A_b n > M_{con}/\, arm\,; \qquad \phi = 0.75 \tag{3.14}$$

where F_n is the nominal shear strength of the bolt,

A_b is the nominal unthreaded body area of the bolt,

n is the number of bolts in the end-plate at the flange, and

arm is the distance from outside edge of the end-plate to point of beam load.

Step 10: Check material bearing design strength. (The end-plate side of the connection is generally more critical than the column side due to thickness.)

Assuming that for the end-plate $L_e \geq 1.5d$ and $s \geq 3d$.

$$\phi R_n = \phi 2.4 d_b t_p F_u > M_{con}/\, arm; \qquad \phi = 0.75 \qquad \{J3\text{-}1a\}$$

Step 11: Check End-Plate shear design strength at the flange.

$$\phi R_n = \phi 0.6 A_g F_y > F_f/2\,; \qquad \phi = 0.90 \qquad \{J5\text{-}3\}$$

where A_g is the gross cross sectional area of the end-plate.

3.2.4 Beam-to-End-Plate Weld

All beam-to-end-plate welds are shop welded and full penetration welds are recommended to fully develop the forces in the beam flanges and web.

3.2.5 Column Design

In addition to axial loading and frame stiffness requirements, the supporting column must be designed for adequate strength to resist the concentrated forces imparted by the beam loading through the bolts. The required column flange and web strengths are determined using the limit states in Chapter K, AISC (LRFD) Specification for Structural Steel Buildings. The limit states to be checked are the following:

Step 1: Column Flange Bending

$$\phi = 0.90$$

$$\phi R_n = \phi 6.25 t_{fc}^2 F_{yf} \qquad \{K1\text{-}1\}$$

where t_{fc} = column flange thickness.

Step 2: Column Web Yielding

$$\phi = 1.0$$

$$\phi R_n = \phi (5k + N) F_{yw} t_{wc} \qquad \{K1\text{-}2\}$$

where $N = t_{fb}$

and t_{wc} = column web thickness.

Step 3: Column Web Crippling

$$\phi = 0.75$$

$$\phi R_n = \phi 135 t_{wc}^2 \left[1 + 3\left(\frac{N}{d}\right)\left(\frac{t_{wc}}{t_{fc}}\right)^{1.5} \right] \sqrt{\frac{F_{yw} t_{fc}}{t_{wc}}} \qquad \{K1\text{-}4\}$$

where $N = t_{fb}$

t_{fc} = column flange thickness

and t_{wc} = column web thickness.

Step 4: Column Web Buckling

$$\phi = 0.90$$

$$\phi R_n = \phi \frac{4{,}100 t_{wc}^3 \sqrt{F_{yw}}}{h} \qquad \{K1\text{-}8\}$$

where h = depth of the column

and t_{wc} = column web thickness.

3.3 SHIMMED FOUR-BOLT EXTENDED MOMENT END-PLATE CONNECTIONS

3.3.1 Beam Selection

The design procedure for the connection begins with the assumption that an adequate beam section has already been determined.

3.3.2 Type and Size of Bolts

The following six steps determine the design load strength of the connection and a preliminary bolt type and size adequate for the connection.

Step 1: Calculate the plastic moment strength of the beam.

$$M_p = F_y * Z_x \qquad (3.1)$$

Step 2: Calculate the required moment strength of the connection. (Because the plastic hinge forms at approximately d/2 inboard from the connection and not at the connection, an additional 10% connection strength above the plastic moment strength of the beam is used for the design.)

$$M_c = 1.10\ M_p \qquad (3.2)$$

Step 3: Calculate the flange force for the required connection moment strength, M_c.

$$F_f = M_c / (d - t_f) \qquad (3.3)$$

Step 4: Divide the flange force by the number of tension side bolts, 4 for this design.

$$T_b = F_f / 4 \qquad (3.4)$$

Step 5: Select a bolt type (A325 or A490) and diameter from Table J3.2 of the AISC Specification (Load 1993) which has greater design strength than the required bolt force, T_b, determined in Step 4.

Step 6: Calculate the moment design strength of the connection using selected type and size bolts.

$$M_{con} = 4\ \phi T_n\ (d - t_f) \geq M_c \qquad (3.5)$$

where ϕT_n is the value obtained from Table J3.2 of the AISC Specification (Load 1993).

3.3.3 End-Plate Thickness

The following steps determine the geometric configuration and thickness of the moment end-plate as shown in Figure 3.1.

Step 1: Establish values (b_p, g and p_f) to define end-plate geometry as in Section 3.2.3.

Step 2: Calculate required end-plate thickness using Equation 2.17.

$$t_p = \sqrt{8B_t p_f / (F_{yp} b_p)} \qquad (2.17)$$

where $B_t = \phi T_n$ determined in Step 5 of Type and Size Bolt.

Step 3: Determine Length of the End-Plate (Figure 3.1).

$$L_p = h + 2\, p_{ext} \qquad (3.13)$$

The remaining steps for plate design, weld and column design checks are as outlined in the previous section.

3.4 FOUR-BOLT WIDE EXTENDED MOMENT END-PLATE CONNECTION

The four-bolt wide extended moment end-plate was designed based on the AISC procedures as outlined in Part 10, page 10-24, of AISC (LRFD) Manual of Steel Construction (1994).

3.4.1 Beam Selection

The design procedure for the connection begins with the assumption that an adequate beam section has already been determined.

3.4.2 Type and Preliminary Size of Bolts

The following six steps determine the design load strength of the connection and a preliminary bolt type and size adequate for the connection.

Step 1: Calculate the plastic moment strength of the beam.

$$M_p = F_y * Z_x \tag{3.1}$$

Step 2: Calculate the required moment strength of the connection. (Because the plastic hinge forms approximately at d/2 inboard from the connection and not at the connection, an additional 10% connection strength above the plastic moment strength of the beam is used for the design.)

$$M_c = 1.10\ M_p \tag{3.2}$$

Step 3: Calculate the flange force for the required connection moment strength, M_c.

$$F_f = M_c / (d - t_f) \tag{3.3}$$

Step 4: Divide the flange force by the number of tension side bolts, 8 for this design.

$$T_b = F_f / 8 \tag{3.4}$$

Step 5: Select a bolt type (A325 or A490) and diameter from Table J3.2 of the AISC Specification (Load 1993) which has greater design strength than the required bolt force, T_b, determined in Step 4.

Step 6: Calculate the moment design strength of the connection using selected type and size bolts.

$$M_{con} = 8\ \phi T_n\ (\ d - t_f\ )\ \geq\ M_c \qquad (3.14)$$

where ϕT_n is the value obtained from Table J3.2 of the AISC Specification (Load 1993).

3.4.3 End-Plate Thickness

Procedures utilized to determine the end-plate thickness are based on Part 10, page 10-24, of AISC (LRFD) Manual of Steel Construction. This design procedure is for the four-bolt unstiffened extended end-plate, but for this research it is applied to the four-bolt wide configuration.

Step 1: Establish values (b_p, g and p_f) to define end-plate geometry as in Section 3.2.3.

Step 2: Calculate required end-plate thickness.

$$t_p = \sqrt{\frac{4M_{eu}}{\phi F_y b_p}} \qquad (3.15)$$

where $M_{eu} = \dfrac{\alpha_m P_{uf} P_e}{4}$

F_y - yield strength of the end-plate material

A_f - area of the beam tension flange

A_w - area of beam web, clear of flanges

b_p - effective end-plate width

b_f - beam flange width

d_b - bolt diameter

p_f - bolt pitch distance

w_i - fillet weld throat size or size of reinforcement for groove weld

$$\alpha_m = C_a C_b \left(A_f / A_w \right)^{1/3} \left(P_e / d_b \right)^{1/4}$$

$P_{uf} = F_f$; factored beam flange force determined in Step 4 of Bolt type and size

$P_e = p_f - \left(d_b / 4 \right) - w_t$; - effective pitch

C_a - constant from Table 10-1, AISC Manual of Steel Construction

$$C_b = \left(b_f / b_p \right)^{1/3}$$

Step 3: Determine Length of the End-Plate (Figure 3.1).

$$L_p = h + 2\, p_{ext} \qquad (3.13)$$

The remaining steps for plate design and weld design checks are as outlined in Sections 3.2.3 and 3.2.4. For column side design checks, refer to Murray (1990) *Steel Design Guide Series 4; Extended End-Plate Moment Connections.*

3.5 EXTENDED, STIFFENED MOMENT END-PLATE CONNECTIONS

The extended, stiffened moment end-plate connection, either four-bolt or four-bolt wide, is intended to be tested with shims. The shimmed end-plate designed in Section 3.3 is an excessively "thick" plate and unacceptable to many steel designers. The stiffeners are added to the conventionally designed end-plate to provide additional bending strength

while retaining a thinner and more acceptable end-plate. The five design steps presented in this section are only for the end-plate stiffener which is added to the connection design of Sections 3.2 or 3.4. Refer to the appropriate section for the design of bolts, end-plate, and column side design.

Step 1: Determine the end-plate bending moment caused by bolt tension.

$$Mp = n * B_t * p_f \tag{3.16}$$

Step 2: Determine moment of inertia and elastic strength of the end-plate.

$$I_x = \frac{b_p t_p^3}{12}$$

$$M_{plate} = \frac{2F_{yp}I_x}{t_p} \tag{3.17}$$

Step 3: Estimate the thickness of stiffener, but less than beam flange thickness. (Based on good engineering judgment.)

Step 4: Calculate the required length of the stiffener along the beam flange such that:

$$M_p < F_y I_X / y \tag{3.18}$$

where I_X - moment of inertia of plate and stiffener

and y - distance to maximum stress.

Step 5: Calculate required stiffener fillet weld size.

$$D_{min} = \frac{0.9F_y t_s}{2x1.392} \tag{3.19}$$

where D_{min} is the fillet weld size in sixteenths.

3.6 SUMMATION

The preceding design procedures were followed to design the connections used in the experimental portion of this research. Both university and commercial fabrication and welding of the moment end-plate-to-beam specimens were used. The following section presents the results of the tests and discusses the validity of the designs.

CHAPTER IV

EXPERIMENTAL RESULTS

4.1 TESTING METHODOLOGY

Full scale testing was conducted using several different size A36 steel wide flange sections and one built-up beam section of Grade 50 steel. All testing was conducted to failure, with failure determined by attaining one of several failure modes. Possible failure modes include: local buckling of the beam flange, fracture of the beam flange, fracture or tearing of the beam to end-plate weld, bolt fracture, end-plate shear failure, and column flange or web buckling. For a properly designed and fabricated connection, the desirable failure mode is local flange buckling of the beam (formation of a plastic hinge).

The physical test setup for the evaluation of the connections is a cantilevered beam connected to a column section by bolts as shown in Figure 4.1. The test setup was erected in the horizontal plane for use of available reaction floor beams and safety of testing. Popov and Tsai (1989) used a similar testing arrangement. Lateral bracing was placed at intervals such that compact section behavior was assured. The free end of the beam was supported by a roller device to eliminate any moment caused by gravity forces perpendicular to the loading plane. No axial loads were applied to the column or beam sections. Instrumentation for recording of test data included a 200 kip tension-compression load cell, a displacement transducer to measure beam deflections at the loading point, instrumented calipers to measure end-plate and column flange separation, a displacement transducer to measure end-plate slip parallel to loading, strain gauges to measure beam flange strain and instrumented bolts to measure bolt strain. The displacement transducer at the loading point was secured to a steel angle which was

Figure 4.1 Test Setup

welded to the column. This method of attachment maintains rigid body motion with the column and allows direct measurement of beam deflection.

All bolts used for the full-scale connection tests were "instrumented" with an internal strain gauge to indicate real time strain within each bolt. During testing, if the bolt strain increased too rapidly or to an unacceptable level, the test could be halted without failure of the bolts and/or damage to test equipment. In addition to monitoring and recording bolt tension (strain) during the tests, the "instrumented" bolts allowed an accurate tightening force to be applied during assembly of the connection.

To prepare these "instrumented" bolts, a 2 mm hole was drilled in the head of the bolt to a depth such that a "bolt" strain gauge could be installed below the head of the bolt but above the threaded portion of the shank. (The 2 mm hole does not reduce the strength of the bolt as its reduction of the bolt shank area is much less than the reduction of area in the threaded portion of the bolt.) After insertion of the strain gauge, an epoxy was injected into the hole which, upon curing, formed a tight bond between the gauge and bolt material. Each bolt was then calibrated for tension load versus strain using a tensile test machine.

Quasi-static or "slow cyclic" loading was applied to the end of the cantilever beam using a hydraulic actuator. The loading history prescribed by ATC-24 and previously discussed in Chapter II was used for all testing. Actual load histories are included in appropriate appendices with each beam section. Data from each test was recorded from test setup to eventual failure, through the use of a MEGADAC, Optim Electronics Corporation, data acquisition system. The data was transferred via disk media to commercial software for analysis in spread sheet and graphical software. All presented data and graphical representations are generated from actual test data. Appendices C through G contain end-plate and connection detailing, strain gauge and bolt location, tensile coupon test results, load history, connection performance curves, and bolt tension curves. Similar beam sections are located in the same appendix.

4.2 TESTS USING THE W18X35 BEAM SECTION

Four different four-bolt extended moment end-plate connections with a W18x35 nominally A36 beam section were designed, fabricated and tested. For each test, university personnel welded the end-plate using full penetration welds to a W18x35, A36 steel, beam section and bolted it to the flange of a W14x145, A36 steel, column section. The connections did not have weld access holes. The initial four-bolt extended moment end-plate connection tests were intended to validate the developed design procedures and to develop and refine the testing technique of cyclic loading to be used in subsequent testing. Two of the connections were of a conventional extended configuration. The third connection was designed with end-plate stiffeners and the fourth, which had a thick end-plate, was designed to be tested with shims. Table 4.1 shows the end-plate and bolt dimensions, measured beam material strengths, number of cycles tested, and failure mode for each of the four tests. The actual yield strength of the beam sections, 55 ksi, was much greater than the design strength, 45 ksi, used in calculations. Connection configuration and individual test results are presented in detail in Appendix C.

Table 4.1
Test Specimen Dimensions and Material Properties (W18x35)

Test No.	t_p in.	(A-325) d_b in.	Beam** F_y ksi	Beam** F_u ksi	Maximum Loading Cycles	Failure Mode	Remarks
1 / 95	1.0	1.0	55	71.7	19	Local Flange Buckling	
2 / 95	1.5	1.0	55	71.7	20	Local Flange Buckling	Shims
3 / 95	1.0	1.0	55	71.7	20	Local Flange Buckling	Shims Stiffened
4 / 95	1.0	1.0	55	71.7	20	Local Flange Buckling	

* End-Plate Dimensions: $b_p = 7.0$ in.; $g = 4.5$ in.; $p_f = 1.5$ in.
** Based on Tensile Coupon Tests of Beam Flanges and Web

Test 1/95 was conducted with a conventional four-bolt connection configuration. The instrumented A325 (1 in. diameter) bolts were tightened to 51 kips, which is the minimum bolt tension force prescribed in the AISC Specification (Load 1993). The applied load versus deflection and beam moment rotation histories from the test are shown in Figure 4.2. Figure 4.3 shows the corresponding interior and exterior bolt force versus beam flange force. Local buckling of the beam flanges occurred during the 16th cycle when the beam deflection was 4 times δ_y. The buckling was located 9 in. - 11 in. from the face of the end-plate. The test was terminated after 19 cycles of testing due to noticeable deterioration of beam strength. As the load history deflection was increased beyond 2 in., the connection displayed a loss of stiffness as evidenced by increase in deflection and decrease in the applied load (see Figure 4.2). The loss of connection stiffness is primarily due to the formation of a plastic hinge in the beam and the beam's ability to resist the applied bending moment.

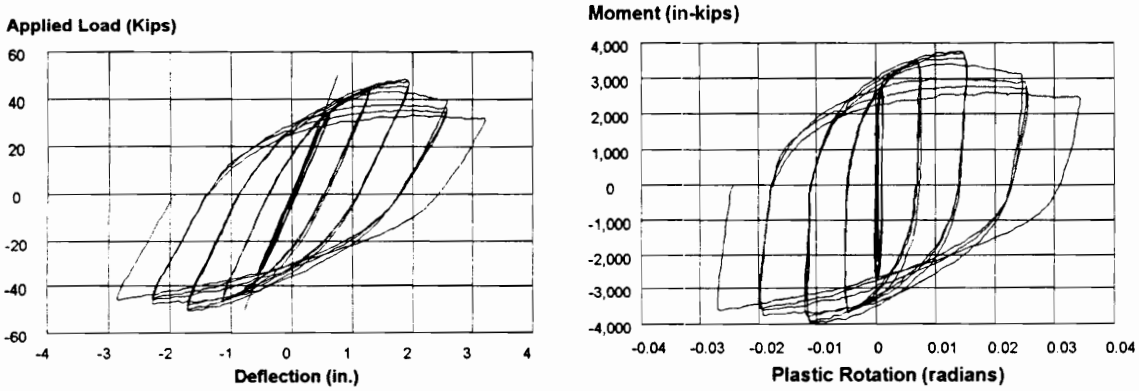

Figure 4.2 Loading and Connection Rotation Histories, Test 1/95

Neither the end-plate, welds, bolts nor column flange showed any distress during the test. The hysteresis loops shown in Figure 4.2 are robust and significantly wider than those reported for fully welded connections. The connection rotation is greater than 0.02 radians. As seen in Figure 4.3, there was a complete loss of bolt tension for the inner bolt

and a substantial loss of bolt force for the outer bolt. However, these losses did not affect the strength of the connection.

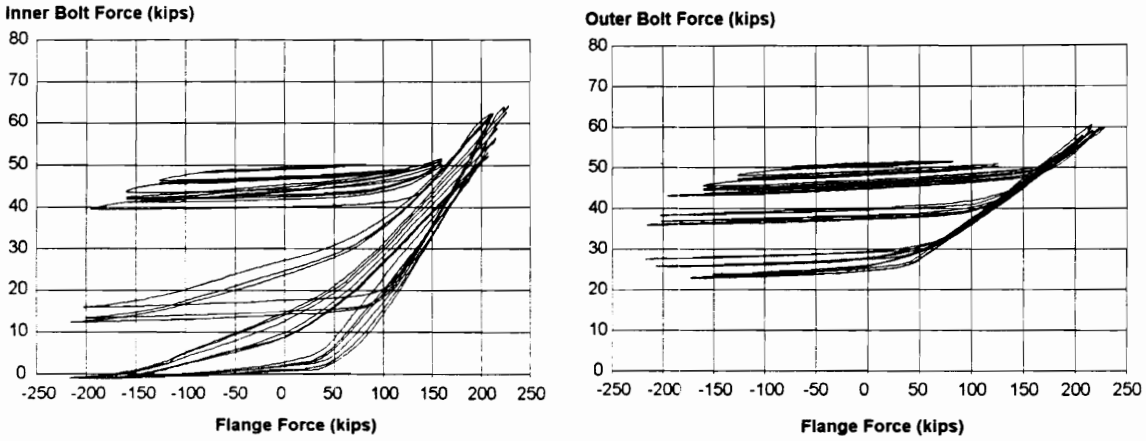

Figure 4.3 Inner and Outer Bolt Forces, Test 1/95

Test 2/95 was conducted with 0.50 in. thick shims placed as shown in Figure 4.4. The bolts were tightened to the minimum bolt tension as measured by the instrumented bolts. Local buckling of the beam flange occurred during cycle 13 without end-plate, weld, bolt or column flange distress. Testing was terminated after 20 cycles. The load-deflection, moment rotation and bolt force-flange force histories were similar to those from Test 1/95 (see Appendix C for Test 2/95 data). Again, the hysteresis loops were wide, but bolt forces decreased unexpectedly, possibly because of compression yielding of the shim plates and yielding of the end-plate. The shim plate original thickness was reduced by 0.025 in. due to compression.

For Test 3/95, an extended, stiffened end-plate was tested with shims. The bolts were tightened to the minimum bolt tension force. Failure was again by local flange buckling of the beam flanges. The load-deflection, moment rotation and bolt force-flange force histories were similar to those from Test 1/95 (see Appendix C for Test 3/95 data). The bolt forces decreased similar to Test 2/95 again due to yielding of the shim in compression (0.025 in.) and deformation of the end-plate at high tensile loading.

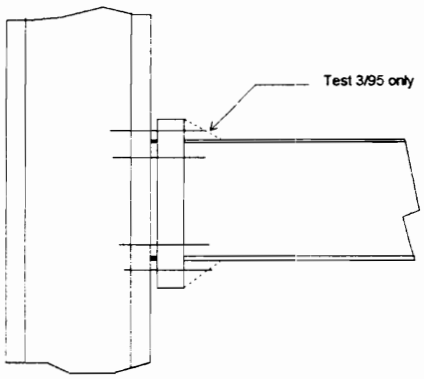

Figure 4.4 Shimmed End-Plate Connection

Test 4/95 was identical to Test 1/95 except that the bolts were tightened using the turn-of-nut method (Load 1993). This tightening method resulted in larger strains in the bolts at completion of tightening. Again, failure was local buckling of the beam flanges without end-plate, weld, bolt or column flange distress. Resulting load-displacement and moment rotation histories were similar to those from Test 1/95. The bolt forces decreased as in Test 1/95 but not as significantly (see Appendix C for Test 4/95 data).

4.3 TESTS USING THE W24X62 BEAM SECTION

Six different four-bolt extended moment end-plate connections with a W24x62 nominally A36 beam section were designed and tested. For each test, the end-plate was welded using full penetration welds to a W24x62, A36 steel, beam section and bolted to the flange of a W14x257, A36 steel, column section. The first two connections were part of the initial research plan to test the design validity for moderate-to-small size beam connections. Due to beam flange fractures encountered during the first two tests, four additional connections were fabricated to investigate and identify the cause of the fractures. One configuration was the conventional unstiffened four-bolt style, a second configuration employed a conventional unstiffened end-plate with shims and the third was a stiffened end-plate also with shims.

The first two of the end-plate-to-beam welds were welded by a commercial steel fabricator using weld access holes. The remaining four end-plates were welded by university personnel without weld access holes. Weld access holes are cut in the web adjacent to the beam flange where the end-plate and beam are welded together (see Figure 4.5). The holes provide access for the welder's torch during end-plate to beam welding to ensure a continuous full-penetration weld is obtained behind the web-flange fillet area of the beam. The size of the hole must be at least 1 1/2 times the web thickness in accordance with AISC Specification (Load 1993), but it is often slightly larger due to the difficulty of cutting a proper hole in sections with a thin web.

Table 4.2 shows the end-plate and bolt dimensions, measured beam material strengths, number of cycles tested, and failure mode for each of the six tests. The actual yield strength of the first three beam sections, 53 ksi, was much greater than the design strength, 45 ksi, used in calculations. The actual yield strength of the remaining beam sections, 47 ksi, was very close to the design strength, 45 ksi, used in calculations. Connection configuration and individual test results are presented in detail in Appendix D.

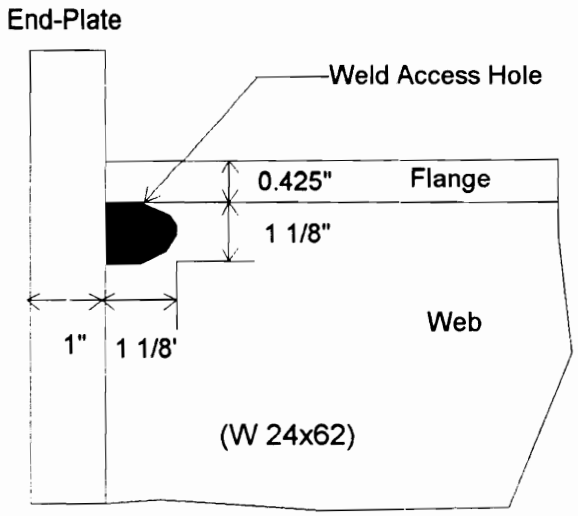

Figure 4.5 Weld Access Hole

Test 5/95 utilized a commercially welded end-plate to beam with weld access holes, 1 1/8 in. x 1 1/8 in. The 1 1/4 in. A325 bolts were tightened using the turn-of-the-nut method, but not less than 85 kips. The test was terminated during cycle 15 when a beam flange fracture occurred between 1 and 2 in. from the face of the end-plate. The fracture occurred within the length of the weld access hole, (see Figure 4.6). Neither the welds, bolts nor column flange showed any distress during the test. Maximum end-plate separation from the column flange was 0.040 in. during the inelastic cycles 12 - 15.

Table 4.2
Test Specimen Dimensions and Material Properties (W24x62)

Test No.	t_p in.	(A-325) d_b in.	Beam** F_y ksi	Beam** F_u ksi	Maximum Loading Cycles	Failure Mode	Remarks
5 / 95	1.0	1.25	53	69	15	Flange Fracture	weld access
6 / 95	2.0	1.25	53	69	13	Flange Fracture	weld access Shims
7 / 95	1.0	1.25	53	69	20	Local Flange Buckling	stiffened Shims
RH - 2	1.0	1.25	47	63	20	Local Flange Buckling	
RH - 2A	1.0	1.25	47	63	19	Flange Fracture	weld access
RH - 3	1.0	1.25	47	63	15	Flange Fracture	weld access

* End-Plate Dimensions: $b_p = 8.0$ in.; $g = 4.75$ in.; $p_f = 1.75$ in.
** Based on Tensile Coupon Tests of Beam Flanges and Web

Test 6/95 was conducted with another commercially welded specimen with weld access holes. Half inch high-strength steel shims were placed in the connection as shown in Figure 4.4. The bolts were tightened to a minimum of 85 kips as prescribed in the AISC Specification (Load 1993). During cycle 13 of loading, the beam flange within the length of the weld access hole fractured. The end-plate, thicker than usual because of the design method, did not display signs of yielding or permanent distress. The bolt forces

Figure 4.6 Flange Fracture, TEST 5/95

displayed a loss in tension as previously noted in shim tests due to shim compression (measured to be 0.012 in.) and yielding and elastic flexure of the heavy end-plate. Neither the bolts nor the welds displayed any distress or indications of failure. End-plate slip parallel to loading was measured at 0.012 inches.

Test 7/95 used a stiffened end-plate welded by university personnel without weld access holes. High-strength steel shims were used as previously discussed. All interior bolts were tightened to 85 kips. and the external bolts were tightened to 60 kips due to flexure of the end-plate during bolt tensioning. Testing was terminated after 20 cycles as beam strength deteriorated. Failure due to local flange buckling occurred 10 to 12 in. from the end-plate during cycle 16. Severe yielding of the end-plate occurred in the later cycles. Bolt forces dropped to zero when the flange force was in compression, and the shims moved freely when the flange force was in tension. No distress was noted in the welds or column flange.

Test RH-2 utilized a university personnel (certified welder) welded end-plate without weld access holes. Shims were not used in this test. The 1 1/4 in. A325 bolts were tightened to 85 kips prior to the test. Local flange buckling was noted during cycle 13 with severe buckling occurring during cycle 16. Testing was terminated after 20 complete cycles as beam strength deteriorated. Figure 4.7 shows the applied load versus deflection and beam moment rotation histories from the test. Figure 4.8 shows the corresponding interior and exterior bolt force versus beam flange force. As with other successful tests, the hysteresis loops are robust and full, displaying the desired energy dissipation of the connection. Connection rotation exceeded 0.03 radians prior to test completion. Figure 4.8 illustrates a substantial loss of bolt forces.

Test RH-2A was conducted with a university personnel welded end-plate with weld access holes. The end-plate was bolted to the column flange without shims. The 1 1/4 in. A325 bolts were tightened to 85 kips. as measured by the instrumented bolts. Local flange buckling of the beam occurred during cycle 16, but during cycle 19 the beam flange fractured. The location of the fracture was again within the weld access hole

length. Prior to beam flange fracture, the connection displayed good characteristics with connection rotation exceeding 0.02 radians. The forces for inner and outer bolts decreased similarly to their respective counterparts in Test RH - 2.

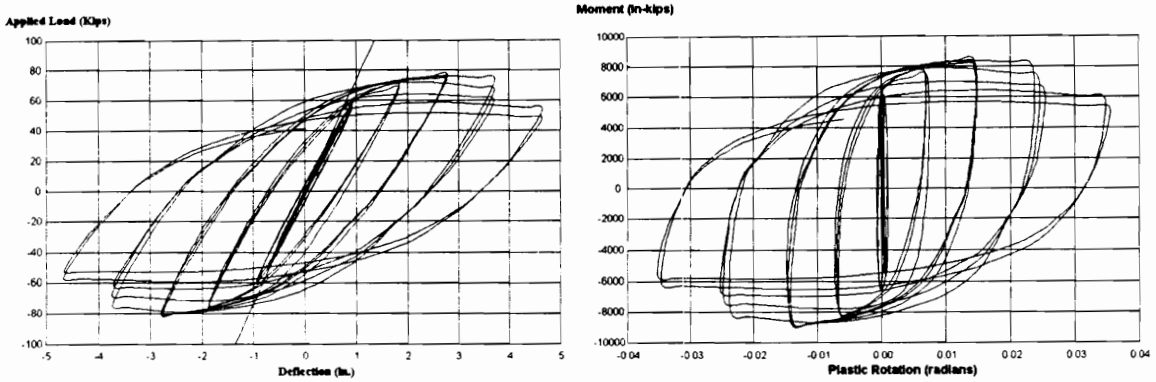

Figure 4.7 Loading and Connection Rotation Histories, Test RH-2

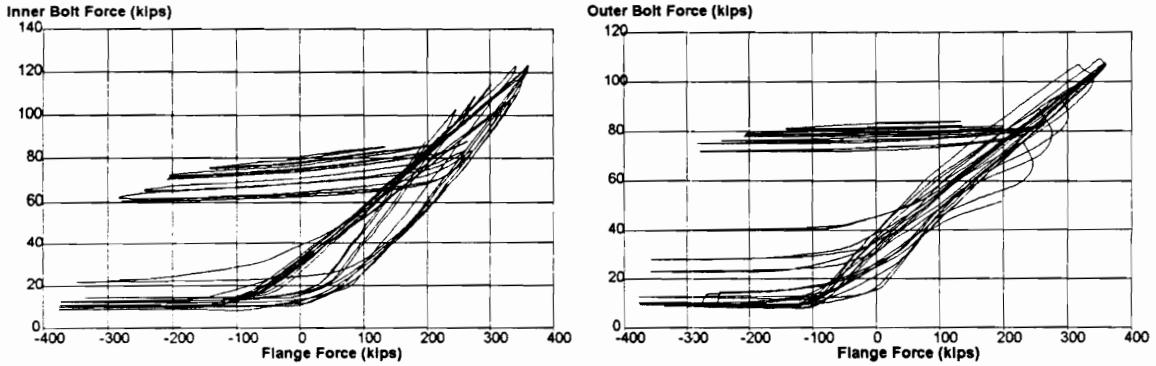

Figure 4.8 Inner and Outer Bolt Forces, Test RH-2

Test RH - 3 utilized a university personnel (certifed welder) welded end-plate with two different sized weld access holes. The access holes were elongated at different lengths to investigate the effects of varied hole size on connection behavior and to measure beam flange strain in the access hole area. The access holes were 2 and 3 times the length of the "normal" hole size; the width remained at 1 1/8 in. Figure 4.9 depicts the

connection with the elongated access holes. The 1 1/4 in. A325 bolts were tightened to 85 kips prior to testing. During cycle 10, a small crack began to develop in the bottom beam flange as shown in Figure 4.10. Minor flange buckling was noted during cycles 13 and 14. During cycle 15, the flange crack propagated rapidly through the flange and the test was terminated, (see Figure 4.10). The cause of the initial crack was that a stress riser located at a rough spot in the flame cut of the web had developed. Grinding of the access hole area was performed but was not sufficient to prevent a stress riser from developing.

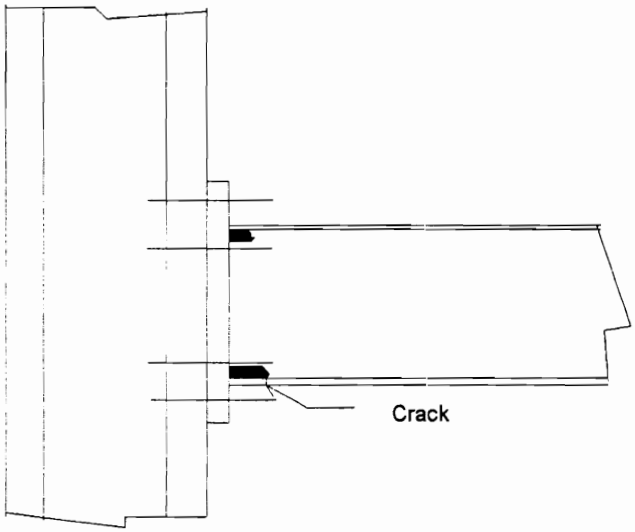

Figure 4.9 Elongated Weld Access Holes

4.4 TESTS USING THE W24X76 BEAM SECTION

Five separate tests were conducted with three different four-bolt extended moment end-plate connection specimens using the W24x76 beam section. For each test, a commercial fabricator welded the end-plate using full penetration welds to a W24x76, A36 steel, beam section and university personnel bolted it to the flange of a W14x257,

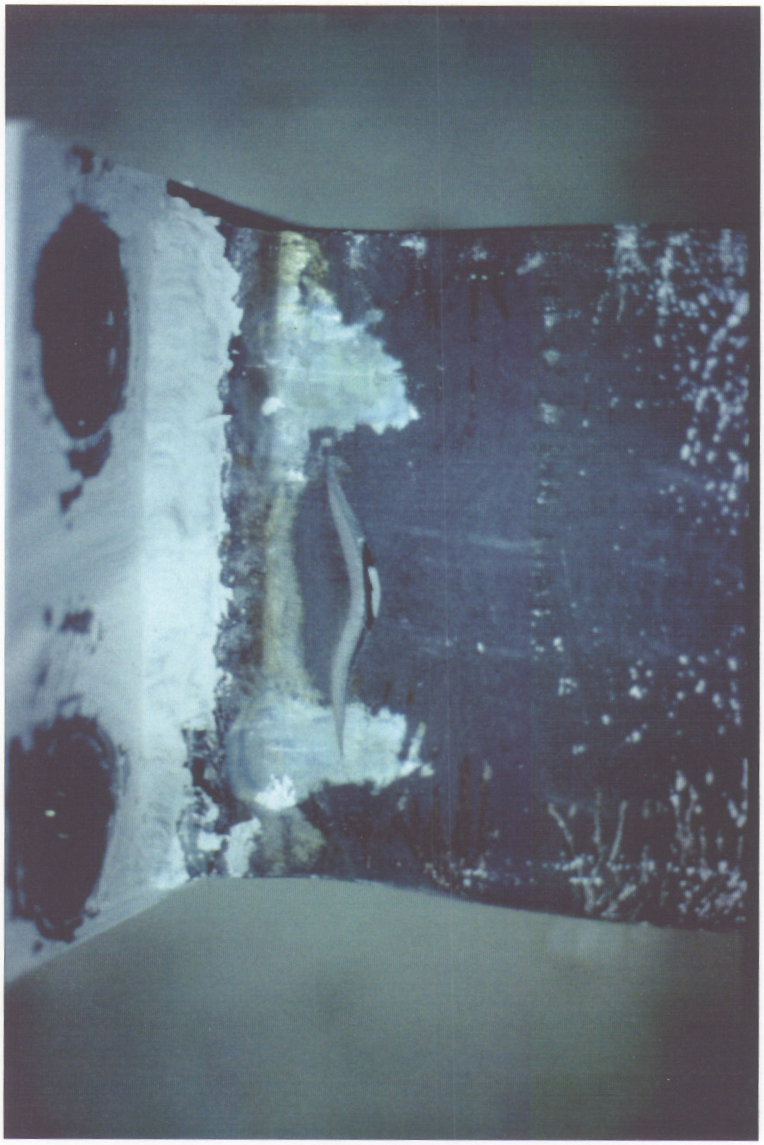

Figure 4.10 Crack Due to Stress Riser

A36 steel, column section. The purpose of the first three tests was to continue design validation while attempting to determine the cause of previous beam flange fracture. The first connection specimen was tested with three different size weld access holes. Each hole size configuration is defined as an independent test; RH-1, RH-1A and RH-1B. The remaining tests, 8/95 and 9/95, incorporated the "dog bone" beam reduction and were intended to again validate design procedures as well as test the beam reduction method as discussed in Section 2.7.

During the first test with this size connection, a much greater load was applied to the specimen than was anticipated. It was conjectured, and later confirmed by tensile coupon testing of beam flange and web material, that the actual material strength of the beam was appreciably higher than designed strength. This greater strength caused the connection moment and flange force to exceed expected values, causing unexpected forces in the A490 bolts and eventual bolt fracture. To utilize the welded end-plate specimens, a method to reduce beam bending strength to near design strength was employed. The "dog bone" method reduced the plastic bending strength of the beam from 11,000 in-kips to 8,040 in-kips. The original design strength was 9,000 in-kips. Table 4.3 shows the end-plate and bolt dimensions, measured beam material strengths, number of cycles tested, and failure mode for each of the five tests. Connection configuration and individual test results are presented in detail in Appendix E.

Test RH-1 was designed to investigate the effects of different length weld access holes on beam flange strain. The beam was prepared with additional strain gauges on the beam flanges for data acquisition. The initial size of the weld access holes was 1 1/8 in. from end-plate to edge by 1 1/8 in. from beam flange to edge. The 1 1/4 in. A490 bolts were tightened by the turn-of-the-nut method prior to the test. The beam underwent 10 cycles of loading with the original size access holes. During the 10th cycle, beam flange yielding was noted by white-wash flaking and strain gauge readings. Testing was stopped at this point because measured and observed yielding of the flange had occurred but strain hardening had not begun. The weld access holes were elongated along the flange,

doubling the length to 2 1/4 in. The width from flange to edge was not changed. Figure 4.11 illustrates the original size access hole and the later elongation sizes. The first loading cycle after hole elongation was evaluated to determine if the data was repeated or if adjustments were needed to the test data. No adjustment was needed. After two additional cycles, yielding of the column flange was noted from white-wash flaking. During the next cycle, an interior bolt fractured at a calculated flange force of 528 kips; the design flange force was 416 kips. From strain gauge data, there appeared to be a slight reduction in beam flange strain with the increase in access hole size.

Table 4.3

Test Specimen Dimensions and Material Properties (W24x76)

Test No.	t_p in.	(A-490) d_b in.	Beam** F_y ksi	Beam** F_u ksi	Maximum Loading Cycles	Failure Mode	Remarks
RH - 1	1.25	1.25	58	74	13	N/A	weld access
RH - 1A	1.25	1.25	58	74	2	N/A	weld access
RH - 1B	1.25	1.25	58	74	16	Flange Fracture	weld access "dog bone"
8 / 95	1.25	1.25	58	74	14	Flange Fracture	weld access "dog bone"
9 / 95	2.25	1.25	58	74	21	Local Flange Buckling	weld access "dog bone"

* End-Plate Dimensions: $b_p = 9.0$ in.; $g = 5.0$ in.; $p_f = 2.0$ in.
** Based on Tensile Coupon Tests of Beam Flanges and Web

Test RH-1A was performed with the same specimen used in Test RH-1. During the 10th cycle of Test RH-1, it was noted that several bolts were loose when the flange force was in compression. Prior to the start of Test RH-1A, the loose bolts were snug tightened and the previously fractured bolt was replaced and also snug tightened. During the first cycle of loading another bolt fractured. (Section 6.2 discusses the cause of bolt

fracture and methods of preventing its occurrence.) The bolt was replaced and snug tightened. An additional 2 loading cycles were conducted to obtain flange strain data with a reduced maximum deflection of the loading to prevent further bolt fracture. The testing was stopped and the weld access holes were elongated to three times the original size along the beam flange. (Figure 4.11) Two loading cycles identical in deflection to the previous ones were then performed with the three times elongated holes to determine a flange strain comparison. The beam flange strain showed a slight increase in all gauges ranging from 100 to 1,000 με.

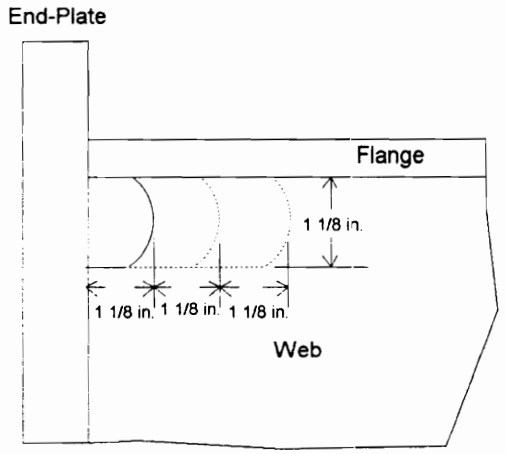

Figure 4.11 Weld Access Hole Elongation Cuts

Test RH-1B utilized the same specimen as did RH-1 and RH-1A. The specimen was removed from the test bed and the beam flanges were "dog boned" to reduce their size and the beam's overall strength. Figure 4.12 depicts the cuts performed in both beam flanges. This procedure prevented bolt fracture by reducing the beam plastic moment strength. New instrumented bolts were installed and tightened to values near the minimum tension force of 104 kips from the AISC Specification (Load 1993). After 14 cycles, a small crack was noted in the beam flange near the end of the weld access hole. During cycle 16, the crack had propagated through the entire beam flange and testing was terminated. The reduced strength of the beam due to the "dog bone" allowed the beam to

perform in a more ductile manner and decrease flange forces so that bolt fracture did not occur. Strain gauges indicated a reduction of strain, for similar deflection after the flange reduction was applied, of 1,000 με to 2,000 με depending on the gauge.

Test 8/95 was conducted with "dog boned" beam flanges as shown in Figure 4.12. Weld access holes were the original size, 1 1/8 in. x 1 1/8 in. The 1 1/4 in. A490 bolts were tightened to only 60-70 kips to investigate the effect of less than fully tightened bolts. After 13 cycles, local beam flange and web buckling was noted. During cycle 14, beam flange fracture occurred. The cause of the fracture was a crack propagation from a rough cut spot in the "dog bone" region of the flange. During the test, bolt tension was lost during flange compression and was greater during flange tension than in other W24x76 beam section connections. A greater variation of bolt strain resulted from the less than fully tightened bolts.

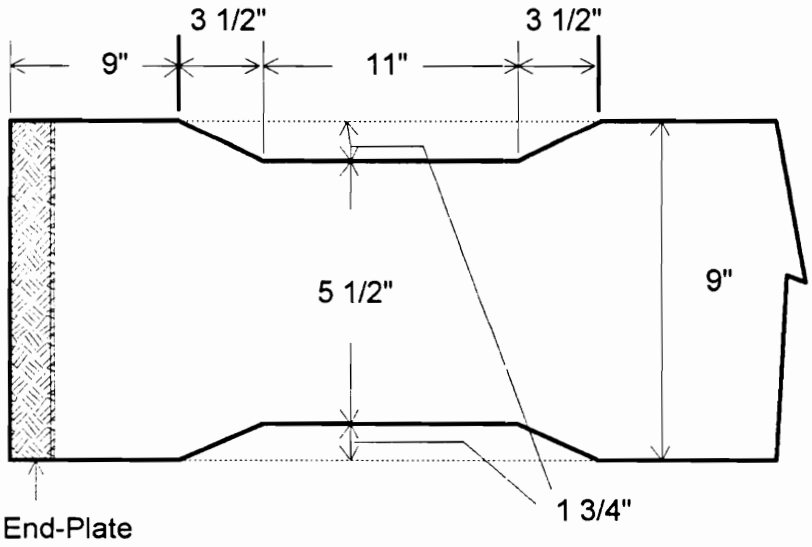

Figure 4.12 Beam Flange Reduction Geometry

Test 9/95 was conducted using a "thick" end-plate and the "dog boned" beam flanges. The bolts were tightened to ± 100 kips. Weld access holes were the original size, 1 1/8 in. x 1 1/8 in. Beam flange and web buckling occurred during cycle 13 and became

severe during cycle 16. The test was terminated after 21 cycles; the mode of failure was local flange buckling. Figure 4.13 records the applied load versus deflection and beam moment rotation histories from the test. Figure 4.14 shows the corresponding interior and exterior bolt force versus beam flange force. The connection rotation is greater than 0.03 radians. As Figure 4.14 indicates, there was a substantial loss of bolt forces, but the maximum forces were well below that to cause bolt fracture. There was no distress noted in the welds or the column flanges.

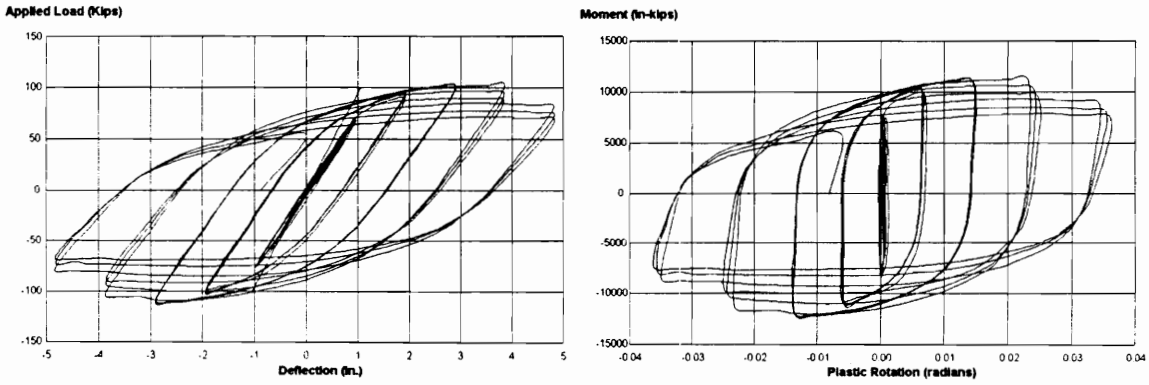

Figure 4.13 Loading and Connection Rotation Histories, Test 9/95

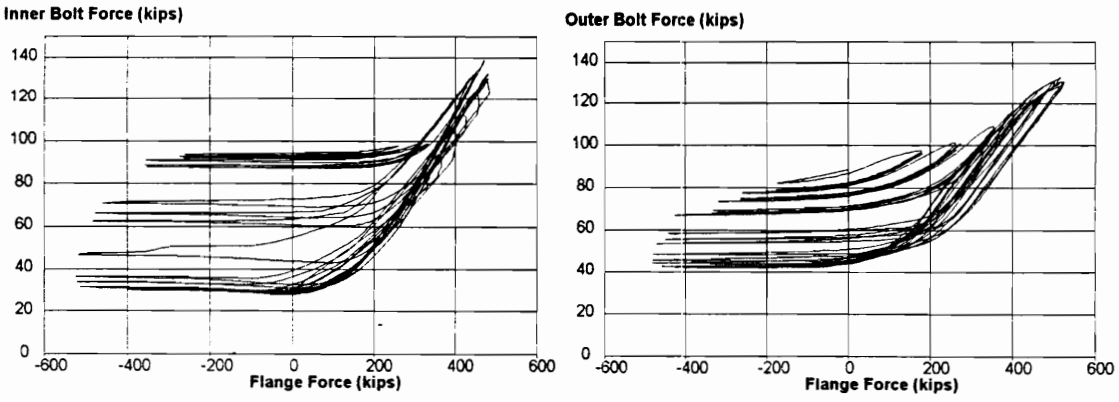

Figure 4.14 Inner and Outer Bolt Forces, Test 9/95

4.5 TESTS USING THE W36X135 BEAM SECTION

Two four-bolt wide extended moment end-plate connections were designed and tested with a W36x135 beam section requiring sixteen A-325 1 1/4 in. diameter bolts each. For each test, a commercial fabricator welded the end-plate using full penetration welds to a W36x135, A36 steel, beam section and university personnel bolted it to the flange of a W14x311, A36 steel, column section. The four-bolt wide end-plate connection has four rows of four bolts each, with the rows parallel to the beam flange, Figure 1.1. Both connections tested had weld access holes. The beam size was selected to investigate large beam connection behavior and determine if the four-bolt extended connection design methods were applicable to the four-bolt wide connection. Table 4.4 shows the end-plate and bolt dimensions, measured beam material strengths, number of cycles tested, and failure mode for both tests. The actual yield strength of the beam section was 45 ksi, which was the same strength used in the design calculations. Connection configuration and individual test results are presented in detail in Appendix F.

Table 4.4
Test Specimen Dimensions and Material Properties (W36x135)

Test No.	t_p in.	(A-325) d_b in.	Beam** F_y ksi	Beam** F_u ksi	Maximum Loading Cycles	Failure Mode	Remarks
10 / 95	1.50	1.25	45	60	13	Flange Fracture	weld access
12 / 95	1.50	1.25	45	60	19	Local Flange Buckling	weld access Stiffened

* End-Plate Dimensions: b_p = 15.0 in.; g = 5.0 in.; p_f = 1.75 in.
** Based on Tensile Coupon Tests of Beam Flanges and Web

Test 10/95 was conducted using a four-bolt wide, extended end-plate connection with weld access holes. The 16 1 1/4 in. A325 bolts were tightened to 85 kips. The bolt tightening process required additional time due to the interaction of bolt tension within the

same flange group. The increase or decrease of tension in any bolt directly affects the tension of the other seven bolts within that flange group. After 10 cycles of testing, yielding was observed in the column flange due to white-wash flaking. Figure 4.15 is a

Figure 4.15 Flange Fracture, W36x135

picture of the beam flange fracture within the weld access hole length which occurred during cycle 13 of the test.

Test 12/95 involved a stiffened four-bolt wide extended end-plate connection with weld access holes. The 1 1/4 in. A325 bolts were tightened to a minimum tension force of 85 kips. Similar tightening difficulties occurred as in Test 10/95. Local beam flange buckling occurred during cycle 13. Because of the actuator ram extension and load capacity, full increments in the cyclic loading could not be performed. During cycle 13 and subsequent cycles, the load displacement was limited to four inches because of actuator limits. In accordance with ATC-24, the cyclic loading was continued at the maximum loading/displacement possible due to actuator limitations. Testing was terminated after 19 cycles due to local flange buckling and a noted deterioration of beam strength. The applied load versus deflection and beam moment rotation histories from the test are shown in Figure 4.16. The connection rotation is just under 0.02 radians, but this is due to the limits of the test actuator and not the connection. Figure 4.17 shows the corresponding interior and exterior bolt force versus beam flange force. The bolts displayed a loss of tension, with the bolts closer to the beam web displaying much less deterioration and variation in tension than did the bolts farther from the beam web. In Figure 4.17, Interior/Exterior refers to the beam flange and Near/Far refers to the bolt's relationship to the beam web.

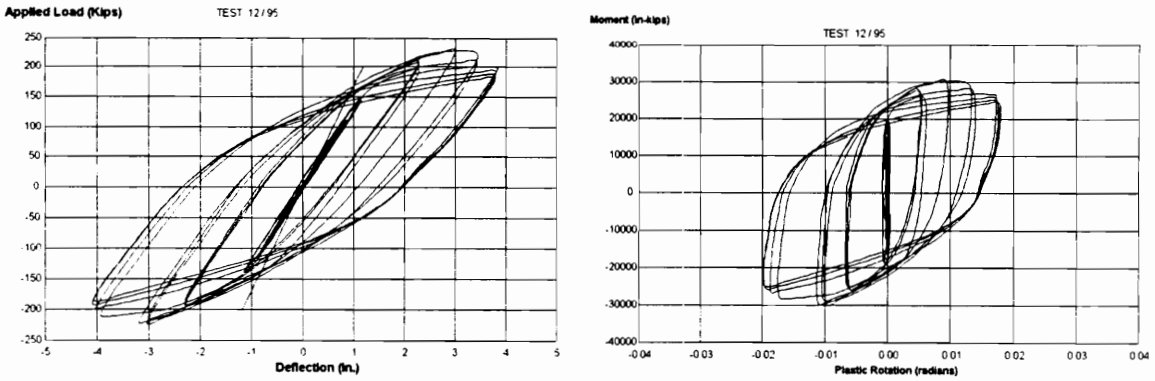

Figure 4.16 Loading and Connection Rotation Histories, Test 12/95

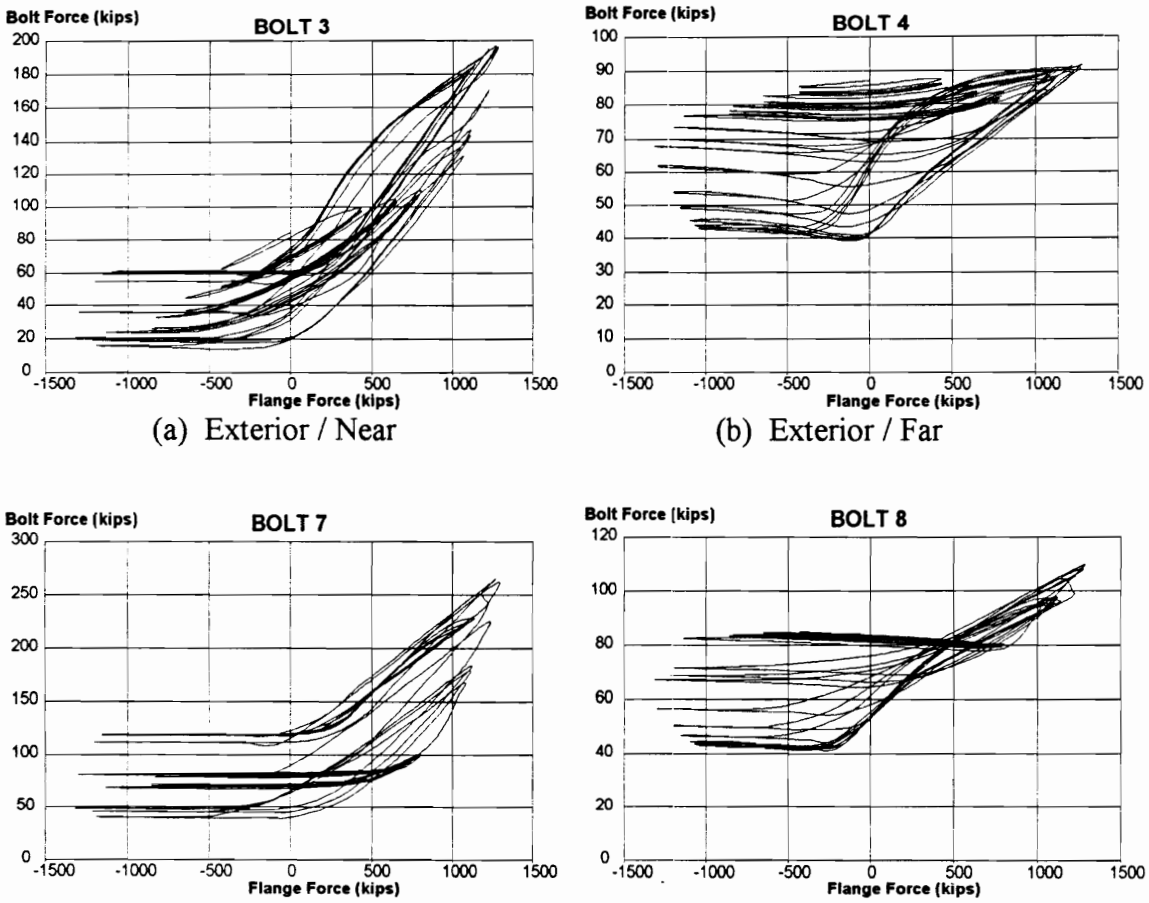

Figure 4.17 Bolt Forces, Test 12/95

4.6 TESTS USING THE BUILT-UP BEAM SECTION

Four four-bolt extended moment end-plate connections were tested using a Grade-50 steel end-plate welded to a Grade-50 steel built-up beam section. The specimen size approximated the W24x62, A-36 steel beam and end-plate connections previously tested. The specimens were fabricated by a metal building manufacturer using current industry welding methods and specifications. Each end-plate was welded to the built-up beam section using full penetration welds. All welds underwent successful non-destructive testing. The actual yield strength of the beam sections, 63-65 ksi, was greater than the

design strength, 55 ksi, used in calculations. Connection configuration and individual test results are presented in detail in Appendix G.

The primary purpose of the built-up specimen tests was to investigate the use of weld access holes and their effects on previous flange fractures failures. The end-plate and beam sections were manufactured identically except for weld access holes (1 1/8 in. diameter) in two of the specimens. Table 4.5 shows the end-plate and bolt dimensions, measured beam material strengths, number of cycles tested, and failure mode for each of the four tests.

Table 4.5
Test Specimen Dimensions and Material Properties (Built-up Section)

Test No.	t_p in.	(A-490) d_b in.	Beam** F_y ksi	Beam** F_u ksi	Maximum Loading Cycles	Failure Mode	Remarks
BuS 1	1.0	1.25	65	90	18	W-F Weld Fracture	access hole
BuS 2	1.0	1.25	65	90	16	W-F Weld Fracture	
BuS 1A	1.0	1.25	63	90	19	Flange Fracture	access hole added weld
BuS 2A	1.0	1.25	63	90	20	W-F Weld Fracture	added weld

* End-Plate Dimensions: $b_p = 8.0$ in.; $g = 4.75$ in.; $p_f = 1.75$ in.

** Based on Tensile Coupon Tests of Beam Flanges and Web

Due to web-to-flange weld failures in the first two tests (BuS 1 and BuS 2), the two remaining specimens had both sides of the webs welded from the end-plate along the flange for a length of two feet. Normal metal building industry practice is to weld only one side of the web to flange joint.

Test BuS 1 used a single sided web-to-flange welded beam which did have weld access holes. The 1 1/4 in. A490 bolts were tightened to 95 kips. After 13 cycles, local flange buckling was observed in the beam flanges. Beam strength deteriorated in

subsequent cycles. At the beginning of cycle 19, a large "tear" in the web-to-flange weld was noted about 12 in. from the end-plate and the test was terminated. Prior to test termination, the connection rotation exceeded 0.02 radians. The bolts did lose tension during the test. No distress was noted in the column flange or end-plate weld.

Test BuS 2 involved a single sided web-to-flange welded beam which did not have weld access holes. The 1 1/4 in. A490 bolts were tightened in excess of 90 kips. After 13 cycles, local flange buckling was observed in the beam flanges. Beam strength deteriorated in subsequent cycles. During cycle 16, a web-to-flange weld failure was again noted about 1 ft. from the end-plate. Prior to test termination, the connection rotation exceeded 0.02 radians. The bolts did lose tension during the test. No distress was noted in the column flange or end-plate weld.

Test BuS 1A was conducted after web-to-flange weld was added on the unwelded side of the web. The weld extended from the end-plate along the flange for a length of 2 ft. The beam section had weld access holes. The 1 1/4 in. A490 bolts were tightened to 103 kips. After 14 cycles, local flange buckling was observed in the beam flanges and severe buckling occurred during cycle 18. Beam strength also deteriorated in these subsequent cycles. During cycle 19, a beam flange fracture occurred and the test terminated.

Test BuS 2A was also conducted after a web-to-flange weld was added on the unwelded side of the web. The weld extended from the end-plate along the flange for a length of 2 ft. The beam section did not have weld access holes. The 1 1/4 in. A490 bolts were tightened to 103 kips. After 10 cycles, beam flange yielding was noted and local flange buckling occurred during cycle 13. Severe buckling developed during cycle 15 as the beam strength deteriorated. During cycle 20, a web-to-flange weld failure was noted about 12 in. from the end-plate. Prior to test termination, the connection rotation exceeded 0.02 radians as seen in Figure 4.18. Figure 4.19 shows that the bolts did lose tension during the test. No distress was noted in the column flange or end-plate weld.

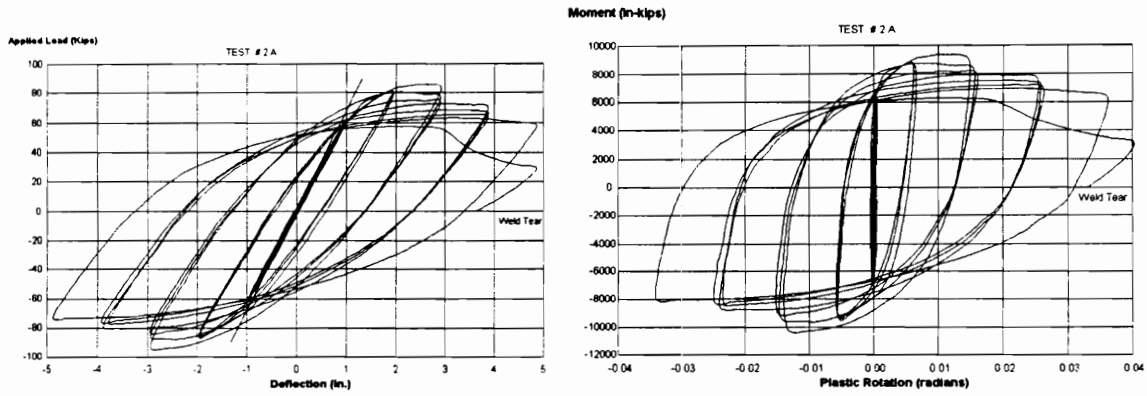

Figure 4.18 Loading and Connection Rotation Histories, Test BuS 2A

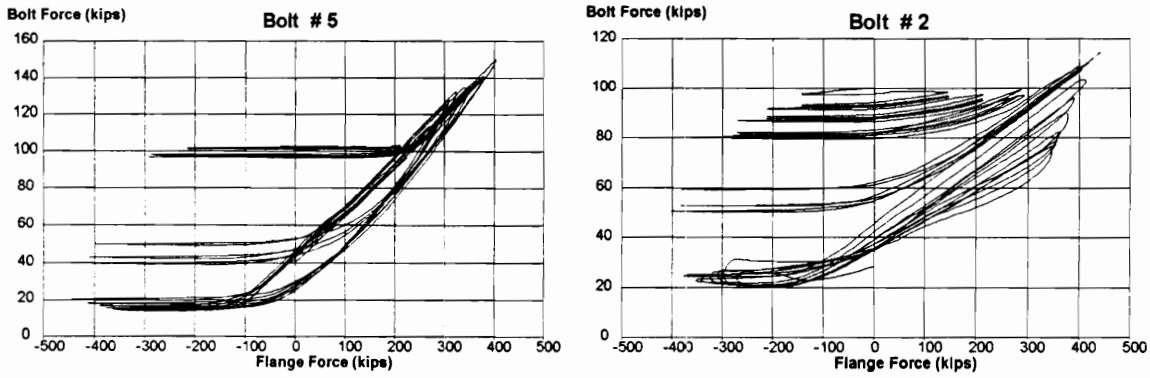

Figure 4.19 Inner and Outer Bolt Forces, Test BuS 2A

4.7 SUMMATION

This chapter presents a discussion of individual tests and their resulting responses to cyclic loading. In Chapter VI, the results obtained during testing are further analyzed and discussed by connection response and configuration specifics.

CHAPTER V

FINITE ELEMENT ANALYSIS

5.1 INTRODUCTION

The objective of the finite element analyses conducted in conjunction with this research was to model full-scale test connections for comparison of beam flange strain for different connection configurations. Beam flange fracture was an unexpected failure mode of several full-scale test specimens during the early stages of the experimental research. The fracture failures occurred in connections which had weld access holes. Finite element analyses of the four-bolt connections were intended to determine the qualitative effects that weld access holes have on the strain developed in the beam flanges. Various techniques or approaches to modeling were investigated, including absence of bolt holes in the end-plate and use of spring elements for bolts. End-plate deformation during loading and the difficulty to accurately model its behavior was noted during review of previous finite element analysis. As this research was to determine the cumulative effects during seismic activity, minor deformation and variations of the end-plate shape were not a primary consideration for the finite element analyses. Modeling to include fracture of the flange was considered beyond the scope of this research and was not attempted.

5.2 CONNECTION MODELING

5.2.1 Initial Two-Dimensional Analysis

A two-dimensional (2-D) analysis of each specimen configuration was performed before actual testing of any specimen was conducted. These analyses were performed to

determine the elastic load-deflection relationship (connection stiffness) which became a baseline for the actual test. The software program utilized to perform the 2-D analysis was RISA-2D (Users Manual). Properly sized column and beam members, their lengths and boundary conditions are represented in the 2-D model. Although only an estimated elastic response is obtained from this analysis, it did provide confirmation of actual test response for the elastic range of cyclic testing, which included the first 9 cycles of loading.

5.2.2 Finite Element Three-Dimensional Analysis

Specimen modeling using ABAQUS (Users Manual) consisted of a two step process. The first was to construct a geometric, three-dimensional (3-D), non-contact model of the entire end-plate and beam. Second, the beam loading versus deflection results of the 3-D model and the actual test data were compared to determine model validity.

Modeling of symmetrical effects of the end-plate and beam was not attempted. The use of symmetric affects perpendicular to the web were ignored because of the full-scale flange fracture failures and the desire to investigate full flange response. Symmetric effects parallel to the web were not utilized due to the load reversal technique used. Full beam length was modeled to develop accurate connection forces, moments and curvature to match full-scale test situations.

5.2.3 W18x35 Beam Model

The first connection to be modeled was the W18x35 beam connection with a 1 in. by 7 in. by 2 ft. 0 in. A36 steel end-plate. This connection was selected as full-scale testing had been completed and test data was available for comparison and calibration of the model.

A three-dimensional 8-node shell element (S8R) was initially selected for beam and end-plate elements. A favorable correlation of modeling and test results prompted the continued use of this shell element for both beam and end-plate. Beam and end-plate

material properties were modeled to represent elastic and plastic behavior using the results from respective coupon tests. An idealized stress-strain curve was modeled using 50 ksi and 72 ksi for yield and tensile beam material strengths, respectively, and 40 ksi and 62 ksi for yield and tensile end-plate material strengths, respectively. A pictorial representation of each respective material strength model can be seen in Appendix H, Figures H.1 and H.2.

The bolts were modeled with non-linear, one dimensional spring elements (SPRING 1). Four identical spring elements were used to represent each bolt to more evenly distribute the tension effects around the bolt hole perimeter. The non-linear spring properties were modeled using existing load-strain data for A325 bolts (Figure H.3). Bolt forces caused by tightening of the bolts are represented in the bolt model. The three-dimensional ABAQUS model of the connection is located in Appendix H.

Incremental loading was modeled to simulate actual testing of the beam. The loading point was the same as in the full-scale tests, 79 in. from the outer edge of the end-plate. Load versus beam deflection results of the models were tabulated and plotted with the actual test data. The projected elastic solution from RISA-2D for comparison of initial connection stiffness is also included. The results of modeling the W18x35 beam connection compared to the actual test data is shown in Figure 5.1. Excellent correlation to shape and magnitude of the load versus deflection curves can be seen. Initial connection stiffness, for both 2-D and 3-D methods, is identical to that of the actual specimen.

5.2.4 W 24x62 Beam Model

A model of the W24x62 beam connection with a 1 in. by 8 in. by 2 ft 6 1/2 in. end-plate was created similar to that described in Section 5.2.3. A finer mesh for both the end-plate and the beam was generated. The three-dimensional ABAQUS model is presented in Appendix H. The W24x62 beam material strengths are 53 ksi (yield) and 69 ksi (tensile). The actual end-plate material strengths are not known. The full-scale connections were

welded by a commercial fabricator and although coupon specimens for the end-plate material were requested, none could be provided. Because the actual material strength values were not known, the end-plate model strength values were iterated until a reasonable relationship was obtained. The material strength values that seemed to provide a reasonable correlation were 50 ksi and 72 ksi (yield and tensile, respectively). Pictorial representations of the beam material strength, the end-plate material strength and the 1 1/4 in. A325 bolt strength are provided in Appendix H, Figures H.4, H.5 and H.6 respectively.

Figure 5.2 depicts the comparison of the final model to actual test data. The model does provide an excellent correlation for most of the load-deflection curve. One possibility for the lack of complete agreement is the effect of material strain hardening. Strain hardening effects are seen in the test data curve where it departs from the finite element model at 1.5 in. This effect can only be accurately modeled with actual tensile coupon data. Without such data, attempts to accurately model the curve are strictly trial and error.

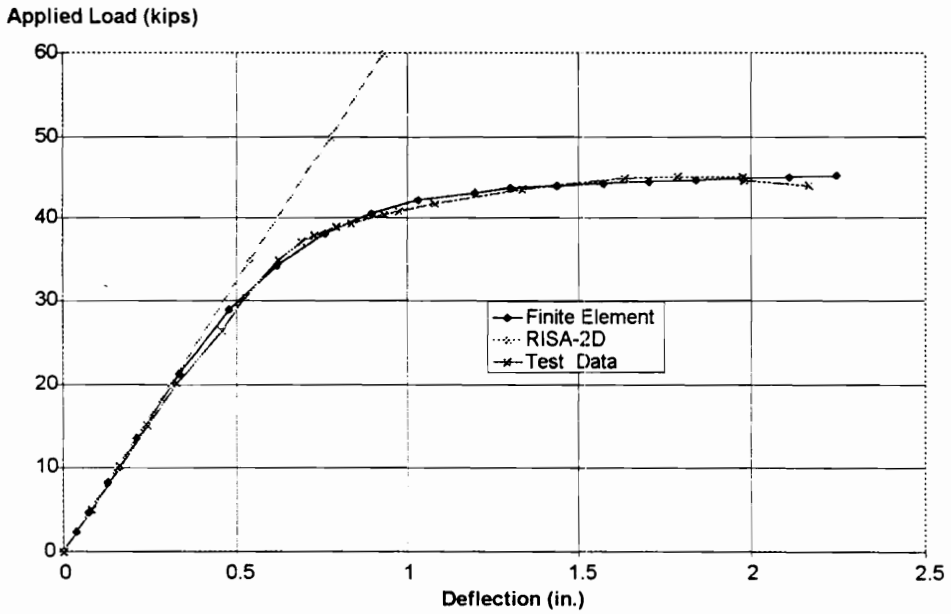

Figure 5.1 Load-Deflection for the W18x35 Beam Model

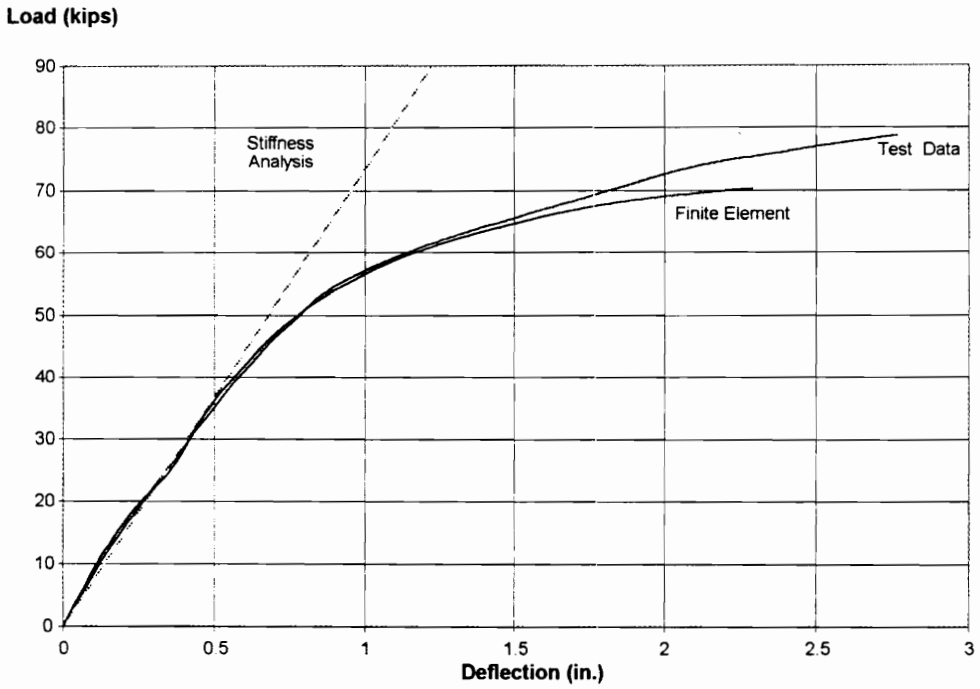

Figure 5.2 Load-Deflection for the W24x62 Beam Model

5.3 WELD ACCESS HOLE MODELING

Investigation of a relationship between weld access holes and beam flange fracture was initiated because several full-scale tests were terminated due to beam flange fracture in the area of the weld access holes. Previously, successful tests conducted did not have these access holes. Therefore, several full-scale tests were designed to determine if the weld access holes or variation in their size would affect eventual failure.

Prior to the actual full-scale testing to investigate beam response to weld access holes, finite element analysis was used to determine if there is an optimal weld access hole size which creates the minimal flange strain. Initial full-scale testing indicated a variation of beam flange strain with varying weld access hole size. The criterion for investigation was to determine a size weld access hole that resulted in the lowest (minimal) beam flange

strain. Weld access hole sizes were modified during the finite element analyses in order to determine the optimal hole size.

The models of the two beam connections described above were modified to model the weld access holes in the beam web. AISC Specification (Load 1993) requires that the holes be a minimum of 1 1/2 times the thickness of the beam web. This requires a minimum weld access hole of slightly larger than 5/8 in. (0.645 in.) for the W24x62 beam. To accommodate the AISC requirement, yet being realistic in size, 1 in. weld access holes were initially generated in the beam web. This size is also consistent with actual access hole size in the full scale test specimens and of a size needed for efficient welding. Additional models were developed which increased the length of the access hole along the flange while the distance from the flange was maintained, e.g. length was increased without increasing the depth.

5.3.1 W18x35 Beam Model

Although weld access holes were not tested in the full-scale W18x35 beam connection, finite element analysis was conducted to determine beam response to varying size access holes. A modification to web elements near the flange-web fillet was made to create a hole 1 in. by 1 in. adjacent to the end-plate. Incremental loading was applied to the weld access hole model. The web elements were changed two additional times to allow for a 1 in. by 1 1/2 in. and a 1 in. by 2 in. access hole. Figure 5.3 shows the relationship of the four different models and the increase in flange strain at the weld access hole area. Each increase of access hole subsequently caused a larger flange strain. The strain values obtained from the model without access holes correspond well with test strain data (Figure 5.4). The test data was derived from an average of the strain gauges located in the approximate location of the model values. No test data is available for comparison of the weld access hole model data.

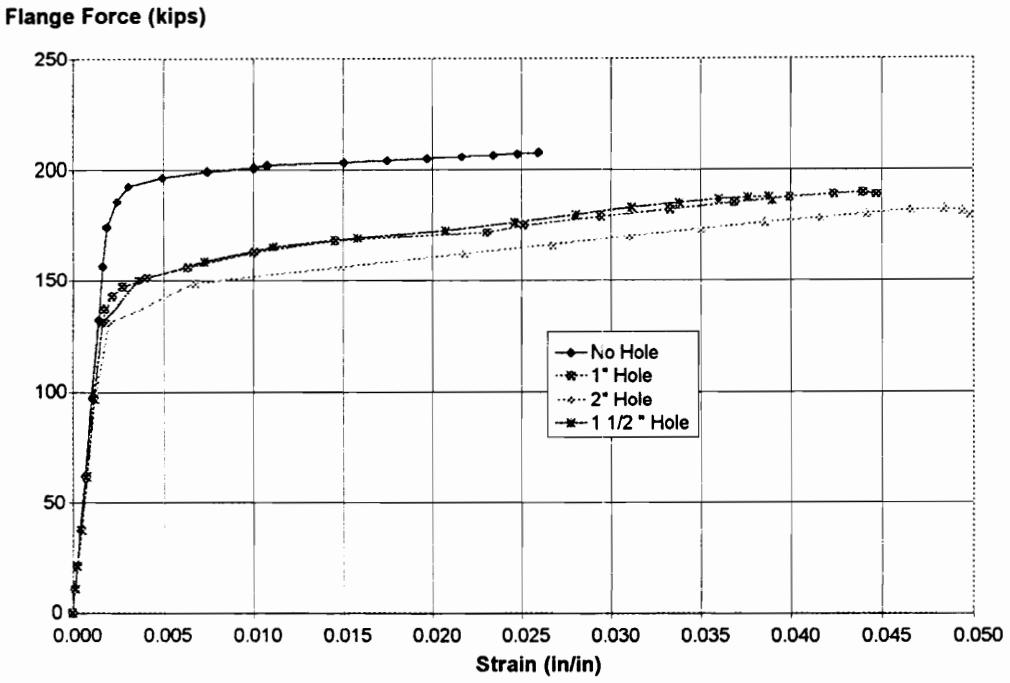

Figure 5.3 Model Flange Strain with Weld Access Holes (W 18x35)

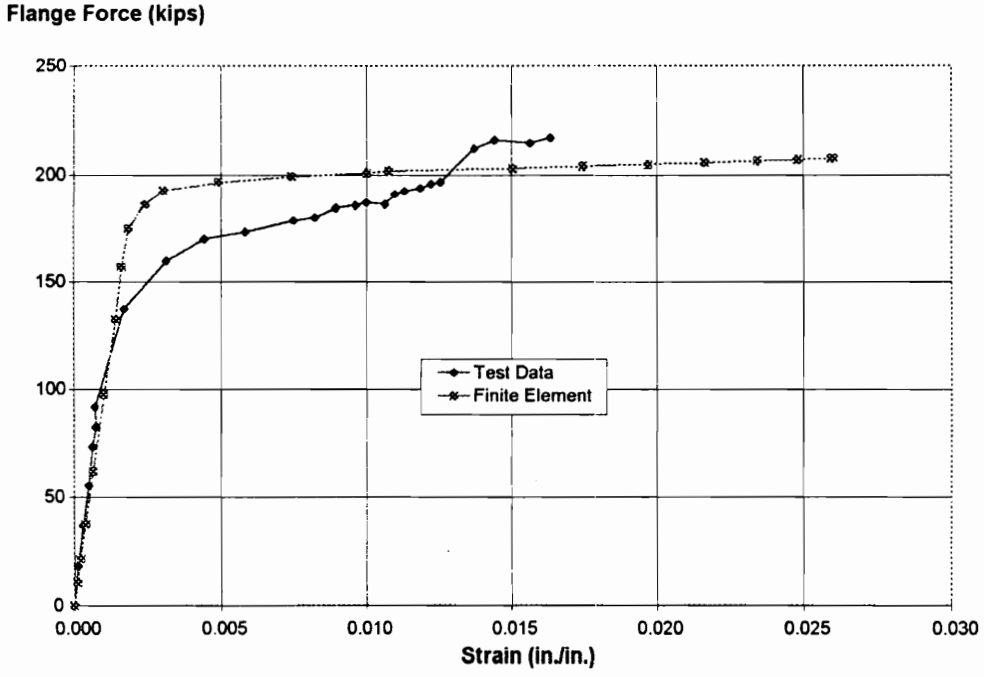

Figure 5.4 Model versus Test Flange Strain (W18x35)

5.3.2 W24x62 Beam Model

The modeling procedures described in Section 5.3.1 were repeated for the W24x62 beam connection. Two weld access hole sizes were used: 1 in. by 1 in. and 1 in. by 2 in. Figure 5.5 graphically portrays the numerical results of each model in response to the incremental loading. As with the other beam model, as the hole size increased, beam flange strain increased. The flange strain in connections with weld access holes was greater than the connection without access holes for the entire range of loading.

The strain values obtained from the model compared to actual test strain values indicate a good correlation (Figure 5.6). Both strain curves indicate a non-linear response and a plateau with the strain values of the model higher than the test data. The erratic curve of the test data is caused by the slight variations with individual strain gauges.

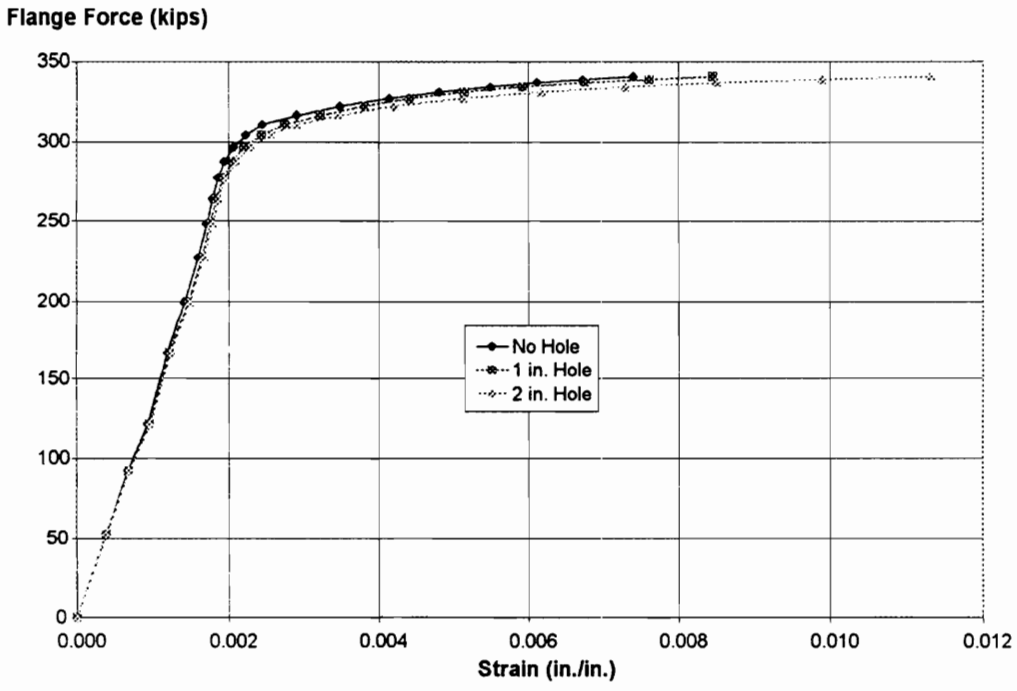

Figure 5.5 Model Flange Strain with Weld Access Holes (W24x62)

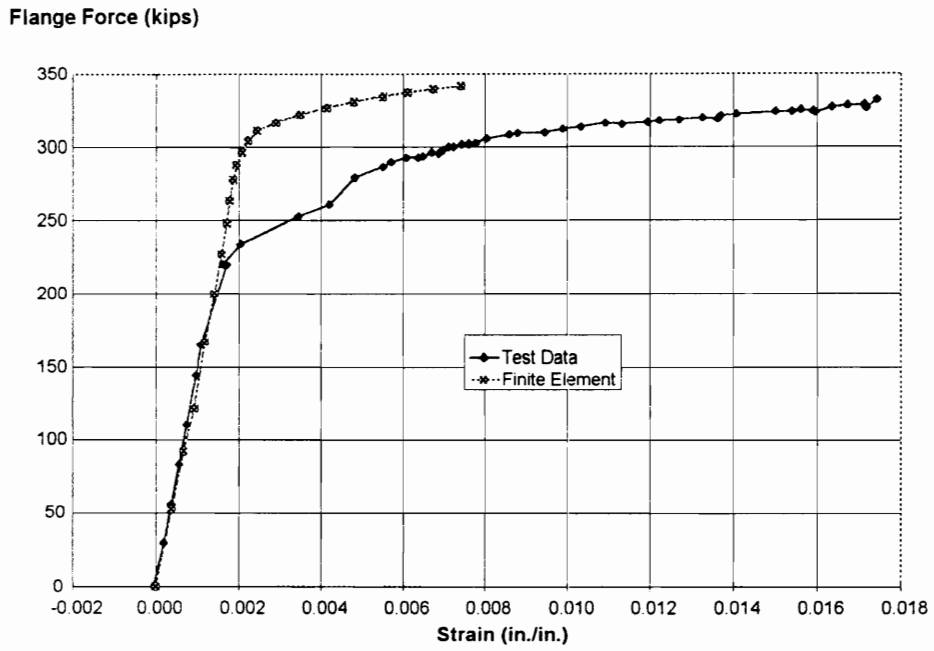

Figure 5.6 Model versus Test Flange Strain (W24x62)

5.4 LOAD-DEFLECTION HYSTERESIS MODEL

Loading reversal or hysteresis loop generation was attempted to determine if the same finite element model could accurately model a full cycle of loading. Using the model for the W18x35 beam connection, a load reversal technique was applied to simulate reverse bending of the beam. After several direction reversals in the loading, a hysteresis loop of the load-deflection parameters is generated. The model data along with full-scale test data is shown in Figure 5.7. The initial loading shows excellent correlation of the test data and model. The second loading, or reversal of original loading direction, does not display the reduction of connection stiffness as indicated by the slope of the line. The third loading also displays original connection stiffness.

The reversal points of both curves correlate well. The model generates a fuller loop due to the constant connection stiffness, which indicates more energy dissipation in the model than in the actual test connection. From the results of this modeling technique, it is possible to obtain an accurate full hysteresis loop of the beam load versus deflection.

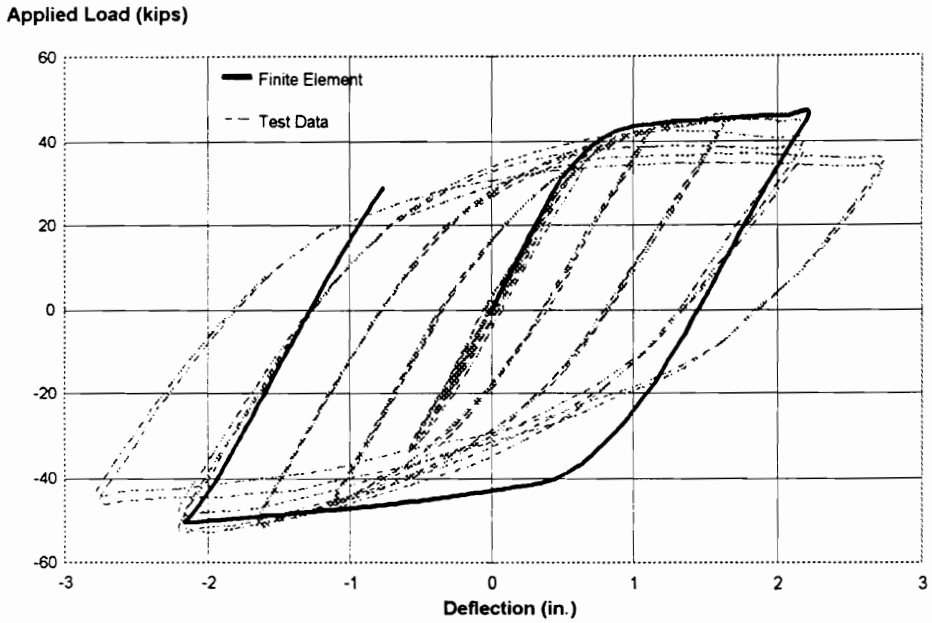

Figure 5.7 Load-Deflection Hysteresis Curves for W18x35 Beam

5.5 SUMMATION

The main objective of the finite element analysis was accomplished. The beam flange strain is affected in the region of the weld access hole by the size of the access hole. The beam flange longitudinal strain in the access hole area increases as the size of the weld access holes is increased. It was determined that end-plate connections without weld access holes result in the lowest beam flange strain and are, therefore, least likely to cause flange fracture.

The model developed for the W18x35 beam section shows excellent correlation to actual test data for load versus deflection. This was displayed both in a single load excursion as well as the load reversal and hysteresis loop generation. The model developed for the W24x62 beam section also displayed excellent qualitative correlation and good quantitative relationship as compared to the actual test data.

CHAPTER VI

DISCUSSION OF RESULTS

6.1 INTRODUCTION

After 22 full-scale, moment end-plate connection tests, four tee-stub tests and 13 different finite element models, there is an enormous multitude of data and information available for analysis and understanding. To examine all the information, specific topics and/or aspects of the research have been selected and arranged in a logical and orderly fashion and described in sufficient detail to support reasonable and accurate conclusions. The following sections will discuss and analyze research data and findings organized into nine sections. Some data may affect and be discussed in more than one section when applicable. The sections were selected as key for reporting and understanding the research and as a basis for the conclusions and recommendations. The results are generalized as to connection configuration and phenomena and are not connection size specific.

6.2 BOLT BEHAVIOR

Review of previous research indicated that bolt fracture was a major cause of failure in most moment end-plate tests. Therefore, reduction of bolt tension and elimination of bolt fracture was a primary concern during the early stages of this research. To monitor bolt tension and preclude premature bolt fracture, all bolts used for the full-scale connection tests were instrumented with an internal strain gauge as described in Section 4.1. During testing, the bolt strain was continuously monitored to preclude any bolt failure and/or damage to test equipment. In addition to monitoring and recording bolt

tension (strain) during the tests, the instrumented bolts were exceedingly helpful when tightening the bolts during assembly of the connection.

Although all bolts were instrumented and calibrated, the calibration factor applied to the recorded strain value by the acquisition system was only for the linear elastic range of each bolt. The acquisition software did not correct for the nonlinearity of the bolt force-strain curve. Therefore, when tension (strain) in the bolts exceeded the elastic range, higher than actual forces were indicated and recorded. The high bolt forces as seen in the bolt force diagrams have not been corrected for this nonlinearity. (Actual ultimate strength values for 1 1/4 in. A325 and A490 bolts are approximately 120 kips and 150 kips, respectively.) The bolt force diagrams must be corrected if values of actual bolt forces above the linear range are needed. Actual or corrected bolt force is obtained by comparing actual bolt strain obtained during testing to the force-strain curve for the appropriate bolt type. As is seen in Figure 6.1 (a typical bolt force diagram and its corrected bolt force), the only portion of the plot that changes is the high bolt force data, above 90 kips for A325 bolts and 113 kips for A490 bolts.

Overall, bolt behavior during full-scale testing is considered extremely satisfactory. Of the nearly 200 bolts utilized during the tests, there were only two failures due to fracture. The first fracture was due to an applied end-plate moment that was much higher than designed. The moment, and eventual flange force which developed, far exceeded that which was anticipated due to higher material strength of the beam than designed or realized. (Properties of beam strength are further explained in Sections 2.6 and 6.4.) The second bolt fracture was caused by improper tightening of a strained bolt. When the first fractured bolt was replaced, all bolts in the connection were mistakenly retightened. Most of these bolts had already undergone permanent strain, and during the next loading sequence the second bolt fractured. This second failure emphasized the importance of not tightening a loose bolt found during routine building inspections, but replacing it with a new bolt before applying proper torque.

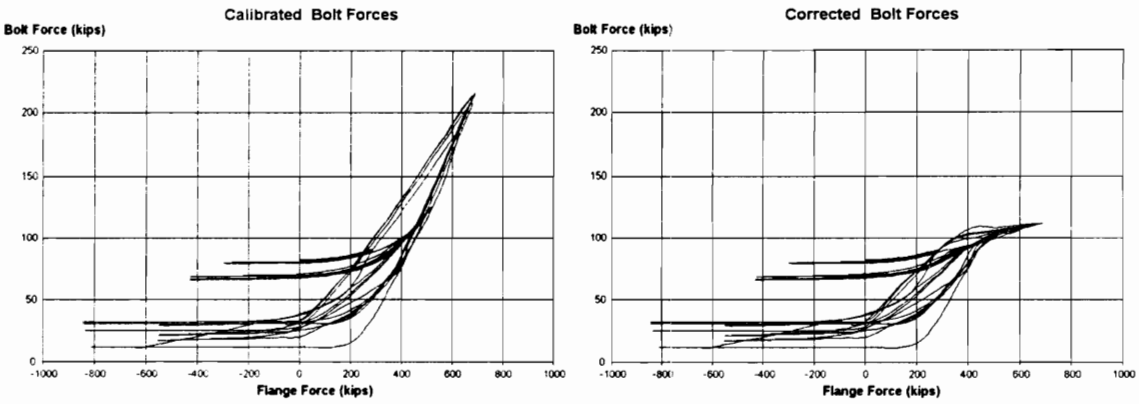

FIGURE 6.1 Calibrated versus Corrected Bolt Force

The bolts do absorb an appreciable amount of the energy imparted to the connection by the seismic loading, as evidenced by most of the bolts undergoing permanent strain deformation without fracture. This permanent deformation does contribute to the overall loss of connection stiffness and when modeling a bolt for finite element analysis, the strain of the bolt must be properly included to obtain valid representation of the connection. Interior bolts carry a greater bolt tension force than the outer bolts, as was predicted.

No notable difference in behavior of the A325 versus A490 bolt was perceived during any of the tests. With the exception of the magnitude of the bolt strength, all bolt responses, calibration, tightening and variation of bolt strain during tests were comparable for both types of bolts. The tension of the tightened bolts did affect end-plate behavior, slip and separation, but not the bolt force diagram generalized shape nor behavior.

6.3 END-PLATE THICKNESS

End-plate thickness of the four-bolt extended moment end-plate connection is determined by the plastic moment capacity of the beam and the type and size of bolts selected. Section 3.2 discuses the relationship of beam size and bolts to the ultimate design moment used for calculation of t_p, end-plate thickness. Many steel fabricators and designers have stated that a major disadvantage of the use of moment end-plate

connections in high-rise structures is the excessive thickness of the end-plates. Table 6.1 compares end-plate thickness as determined by current AISC design methods to the proposed design procedures. An average 20% reduction in required end-plate thickness is achieved by the proposed design over current AISC design. With the proposed design, the end-plate thickness to beam flange thickness ratio is 1.67 to 1.88 as compared to 2.05 to 2.38 in accordance with AISC current design. The test results verify acceptable connection performance with these thinner proposed end-plates. How much thinner the end-plate can be before they are involved in the failure mode is not known and was not an intended aspect of this research.

TABLE 6.1
Four-Bolt Unstiffened, Extended Moment End-Plate Thickness Summary

Beam Size	Thick Plate Limit (in.)	Thin Plate Limit (in.)	AISC Design (in.)	Proposed Design (in.)	Plate Sizes Tested (in.)
W 18x35	1.10	0.76	0.976	0.80	1.0 & 1.5
W 24x62	1.43	1.00	1.209	1.02	1.0 & 2.0
W 24x76	1.97	1.43	1.495	1.138	1.25 & 2.25
Built-Up	1.36	0.94	1.19 (1)	0.94	1.0

(1) AISC design procedure is restricted to A-36 steel

Table 6.1 also indicates the calculated thick and thin plate limits as outlined by Kennedy *et al.* (1981). Comparison of these values to those of test connection end-plates reveals that all three plate behavior stages were tested. Thin plate behavior was present in the W24x62 and W24x76 beam connections with end-plate thicknesses of 1 in. and 1 1/4 in., respectively. Intermediate plate behavior was present in the W18x35 and built-up GRADE-50 Steel beam connections with 1 in. plate thickness. Thick plates were investigated in the W18x35, W24x62 and W24x76 beam connections with 1 1/2 in., 2 in. and 2 1/4 in. thickness respectively. The behavior stage of the W36x135 beam connection cannot be specifically determined because the Kennedy behavior approach was not used in that design, but from test results of its behavior, it can be listed as a thin plate.

The behavior stage of the end-plate was not a common factor in the connection mode of failure. Two thick end-plate connections failed due to local flange buckling, while the other thick plate connection failed due to flange fracture. Of the intermediate thickness end-plates, failure modes of flange fracture, local flange buckling and web-to-flange web fracture were observed. Similarly, the thin end-plate connection experienced both flange fracture and local flange buckling failures.

A direct consequence of the end-plate thickness was the amount of deformation that the plate underwent during a test. As seen in Table 6.2, plate deformation was greatest in the connections with a thin plate behavior, and conversely the least deformation was in the thick plate behavior.

TABLE 6.2
End-Plate Test Deformation

Beam Size	End-Plate Type	End-Plate Slip (in.)	End-Plate Separation (in.)
W 18x35	All - 4-bolt extended Two - with shims One - stiffened	Not Measured	.033-.053
W 24x62	All - 4-bolt extended Two - with shims One - stiffened	.001-.022	.010-.177
W 24x76	All - 4-bolt extended	.011-.033	.033-.137
W 36x135	All - 4-bolt wide extended One - stiffened	.012-.013	.067-.077
Built-Up	All - 4-bolt extended	.001-.080	.057-.093

The largest end-plate separation measured was 0.137 in. and the largest end-plate slip in the direction of loading was 0.080 in. Slip values in Table 6.2 are an absolute maximum value regardless of direction. No special preparation of the end-plate or column flange was performed prior to any tests. Separation values in Table 6.2 are the sum of maximum compression and maximum tension of the connection. The compression measurements were discernible only for the shimmed connections.

6.4 MATERIAL STRENGTH

Tensile coupon tests from the beam flanges and web were conducted on all beam specimens tested. Detailed information of beam strengths is located in the appendix for each beam size. Beam yield stress varied from 45 ksi to 58 ksi and ultimate strength varied from 60 ksi to 74 ksi for the A-36 steel beams. The Grade-50 steel beams had a yield stress of 63 ksi to 65 ksi and an ultimate strength of 90 ksi. End-plate material tensile coupons were tested for the W 18x35 connection only. These end-plate values ranged from 35 ksi to 40 ksi. The majority of the other connections were commercially fabricated and plate samples could not be obtained, and deformation of test specimens precluded their use for test samples.

There was a significant increase in actual beam strength over design strength for the W24x76 beam. A design yield stress of 45 ksi was used, but actual yield stress was determined to be 58 ksi, a 28.9% increase. As discussed in Theory and Experimental Results, this increase resulted in almost a 1/3 greater flange force and corresponding bolt force. It was this increased beam yield stress that caused the first bolt fracture and originated the need for reducing the beam's cross section. The eventual reduction of beam flange area allowed successful testing of these high yield stress specimens.

The first test using the "dog bone" method, Test 8/95, did terminate due to flange fracture as a direct result of the reduction. The flanges were torch cut and then ground to remove flame cuts and to smooth the flange. The lack of success of smoothing was evident with Test 8/95, as a crack developed from a small imperfection and eventually caused flange fracture. In preparation for Test 9/95, much greater time and attention was given to the flange reduction grinding. Additional grinding was conducted to eliminate any visible flaw in the flange as a result of the flame cut. Because of the greater attention, no cracks developed during the second test of the "dog bone" method and a successful test resulted.

The "dog bone" method is a potential method to reduce the beam section to maintain beam strength at or near design strength. The main disadvantage of the method

is the added time, effort and eventual expense of proper section reduction. Although not substantiated, it may be less harmful to have an over-strength beam than one with an area awaiting stress risers and perpetrators of cracks and fractures.

The over-strength steel beam problem was confined to only a few tests. An early hypothesis as to the cause of flange fracture was the higher strength steel with less ductility, as the failure appeared to be brittle. This conjecture was proven wrong as use of the same over-strength beam resulted in successful tests with local flange buckling failures. Therefore, the beam material strength was not the cause of the earlier flange fractures and another phenomenon caused the flange fractures.

6.5 CONNECTION PERFORMANCE

Three different failure modes resulted from cyclic load testing of the full-scale specimens, as discussed in Section 2.6. Beam flange fracture and local beam flange buckling (beam strength deterioration) were observed in the hot rolled beam section tests, and an additional failure mode of web-to-flange weld fracture was noted in testing of the built-up Grade-50 steel beam sections. Nine of the 20 connections tested failed due to a ductile failure, local beam flange buckling. This was the desired mode of failure and considered a successful connection design. All connection sizes with hot rolled steel beam sections did result in at least one ductile failure. The built-up beam connection did not reach a complete ductile failure due to inadequate web-to-flange weld strength. From observation of all testing, it is believed that with adequate weld size/strength, the built-up section could also attain a ductile failure. Eight of the 20 connections tested failed due to a sudden and catastrophic beam flange fracture. Of the hot rolled beam sections, only the W18x35 section did not have this mode of failure. However, due to other variables in these specimens, it was determined that it was not the size that affected eventual failure, but rather it was the absence of weld access holes in the W18x35 specimens. The remaining three failures were web-to-flange weld fractures, which occurred in the Grade-50 steel built-up beam specimens. From all the results, it is with a high probability that the

failure mode is not related to beam size, as fracture and buckling occurred in every size beam.

The performance of the connection was analyzed by two separate measurements, strength and ductility. Both parameters are extremely important for the proper analysis, design and selection of connection component size for seismic loading of structures. Strength of the connection is determined by the maximum load and deflection the connection obtained before failure, while ductility is measured by the amount of connection plastic rotation obtained before failure.

6.5.1 Connection Strength

The strength of a connection is determined by its load capacity before failure. In each case tested, the actual strength of the connection was slightly greater than the calculated value. This increase of strength is probably due to the strain-hardening effects of steel in the connection beam, which is of great advantage by using plastic strength capacity in connection design.

Figure 6.2 is the load-deflection history of the W24x62 beam size connection (Test RH-2). This curve is typical of connections which failed due to local beam flange buckling, and its qualitative shape is similar to test results from previous connection research. The hysteresis loops are full and display exceptional repeatability. The hysteresis loops for the W24x62 beam in Tests 5/95 through 7/95 appear to have a distinctive pinched shape, or narrowing at zero load. This effect is due to the method of data acquisition used during these three tests when the hydraulic actuator was unloaded. This shape is not the case for the general W24x62 size beam as seen in Figure 6.2 and other curves of this beam size. The cyclic loops for repeated loading of the same magnitude essentially overlay one another. This repetition represents properly designed steel members.

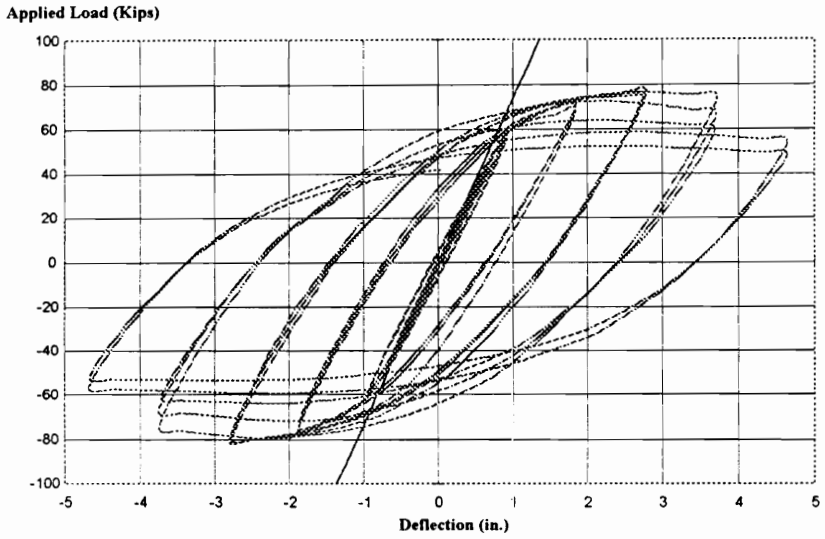

FIGURE 6.2 Typical Load-Deflection History

The area enclosed by the loops represents or defines the energy dissipated by the beam per cycle. A comparison of energy dissipation at maximum applied load showed that the W36x135 beam had 6.7 times greater energy dissipation than the W18x35 beam. Similarly, the W24x62 and W24x76 beams had 2.9 and 4.3 times more energy dissipated, respectively. The Grade-50 steel built-up section displayed 3.0 times greater energy dissipation than the W18x35 beam.

Regardless of the failure mode, the shape and size of the loops were identical for a given beam size up to the fracture failure, which demonstrates the reproducibility of the connection's performance. For beams that experienced a ductile failure, the degradation of beam strength is indicated by the reduced applied load and/or increase in deflection for the same load. For all tests, the initial elastic slope of the connection was slightly less than the calculated slope. This slope difference indicates a greater theoretical stiffness than is demonstrated by the actual connection.

6.5.2 Connection Ductility

A main consideration in the design of moment connections is the maximum available ductility in the beam's inelastic region that is developed during cyclic loading. A consistent technique to express ductility is the maximum connection rotation that occurs in the inelastic region during the inelastic loading cycles. Connection rotation is calculated by transforming the measured linear beam displacement to angular rotation. To obtain plastic rotation values, the respective beam elastic rotation is subtracted from the total connection rotation. These values are then plotted versus the moment loading on the connection. Figure 6.3 is the moment rotation representation of the W 24x62 (RH-2) connection.

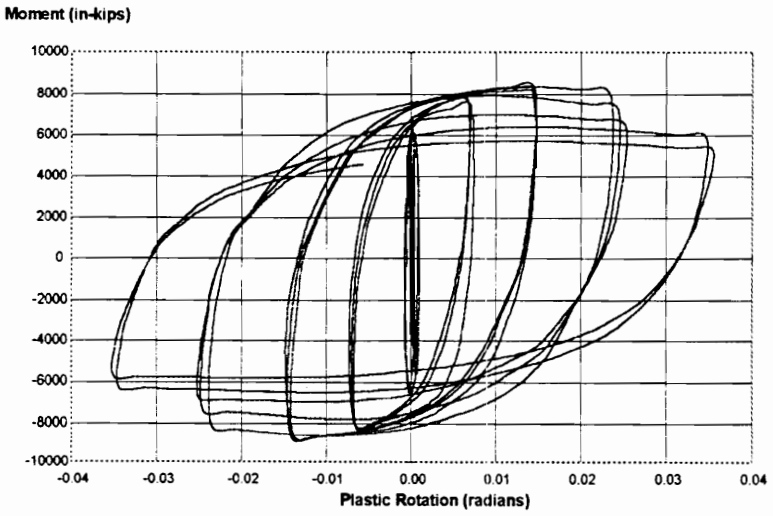

Figure 6.3 Typical Moment Rotation Curve

A research standard of sufficient ductility is that the connection exceed $\pm$ 2% ($\pm$0.02 radians) for acceptable level of performance. In all tests with a ductile failure, a value of $\pm$ 0.02 radians was obtained. Test 12/95 is slightly less than that during the negative loading, but this was due to test apparatus limitation, and if greater loading had been applied, the ductility would have exceeded $\pm$ 0.02 radians. Satisfactory ductile

performance was displayed in several tests even when flange fracture was the mode of failure. Table 6.3 lists the tests conducted and the corresponding connection performance for each test in addition to the ultimate mode of failure.

TABLE 6.3
Test Connection Performance

Test No.	Beam Section	Maximum Applied Load (kips)	Maximum Deflection (in.)	Calculated Maximum Ductility (radians)	Mode of Failure
1 / 95	18 x 35	48	3.22	0.034	Local Flange Buckling
2 / 95	18 x 35	45	3.04	0.028	Local Flange Buckling
3 / 95	18 x 35	46	2.82	0.028	Local Flange Buckling
4 / 95	18 x 35	46	2.73	0.031	Local Flange Buckling
5 / 95	24 x 62	81	3.05	0.016	Flange Fracture
6 / 95	24 x 62	83	2.78	0.014	Flange Fracture
7 / 95	24 x 62	88	4.66	0.034	Local Flange Buckling
8 / 95	24 x 76	112	3.96	0.022	Flange Fracture
9 / 95	24 x 76	110	4.80	0.036	Local Flange Buckling
10 / 95	36 x 135	219	3.35	0.013	Flange Fracture
12 / 95	36 x 135	224	4.02	0.020	Local Flange Buckling
RH - 1B	24 x 76	112	3.43	0.019	Flange Fracture
RH - 2	24 x 62	80	4.62	0.035	Local Flange Buckling
RH - 2A	24 x 62	80	4.22	0.023	Flange Fracture
RH - 3	24 x 62	80	2.70	0.014	Flange Fracture
BuS 1	Built-up	86	3.94	0.027	Weld Tear, Web to Flg
BuS 2	Built-up	94	4.84	0.026	Weld Tear, Web to Flg
BuS 1A	Built-up	90	3.92	0.016	Flange Fracture
BuS 2A	Built-up	93	4.86	0.036	Weld Tear, Web to Flg
1 / 96	24 x 62	82	4.17	0.031	Local Flange Buckling

6.6 FOUR-BOLT EXTENDED MOMENT END-PLATE CONNECTIONS

The main emphasis of investigation during this research was the four-bolt extended moment end-plate connection. This section discusses the observed differences related to the presence or the absence of the weld access holes in four-bolt extended moment end-plate connections. Table 6.4 lists the fourteen different full-scale connection tests with this configuration. Of these tests, six connections did not have weld access holes and the other eight connections did have weld access holes. Initially all test specimens were designed and welded without weld access holes, and it wasn't until specimens from a commercial fabricator were tested that the presence of the access holes became a topic of connection difference. Of the test variables discussed, it appears that for the four-bolt extended connection, the presence of weld access holes determined the failure mode of the connection. When weld access holes were present, flange fracture was most often the mode of failure. Connections without the weld access holes had a ductile failure of local beam flange buckling.

The Grade-50 steel built-up beam connections were initially intended to provide data from identical connections and their response to cyclic loading with and without weld access holes. Although their initial similar behavior was noted, the weld fractures make it impossible to derive any proper or reasonable conclusion as to the effect of the access holes. Therefore, the results of these four tests are not used for final conclusions.

6.6.1 Connections without Weld Access Holes

Two tests without access holes were conducted with a W18x35 beam section, two with a W24x62 beam section and two with a Grade-50 steel built-up beam section. All four hot rolled beam sections failed in the ductile mode of local beam flange buckling, while both built-up beam sections failed due to web-to-flange weld fracture. It is hypothesized that had the web-to-flange weld been sufficient, these two tests also would have resulted in beam flange buckling. During the test of the built-up section beam connections, the beam flanges had begun to severely buckle before the weld fracture was

noted. From testing of the four-bolt connection without weld access holes, the design appears to be sufficient to withstand seismic loading.

TABLE 6.4
Four-Bolt Extended End-Plate Tests

Test No.	Beam Section	Weld Access Holes	Cycles Before Failure	Failure Mode
1/95	W 18x35	No	19	Local Flange Buckling
4/95	W 18x35	No	20	Local Flange Buckling
5/95	W 24x62	Yes	15	Flange Fracture
8/95	W 24x76	Yes	14	Local Flange Buckling
9/95	W 24x76	Yes	21	Local Flange Buckling
RH-1B	W 24x76	Yes	16	Local Flange Buckling
RH-2	W 24x62	No	20	Local Flange Buckling
RH-2A	W 24x62	Yes	19	Local Flange Buckling
RH-3	W 24x62	Yes	15	Local Flange Buckling
BuS 1	Built-up	Yes	18	Web-to-Flange Weld
BuS 2	Built-up	No	16	Web-to-Flange Weld
BuS 1A	Built-up	Yes	19	Flange Fracture
BuS 2A	Built-up	No	20	Web-to-Flange Weld
1/96	W 24x62	No	21	Local Flange Buckling

6.6.2 Connections with Weld Access Holes

Of the eight tests performed with weld access holes, three were commercially fabricated for planned testing. The remaining five connections were tests developed to investigate the phenomenon of the weld access hole, its introduction into the connection and its possible cause of earlier beam flange fractures.

Three of the eight tests were conducted with a W24x62 beam section and all three connections failed due to beam flange fracture. Another three of the eight tests were conducted with a W24x76 beam section. Two of these connections failed due to beam flange fracture and the third by local beam flange buckling. Test 9/95 did successfully complete its cyclic testing with a resulting ductile failure of the beam. This connection had

a "thick" end-plate, 2 1/4 in., and the beam flange was also reduced by the "dog bone" method. It is difficult to discern what effect these two modifications and distinctive differences had on the connection's response.

The two remaining connections tested had a Grade-50 steel built-up beam section. Test BuS 1 was terminated due to the web-to-beam weld fracture, and Test BuS 1A failed due to beam flange fracture. The fracture in Test BuS 1A was initiated by the web-to-flange weld failure and is not similar to the other observed flange fractures. The other flange fractures all occurred in the area of the weld access holes, whereas the Test BuS 1A failure was at the weld failure some 4 inches away from the access holes.

6.7 End-Plate Connections With Shims

As discussed in Chapter II, the use of steel shims was intended to eliminate end-plate prying forces, thus reducing the bolt force and precluding eventual bolt fracture. Before full-scale end-plate connection testing with shims was attempted, four tee-stub tests were conducted to verify the shim concept. The tee-stubs were tested in a universal tensile test machine for savings of time and degree of simplicity for these preliminary tests. The major objective of the tee-stub testing was to investigate the actual concept of shims and validate the concept before extensive and expensive full-scale testing was conducted. Of equal importance in the tee-stub tests was the determination of exact location and dimensions of the shim. An early look at the effects of yielding/bending of the end-plate portion of the tee-stub as the bolts undergo tightening was also desired. Tee-stub testing was conducted with tensioned high-strength instrumented bolts. A cyclic loading of the tee-stubs was performed with varied tension load histories to closely approximate a loading sequence recommended by ATC-24. Table 6.5 provides sizes and specifications of the tee-stubs tested.

From the results of the four tee-stub tests, the theory of shimmed end-plates appeared valid. When the applied tension load on the tee-stub was below the pre-tension bolt force, the bolt forces remained almost constant (7-10% maximum variation in bolt

forces). When the loading exceeded the pre-tension bolt force, bolt and plate yielding occurred and the stiffness of the connection was lost. Intended failure of the connections occurred due to bolt fracture when tension forces, due to applied loading, exceeded the bolt strength.

During the tests, it was observed that the bolts with higher initial tension seemed to carry a greater portion of the load and generally retained higher tension throughout the test. The proper width of the shim was determined to be the thickness of the beam flange for proper transfer of forces between the beam and column, which agreed with the results of Bouwman (1981). A shim thickness of one-half inch was selected through good engineering judgment and was used for all testing.

TABLE 6.5
Tee-Stub Test Specimen Specifications

Test No.	End-Plate thickness (in.)	End-Plate dimensions (in.)	End-Plate type	Bolt Diameter (in.)
1	1/2	6 x 8	Unstiffened	1/2
2	1/2	6 x 8	Stiffened	5/8
3	1/2	6 x 8	Stiffened	5/8
4	3/4	6 x 8	Stiffened	5/8

From the tee-stub tests, it was concluded that the use of shimmed end-plates appeared to be a valid design alternative. The tests provided insight and techniques that were used in later testing as well as answering the major concerns addressed above. It was predicted that the shimmed connections would remain rigid and not fail if designed for a greater moment than the beam plastic strength, as discussed in Chapter II. The design would force the beam to be the weak link in the structure and cause a plastic hinge to form before failure of the end-plate connection.

The shimmed connection design, stiffened and unstiffened, was suspended after four full-scale tests of the concept. Although the concept was extremely promising in theory and during the tee-stub tests, the full scale connection displayed several

disadvantages, making the concept of this design not desirable nor feasible as a practical or economical connection for general use. The main disadvantage of the shimmed connection was its loss of stiffness due to end-plate deformation and shim compression. Maximum separation of the end-plate and column flange varied from 0.133 to 0.15 in. during full-scale testing. This is the total separation and comprises both end-plate deformation and shim compression. With a known shim compression of 0.012 to 0.025 in., the end-plate separation due to deformation was approximately 1/8 in. Although connection strength is not affected by these yielding mechanisms, the degree to which the connection stiffness deteriorates is not acceptable.

A major fabrication and erection difficulty was noted during testing. The initial difficulty was the exact placement and retention of the shim at the proper location during erection. This problem was overcome by spot welding the shim at its proper location on the end-plate prior to erection. The spot welding of the shim also prevented the shim's movement and loss during high seismic activity.

Another drawback of the shims as observed during full-scale testing is the stress level imparted to the column flange and end-plate when in compression. In addition to physical compression of the shim during testing, local yielding of the column flange and end-plate was noted. After disassembly of each shim connection, a visible shim "impression" was observed in the column flange and end-plate caused by the high compressive stresses during the test. Although this "impression" will not cause failure of the connection, it does reduce the stiffness of the connection.

Review of the test results and connection variables indicate that the use of shims did not affect the eventual failure mode of the connection. Of the four tests with shims, three failed due to local flange buckling and the other due to flange fracture. The flange fracture failure was caused by the presence of weld access holes (see discussion of weld access holes, Section 6.6.2).

An advantage of the shimmed connection, other than simplicity of design, is that of all connections tested, the bolts in the shimmed connection displayed the smallest increase

in tension from their tightened tension force. The bolt forces did vary greatly during testing and were often unloaded during bolt group compression, but the overall increase from the initial tightening force never exceeded 25%.

6.8 Stiffened, Extended End-Plate Connection

Three different size connections with stiffened extended end-plates were tested. Two of the connections, one with a W18x35 beam section and the other with a W 24x62 beam section, were tested with shims. The third test, with a W36x135 beam section, did not incorporate shims. The W18x35 beam size connection did not have weld access holes while the W24x62 and W36x135 beam size connections did have access holes.

All three connections displayed identical ductile failures, local flange buckling of the beam accompanied by degradation of beam strength. Severe yielding was noted in the stiffeners as evidenced by the flaking of the white-wash. Each connection experienced 20-21 complete loading cycles before test termination.

Testing of the same design connection without stiffeners was conducted on the W24x62 and W36x135 beam section. In both cases the flange fractured in the area of the weld access holes. The W18x35 beam section connection was not tested with weld access holes.

The results of these tests and comparison of the results to tests without stiffeners lends more credibility to the fact that the weld access holes are the cause of flange fracture in the test specimens. The added information gained in the stiffened, extended connections is that the stiffener appears to carry a critical portion of the flange loading so that flange fracture is avoided. Due to the small test sample, more tests should be conducted to verify these preliminary findings.

6.9 FOUR-BOLT WIDE END-PLATE CONNECTION

Two tests with four-bolt wide extended end-plate connections were conducted. The main purpose of the limited tests performed with a W36x135 beam section was to investigate the application of cyclic loading with larger sized connections and attempt to see if design procedures for the four-bolt connection could be expanded to four-bolt wide connections.

As with the other end-plate connection configurations, the presence of weld access holes seems to be the design variable that ultimately determines the mode of failure. The tests without stiffeners indicate that even in large beam size connections, the weld access holes can cause flange fracture and the tests with stiffeners indicate that their use negates the effects of the access holes and allows the connection to develop its full capacity and fail in a ductile manner.

The two tests are by no means conclusive but do provide positive reinforcement to the use of end-plate connections of larger size beams, and their response is similar to small and moderate size beam connections.

An additional item noted was that the bolt tension in the four-bolt wide connection appears to be affected more by location relative to the web line than inner or outer bolt based on the flange.

6.10 SUMMATION

This section will provide a short, cumulative summary of all the results discussed. If detailed information is desired, the specific section referenced should be consulted.

Bolt design was adequate, as no bolt failures were experienced under normal connection behavior. Although test values were not directly compared to the design tension values, the bolt performance is considered satisfactory. No difference in bolt behavior between the A325 or A490 bolts was noted during tests.

An industry wide problem of actual steel strength well above nominal strength has directly affected the design and response of connections under cyclic loading. When the

beam strength exceeds the design value, the mode of failure changes from the designed ductile failure to bolt fracture for these connections.

The design and selection of end-plate thickness utilized in this research is sufficient to prevent failure of the end-plate. The design method does result in a thinner end-plate than current AISC methods, which should be acceptable to steel designers and fabricators. Although the thinner plate does deform more under loading, its design is adequate to withstand cyclic loading. A thick end-plate experiences less deformation and provides a more even distribution of flange force to the bolts.

The true measure of a connection design is its performance during cyclic loading. All connections displayed excellent strength and ductility when flange fracture failures were eliminated. The connections were slightly stronger than predicted and their ductility was well above the 2% rotation desired.

Of the connection configurations tested, only the connection with shims was disappointing and its overall performance less than desired. The four-bolt extended end-plate connection demonstrated great promise and was very successful. Its design and testing indicates that an acceptable alternative to flange welded connection is available. The four-bolt wide connection also provided positive indications of promise with more research and fine tuning.

The single event of apparent importance and of a critical nature was the presence of weld access holes in the connection's beam section. Either not noted or documented prior to this research, the weld access hole has questionable need and, more importantly, surprising results when present in moment end-plate connections. There has been much discussion amongst designers and fabricators as to whether weld access holes are required under current AWS design codes to meet inspection criteria of beam-to-endplate welds. It should be noted, with the exception of one test connection, that all four-bolt extended moment end-plate connections tested with weld access holes failed due to flange fracture.

The need for weld access holes for welding purposes is not sound, because shop welding permits rotation of the connection to conduct down welding on both flanges.

Even with a less than perfect weld, as was demonstrated by TEST 1/96, the connection without access holes has sufficient strength. In this specially prepared specimen, a 1/8 in. x 1/8 in. x 1/4 in. carbon block was placed at the flange-web juncture before welding. This caused a large inclusion at the critical point of the weld. The test results indicate that even with this size inclusion, the connection weld was adequate to prevent weld failure. No weld access holes were present. Additionally, the metal building industry presently does not use weld access holes and has perfected inspection techniques that satisfactorily determine the quality of end-plate welds. To provide further information for weld access holes, the simple finite element analysis conducted of identical beam models with and without access holes indicated lower flange strain when no weld access holes were present.

CHAPTER VII

SUMMARY, CONCLUSIONS AND RECOMMENDATIONS

7.1 SUMMARY

This final chapter provides conclusions of the research and recommendations for further research required for the extended end-plate moment connections. The conclusions are based upon theory, test design and results discussed in the preceding chapters. The additional research outlined is needed to answer or clarify the questions developed as a result of this research. This further research is needed to confirm several initial indications uncovered and to develop and validate procedures that will expand the acceptance and use of larger moment end-plate connections.

7.2 CONCLUSIONS

The final conclusions relate to the three primary areas of this research: design, test and analysis of results. The conclusions address the key objectives of the research for moment end-plate connections.

7.2.1 Four-Bolt Extended End-Plate Connections

The four-bolt extended end-plate connection design procedures that were developed and tested are satisfactory to develop the strength and ductility of the connection due to cyclic loading. The tests performed with 1 in. and 1 1/4 in. diameter bolts demonstrated successfully the sufficiency of the design and its use as an alternative for flange welded connections of equal size. Although only two bolt diameters were used during tests, no performance difference is expected for intermediate or smaller diameter

bolts. The beam size limitation based on testing is the W24x76 beam with 1 1/4 in. diameter A490 bolts. The selection of larger beams and/or bolts should be investigated and documented before actual use of larger beams and bolts is implemented or attempted.

7.2.2 Weld Access Holes

The results of these tests demonstrate that weld access holes are not needed for the four-bolt extended end-plate connection. In fact, it was demonstrated that the presence of weld access holes causes unacceptable behavior of the connection. The performance of the connections tested convincingly demonstrates that a sufficient quality weld can be obtained without the use of access holes and beam fracture failure can be avoided. The quality can also be proven if appropriate non-destructive testing of beam-to-end-plate welds is conducted to detect welding flaws. Weld access holes affect the beam response and failure mode to cyclic loading regardless of beam size.

7.2.3 Other Extended End-Plate Configurations

The use of shims in moment end-plate connections does not provide an economical or practical solution for the elimination of bolt prying forces as initially conceived. As determined during tests, the connections will survive cyclic loading, but the deformation and loss of bolt tension forces may not be acceptable in most applications. Additionally, as tests demonstrated, a thinner and more efficient moment end-plate can be used successfully to avoid bolt fracture and withstand the effects of cyclic loading.

End-plate stiffeners do provide additional strength to a connection and cause the end-plate to respond as if it were thicker than it is. The stiffener also negates the negative effects of weld access holes and allows the connection to develop its full capability under cyclic loading.

The initial indications are very promising that a satisfactory 8-bolt end-plate connection is conceivable for use with beam sections larger than W24 to withstand the

effects of cyclic loading. Although only limited tests were conducted for the four-bolt wide connection, the results provide positive indications to its satisfactory performance. With additional research and analysis of results, the 8-bolt connection should prove to be a successful alternative to flange weld beam-to-column connections.

7.2.4 BUILT-UP MEMBERS

Four-bolt extended moment end-plate connections with Grade-50 steel built-up beam sections can withstand the effects of cyclic loading, but a redesign of the web-to-flange welds is needed. The ductile behavior of the beam flanges prior to the weld failures provides proof that the connection is capable of sustaining the effects of seismic activity. Additional weld size for the web-to-flange welding should allow the connection to develop its full ductile strength.

7.3 RECOMMENDATIONS

The four-bolt extended moment end-plate connection should be considered adequate for use in construction of steel buildings in areas of any seismic activity. This design should not incorporate the use of weld access holes.

The use of weld access holes should not be included in the design and fabrication of extended moment end-plate connections that are used in a high seismic geographic area.

Built-up beam sections used in extended moment end-plate connections should be welded on both sides of the web-to-flange juncture. The weld strength of this joint should be redesigned to provide greater strength to withstand the forces caused by seismic activity.

Additional research is required for the verification of design procedures for the four-bolt wide extended moment end-plate connections. Further testing of the connection design under cyclic loading is then required for use in seismic areas.

REFERENCES

Abel, M.S.M., (1993) "Four-Bolt Extended Unstiffened Moment End-Plate Connections." Master of Science Thesis, Department of Civil Engineering, Virginia Polytechnic Institute and State University, Blacksburg, Virginia.

Ahuja, V. (1982) "Analysis of Stiffened End-Plate Connections Using Finite Element Method." Master of Science Thesis, School of Civil Engineering and Environmental Science, University of Oklahoma, Norman, Oklahoma.

"AISC Technical Bulletin No 2: Interim Observation & Recommendations on Steel Moment Resisting Frames." (1994) *Modern Steel Construction*, AISC Vol. 34 (12), 22-31.

Agerskov, H. (1976) "High Strength Bolted Connections Subject to Prying." *Journal of the Structural Division*, ASCE, Vol. 102, ST1, 161-175.

Agerskov, H. (1977) "Analysis of Bolted Connections Subject to Prying." *Journal of the Structural Division*, ASCE, Vol. 103 ST11, 2145-2163.

Bahaari, M.R. and Sherbourne, A.N. (1993), "Modeling of Extended End-plate Bolted Connections." *Proceedings of the National Steel Structures Congress*, AISC, 731-736.

Ballio, G., et al. (1987) "Cyclic Behavior of Steel Beam-to-Column Joints, Experimental Research." *Construzioni Metalliche*, 2.

Biswas, P. (1994) "Development of a Finite Element Computer Program to Predict Cyclic Hysteretic Behavior and Failure of End-Plate Connections." Master of Science Thesis, School of Civil Engineering and Environmental Science, University of Oklahoma, Norman, Oklahoma.

Blodgett, O. W. (1992) "Structural Details To Increase Ductility of Connections." *Engineering Journal*, AISC, Vol. 29 No. 4, 132-136.

Bouwman, L.P. (1981) "The Structural Design of Bolted Connections Dynamically Loaded in Tension", *Joints in Structural Steelwork*, eds. J.H. Howlett, W.M. Jenkins, and R. Stainsky, John Wiley & Sons, New York, 1.3-1.16.

Bouwman, L.P., (1982) "Bolted Connections Loaded in Tension", *Journal of the Structural Division*, ASCE, Vol. 108 ST9, 2117-2129.

Bursi, O.S. and Leonelli, L (1994) "A Finite Element Model for the Rotational Behavior of End Plate Steel Connections", *SSRC Proceedings 1994 Annual Task Group Technical Session*, Leigh University, 162-175.

Chasten, C.P., Fleischman, R.B., Driscoll, G.C., and Lu, L. (1989) "Top-and-Seat-Angle Connections and End-Plate Connections: Behavior and Strength Under Monotonic and Cyclic Loading", *Proceedings, National Engineering Conference*, AISC, 6-1-6-32.

Chasten, C.P., Lu, L. and Driscoll, G.C. (1992) "Prying and Shear in End-Plate Connection Design." *Journal of Structural Engineering*, Vol. 118, No. 5, 1295-1311.

Douty, R.T. and McGuire, S. (1965) "High Strength Bolted Moment Connections." *Journal of the Structural Division*, ASCE, Vol. 91 ST2, 101-126.

Engelhardt, M.D., Sabol, T.A., Aboutaha, R.S. and Frank, K.H. (1995) "Testing Connections." *Modern Steel Construction*, AISC, Vol. 35 (5), 36-44.

Ferguson, P.M., *Reinforced Concrete Fundamentals*, Second Edition, John Wiley and Sons, New York, 1965.

Ghassemieh, M. (1983) "Inelastic Finite Element Analysis of Stiffened End-Plate Moment Connections." Master of Science Thesis, School of Civil Engineering and Environmental Science, University of Oklahoma, Norman, Oklahoma.

Ghobarah, A., Osman, A. and Korol, R.M. (1990) "Behavior of Extended End-Plate Connections under Cyclic Loading." *Engineering Structures.*, Vol. 12(1), 15-27.

Ghobarah, A., Korol, R.M. and Osman, A. (1992) "Cyclic Behavior of Extended End-Plate Joints." *Journal of Structural Engineering*, Vol. 118(5), 1333-1353.

Granstrom, A. (1980) "Bolted End-Plate Connections." *Stalbyggnads Institute SBI Report 86.3*, September, 5-12.

"Guidelines for Cyclic Seismic Testing of Components of Steel Structures (ATC-24)" (1992) Applied Technology Council, Redwood City, CA.

Graham, J. (1993) "Observations From the Behaviour of Bolted Beam to Unstiffened Column Rigid Connections." *The Structural Engineer*, Vol. 71 No.6, 99-105.

Griffiths, J.D. (1984) "End-Plate Moment Connections - Their Use and Misuse." AISC *Engineering Journal*, First Qtr., 21, 32-34.

Grundy, P., Thomas, I. and Bennetts, I. (1980) "Beam-To-Column Moment Connections." *Journal of the Structural Division*, ASCE, Vol 106 ST1, 313-330.

Hendrick, R.A. and Murray, T.M. (1984) "Column Web Compression Strength at End-Plate Connections," AISC *Engineering Journal*, 21 (3), 161-169.

Iwankiw, N. (1995) "Some Ultimate Strength Considerations for Reduced Beam Section." Draft Letter.

Kato, B. and McGuire, W.F.,(1973) "Analysis of T-Stub Flange-to-Column Connections", *Journal of the Structural Division*, ASCE, Vol. 99 ST5, 865-888.

Kennedy, N.A., Vinnakota, S. and Sherbourne, A.N. (1981) "The Split-Tee Analogy in Bolted Splices and Beam-Column Connections", *Proceedings of the International Conference on Joints in Structural Steelwork*, 2.138-2.157.

Korol, R.M., Ghobarah, A. and Osman, A. (1991) "Extended End-Plate Connections Under Cyclic Loading: Behavior and Design." *Journal of Constructional Steel Research.*, 16(4), 253-280.

Krishnamurthy, N. (1978) "A Fresh Look at Bolted End-Plate Behavior and Design", *Engineering Journal*, AISC, Vol. 15(2), 39-49.

Krishnamurthy, N. and Graddy, Jr., D.E. (1976) "Correlation Between 2- and 3-Dimensional Finite Element Analysis of Steel Bolted End-Plate Connections." *Computers and Structures*, Vol. 6 No. 415, 381-389.

Krishnamurthy, N., Huang, H., Jeffrey, P. and Avery, L. (1979) "Analytical M-Theta Curves for End-Plate Connections." *Journal of the Structural Division*, ASCE, Vol. 105 ST1, 133-145.

Kukreti, A.R., Ghassemieh, M. and Murray, T.M. (1990) "Behavior and Design of Large-Capacity Moment End-Plates." *Journal of Structural Engineering.*, Vol. 116 (3), 809-828.

Kukreti, A.R., Murray, T.M. and Abolmaali, A. (1987). "End-Plate Connection Moment-Rotation Relationship." *Journal of Constructional Steel Research.*, Vol. 8, 137-157.

Mander, J.B., Pekcan, G. and Chen, S.S. (1995) "Low-Cycle Variable Amplitude Fatigue Modeling of Top-and-Seat Angle Connections." *Engineering Journal*, Vol. 32 (2), 54-62.

Mann, A.P. and Morris, L.J. (1979) "Limit Design of Extended End-Plate Connections." *Journal of the Structural Division*, ASCE, Vol. 105 ST3, 511-526.

"Manual of Steel Construction." (1970), Seventh Edition, American Institute of Steel Construction, Chicago, IL.

"Manual of Steel Construction." (1989) (Allowable Stress Design), Ninth Edition, American Institute of Steel Construction, Chicago, IL.

"Manual of Steel Construction." (1986) (Load & Resistance Factor Design), First Edition, American Institute of Steel Construction, Chicago, IL.

"Manual of Steel Construction." (1994) (Load & Resistance Factor Design), Second Edition, American Institute of Steel Construction, Chicago, IL.

Miller, J.R. (1994) "Performance of Pre-Engineered Buildings in the Northridge Earthquake." Report on Northridge Earthquake, J.R. Miller & Associates, Inc., Brea, California.

Morrison, S.J., Astaneh-Asl, A., Murray, T.M. "Analytical and Experimental Investigation of the Extended Stiffened Moment End-Plate Connection with Four Bolts at the Beam Tension Flange." Report No. FSEL/MBMA 85-05, Fears Structural Engineering Laboratory, University of Oklahoma, Dec. 1985.

Murray, T.M. (1988). "Recent Developments for the Design of Moment End-Plate Connections." *Journal of Constructional Steel Research.*, Vol. 10, 133-162.

Murray, T. M., "Extended End-Plate Moment Connections," (1990), *Steel Design Guide Series, 4*, AISC, Chicago, IL.

Murray, T.M. and Kukreti, A. (1988) "Design of 8-bolt Stiffened Moment End-Plates." *Engineering Journal*, AISC, Vol. 25, No. 2, 2nd Qtr, 45-52.

Murray, T.M. and Meng, R.L. (1995) " Seismic Loading of Moment End-Plate Connections: Some Preliminary Results." Third International Workshop on Connections in Steel Structures, Trento, Italy, May 1995.

Nair, R., Birkemoe, P. and Munse, W. (1974) "High Strength Bolts Subject to Tension and Prying." *Journal of the Structural Division*, ASCE, Vol. 100 ST2, 351-372.

Packer, J. and Morris, L. (1977) "A Limit State Design Method for the Tension Region of Bolted Beam-Column Connections." *The Structural Engineer*, Vol. 55 No. 10,446-458.

Piraprez, E. (1993) "The Effect of Prying Stress Ranges on Fatigue Behaviour of Bolted Connections: The State-of-the-Art." *Journal of Constructional Steel Research*, Vol. 27, 55-68.

Popov, E.P. and Bertero, V.V. (1973) "Cyclic Loading of Steel Beams and Connections." *Journal of the Structural Division*, ASCE, Vol. 99 ST6, 1189-1204.

Popov, E. and Tsai, K.C. (1989) "Performance of Large Seismic Steel Moment Connections Under Cyclic Loads." *Engineering Journal*, 12(2), 51-60.

Salmon, C.G. and Johnson, J.E. (1980) *Steel Structures, Design and Behavior*, 2nd Edition, Harper & Row, New York.

Sanpaolesi, L., et al. (1981) "Experimental Investigation on Strength and Ductility of Structural Connections." *Monographia N. 5, Pubblicazione Italsider*, Nuova Italsider, Genove (in Italian).

Tsai, K.C. and Popov, E. (1988) "Steel Beam-Column Joints in Seismic Moment Resisting Frames." University of California, Berkeley.

Tsai, K.C. and Popov, E. (1990) "Cyclic Behavior of End-Plate Moment Connection." *Journal of Structural Engineering*., Vol. 116 (11), 2917-2930.

Tsai, K.C. and Popov, E (1993) "End-Plate Moment Connections for Cyclic Loads", *Proceedings of the National Steel Structures Congress*, AISC, 569-578.

APPENDIX A

NOMENCLATURE

NOMENCLATURE

ABAQUS - a finite element code

AISC - American Institute of Steel Construction

ANSYS - a finite element code

ASD - Allowable Stress Design

ATC - Applied Technology Council

A_b - bolt cross-sectional area

A_g - end-plate gross cross-sectional area

B - bolt force

B_I - inner bolt force

B_E - outer bolt force

B_{max} - maximum bolt force of the inner and outer bolts

$BF_{plastic}$ - bolt force in plastic region

B_t - specified bolt tension force, (AISC specification)

D_{min} - minimum weld thickness, in sixteenths

E - Young's modulus (modulus of elasticity)

F - force

F_a - bolt material allowable stress

F_B - total bolt tension force

F_b - bolt tension force

F_c - T-section contact force

F_f - flange force

F_{fy} - beam flange yield stress

F_{limit} - possible flange force per bolt at the thin plate limit

F_n - bolt nominal shear rupture strength

F_{py} - end-plate material yield stress

FR - fully restrained

F_t - bolt material tensile strength

- tension force

F_y - material (beam) yield stress

F_y^{act} - actual yield stress of beam

F_{yb} - bolt material yield stress

F_{yf} - flange yield stress

F_{yw} - web yield stress

F' - flange force per bolt at the thin plate limit

F_1 - flange force at the thick plate limit

F_{11} - flange force at the thin plate limit

I - beam moment of inertia

I_x - end-plate moment of inertia

I_X - composite end-plate and stiffener moment of inertia

K_e - connection elastic stiffness

L - clear beam span between columns

L' - reduced span between interior plastic hinges

L_e - edge distance

L_p - length of end-plate

LRFD - Load and Resistance Factor Design

M - moment

M_b - bolt moment capacity

M_{bolt} - bolt failure moment

M_c - moment delivered to supporting column face

M_{con} - moment capacity of a bolted connection

M_{crit} - critical moment

M_F - fixed end moment; yield moment

M_p - predicted failure moment

- plastic moment capacity of the beam

M_{plate} - plate failure moment

M_u - end-plate ultimate moment capacity

M_y^{act} - actual yield moment capacity at beam end

M_{yb} - bolt moment capacity

M_w - working moment

M_1 - plastic moment at first hinge line to form

M_2 - plastic moment at second hinge line to form

N - length of bearing

P - load applied to test specimen by hydraulic ram

PR - partially restrained

P_t - bolt material ultimate tensile load capacity

P_y - bolt material yield load

Q - prying force on bolt

- testing load force

Q_{max} - maximum prying force on bolt

Q_y - estimated load value to cause beam yielding

R - bolt relationship

R_n - nominal strength

R_u - ultimate reaction force

S - beam elastic section modulus

T_b - tension force in a bolt

V_p - beam shear due to reverse curvature bending that results in m_p^{act} limit state

W_e - external virtual work

W_i - internal virtual work

Z - beam plastic section modulus

Z_f - plastic section modulus of the beam flanges

Z_w - plastic section modulus of the beam web

Z_x - plastic section modulus about the x-axis

a - distance from bolt centerline to prying force for an end-plate

b - distance from concentrated load to support for test specimen

b_f - beam flange width

b_p - end-plate width

d - beam depth

d_b - bolt diameter

e - offset of plastic hinge from beam end

g - end-plate bolt gage distance

h - beam depth

k - distance from outer face of flange to web toe of fillet

$m_{elastic}$ - slope of load versus strain in elastic region for bolt material

m_p - plastic moment capacity of plate per unit length

m_p^{act} - actual plastic moment capacity at minimum reduced beam section

n - number of bolts

p_{ext} - end-plate extension outside beam flange

p_f - distance from bolt centerline to near face of beam flange

p_t - distance from bolt centerline to far face of beam flange

r - reduced flange width coefficient

rb_f - reduced flange width

s - distance from bolt centerline to outermost yield-line

t_f - beam flange thickness

t_{fb} - beam flange thickness

t_{fc} - column flange thickness

t_p - end-plate thickness

t_s - stiffener thickness

t_w - beam web thickness

t_{wc} - column web thickness

t_1 - plate thickness at thick plate limit

t_{11} - plate thickness at thin plate limit

w' - end-plate width per bolt less the bolt hole diameter (at bolt line)

x - distance from zero

z - reduced plastic section modulus of the beam

z_f - plastic section modulus of the reduced beam flanges

α - outer end-plate factor

β - inner end-plate factor

- material strain hardening factor

γ - α or β

δ - beam deformation / deflection

δ^* - average deflection of loading point at Q

δy - deflection of beam load point at yield

$\varepsilon_{plastic}$ - bolt material strain in plastic region

ε_y - bolt material yield strain

θ - virtual rotation of end-plate

θ_s - simple span end rotation for any loading

π - mathematical pi

σ - normal stress

σ_y - normal yield stress

τ - shear stress

τ_{cr} - critical shear stress

ϕ - resistance factor

APPENDIX B

DESIGN EXAMPLES

DESIGN EXAMPLE B-1

Four-Bolt Extended Moment End-Plate Connection

Design Parameters:

Beam Section	W 24 x 62, A-36
Beam Material Yield Stress	45 ksi
Column Section	W 14 x 257, A-36
Column Material Yield Stress	45 ksi
End-Plate Material Yield Stress	42 ksi

Beam Properties

W 24 x 62, A-36 beam section properties.

$d =$	23.74 in.	$t_w =$	0.43 in.	$t_f =$	0.59 in.
$Z_x =$	153 in^3	$b_f =$	7.04 in.	$F_y =$	45 ksi*

* Beam material yield stress of 45 ksi is used in calculations due to recommendations of numerous structural articles on new strengths of hot-rolled wide flange sections.

Type and Size of Bolts

Step 1: Calculate the plastic moment capacity of the beam using Equation 3.1.

$$M_p = F_y * Z_x$$

$$M_p = 45 \text{ ksi} * 153 \text{ in}^3 = \underline{6{,}885 \text{ in-kips}}$$

Step 2: Calculate the required moment capacity of the connection using Equation 3.2.

$$M_c = 1.10 \ M_p$$

$$M_c = 1.10 * 6{,}885 \text{ in-kips} = \underline{7{,}574 \text{ in-kips}}$$

Step 3: Calculate the flange force for the required connection moment capacity, M_c.

$$F_f = M_c / (d - t_f)$$

$$F_f = 7{,}574 \text{ in-kips} / (23.74 \text{ in.} - .59 \text{ in}) = \underline{327.1 \text{ kips}}$$

Step 4: Divide the flange force by the number of tension side bolts, 4 for this design.

$T_b = F_f / 4$

$T_b =$ 327.1 kips / 4 = 81.8 kips

Step 5: Select a bolt type (A-325 or A-490) and diameter to be sufficient for each bolt force from Table J3.2, AISC Specification (Load 993).

A-325 minimum diameter bolt is 1 1/4 in. at 82.8 kips
A-490 minimum diameter bolt is 1 1/8 in. at 84.2 kips

Select A-325 1 1/4 in. diameter bolt due to lower unused strength and availability

Step 6: Calculate the actual moment capacity of the connection using selected type and size bolts.

$M_{con} = 4\ \phi T_n\ (d - t_f) \geq M_c$

$M_{con} = 4 * 82.8$ kips (23.74 in. - 0.59 in.) = 7667.3 in-kips > M_c = 7,574 in-kips (Check)

End-Plate Thickness

Step 1: Establish values to define end-plate geometry.

$b_p =$ 8 in. (column section has a k_1 value of 15/16 in.; from Table 8-4 (AISC, Manual of Steel Construction), wrench clearance is 1 1/4 in. from fillet; from Table J3.4 (AISC, Specification), minimum edge distance for 1 1/4 in. diameter bolt is 1 5/8 in. Therefore, sum of spacing is 7 5/8 in.; round up to 8 in..)

$g =$ 4.75 in. (based on 8 in. end-plate width, subtract minimum edge distance from each side; 8 in. - 2 (1.625 in) = 4.75 in.)

$p_f =$ 1.75 in. (bolt diameter plus 1/2 inch)

$F_{yp} =$ 42 ksi (assumed actual yield stress for hot-rolled steel plate material)

Step 2: Calculate distance from inner bolt to the outer yield-line, Equation 2.5.

$$s = \sqrt{b_p g} / 2$$

$$s = \sqrt{8in x 4.75in}/2 = \underline{3.082\ in.}$$

Step 3: Calculate required end-plate thickness using Equation 2.4 with $M_u = M_{con}$.

$$t_p = \left[\frac{M_u / F_{py}}{\left(\frac{b_p}{2}\left(\frac{1}{p_f} + \frac{1}{s} \right) + (p_f + s)\left(\frac{2}{g} \right) \right)(h - p_t) + \frac{b_p}{2}\left(\frac{h}{p_f} + \frac{1}{2} \right)} \right]^{1/2}$$

$$t_p = \left[\frac{7{,}574in\text{-}kips / 42ksi}{\left(\frac{8}{2}\left(\frac{1}{1.75} + \frac{1}{3.082} \right) + (1.75 + 3.082)\left(\frac{2}{4.75} \right) \right)(23.74 - 2.34) + \frac{8}{2}\left(\frac{23.74}{1.75} + \frac{1}{2} \right)} \right]^{1/2}$$

$$tp = \underline{1.02\ in.}\ ,\ \underline{\text{round off to 1 in. plate}}$$

Step 4: Calculate actual moment capacity of end-plate with selected thickness.

$$M_{plate} = F_{py} t_p^2 \left[\left(\frac{b_p}{2}\left(\frac{1}{p_f} + \frac{1}{s} \right) + (p_f + s)\left(\frac{2}{g} \right) \right)(h - p_t) + \frac{b_p}{2}\left(\frac{1}{2} + \frac{h}{p_f} \right) \right]$$

$$M_{plate} = 42 x 1^2 \left[\left(\frac{8}{2}\left(\frac{1}{1.75} + \frac{1}{3.082} \right) + (1.75 + 3.082)\left(\frac{2}{4.75} \right) \right)(23.74 - 2.34) + \frac{8}{2}\left(\frac{1}{2} + \frac{23.74}{1.75} \right) \right]$$

$$M_{plate} = \underline{7{,}412.6\ in\text{-}kips}$$

Step 5: Determine behavior category of selected end-plate.

$$t_1 = \sqrt{2.11 p_f t_f \frac{b_f}{b_p} \frac{F_{fy}}{F_{py}}}$$

$$t_1 = \sqrt{2.11 x 1.75 x 0.59 \frac{7}{8} \frac{45}{42}} = \underline{1.43\ in.}\ \text{(thick plate limit)}$$

$$t_{11} = \sqrt{\frac{\left(b_f t_f F_{fy} p_f - \frac{\pi}{8} d_b^3 F_{yb}\right)}{F_{yp}\left(0.425 b_p + 0.80 w'\right)}}$$

$$t_{11} = \sqrt{\frac{\left(7x0.59x45x1.75 - \frac{\pi}{8} x1.25^3 x90\right)}{42\left(0.425x\frac{8}{2} + 0.80x7.6875\right)}} \quad = \underline{1.05 \text{ in.}} \quad \text{(thin plate limit)}$$

Since $t_p < t_{11}$; end-plate behavior is thin. NOTE: The exact values for thick and thin plate behavior are 1.43 in. and 1.00 in., respectively, using Kennedy *et al.* (1981) exact value equations.

Step 6: Calculate Inner and Outer Bolt Forces.

Calculate values for Thin plate behavior,

$$a = 3.682 \left(t_p / d_b\right)^3 - 0.085 \; ; \qquad [a \leq (p_{ext} - p_f) \text{ for } B_E]$$

$$a = 3.682 \text{ x } \left(1.0 / 1.25\right)^3 - 0.085 = \underline{3.082 \text{ in.}}$$

Since $a > (p_{ext} - p_f) = 1.625$; "a" for B_E is; $a = (p_{ext} - p_f) = 1.625$

$$w' = \frac{b_p}{2} - d_b - \frac{1}{16} = \frac{8}{2} - 1.25 - \frac{1}{16} = \underline{2.6875 \text{ in.}}$$

$$F' = F_{11}/2 = \frac{t_p^2 F_{py}\left[0.85\left(b_f / 2\right) + 0.80 w'\right] + \left[\left(\pi d_b^3 F_{yb}\right)/8\right]}{4 p_f}$$

$$F' = \frac{1^2 x42\left[0.85(7/2) + 0.80x2.6875\right] + \left[\left(\pi x1.25^3 x90\right)/8\right]}{4x1.75} = \underline{43.16 \text{ kips}}$$

$$Q_{max} = \frac{w' t_p^2}{4a}\sqrt{F_{py}^2 - 3\left(F'/w' t_p\right)^2}$$

$$Q_{max} = \frac{2.6875x1^2}{4x3.082}\sqrt{42^2 - 3(43.16/2.6875x1)^2} = \underline{11.74} \text{ kips. for the inner bolt}$$

$$Q_{max} = \frac{2.6875x1^2}{4x1.625}\sqrt{42^2 - 3(43.16/2.6875x1)^2} = \underline{13.01} \text{ kips. for the outer bolt}$$

Therefore;

$B_I = \beta F_f / 2 + Q_{max} = F_f / 4 + Q_{max} = 327.1 \text{ kips} / 4 + 11.74 \text{ kips} = \underline{94.6} \text{ kips}$

$B_E = \alpha F_f / 2 + Q_{max} = F_f / 4 + Q_{max} = 327.1 \text{ kips} / 4 + 13.01 \text{ kips} = \underline{95.9} \text{ kips}$

Step 7: Determine if selected bolt size and type are sufficient for loading.

$B_I = 94.6 \text{ kips} < \frac{4}{3} T_b = 110.4 \text{ kips}$; and $B_E = 95.9 \text{ kips} < \frac{4}{3} T_b = 110.4 \text{ kips}$

Since, B_I and B_E are less than $\frac{4}{3} T_b$, larger sized bolts are not required. (Check)

Step 8: Determine Length of the End-Plate, Equation 3.13.

$L_p = h + 2 p_{ext}$

$L_p = 23.74 \text{ in.} + 2 (3.375 \text{ in.}) = \underline{30.49 \text{ in.}}$ round off to $\underline{30.50 \text{ in.}}$

Therefore; Plate 1 x 8 x 2 - 6 1/2 , A-36

Step 9: Check Bolt Shear.

$\phi R_n = \phi F_n A_b n > M_{con}/\text{arm}$; $\phi = 0.75$

$\phi R_n = 0.75 \text{ x } (60 \text{ ksi}) \text{ x } 1.2272 \text{ in.}^2 \text{ x } 8 = 441.8 \text{ kips}$

$\phi R_n = 441.8 \text{ kips} > 7667.3 \text{ in-kips} / 79 \text{ in.} = 97.1 \text{ kips}$ (Check)

Step 10: Check material bearing strength (The end-plate side of the connection is generally more critical than the column side due to thickness.)

Check that for the end-plate $L_e \geq 1.5d$ and $s \geq 3d$.

Le = 1.625 in. /> 1.5 (1.25 in.) No Good; s = 4.09 in. > 3 (1.25 in.) check

Therefore; $\phi R_n = \phi L_e t_p F_u \leq \phi 2.4 d_b t_p F_u$ for the exterior bolt and,

$\phi L_e t_p F_u = 0.75 \times 1.625$ in x 1 in. x 58 ksi = 70.7 kips

$\phi 2.4 d_b t_p F_u = .75 \times 2.4 \times 1.25$ in x 1 in. x 58 ksi = 130.5 kips (Check)

$\phi R_n = \phi(s - d_b/2) t_p F_u \leq \phi 2.4 d_b t_p F_u$ for the interior bolt.

$\phi(s - d_b/2) t_p F_u = 0.75$ (4.09 - 1.25 in/2) 1 in x 58 ksi = 150.7 kips

$\phi 2.4 d_b t_p F_u = 0.75 \times 2.4 \times 1.25$ in x 1 in. x 58 ksi = 130.5 kips (Check)

Step 11: Check End-Plate shear strength.

$\phi R_n = \phi 0.6 A_g F_y > F_f/2$; $\phi = 0.90$

$\phi R_n = 0.90 \times 0.6 \times (8$ in. x 1 in.) x 42 ksi = 181.4 kips > 163.5 kips (Check)

Beam-to-End-Plate Weld

Full penetration welds are recommended for all beam-to-end-plate welds.

Column Design

The column section is assumed to have been designed for axial loading and frame stiffness requirements. It must also be checked for adequate strength to resist the concentrated forces imparted by the beam loading through the bolts.

Step 1: Column Flange Bending

$\phi R_n = \phi 6.25 t_{fc}^2 F_{yf} > F_f$ $\phi = 0.90$

$\phi Rn = 0.90 \times 6.25 \times (1.89$ in.$)^2 \times 45$ ksi = 904.2 kips > 327.1 kips (Check)

Step 2: Column Web Yielding

$\phi R_n = \phi(5k + N) F_{yw} t_w$ $\phi = 1.0$

ϕRn = 1.0 (5 x 2 15/16 in + .59 in.) 45 ksi x 1.41 in. = 969.4 kips > 327.1 kips (Check)

Step 3: Column Web Crippling

$$\phi R_n = \phi 135 t_w^2 \left[1 + 3\left(\frac{N}{d}\right)\left(\frac{t_w}{t_f}\right)^{1.5} \right] \sqrt{\frac{F_{yw} t_f}{t_w}} \quad , \ \phi = 0.75$$

$$\phi R_n = .75 \text{x} 135 \text{x} 1.175^2 \left[1 + 3\left(\frac{.59}{16.38}\right)\left(\frac{1.175}{1.89}\right)^{1.5} \right] \sqrt{\frac{45 \text{x} 1.89}{1.175}} = 1{,}252.3 \text{ kips} > 327.1 \text{ kips}$$

(Check)

Step 4: Column Web Buckling

$$\phi R_n = \phi \frac{4{,}100 t_w^3 \sqrt{F_{yw}}}{h} \qquad \phi = 0.90$$

$$\phi R_n = 0.90 \frac{4{,}100 \text{x} 1.175^3 \sqrt{45}}{16.38} = 2{,}451.5 \text{ kips} > 327.1 \text{ kips} \quad \text{(Check)}$$

Design Example B-2

Shimmed Four-Bolt Extended Moment End-Plate Connection

Design Parameters:

Beam Section	W 18x35, A-36
Beam Material Yield Stress	48 ksi
Column Section	W 14 x 145, A-36
Column Material Yield Stress	45 ksi
End-Plate Material Yield Stress	42 ksi

Beam Properties

W 18x35, A-36 beam section properties.

$d =$	17.7 in.	$t_w =$	0.30 in.	$t_f =$	0.425 in.
$Z_x =$	66.5 in^3	$b_f =$	6.00 in.	$F_y =$	48 ksi*

* Beam material yield stress of 48 ksi is used in calculations due to recommendations of numerous structural articles on new strengths of hot-rolled wide flange sections.

Type and Size of Bolts

Step 1: Calculate the plastic moment capacity of the beam using Equation 3.1.

$$M_p = F_y * Z_x$$

$$M_p = 48 \text{ ksi} * 66.5 \text{ in}^3 = \underline{3{,}192 \text{ in-kips}}$$

Step 2: Calculate the required moment capacity of the connection using Equation 3.2.

$$M_c = 1.10 \ M_p$$

$$M_c = 1.10 * 3{,}192 \text{ in-kips} = \underline{3{,}511 \text{ in-kips}}$$

Step 3: Calculate the flange force for the required connection moment capacity, M_c.

$$F_f = M_c / (d - t_f)$$

$$F_f = 3{,}511 \text{ in-kips} / (17.7 \text{ in.} - 0.425 \text{ in}) = \underline{203.3 \text{ kips}}$$

Step 4: Divide the flange force by the number of tension side bolts, 4 for this design.

$T_b = F_f / 4$

$T_b =$ 203.3 kips / 4 = 50.8 kips

Step 5: Select a bolt type (A-325 or A-490) and diameter to be sufficient for each bolt force from Table J3.2, AISC Specification (Load 1993).

A-325 minimum diameter bolt is 1 in. at 53 kips
A-490 minimum diameter bolt is 1 in. at 66.3 kips

Select A-325 1 in. diameter bolt

Step 6: Calculate the actual moment capacity of the connection using selected type and size bolts.

$M_{con} = 4 \ \phi T_n (d - t_f) \geq M_c$

$M_{con} = 4 * 53$ kips (17.7 in. - 0.425 in.) = 3,662 in-kips > M_c = 3,511 in-kips (Check)

End-Plate Thickness

Step 1: Establish values to define end-plate geometry.

$b_p =$ 7 in. (assumed column section selection have a k_1 value of about 1 1/8 in.; from Table 8-4 (AISC, Manual of Steel Construction), wrench clearance is 1 in. from fillet; from Table J3.4 (AISC, Specification), minimum edge distance for 1 in. diameter bolt is 1 1/4 in. Therefore, sum of spacing is 6 3/4 in.; round up to 7 in..)

$g =$ 4.5 in. (based on 7 in. end-plate width, subtract minimum edge distance from each side; 7 in. - 2 (1.25 in) = 4.5 in.)

$p_f =$ 1.5 in. (bolt diameter plus 1/2 inch.)

$F_{yp} =$ 42 ksi (assumed actual yield stress for hot-rolled steel plate material)

Step 2: Calculate required end-plate thickness using Equation 2.17.

$$t_p = \sqrt{8B_t p_f / \left(F_{yp} b_p\right)}$$

$$t_p = \sqrt{8(53\text{kips})(1.5\text{in.}) \Big/ (42\text{ksi})(7\text{in.})} = \quad \underline{1.44 \text{ in.}};\ \text{Select}\ \underline{1.5 \text{ in.}}\ \text{A-36 plate}$$

Step 3: Determine Length of the End-Plate, Equation 3.13.

$$L_p = h + 2\, p_{ext}$$

L_p = 17.7 in. + 2 (2.75 in.) = 23.7 in. round off to 24.0 in.

Therefore; Plate 1 1/2 x 7 x 2 - 0 , A-36

Step 4: Check Bolt Shear.

$\phi R_n = \phi F_n A_b n > M_{con}/arm$; $\phi = 0.75$

ϕR_n = 0.75 (60 ksi) (.7854 in^2) 8 = 282.7 kips

ϕR_n = 282.7 kips > 7667.3 in-kips/ 79 in. = 97.1 kips (Check)

Step 5: Check material bearing strength (The end-plate side of the connection is more critical because its thickness is less than the column side.)

Check that for the end-plate $L_e \geq 1.5d$ and $s \geq 3d$.

Le = 1.625 in. > 1.5 (1 in.) check; s = 3.425 in. > 3 (1 in.) check

$\phi R_n = \phi 2.4 d_b t_p F_u > M_{con}/arm$; $\phi = 0.75$

ϕR_n = 0.75 (2.4) (1 in.) (1.5 in.) 58 ksi = 156.6 kips > 97.1 kips (Check)

Step 6: Check End-Plate shear strength.

$\phi R_n = \phi 0.6 A_g F_y > F_f/2$; $\phi = 0.90$

ϕR_n = 0.90 (0.6) 1.5 in. x 7 in. x 42 ksi = 238.0 kips > 101.6 kips (Check)

Beam-to-End-Plate Weld

Full penetration welds are recommended for all beam-to-end-plate welds.

Column Design

Design procedures are similar to the four-bolt extended moment end-plate connection. See Design Example B-1.

Design Example B-3

Four-Bolt Wide Extended Moment End-Plate Connection

Design Parameters:

Beam Section	W 36x135, A-36
Beam Material Yield Stress	48 ksi
Column Section	W 14 x 311, A-36
Column Material Yield Stress	45 ksi
End-Plate Material Yield Stress	42 ksi

Beam Properties

W 36 x 135, A-36 beam section properties.

$d =$	35.55 in.	$t_w =$	0.60 in.	$t_f =$	0.79 in.
$Z_x =$	509 in^3	$b_f =$	11.95 in.	$F_y =$	48 ksi*

* Beam material yield stress of 48 ksi is used in calculations due to recommendations of numerous structural articles on new strengths of hot-rolled wide flange sections.

Type and Size of Bolts

Step 1: Calculate the plastic moment capacity of the beam using Equation 3.1.

$$M_p = F_y * Z_x$$

$$M_p = 48 \text{ ksi} * 509 \text{ in}^3 = \underline{24,432 \text{ in-kips}}$$

Step 2: Calculate the required moment capacity of the connection using Equation 3.2.

$$M_c = 1.10 \ M_p$$

$$M_c = 1.10 * 24,432 \text{ in-kips} = \underline{26,875 \text{ in-kips}}$$

Step 3: Calculate the flange force for the required connection moment capacity, M_c.

$$F_f = M_c / (d - t_f)$$

$$F_f = 26,875 \text{ in-kips} / (35.55 \text{ in.} - 0.79 \text{ in}) = \underline{773.2 \text{ kips}}$$

Step 4: Divide the flange force by the number of tension side bolts, 8 for this design.

$T_b = F_f / 8$

$T_b =$ 773.2 kips / 8 = 96.6 kips

Step 5: Select a bolt type (A-325 or A-490) and diameter to be sufficient for each bolt force from Table J3.2, AISC Specification (Load 1993).

A-325 minimum diameter bolt is 1 3/8 in. at 100.2 kips
A-490 minimum diameter bolt is 1 1/4 in. at 104.0 kips

Select A-490 1 1/4 in. diameter bolt.

Step 6: Calculate the actual moment capacity of the connection using selected type and size bolts.

$M_{con} = 8\ \phi T_n\ (d - t_f) \geq M_c$

M_{con} = 8 x 104.0 kips (35.55 in. - 0.79 in.)

= 28,920 in-kips > M_c = 26,875 in-kips (Check)

End-Plate Thickness

Step 1: Establish values to define end-plate geometry.

$b_p =$ 15 in. (assumed column section selection have a k_1 value of about 1 5/16 in.; from Table 8-4 (AISC, Manual of Steel Construction), wrench clearance is 1 1/4 in. from fillet; from Table J3.4 (AISC, Specification), minimum edge distance for 1 1/4 in. diameter bolt is 1 5/8 in. Minimum bolt spacing (Section J3.4, AISC Specification) is 2 2/3 bolt diameter, 3.33 in. Therefore, sum of all spacing is 15.04 in.; round off to 15 in..)

$p_f =$ 1.75 in. (bolt diameter plus 1/2 inch.)

$F_{yp} =$ 45 ksi (assumed actual yield stress for hot-rolled steel plate material)

Step 2: Calculate required end-plate thickness. (Procedures from AISC, Manual of Steel Construction, LRFD)

Assume $P_{uf} = F_f$; Therefore, P_{uf} = 773.2 kips,

C_a = 1.36 (Table 10-1)

$C_b = \left(b_f / b_p\right)^{1/3}$ = (11.95 in. / 12.95 in.) $^{1/3}$ = 0.960

(used only effective end-plate width, beam flange width plus 1 inch.)

$\left(A_f / A_w\right)$ = 0.463 (Table 10-2, Load 1993)

$P_e = p_f - \left(d_b / 4\right) - w_t$ = 1.75 in. - (1.25 in. / 4) = 1.4375 in.

(assume penetration weld with no weld fillet, w_t = 0.0 , conservative estimate.)

$$\alpha_m = C_a C_b \left(A_f / A_w\right)^{1/3} \left(P_e / d_b\right)^{1/4}$$

$$= 1.36 \times .9606 \times (.463)^{1/3} \left(1.4375 / 1.25\right)^{1/4} = 1.0466$$

$$t_p = \sqrt{\frac{4M_{eu}}{\phi F_y b_p}} \quad \text{and with} \quad M_{eu} = \frac{\alpha_m P_{uf} P_e}{4}$$

$$t_p = \sqrt{\frac{1.0466 \times 773.2 \times 1.4375}{.9 \times 45 \times 12.95}} = \underline{1.489 \text{ in.}} \quad \text{round off to} \quad \underline{1.50 \text{ in.}}$$

Step 3: Determine Length of the End-Plate.

$L_p = h + 2\, p_{ext}$

L_p = 35.55 in. + 2 (3.375 in.) = <u>42.3 in.</u> round off to <u>42.5 in.</u>

Therefore; <u>Plate 1 1/2 x 15 x 3 - 6 1/2 , A-36</u>

Step 4: Check Bolt Shear.

$\phi R_n = \phi F_n A_b n > M_{con}/arm;$ $\phi = 0.75$

ϕR_n = 0.75 (75 ksi) (1.2272 in^2) 16 = <u>1,104.5 kips</u> > 215.8 kips (Check)

Step 5: Check material bearing strength (The end-plate side of the connection is more critical because its thickness is less than the column side.)

Check that for the end-plate $L_e \geq 1.5d$ and $s \geq 3d$.

L_e = 1.625 in. > 1.5 (1 in.) check; s = 4.29 in. > 3 (1.25 in.) check

$\phi R_n = \phi 2.4 d_b t_p F_u > M_{con}/arm$; $\phi = 0.75$

ϕR_n = 0.75 (2.4) (1.25 in.) (1.5 in.) 58 ksi = 200 kips < 215.8 kips (Check)

Step 6: Check End-Plate shear strength.

$\phi R_n = \phi 0.6 A_g F_y > F_f/2$; $\phi = 0.90$

ϕR_n = 0.90 (0.6) 1.5 in. x 15 in. x 45 ksi. = 546.8 kips > 386.6 kips (Check)

Beam-to-End-Plate Weld

Full penetration welds are recommended for all beam-to-end-plate welds.

Column Design

For column side design checks, refer to Murray (1990) *Steel Design Guide Series 4; Extended End-Plate Moment Connections.*

Design Example B-4

Extended, Stiffened Moment End-plate Connection

Design Parameters:		
	Beam Section	W 24x76 , A-36
	Column Section	W 14x257 , A-36
	End-Plate	A-36, F_y = 42 ksi.
	Dimension	1 1/4 x 9 x 2 - 8, A-36
	Bolts	1 1/4 in. diameter, A-490
	B_t	102 kips

Beam Properties

W 24 x 76, A-36 beam section properties.

d =	23.92 in.	t_w =	0.44 in.	t_f =	0.68 in.
Z_x =	200 in^3	b_f =	8.99 in.	F_y =	48 ksi*

* Beam material yield stress of 48 ksi is used in calculations due to recommendations of numerous structural articles on new strengths of hot-rolled wide flange sections.

(Only the stiffener design is presented here. The end-plate and bolt specifications are determined by procedures for a four-bolt extended or four-bolt wide moment end-plate connection.)

Step 1: Determine the bending moment caused by bolt tension.

$$Mp = n * B_t * pf$$

$$Mp = 2\ (102 \text{ kips})\ 2 \text{ in.} = \underline{408 \text{ in-kips}}$$

Step 2: Determine Moment of Inertia and elastic capacity of the end-plate.

$$I_x = \frac{b_p t_p^3}{12} = 9 \text{ in. } (1.25 \text{ in.})^3 / 12 = \underline{1.465 \text{ in}^4}$$

$$M_{plate} = \frac{2F_{yp}I_x}{t_p} = 2\ (42 \text{ ksi.})\ 1.465 \text{ in}^4 / 1.25 \text{ in.} = \underline{98.4 \text{ in-kips}}$$

Step 3: Estimate the thickness of stiffener

Step 4: Calculate the required length of the stiffener along the beam flange

(Best method to calculate stiffener size is to set up a spread sheet with basic static quantities of material and iterate until acceptable solution is determined.)

Results of Spread Sheet Calculations

	length	thickness	Area	y	A*y	I'	A*d2
Plate	9	1.25	11.25	0.625	7.03125	1.46484	13.4583
Stiffener	7.5	0.5	3.75	5	18.75	17.578	40.3748
Total			15		25.7813	19.043	53.833
		Ycg =	1.719		Ix =	72.876	
	y max	stress =	7.031	My =	435.31	> M(load)	= 416

Alternative Stiffener Selection

	length	thickness	Area	y	A*y	I'	A*d2
Plate	9	1.25	11.25	0.625	7.03125	1.46484	14.3405
Stiffener	8.75	0.375	3.28125	5.625	18.457	20.935	49.1675
Total			14.5313		25.4883	22.3999	63.5081
		Ycg =	1.754		Ix =	85.908	
	y max	stress =	8.246	My =	437.56	> M(load)	= 416

Select the 1/2 in. thick stiffener due to shorter length and similar thickness to other beam stiffener requirements.

Therefore: Stiffener, 1/2 x 4 x 0 - 7 1/2, A-36

Step 5: Calculate required stiffener filler weld size.

$$D_{min} = \frac{0.9F_y t_s}{2x1.392} = 0.9\ (42\ ksi)\ 0.5\ in.\ /\ 2 \times 1.392\ ksi/in. = 6.79$$

round up to 7/16 in. weld required. Minimum weld required is 3/16 in. (Table J2.4, AISC, Specification (Load 1993))

Therefore: Apply 1/4 in. weld both sides of the stiffener.

APPENDIX C

W 18 X 35 BEAM TEST RESULTS AND DATA

TESTS 1 / 95 - 4 / 95

Beam Section W 18 x 35, A-36 Steel

$d = 17.7$ in. $t_w = 0.30$ in. $t_f = 0.425$ in $b_f = 6.00$ in.

$S_x = 57.6$ in^4. $Z_x = 66.5$ in^3.

Specimen Preparation and Welding Technique

End-Plates were saw cut to length and ground if required to smooth rough edges. No preheating of end-plate or beam was conducted. Connection was stick welded with 1/8 in. 7018 Low Hydrogen Rods.

Beam Coupon tests of 3/15/95

Web # 1 (#976)

.324 x 1.507 = area of 0.4883

Lower Yield Stress - 60,560 psi.
Tensile Strength - 65,726 psi.
Elongation (2 in. base) - 38%

Web # 2 (#977)

.324 x 1.507 = area of 0.4883

Lower Yield Stress - 59,285 psi.
Tensile Strength - 78,278 psi.
Elongation (2 in. base) - 39%

Flange # 1 (#978)

.400 x 1.508 = area of 0.6032

Lower Yield Stress - 50,180 psi.
Tensile Strength - 71,550 psi.
Elongation (2 in. base) - 39%

Flange # 2 (#980)

.398 x 1.505 = area of 0.5990

Lower Yield Stress - 50,465 psi.
Tensile Strength - 71,538 psi.
Elongation (2 in. base) - 49%

Web Strengths:	**59,922 psi (yield)**	**72,000 psi (ultimate)**
Flange Strengths:	**50,322 psi (yield)**	**71,544 psi (ultimate)**

TEST 1 / 95

Connection End-Plate: Extended Four-Bolt, 1 in. Thick

Cycles Completed: 19

Failure Mode: Local Flange Buckling

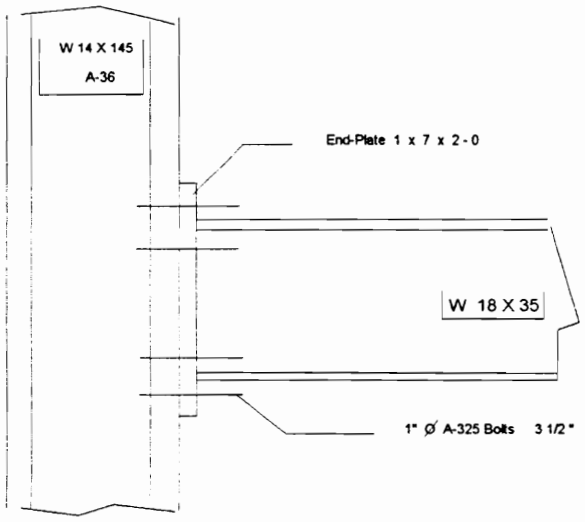

End-Plate Connection

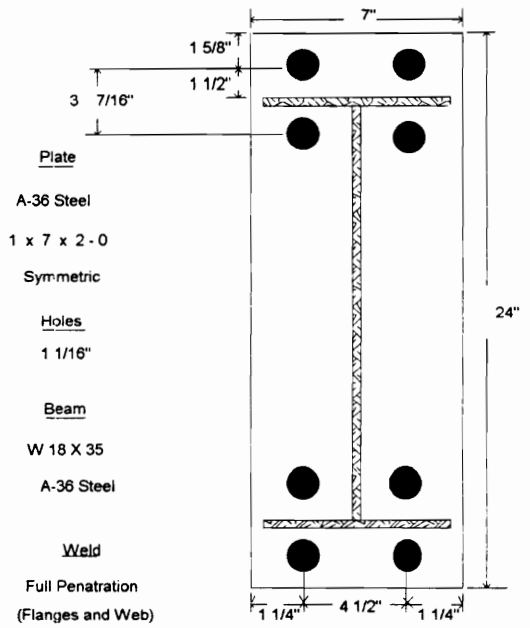

End-Plate Detailing

1 in. End-Plate Coupon tests of 3/15/95

End-Plate 1 in. # 1 (#983)

1.020 x 1.503 = area of 1.5331

Lower Yield Stress - 41,577 psi.
Tensile Strength - 62,437 psi.
Elongation (2 in. base) - 61%

End-Plate 1 in. # 2 (#984)

1.021 x 1.504 = area of 1.5356

Lower Yield Stress - 39,031 psi.
Tensile Strength - 62,015 psi.
Elongation (2 in. base) - 62%

1 in. End-Plate Strengths: **40,304 psi (yield)** **62,226 psi (ultimate)**

Loading History for TEST 1 / 95

Cycle 1	Cycle 2	Cycle 3	Cycle 4	Cycle 5	Cycle 6	Cycle 7	Cycle 8	Cycle 9	Cycle 10	Cycle 11	Cycle 12	Cycle 13	Cycle 14	Cycle 15	Cycle 16	Cycle 17	Cycle 18	Cycle 19
0	0	0	0	0	0	0	0	0	0	0	0	0	0	0	0	0	0	0
4	4	4	5	5	5	10	10	10	0.322	0.322	0.322	0.322	0.322	0.322	0.644	0.644	0.644	0.644
8	8	8	10	10	10	20	20	20	0.483	0.483	0.483	0.644	0.644	0.644	0.966	0.966	0.966	1.288
12	12	12	15	15	15	30	30	30	0.644	0.644	0.644	0.966	0.966	0.966	1.288	1.288	1.288	1.610
16	16	16	20	20	20	35	35	35	0.859	0.859	0.859	1.288	1.288	1.288	1.610	1.610	1.610	1.932
18	18	18	27.7	27.7	27.7	36.9	36.9	36.9	1.073	1.073	1.073	1.503	1.503	1.503	1.932	1.932	1.932	2.254
16	16	16	20	20	20	35	35	35	1.288	1.288	1.288	1.717	1.717	1.717	2.147	2.147	2.147	2.576
12	12	12	15	15	15	30	30	30	1.073	1.073	1.073	1.932	1.932	1.932	2.361	2.361	2.361	2.791
8	8	8	10	10	10	20	20	20	0.859	0.859	0.859	1.717	1.717	1.717	2.576	2.576	2.576	3.005
4	4	4	5	5	5	10	10	10	0.644	0.644	0.644	1.503	1.503	1.503	2.361	2.361	2.361	3.220
0	0	0	0	0	0	0	0	0	0.483	0.483	0.483	1.288	1.288	1.288	2.147	2.147	2.147	3.005
-4	-4	-4	-5	-5	-5	-10	-10	-10	0.322	0.322	0.322	0.966	0.966	0.966	1.932	1.932	1.932	2.791
-8	-8	-8	-10	-10	-10	-20	-20	-20	0	0	0	0.644	0.644	0.644	1.61	1.61	1.61	2.576
-12	-12	-12	-15	-15	-15	-30	-30	-30	-0.286	-0.286	-0.286	0.322	0.322	0.322	1.288	1.288	1.288	2.254
-16	-16	-16	-20	-20	-20	-30	-30	-30	-0.429	-0.429	-0.429	0	0	0	0.966	0.966	0.966	1.932
-18	-18	-18	-27.7	-27.7	-27.7	-36.9	-36.9	-36.9	-0.572	-0.572	-0.572	-0.286	-0.286	-0.286	0.644	0.644	0.644	1.610
-16	-16	-16	-20	-20	-20	-35	-35	-35	-0.763	-0.763	-0.763	-0.572	-0.572	-0.572	0	0	0	1.288
-12	-12	-12	-15	-15	-15	-30	-30	-30	-0.953	-0.953	-0.953	-0.858	-0.858	-0.858	-0.572	-0.572	-0.572	0.644
-8	-8	-8	-10	-10	-10	-20	-20	-20	-1.144	-1.144	-1.144	-1.144	-1.144	-1.144	-0.858	-0.858	-0.858	0
-4	-4	-4	-5	-5	-5	-10	-10	-10	-0.953	-0.953	-0.953	-1.335	-1.335	-1.335	-1.144	-1.144	-1.144	-0.572
0	0	0	0	0	0	0	0	0	-0.763	-0.763	-0.763	-1.525	-1.525	-1.525	-1.430	-1.430	-1.430	-1.144
									-0.572	-0.572	-0.572	-1.716	-1.716	-1.716	-1.716	-1.716	-1.716	-1.430
									-0.429	-0.429	-0.429	-1.525	-1.525	-1.525	-1.907	-1.907	-1.907	-1.716
									-0.286	-0.286	-0.286	-1.335	-1.335	-1.335	-2.097	-2.097	-2.097	-2.002
									0	0	0	-1.144	-1.144	-1.144	-2.288	-2.288	-2.288	-2.288
								<=	=>			-0.858	-0.858	-0.858	-2.097	-2.097	-2.097	-2.479
								Load	Deflect			-0.572	-0.572	-0.572	-1.907	-1.907	-1.907	-2.669
								(kips)	(in.)			-0.286	-0.286	-0.286	-1.716	-1.716	-1.716	-2.860
												0	0	0	-1.430	-1.430	-1.430	-2.699
															-1.144	-1.144	-1.144	-2.479
															-0.858	-0.858	-0.858	-2.288
															-0.572	-0.572	-0.572	-2.002

positive delta = 0.644 in.

negative delta = -0.572 in.

TEST 1 / 95
W 18 x 35
1 in. End-Plate

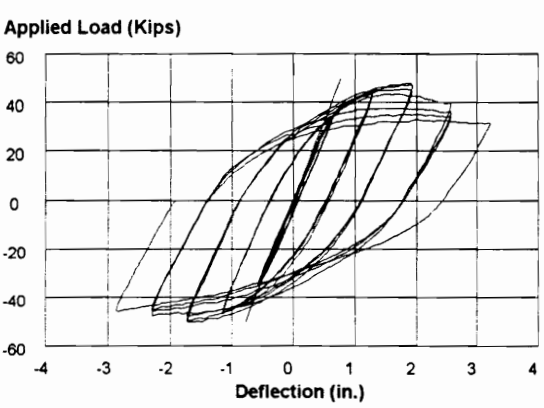

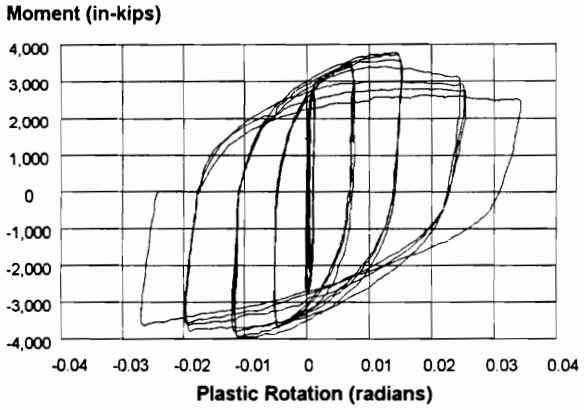

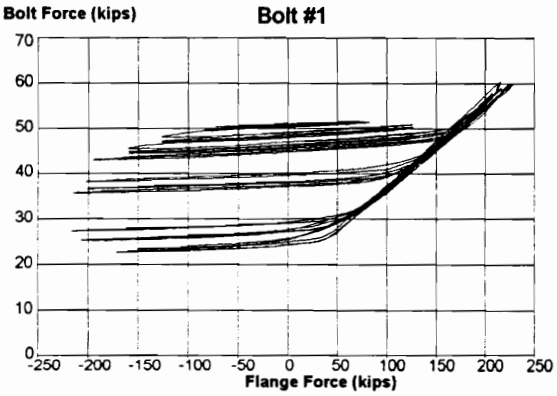

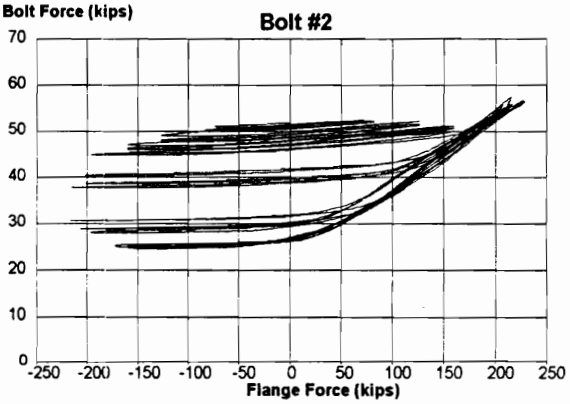

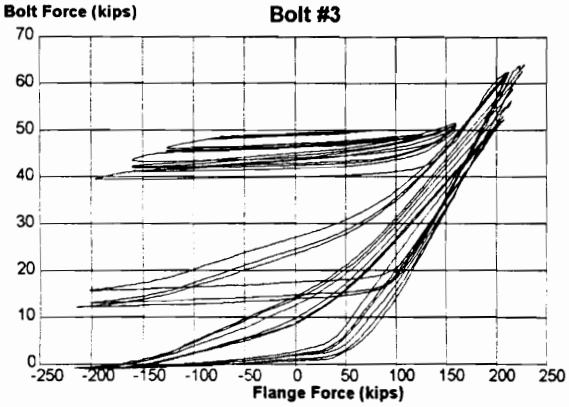

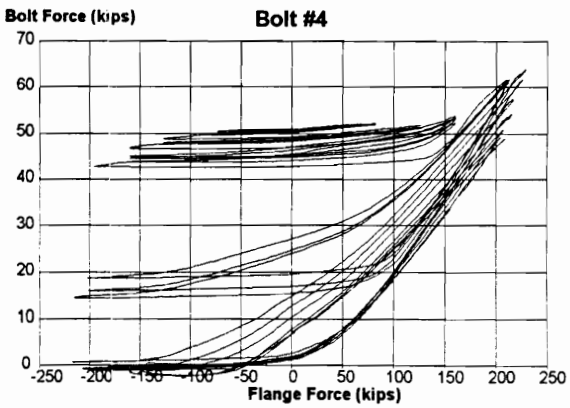

TEST 1 / 95
W 18 x 35
1 in. End-Plate

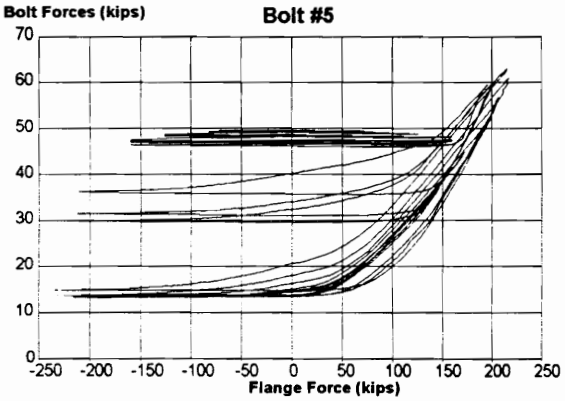

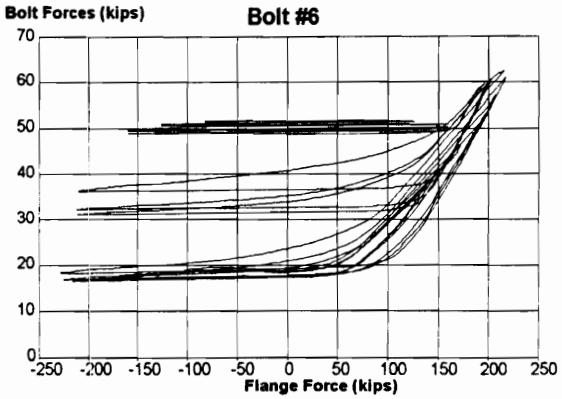

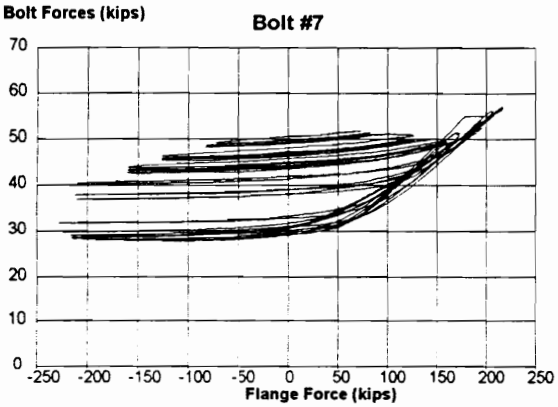

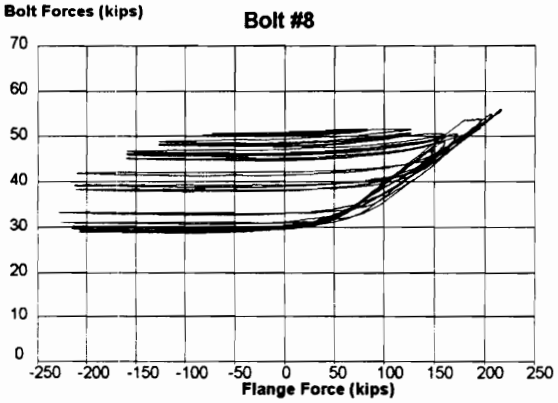

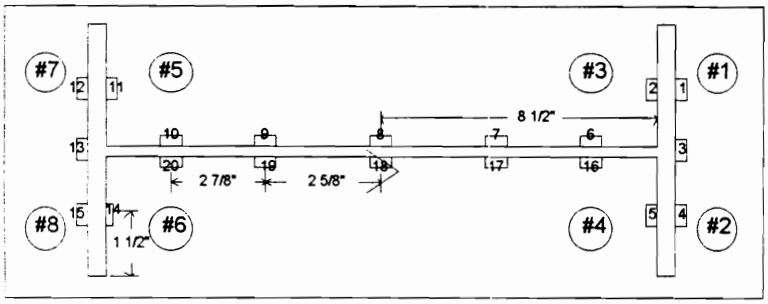

Strain Gauge and Bolt Location

TEST 2 / 95

Connection End-Plate: Extended Four-Bolt, 1 1/2 in. Thick, with Shims

Cycles Completed: 20

Failure Mode: Local Flange Buckling

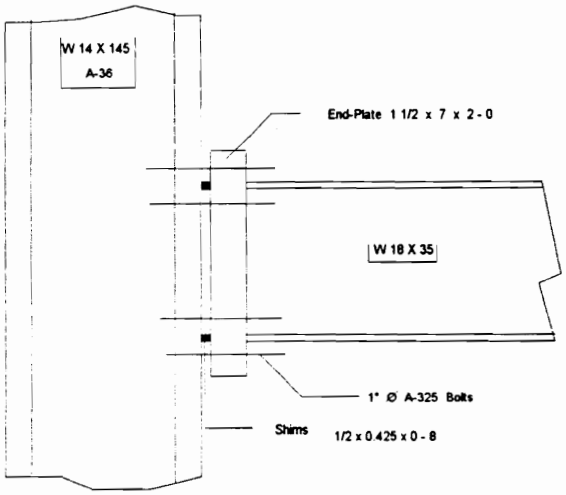

End-Plate Connection

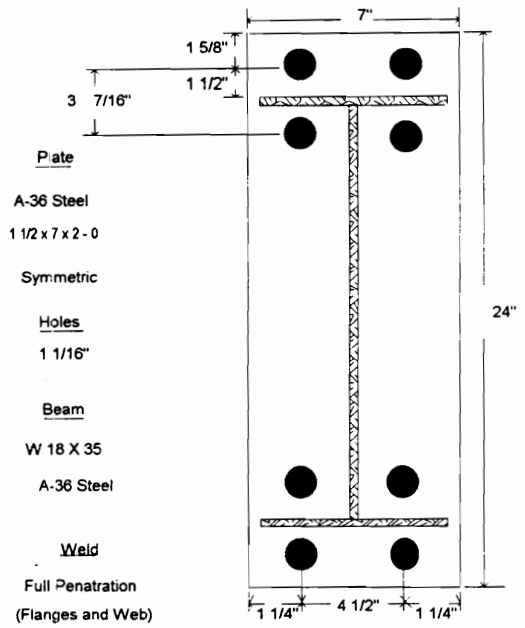

End-Plate Detailing

1 1/2 in. End-Plate Coupon tests of 3/15/95

End-Plate 1 1/2 in. # 1 (#993)

1.523 x 1.505 = area of 2.2921

Lower Yield Stress - 35,127 psi.
Tensile Strength - 39,112 psi.
Elongation (2 in. base) - 62%

End-Plate 1 1/2 in. # 1 (#1025)

1.525 x 1.504 = area of 2.2951

Lower Yield Stress - 35,187 psi.
Tensile Strength - 67,245 psi.
Elongation (2 in. base) - 59%

End-Plate Strengths: **35,162 psi (yield)** **53,178 psi (ultimate)**

Loading History for TEST 2 / 95

Load (kips) <= => Deflection (in.)

Cycle 1	Cycle 2	Cycle 3	Cycle 4	Cycle 5	Cycle 6	Cycle 7	Cycle 8	Cycle 9	Cycle 10	Cycle 11	Cycle 12	Cycle 13	Cycle 14	Cycle 15	Cycle 16	Cycle 17	Cycle 18	Cycle 19	Cycle 20
									0	0	0	0	0	0	0	0	0	0	0
0	0	0	0	0	0	0	0	0	0.304	0.304	0.304	0.304	0.304	0.304	0.608	0.608	0.608	0.608	0.608
4	4	4	5	5	5	10	10	10	0.456	0.456	0.456	0.608	0.608	0.608	0.912	0.912	0.912	1.216	1.216
8	8	8	10	10	10	20	20	20	0.608	0.608	0.608	0.912	0.912	0.912	1.216	1.216	1.216	1.520	1.520
12	12	12	15	15	15	30	30	30	0.811	0.811	0.811	1.216	1.216	1.216	1.520	1.520	1.520	1.824	1.824
16	16	16	20	20	20	32.5	32.5	32.5	1.013	1.013	1.013	1.419	1.419	1.419	1.824	1.824	1.824	2.128	2.128
18	18	18	26.5	26.5	26.5	35.3	35.3	35.3	1.216	1.216	1.216	1.621	1.621	1.621	2.027	2.027	2.027	2.432	2.432
16	16	16	20	20	20	32.5	32.5	32.5	1.013	1.013	1.013	1.824	1.824	1.824	2.229	2.229	2.229	2.635	2.635
12	12	12	15	15	15	30	30	30	0.811	0.811	0.811	1.621	1.621	1.621	2.432	2.432	2.432	2.837	2.837
8	8	8	10	10	10	20	20	20	0.608	0.608	0.608	1.419	1.419	1.419	2.229	2.229	2.229	3.040	3.040
4	4	4	5	5	5	10	10	10	0.456	0.456	0.456	1.216	1.216	1.216	2.027	2.027	2.027	2.837	2.837
0	0	0	0	0	0	0	0	0	0.304	0.304	0.304	0.912	0.912	0.912	1.824	1.824	1.824	2.635	2.635
									0	0	0	0.608	0.608	0.608	1.520	1.520	1.520	2.432	2.432
												0.304	0.304	0.304	1.216	1.216	1.216	2.128	2.128
												0	0	0	0.912	0.912	0.912	1.824	1.824
															0.608	0.608	0.608	1.520	1.520
															0	0	0	1.216	1.216
																		.608	.608
																		0	0

delta = $\pm$ 0.608 in.

Note: For more efficient use of space, only positive load and deflection values are tabulated.
A complete cycle included both positive and negative (load or deflection) excursions of equal magnitude

TEST 2 / 95
W 18 x 35
1 1/2 in. End-Plate, with Shims

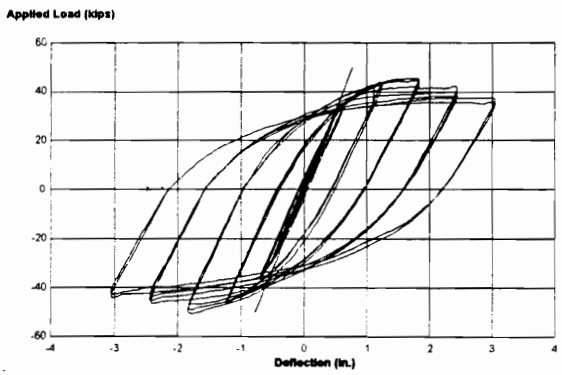

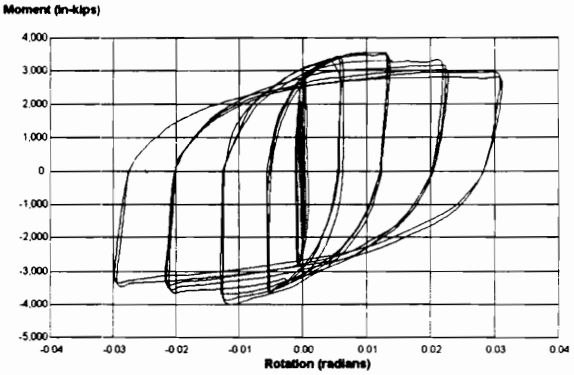

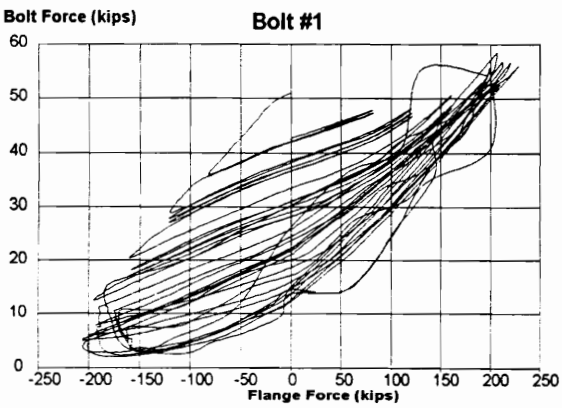

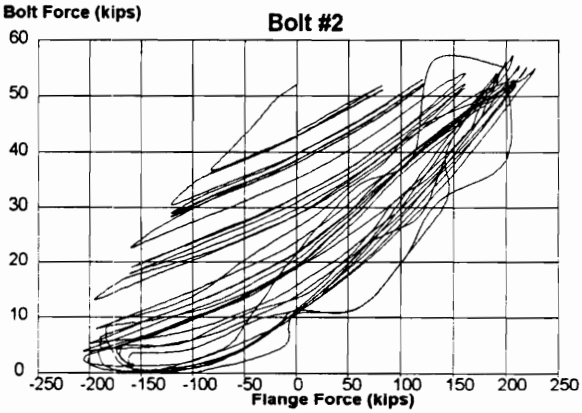

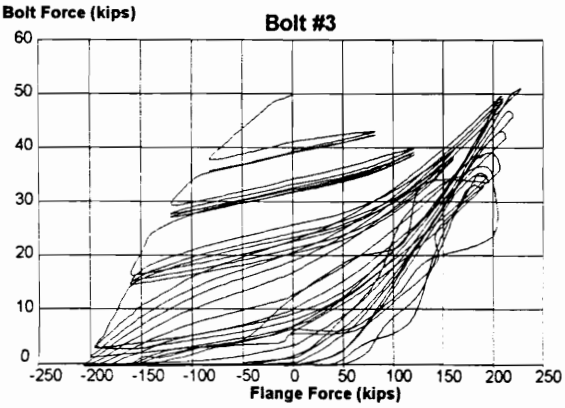

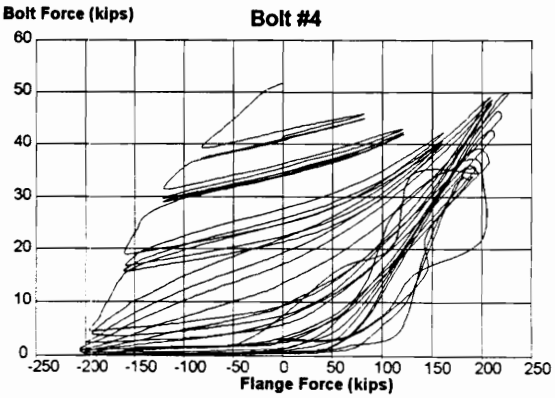

TEST 2 / 95
W 18 x 35
1 1/2 in. End-Plate, with Shims

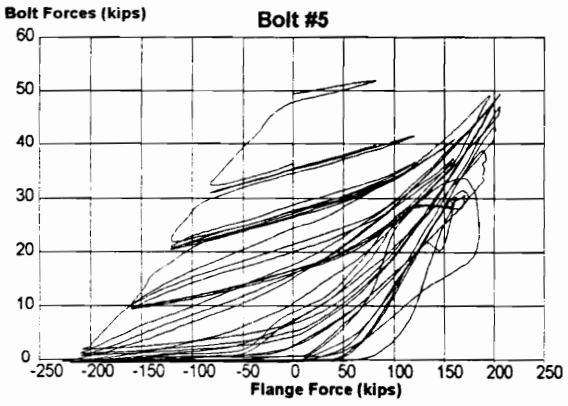

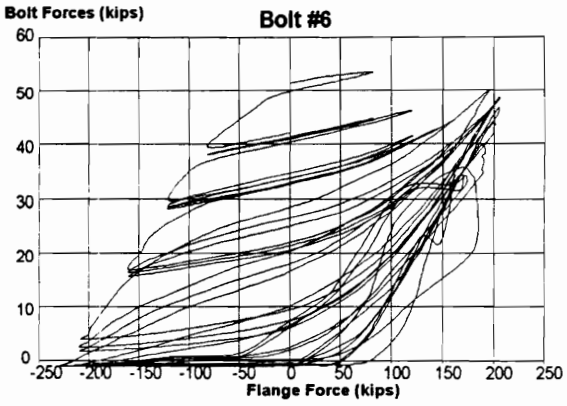

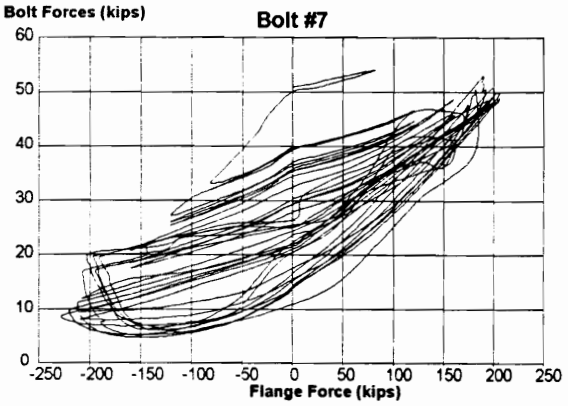

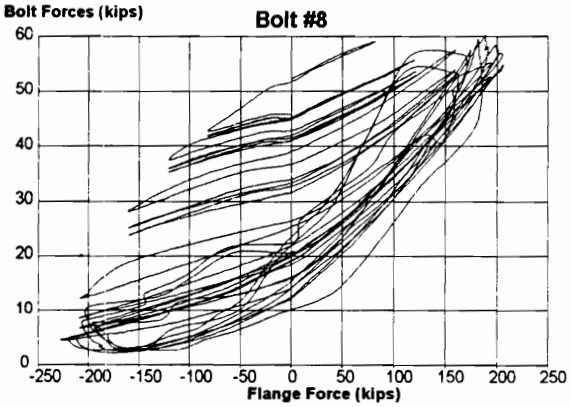

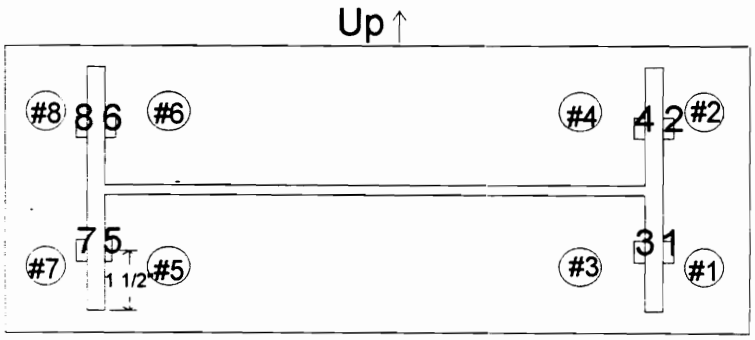

Strain Gauge and Bolt Location

TEST 3 / 95

Connection End-Plate: Extended, Stiffened Four-Bolt, 1 in. Thick, with Shims

Cycles Completed: 20

Failure Mode: Local Flange Buckling

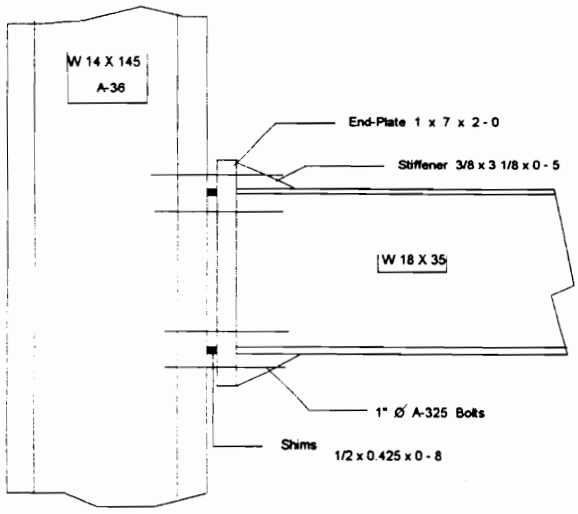

End-Plate Connection

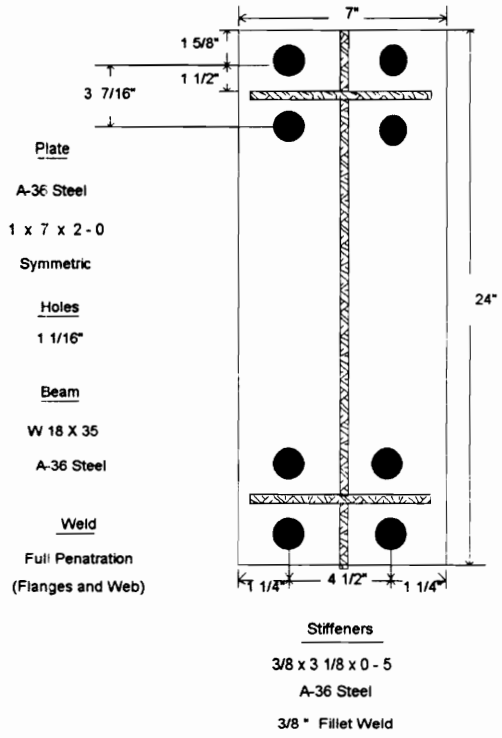

End-Plate Detailing

1 in. End-Plate Coupon tests of 3/15/95

End-Plate 1 in. # 1 (#983)

1.020 x 1.503 = area of 1.5331

Lower Yield Stress - 41,577 psi.
Tensile Strength - 62,437 psi.
Elongation (2 in. base) - 61%

End-Plate 1 in. # 2 (#984)

1.021 x 1.504 = area of 1.5356

Lower Yield Stress - 39,031 psi.
Tensile Strength - 62,015 psi.
Elongation (2 in. base) - 62%

1 in. End-Plate Strengths: **40,304 psi (yield)** **62,226 psi (ultimate)**

Loading History for TEST 3 / 95

Load (kips) <= => Deflection (in.)

Cycle 1	Cycle 2	Cycle 3	Cycle 4	Cycle 5	Cycle 6	Cycle 7	Cycle 8	Cycle 9	Cycle 10	Cycle 11	Cycle 12	Cycle 13	Cycle 14	Cycle 15	Cycle 16	Cycle 17	Cycle 18	Cycle 19	Cycle 20
									0	0	0	0	0	0	0	0	0	0	0
0	0	0	0	0	0	0	0	0	0.282	0.282	0.282	0.282	0.282	0.282	0.564	0.564	0.564	0.564	0.564
4	4	4	5	5	5	10	10	10	0.423	0.423	0.423	0.564	0.564	0.564	0.846	0.846	0.846	1.128	1.128
8	8	8	10	10	10	20	20	20	0.564	0.564	0.564	0.846	0.846	0.846	1.128	1.128	1.128	1.410	1.410
12	12	12	15	15	15	30	30	30	0.752	0.752	0.752	1.128	1.128	1.128	1.410	1.410	1.410	1.692	1.692
16	16	16	20	20	20	32	32	32	0.940	0.940	0.940	1.316	1.316	1.316	1.692	1.692	1.692	1.974	1.974
18	18	18	25	25	25	34	34	34	1.128	1.128	1.128	1.504	1.504	1.504	1.880	1.880	1.880	2.256	2.256
16	16	16	20	20	20	32	32	32	0.940	0.940	0.940	1.692	1.692	1.692	20.68	20.68	20.68	2.444	2.444
12	12	12	15	15	15	30	30	30	0.752	0.752	0.752	1.504	1.504	1.504	2.256	2.256	2.256	2.632	2.632
8	8	8	10	10	10	20	20	20	0.564	0.564	0.564	1.316	1.316	1.316	2.068	2.068	2.068	2.820	2.820
4	4	4	5	5	5	10	10	10	0.423	0.423	0.423	1.128	1.128	1.128	1.880	1.880	1.880	2.632	2.632
0	0	0	0	0	0	0	0	0	0.282	0.282	0.282	0.846	0.846	0.846	1.692	1.692	1.692	2.444	2.444
									0	0	0	0.564	0.564	0.564	1.410	1.410	1.410	2.256	2.256
												0.282	0.282	0.282	1.128	1.128	1.128	1.974	1.974
												0	0	0	0.846	0.846	0.846	1.692	1.692
															0.564	0.564	0.564	1.410	1.410
															0	0	0	1.128	1.128
																		0.564	0.564
																		0	0

delta = $\pm$ 0.564 in.

Note: For more efficient use of space, only positive load and deflection values are tabulated.
A complete cycle included both positive and negative (load or deflection) excursions of equal magnitude

TEST 3 / 95
W 18 x 35
1 in. Stiffened End-Plate, with Shims

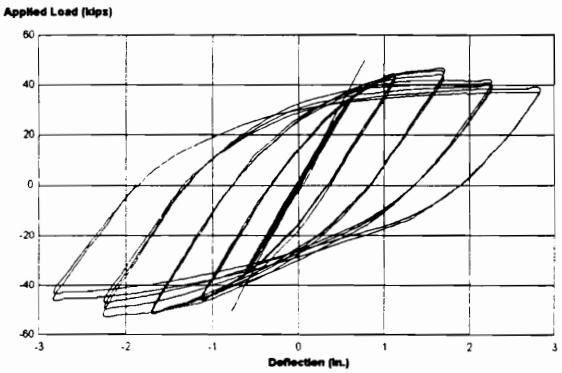

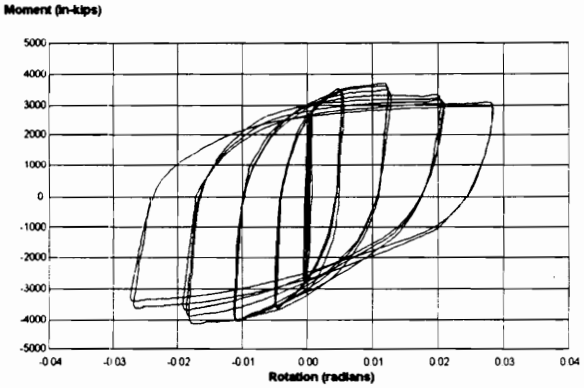

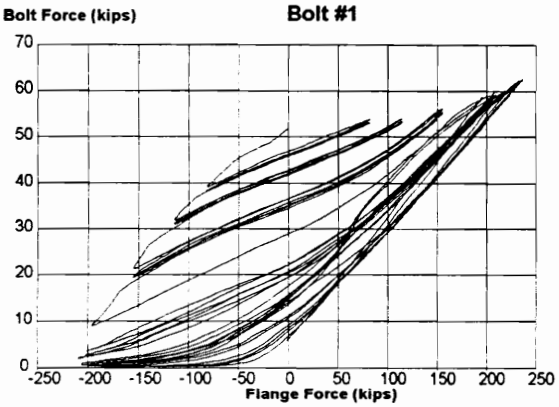

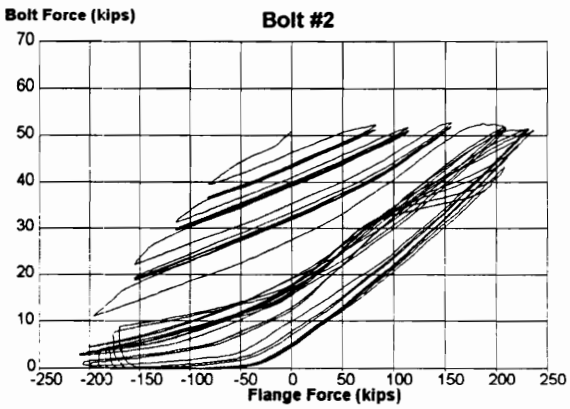

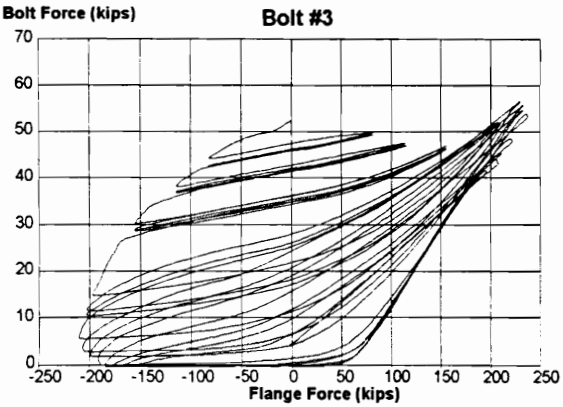

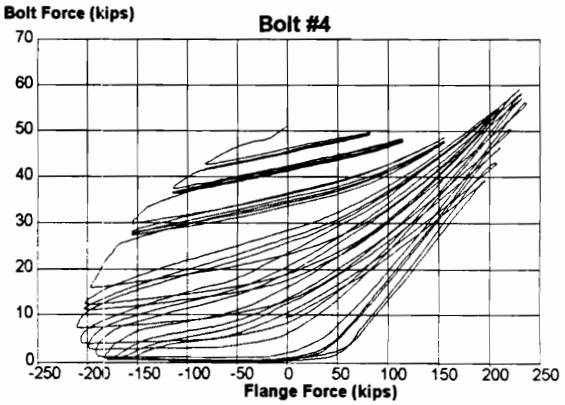

TEST 3 / 95
W 18 x 35
1 in. Stiffened End-Plate, with Shims

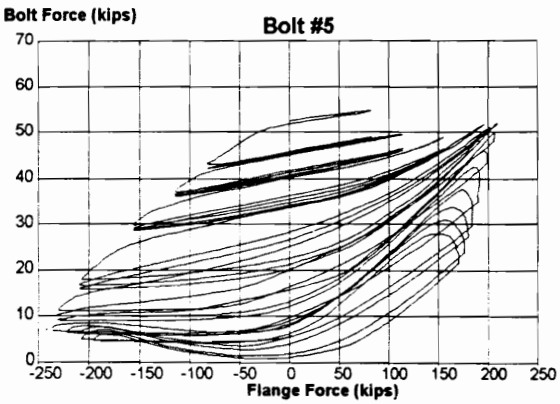

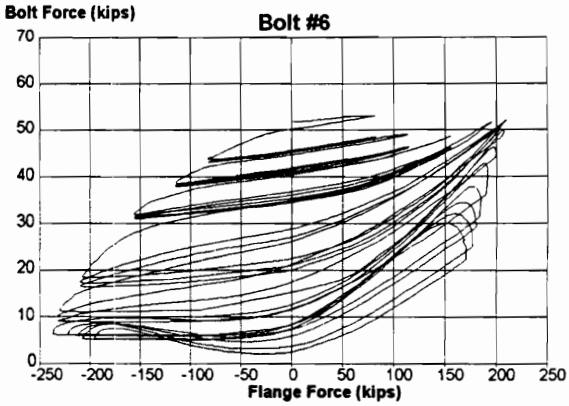

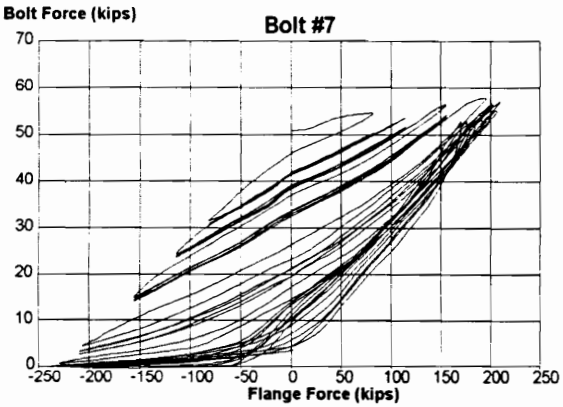

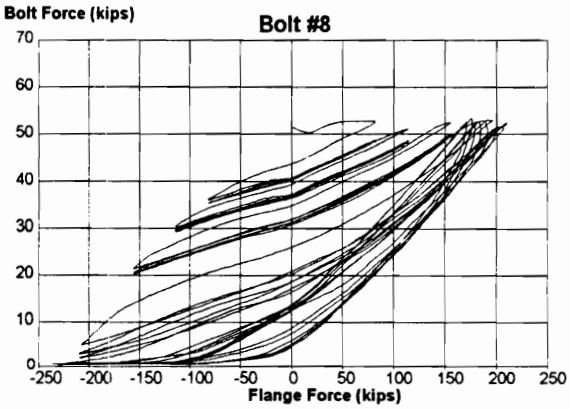

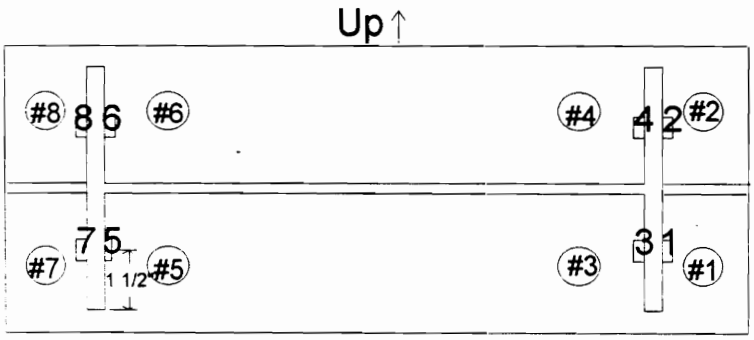

Strain Gauge and Bolt Location

TEST 4 / 95

Connection End-Plate: Extended Four-Bolt, 1 in. Thick

Cycles Completed: 20

Failure Mode: Local Flange Buckling

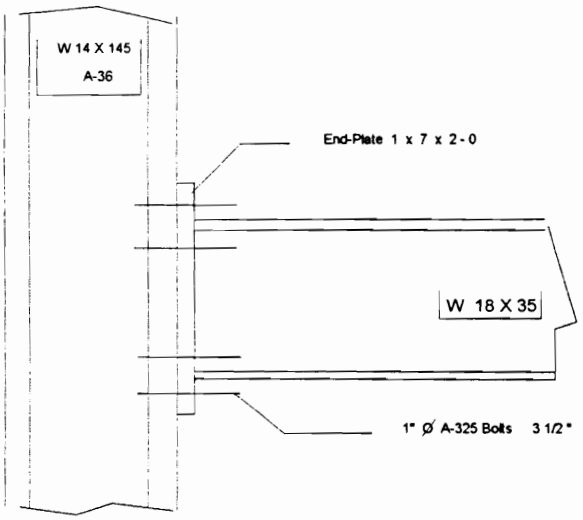

End-Plate Connection

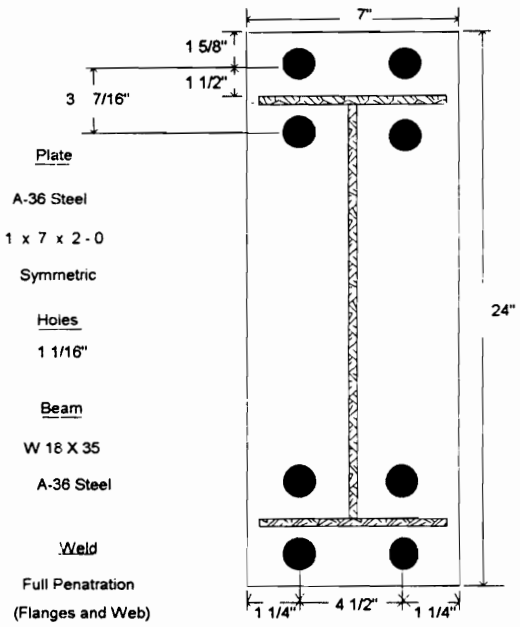

End-Plate Detailing

1 in. End-Plate Coupon tests of 3/15/95

End-Plate 1 in. # 1 (#983)

1.020 x 1.503 = area of 1.5331

Lower Yield Stress - 41,577 psi.
Tensile Strength - 62,437 psi.
Elongation (2 in. base) - 61%

End-Plate 1 in. # 2 (#984)

1.021 x 1.504 = area of 1.5356

Lower Yield Stress - 39,031 psi.
Tensile Strength - 62,015 psi.
Elongation (2 in. base) - 62%

1 in. End-Plate Strengths: **40,304 psi (yield)** **62,226 psi (ultimate)**

Loading History for TEST 4 / 95

Load (kips) <= => Deflection (in.)

Cycle 1	Cycle 2	Cycle 3	Cycle 4	Cycle 5	Cycle 6	Cycle 7	Cycle 8	Cycle 9	Cycle 10	Cycle 11	Cycle 12	Cycle 13	Cycle 14	Cycle 15	Cycle 16	Cycle 17	Cycle 18	Cycle 19	Cycle 20
									0	0	0	0	0	0	0	0	0	0	0
0	0	0	0	0	0	0	0	0	0.273	0.273	0.273	0.273	0.273	0.273	0.545	0.545	0.545	0.545	0.545
4	4	4	5	5	5	10	10	10	0.409	0.409	0.409	0.545	0.545	0.545	0.818	0.818	0.818	1.090	1.090
8	8	8	10	10	10	20	20	20	0.545	0.545	0.545	0.819	0.819	0.819	1.090	1.090	1.090	1.363	1.363
12	12	12	15	15	15	30	30	30	0.727	0.727	0.727	1.090	1.090	1.090	1.363	1.363	1.363	1.635	1.635
16	16	16	20	20	20	32	32	32	0.908	0.908	0.908	1.272	1.272	1.272	1.635	1.635	1.635	1.908	1.908
18	18	18	25	25	25	34	34	34	1.090	1.090	1.090	1.453	1.453	1.453	1.817	1.817	1.817	2.180	2.180
16	16	16	20	20	20	32	32	32	0.908	0.908	0.908	1.635	1.635	1.635	1.998	1.998	1.998	2.362	2.362
12	12	12	15	15	15	30	30	30	0.727	0.727	0.727	1.453	1.453	1.453	2.180	2.180	2.180	2.543	2.543
8	8	8	10	10	10	20	20	20	0.545	0.545	0.545	1.272	1.272	1.272	1.998	1.998	1.998	2.725	2.725
4	4	4	5	5	5	10	10	10	0.409	0.409	0.409	1.090	1.090	1.090	1.817	1.817	1.817	2.543	2.543
0	0	0	0	0	0	0	0	0	0.273	0.273	0.273	0.818	0.818	0.818	1.635	1.635	1.635	2.362	2.362
									0	0	0	0.545	0.545	0.545	1.363	1.363	1.363	2.180	2.180
												0.273	0.273	0.273	1.090	1.090	1.090	1.908	1.908
												0	0	0	0.818	0.818	0.818	1.635	1.635
															0.545	0.545	0.545	1.363	1.363
															0	0	0	1.090	1.090
																		0.545	0.545
																		0	0

delta = $\pm$ 0.545 in.

Note: For more efficient use of space, only positive load and deflection values are tabulated.
A complete cycle included both positive and negative (load or deflection) excursions of equal magnitude

TEST 4 / 95
W 18 x 35
1 in. End-Plate

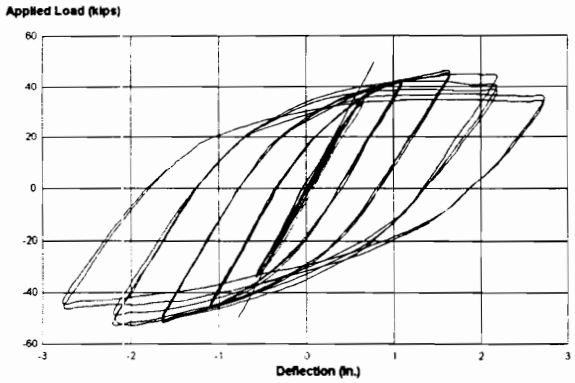

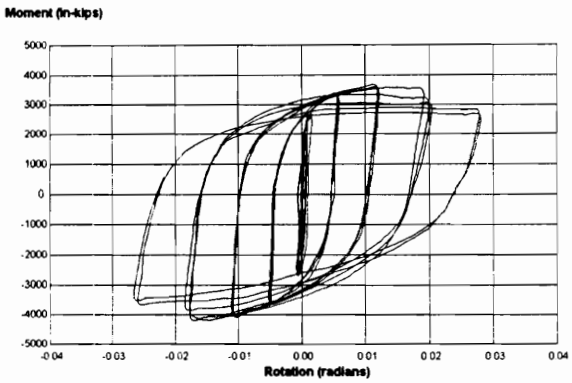

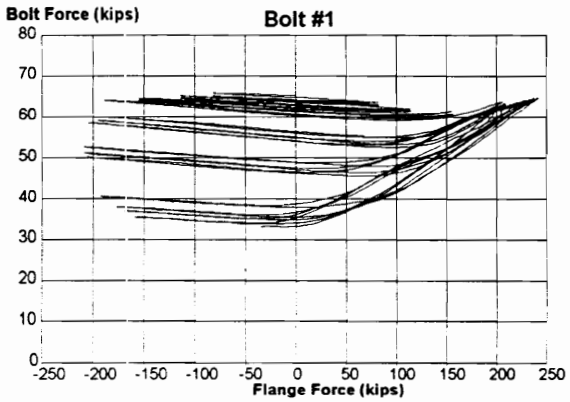

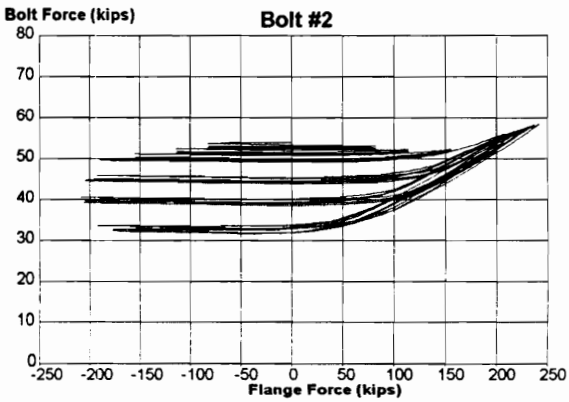

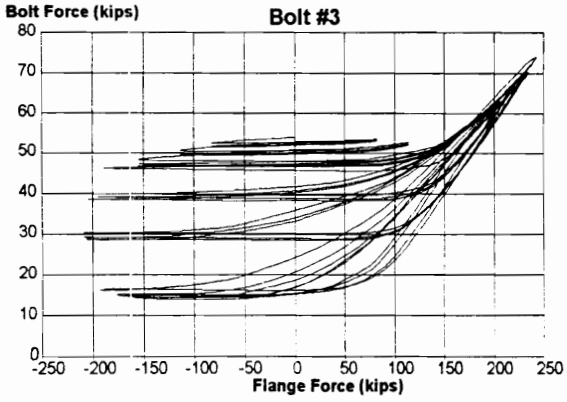

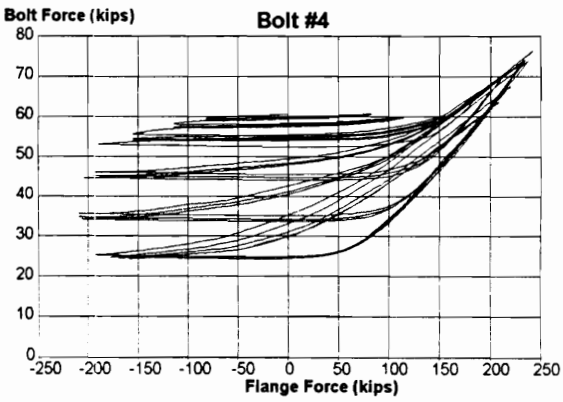

TEST 4 / 95
W 18 x 35
1 in. End-Plate

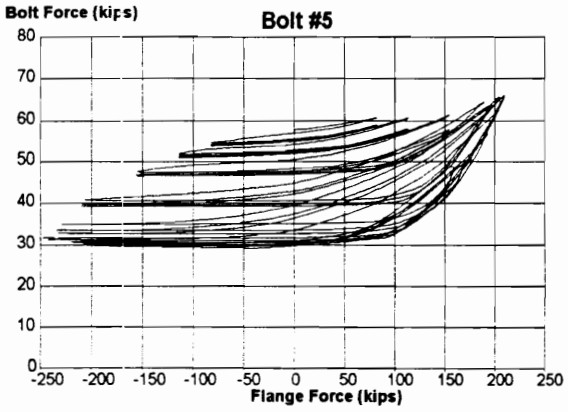

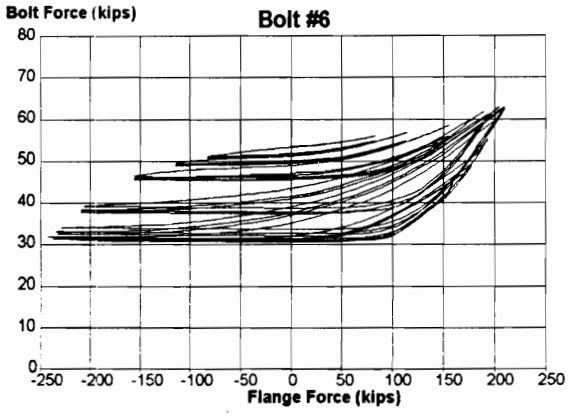

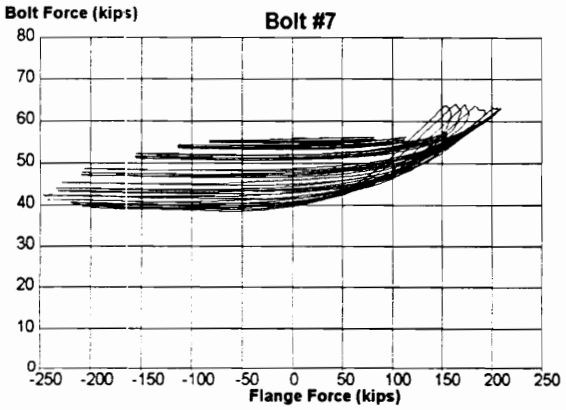

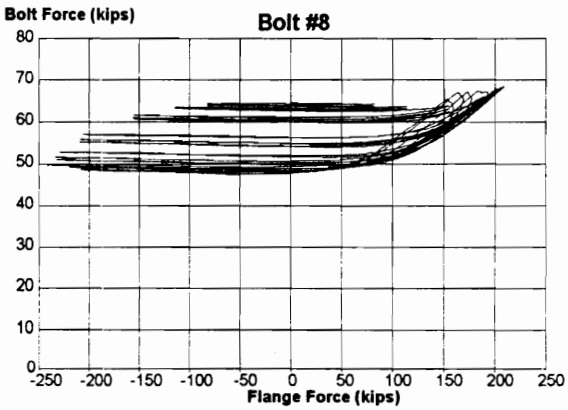

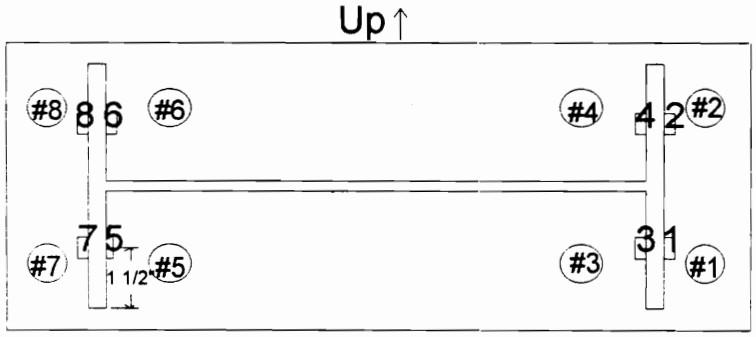

Strain Gauge and Bolt Location

APPENDIX D

W 24 X 62 BEAM TEST RESULTS AND DATA

TESTS 5 / 95 - 7 / 95

Beam Section W 24 x 62, A-36 Steel

$d = 23.74$ in. $t_w = 0.43$ in. $t_f = 0.59$ in $b_f = 7.04$ in.

$S_x = 131$ in^4. $Z_x = 153$ in^3.

Specimen Preparation and Welding Technique

End-Plates were flame cut to length and ground if required to smooth rough edges. Preheating of end-plate and/or beam was conducted as required by AWS. Connection was welded via flux core technique utilizing 5/64 in. E70 electrode Lincoln wire.

Beam Coupon Tests of 07/14/95

Web # 1

.420 x 1.503 = area of 0.6313

Lower Yield Stress - 53,385 psi.
Tensile Strength - 69,068 psi.
Elongation (8 in. base) - 28.1%

Flange # 1 Top Flange

.552 x 1.500 = area of 0.8280

Lower Yield Stress - 51,449 psi.
Tensile Strength - 68,116 psi.
Elongation (8 in. base) - 28.0%

Flange # 3 Bottom Flange

.565 x 1.503 = area of 0.8492

Lower Yield Stress - 53,816 psi.
Tensile Strength - 69,242 psi.
Elongation (8 in. base) - 18.84%

Web # 2

.420 x 1.503 = area of 0.6313

Lower Yield Stress - 53,068 psi.
Tensile Strength - 68,593 psi.
Elongation (8 in. base) - 28.9%

Flange # 2 Top Flange

.552 x 1.500 = area of 0.8280

Lower Yield Stress - 50,966 psi.
Tensile Strength - 67,512 psi.
Elongation (8 in. base) - 25.0%

Flange # 4 Bottom Flange

.553 x 1.502 = area of 0.8312

Lower Yield Stress - 53,068 psi.
Tensile Strength - 68,593 psi.
Elongation (8 in. base) - 28.9%

Web Strengths:	**53,227 psi (yield)**	**68,830 psi (ultimate)**
Flange Strengths:	**53,086 psi (yield)**	**68,692 psi (ultimate)**

TEST 5 / 95

Connection End-Plate: Extended Four-Bolt, 1 in. Thick

Cycles Completed: 15

Failure Mode: Beam Flange Fracture

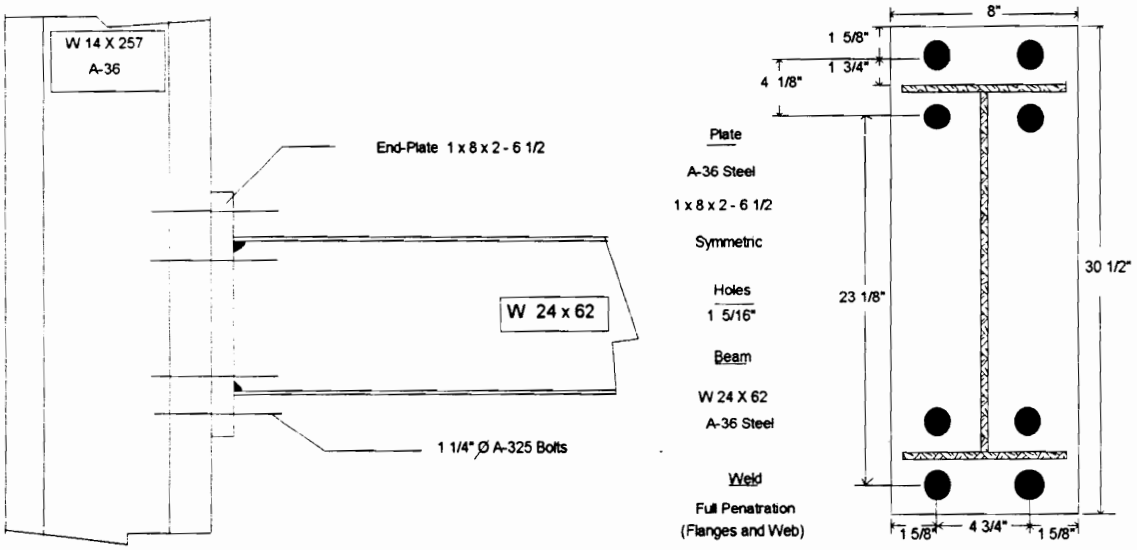

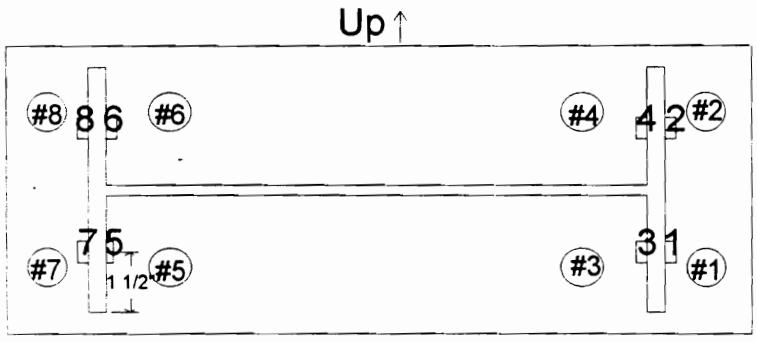

Strain Gauge and Bolt Location

Loading History for TEST 5/95

Load (kips) =>						Deflection (in.) =>								
Cycle 1	Cycle 2	Cycle 3	Cycle 4	Cycle 5	Cycle 6	Cycle 7	Cycle 8	Cycle 9	Cycle 10	Cycle 11	Cycle 12	Cycle 13	Cycle 14	Cycle 15
0	0	0	0	0	0	0	0	0	0	0	0	0	0	0
6	6	6	9	9	9	0.204	0.204	0.204	0.509	0.509	0.509	0.509	0.509	0.509
12	12	12	18	18	18	0.407	0.407	0.407	0.764	0.764	0.764	1.018	1.018	1.018
18	18	18	27	27	27	0.611	0.611	0.611	1.018	1.018	1.018	1.527	1.527	1.527
24	24	24	36	36	36	0.814	0.814	0.814	1.357	1.357	1.357	2.036	2.036	2.036
31.5	31.5	31.5	48	48	48	1.018	1.018	1.018	1.697	1.697	1.697	2.375	2.375	2.375
24	24	24	36	36	36	0.814	0.814	0.814	2.036	2.036	2.036	2.715	2.715	2.715
18	18	18	27	27	27	0.611	0.611	0.611	1.697	1.697	1.697	3.054	3.054	3.054
12	12	12	18	18	18	0.407	0.407	0.407	1.257	1.257	1.257	2.715	2.715	2.715
6	6	6	9	9	9	0.204	0.204	0.204	1.018	1.018	1.018	2.375	2.375	2.375
0	0	0	0	0	0	0	0	0	0.764	0.764	0.764	2.036	2.036	2.036
									0.509	0.509	0.509	1.527	1.527	1.527
									0	0	0	1.018	1.018	1.018
												0.509	0.509	0.509
												0	0	0

delta = $\pm$ 1.018 in.

Note: For more efficient use of space, only positive load and deflection values are tabulated.
A complete cycle included both positive and negative (load or deflection) excursions of equal magnitude.

TEST 5 / 95
W 24 x 62
1 in. End-Plate

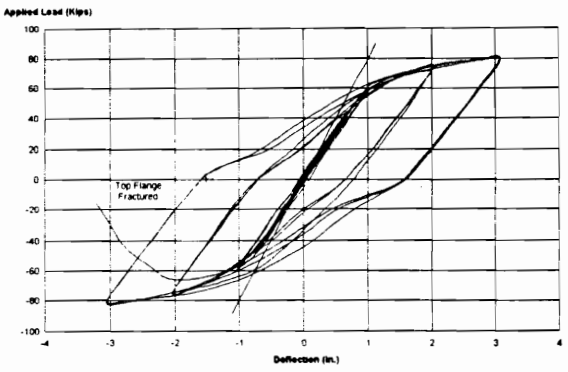

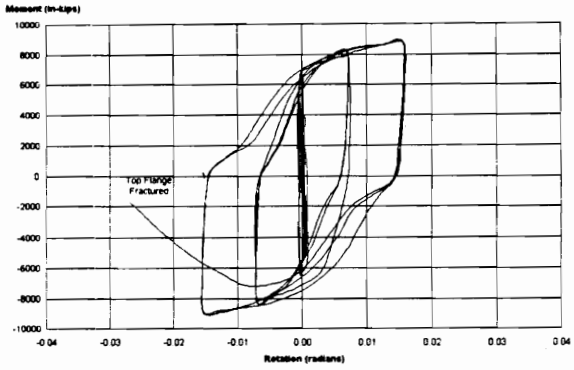

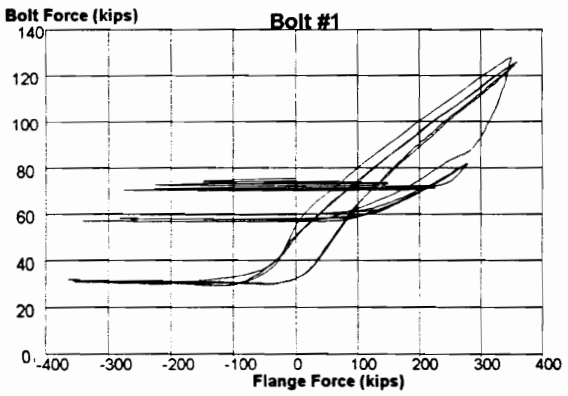

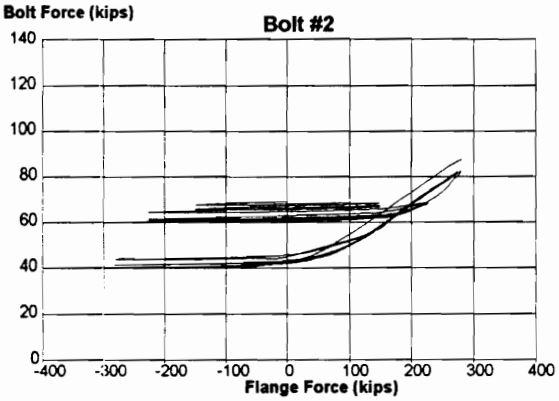

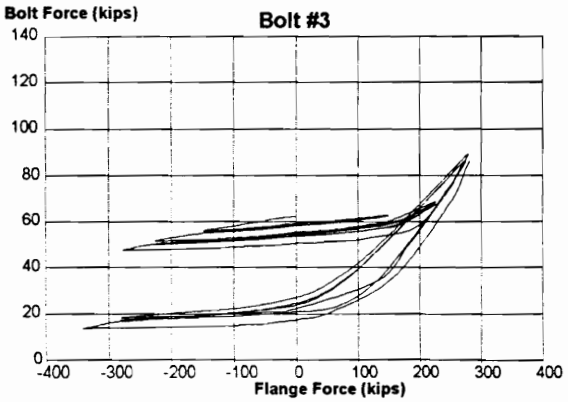

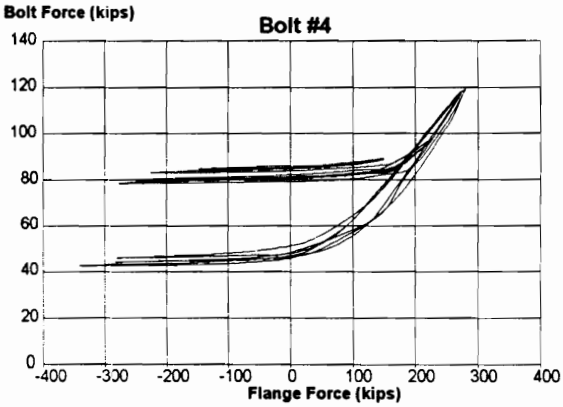

TEST 5 / 95
W 24 x 62
1 in. End-Plate

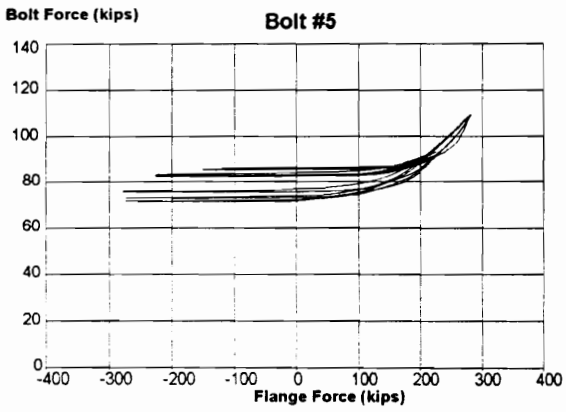

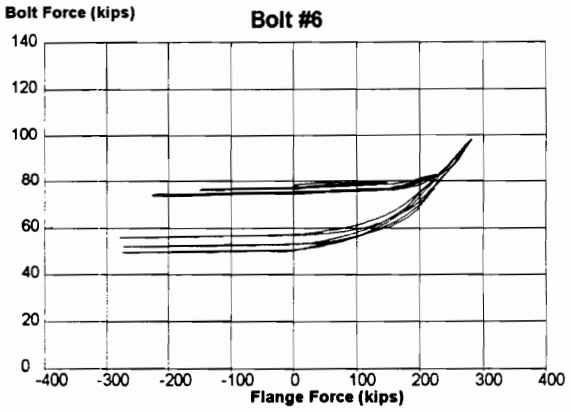

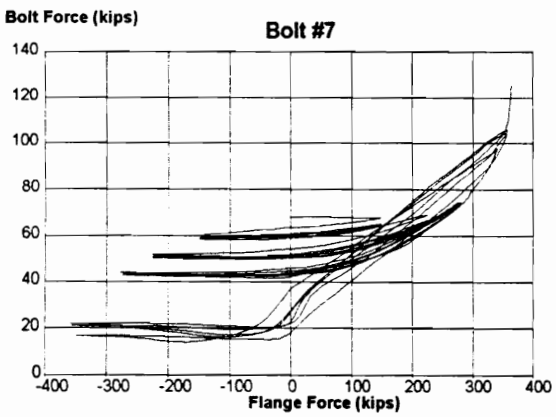

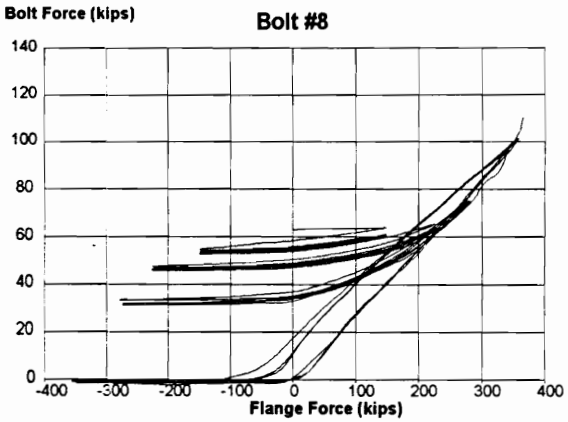

TEST 6 / 95

Connection End-Plate: Extended Four-Bolt, 2 in. Thick with Shims

Cycles Completed: 13

Failure Mode: Beam Flange Fracture

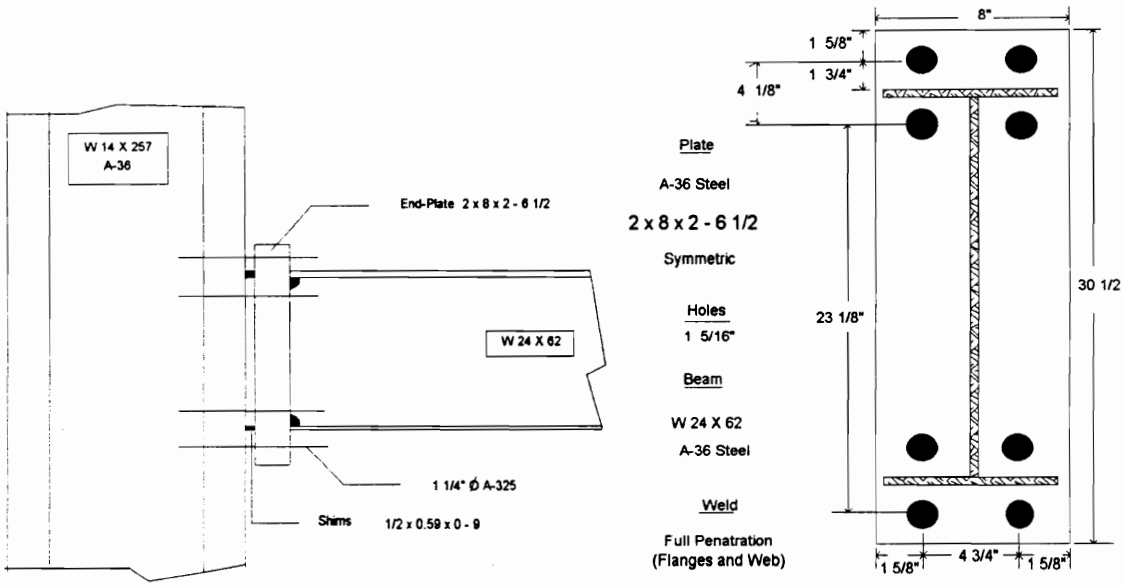

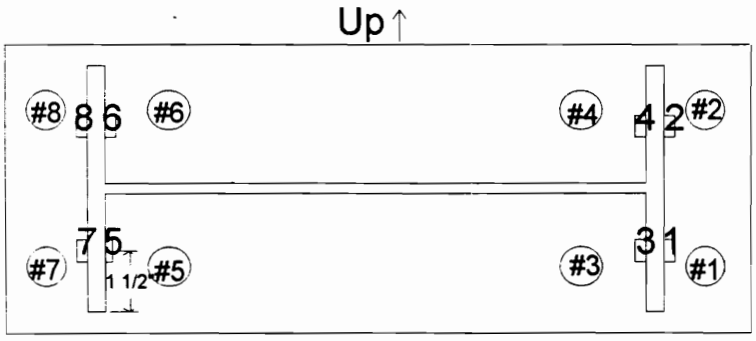

Strain Gauge and Bolt Location

Loading History for TEST 6/95

Load (kips)	=>					Deflection	(in.)	=>				
Cycle 1	Cycle 2	Cycle 3	Cycle 4	Cycle 5	Cycle 6	Cycle 7	Cycle 8	Cycle 9	Cycle 10	Cycle 11	Cycle 12	Cycle 13
0	0	0	0	0	0	0	0	0	0	0	0	0
6	6	6	9	9	9	0.184	0.184	0.184	0.461	0.461	0.461	0.461
12	12	12	18	18	18	0.369	0.369	0.369	0.692	0.692	0.692	0.922
18	18	18	27	27	27	0.553	0.553	0.553	0.922	0.922	0.922	1.383
24	24	24	36	36	36	0.738	0.738	0.738	1.229	1.229	1.229	1.844
30	30	30	45	45	45	0.922	0.922	0.922	1.537	1.537	1.537	2.151
24	24	24	36	36	36	0.738	0.738	0.738	1.844	1.844	1.844	2.459
18	18	18	27	27	27	0.553	0.553	0.553	1.537	1.537	1.537	2.766
12	12	12	18	18	18	0.369	0.369	0.369	1.229	1.229	1.229	2.459
6	6	6	9	9	9	0.184	0.184	0.184	0.922	0.922	0.922	2.151
0	0	0	0	0	0	0	0	0	0.692	0.692	0.692	1.844
									0.461	0.461	0.461	1.383
									0	0	0	0.922
												0.461
												0

delta = $\pm$ 0.922 in.

Note: For more efficient use of space, only positive load and deflection values are tabulated.
A complete cycle included both positive and negative (load or deflection) excursions of equal magnitude.

TEST 6 / 95
W 24 x 62
1 in. End-Plate

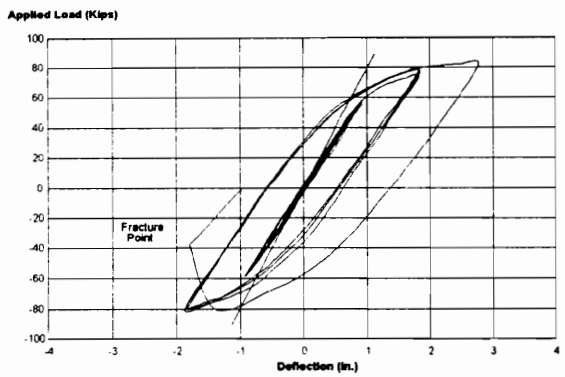

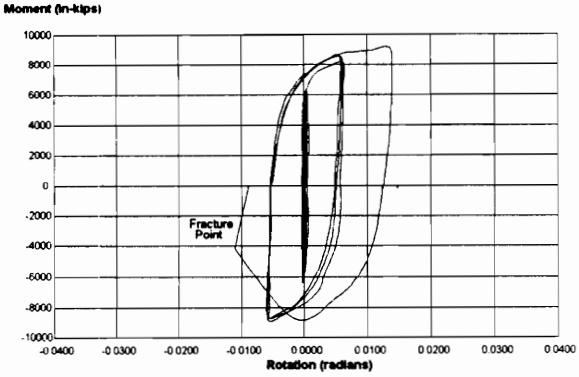

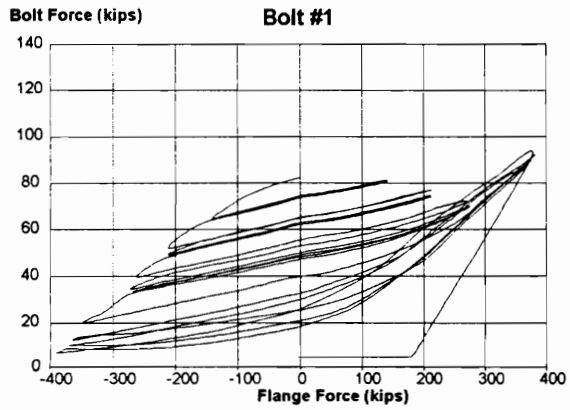

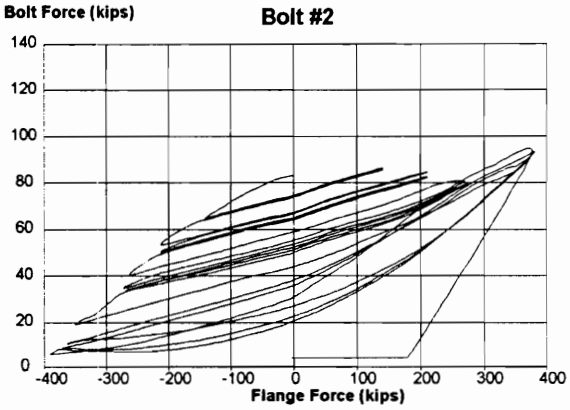

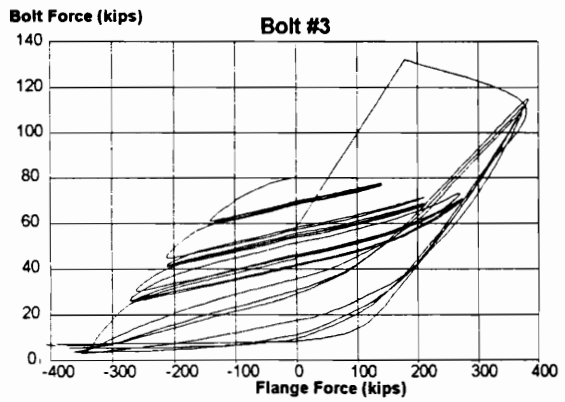

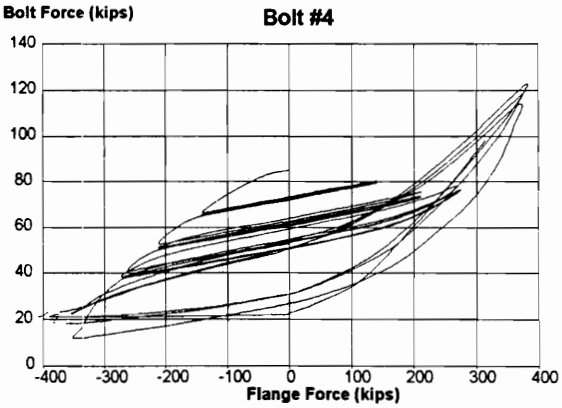

TEST 6/95
W 24 x 62
1 in. End-Plate

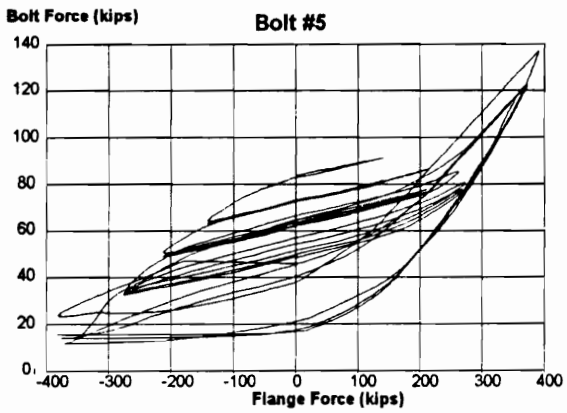

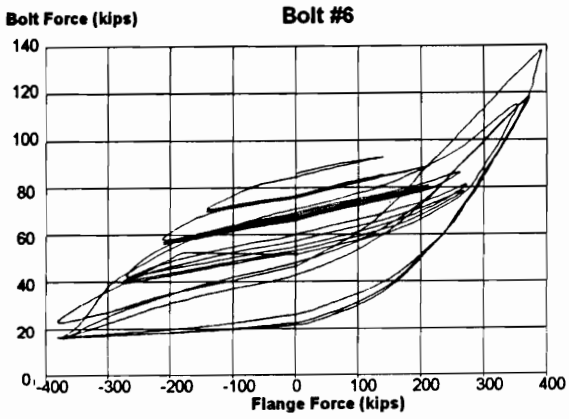

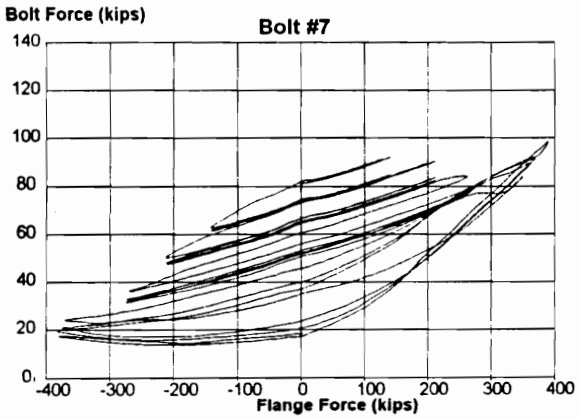

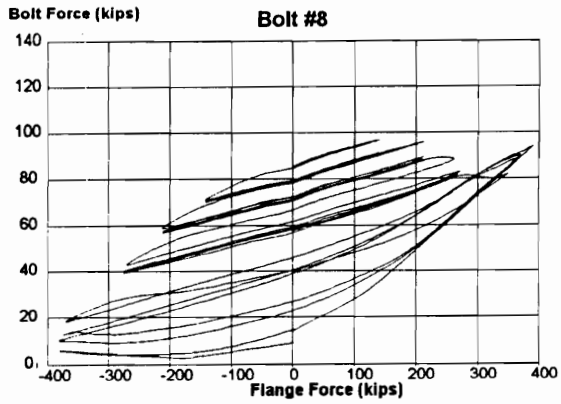

TEST 7 / 95

Connection End-Plate: Stiffened, Extended Four-Bolt, 1 in. Thick

Cycles Completed: 20

Failure Mode: Local Flange Buckling

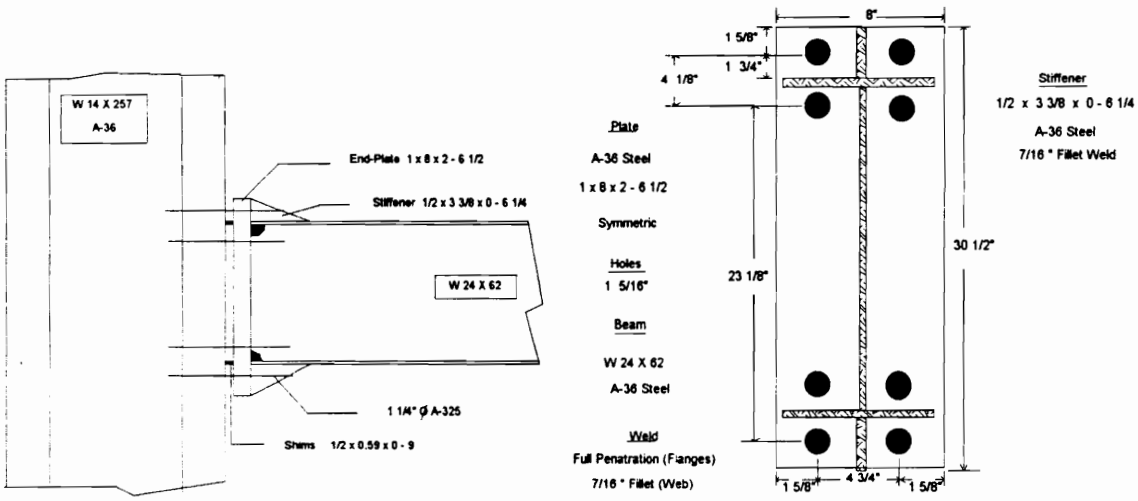

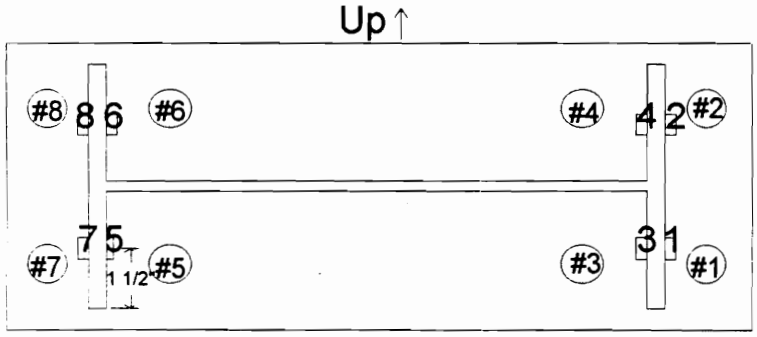

Strain Gauge and Bolt Location

Loading History for TEST 7/95

Load (kips)	=>					Deflection	(in.)		=>										
Cycle 1	Cycle 2	Cycle 3	Cycle 4	Cycle 5	Cycle 6	Cycle 7	Cycle 8	Cycle 9	Cycle 10	Cycle 11	Cycle 12	Cycle 13	Cycle 14	Cycle 15	Cycle 16	Cycle 17	Cycle 18	Cycle 19	Cycle 20
0	0	0	0	0	0	0	0	0	0	0	0	0	0	0	0	0	0	0	0
6	6	6	9	9	9	0.187	0.187	0.187	0.466	0.466	0.466	0.466	0.466	0.466	0.933	0.933	0.933	0.933	0.933
12	12	12	18	18	18	0.373	0.373	0.373	0.700	0.700	0.700	0.933	0.933	0.933	1.399	1.399	1.399	1.866	1.866
18	18	18	27	27	27	0.560	0.560	0.560	0.933	0.933	0.933	1.399	1.399	1.399	1.866	1.866	1.866	2.332	2.332
24	24	24	36	36	36	0.746	0.746	0.746	1.244	1.244	1.244	1.866	1.866	1.866	2.332	2.332	2.332	2.799	2.799
30	30	30	45	45	45	0.933	0.933	0.933	1.555	1.555	1.555	2.177	2.177	2.177	2.799	2.799	2.799	3.265	3.265
24	24	24	36	36	36	0.746	0.746	0.746	1.866	1.866	1.866	2.488	2.488	2.488	3.110	3.110	3.110	3.732	3.732
18	18	18	27	27	27	0.560	0.560	0.560	1.555	1.555	1.555	2.799	2.799	2.799	3.421	3.421	3.421	4.043	4.043
12	12	12	18	18	18	0.373	0.373	0.373	1.244	1.244	1.244	2.488	2.488	2.488	3.732	3.732	3.732	4.353	4.353
6	6	6	9	9	9	0.187	0.187	0.187	0.933	0.933	0.933	2.177	2.177	2.177	3.421	3.421	3.421	4.664	4.664
0	0	0	0	0	0	0	0	0	0.700	0.700	0.700	1.866	1.866	1.866	3.110	3.110	3.110	4.353	4.353
									0.466	0.466	0.466	1.399	1.399	1.399	2.799	2.799	2.799	4.043	4.043
									0	0	0	0.933	0.933	0.933	2.332	2.332	2.332	3.732	3.732
												0.466	0.466	0.466	1.866	1.866	1.866	3.265	3.265
												0	0	0	1.399	1.399	1.399	2.799	2.799
															0.933	0.933	0.933	2.332	2.332
															0	0	0	1.866	1.866
																		0.933	0.933
																		0	0

delta = $\pm$ 0.933 in.

Note: For more efficient use of space, only positive load and deflection values are tabulated.
A complete cycle included both positive and negative (load or deflection) excursions of equal magnitude.

TEST 7 / 95
W 24 x 62
1 in. End-Plate

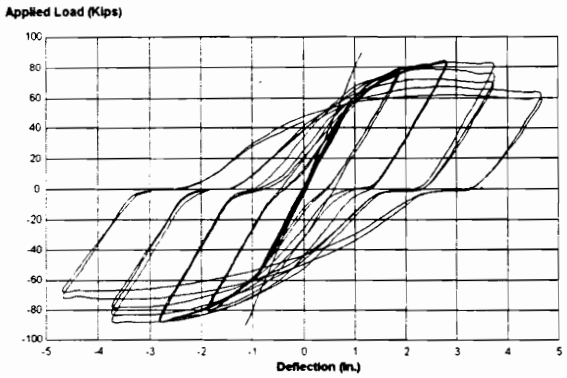

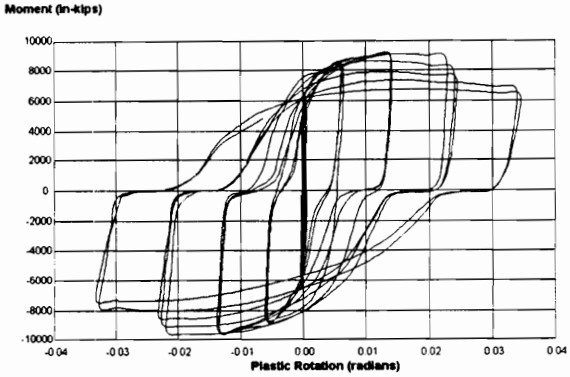

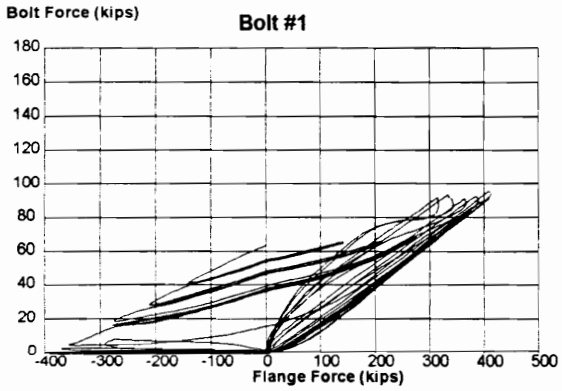

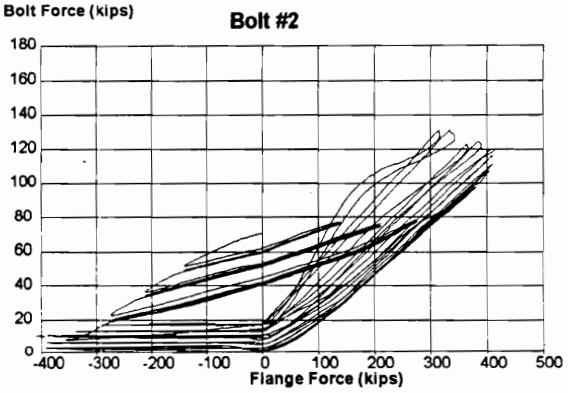

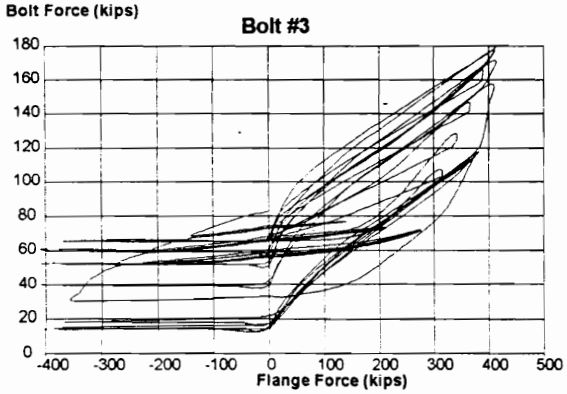

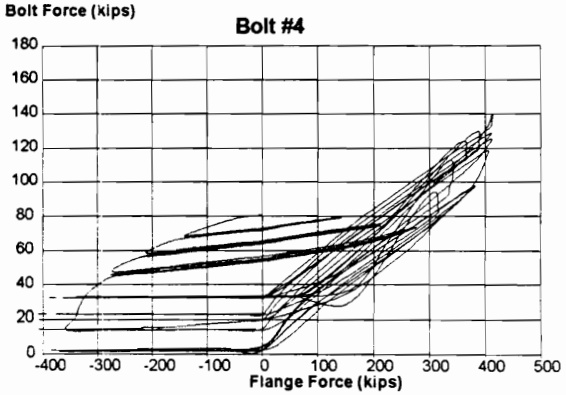

TEST 7 / 95
W 24 x 62
1 in. End-Plate

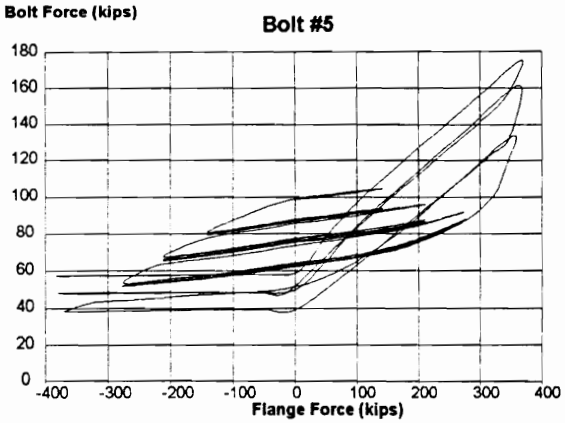

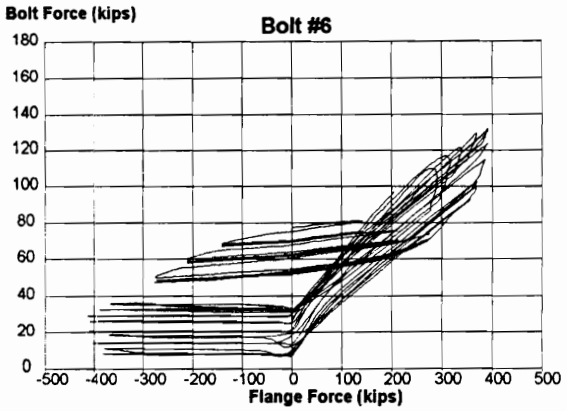

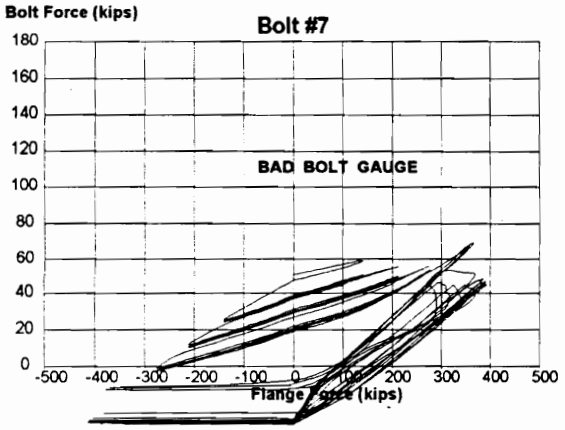

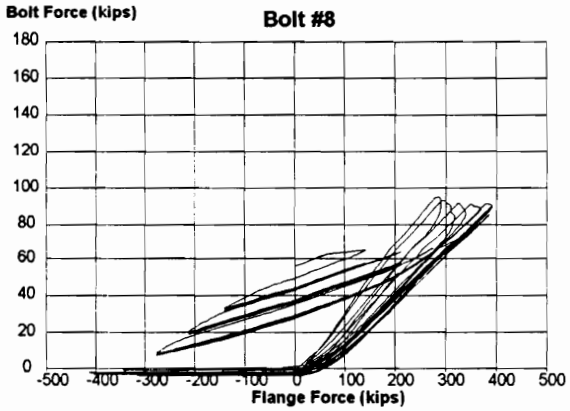

TESTS RH - 2, RH - 2A & RH - 3

Beam Section W 24 x 62, A-36 Steel

$d = 23.74$ in. $t_w = 0.43$ in. $t_f = 0.59$ in $b_f = 7.04$ in.

$S_x = 131$ in^4. $Z_x = 153$ in^3.

Specimen Preparation and Welding Technique

End-Plates were saw cut to length and ground if required to smooth rough edges. No preheating of end-plate and/or beam was conducted. Connection was welded via GMAW technique utilizing .035 in. E70T electrode Lincoln wire.

Beam Coupon Tests of 09/18/95 & 10/30/95

Web # 1 (#1197 & #1198)

.424 x 1.503 = area of 0.6373
Lower Yield Stress - 46,000 psi.
Tensile Strength - 62,100 psi.
Elongation (8 in. base) - 31.3%

Web # 2 (#1199)

.423 x 1.502 = area of 0.6353
Lower Yield Stress - 47,240 psi.
Tensile Strength - 62,250 psi.
Elongation (8 in. base) - 32.8%

Web # 3 (#21)

.419 x 1.500 = area of 0.6285
Lower Yield Stress - 45,400 psi.
Tensile Strength - 62,700 psi.
Elongation (8 in. base) - 33.59%

Web # 4 (#22)

.418 x 1.500 = area of 0.6270
Lower Yield Stress - 47,300 psi.
Tensile Strength - 64,385 psi.
Elongation (8 in. base) - 28.91%

Flange # 1 (#1201)

.558 x 1.501 = area of 0.8376
Lower Yield Stress - 46,620 psi.
Tensile Strength - 63,270 psi.
Elongation (8 in. base) - 21.9%

Flange # 2 (#1202)

.581 x 1.503 = area of 0.8732
Lower Yield Stress - 48,000 psi.
Tensile Strength - 63,700 psi.
Elongation (8 in. base) - 28.1%

Flange # 3 (#23)

.582 x 1.50 = area of 0.8730
Lower Yield Stress - 49,500 psi.
Tensile Strength - 65,000 psi.
Elongation (8 in. base) - 27.34%

Flange # 4 (#24)

.587 x 1.503 = area of 0.8823
Lower Yield Stress - 48,000 psi.
Tensile Strength - 64,250 psi.
Elongation (8 in. base) - 23.44%

Web Strengths:	**46,487 psi (yield)**	**62,858 psi (ultimate)**
Flange Strengths:	**47,940 psi (yield)**	**64,055 psi (ultimate)**

TEST RH - 2

Connection End-Plate: Extended Four-Bolt, 1 in. Thick

Cycles Completed: 20

Failure Mode: Local Flange Buckling

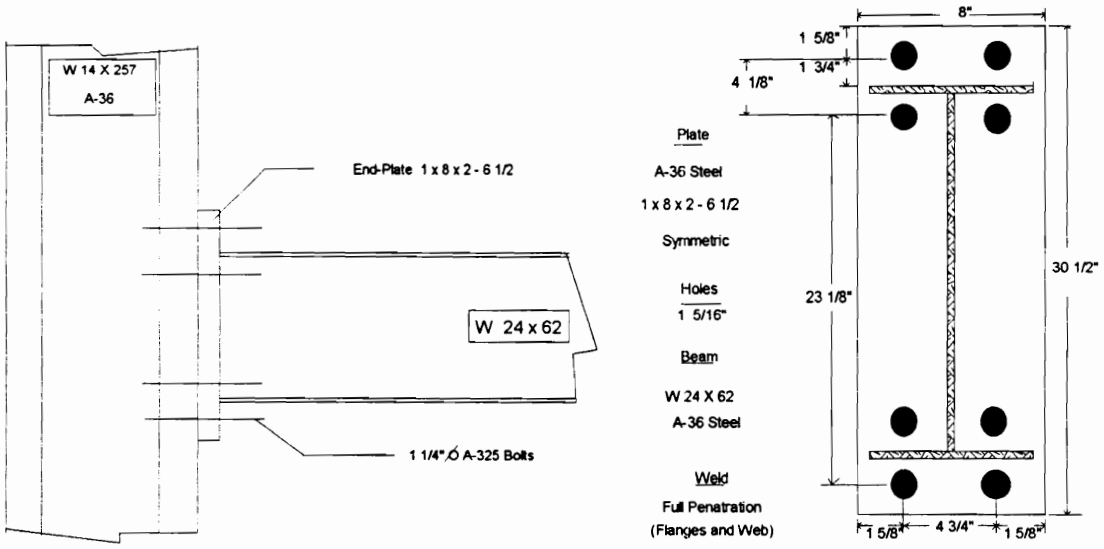

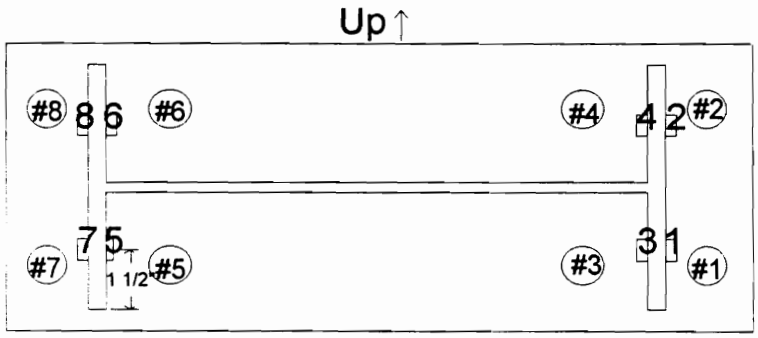

Strain Gauge and Bolt Location

Loading History for TEST RH - 2

Load (kips) => Deflection (in.) =>

Cycle 1	Cycle 2	Cycle 3	Cycle 4	Cycle 5	Cycle 6	Cycle 7	Cycle 8	Cycle 9	Cycle 10	Cycle 11	Cycle 12	Cycle 13	Cycle 14	Cycle 15	Cycle 16	Cycle 17	Cycle 18	Cycle 19	Cycle 20
0	0	0	0	0	0	0	0	0	0	0	0	0	0	0	0	0	0	0	0
6	6	6	9	9	9	0.185	0.185	0.185	0.462	0.462	0.462	0.462	0.462	0.462	0.925	0.925	0.925	0.925	0.925
12	12	12	18	18	18	0.370	0.370	0.370	0.694	0.694	0.694	0.925	0.925	0.925	1.387	1.387	1.387	1.849	1.849
18	18	18	27	27	27	0.555	0.555	0.555	0.925	0.925	0.925	1.387	1.387	1.387	1.849	1.849	1.849	2.312	2.312
24	24	24	36	36	36	0.740	0.740	0.740	1.233	1.233	1.233	1.849	1.849	1.849	2.312	2.312	2.312	2.774	2.774
28	28	28	42	42	42	0.925	0.925	0.925	1.541	1.541	1.541	2.158	2.158	2.158	2.774	2.774	2.774	3.236	3.236
24	24	24	36	36	36	0.740	0.740	0.740	1.849	1.849	1.849	2.466	2.466	2.466	3.082	3.082	3.082	3.699	3.699
18	18	18	27	27	27	0.555	0.555	0.555	1.541	1.541	1.541	2.774	2.774	2.774	3.390	3.390	3.390	4.007	4.007
12	12	12	18	18	18	0.370	0.370	0.370	1.233	1.233	1.233	2.466	2.466	2.466	3.699	3.699	3.699	4.315	4.315
6	6	6	9	9	9	0.185	0.185	0.185	0.925	0.925	0.925	2.158	2.158	2.158	3.390	3.390	3.390	4.623	4.623
0	0	0	0	0	0	0	0	0	0.694	0.694	0.694	1.849	1.849	1.849	3.082	3.082	3.082	4.315	4.315
									0.462	0.462	0.462	1.387	1.387	1.387	2.774	2.774	2.774	4.007	4.007
									0	0	0	0.925	0.925	0.925	2.312	2.312	2.312	3.699	3.699
												0.462	0.462	0.462	1.849	1.849	1.849	3.236	3.236
												0	0	0	1.387	1.387	1.387	2.774	2.774
															0.925	0.925	0.925	2.312	2.312
															0	0	0	1.849	1.849
																		0.925	0.925
																		0	0

delta = $\pm$ 0.925 in.

Note: For more efficient use of space, only positive load and deflection values are tabulated.
A complete cycle included both positive and negative (load or deflection) excursions of equal magnitude.

TEST RH-2
W 24 x 62
1 in. End-Plate

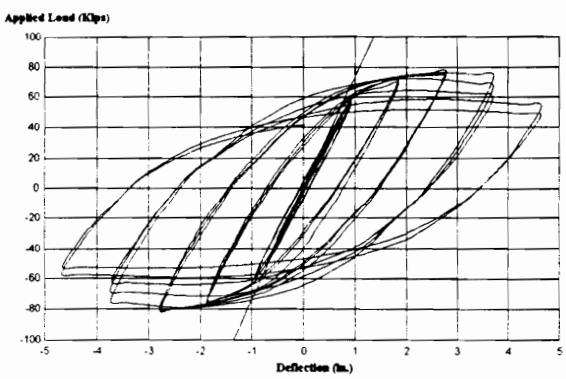

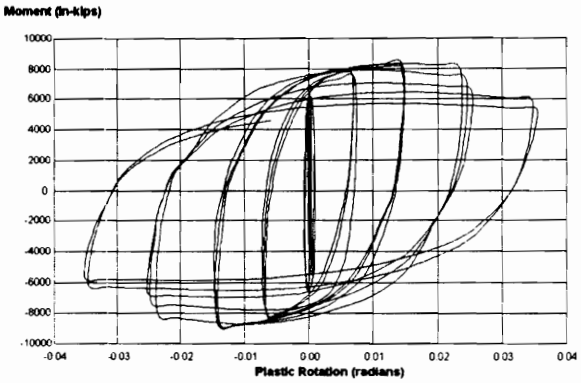

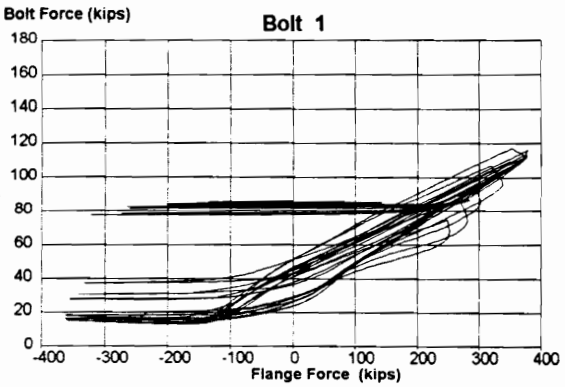

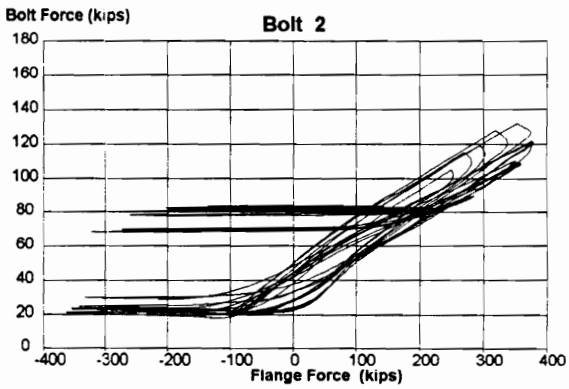

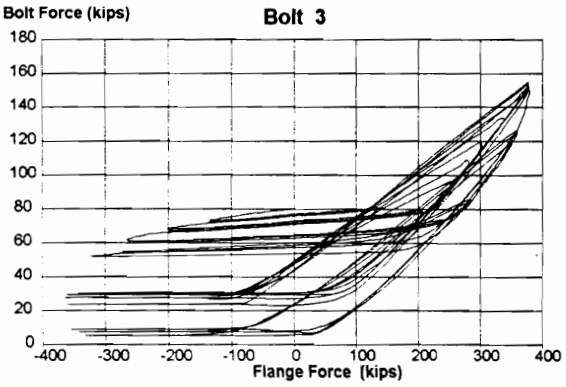

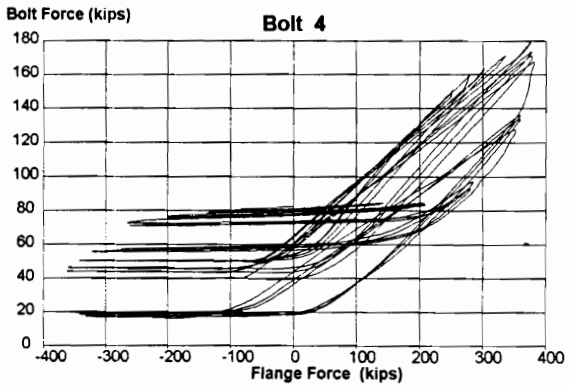

TEST RH-2
W 24 x 62
1 in. End-Plate

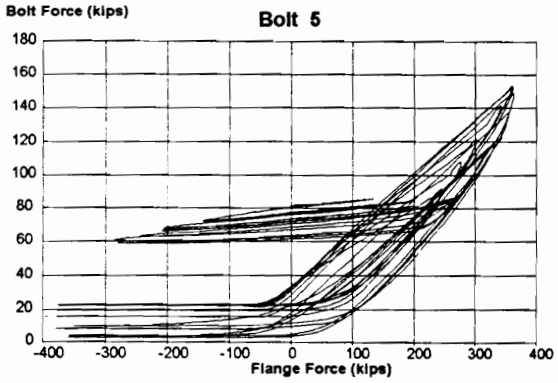

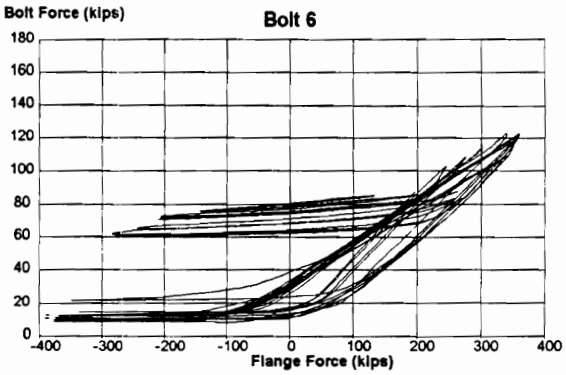

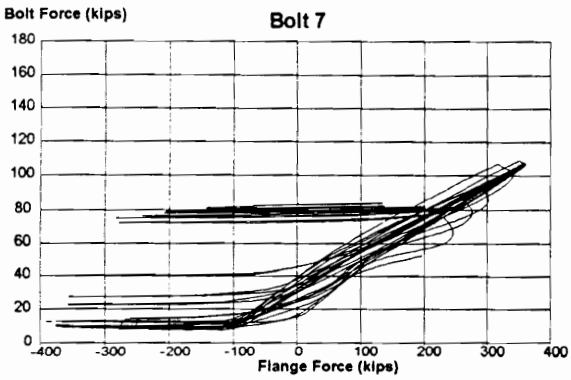

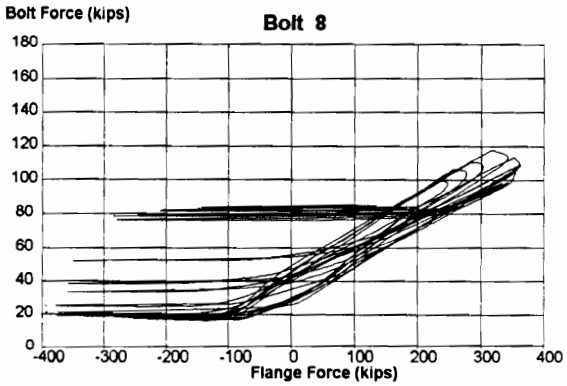

TEST RH - 2A

Connection End-Plate: Extended Four-Bolt, 1 in. Thick

Cycles Completed: 19

Failure Mode: Beam Flange Fracture

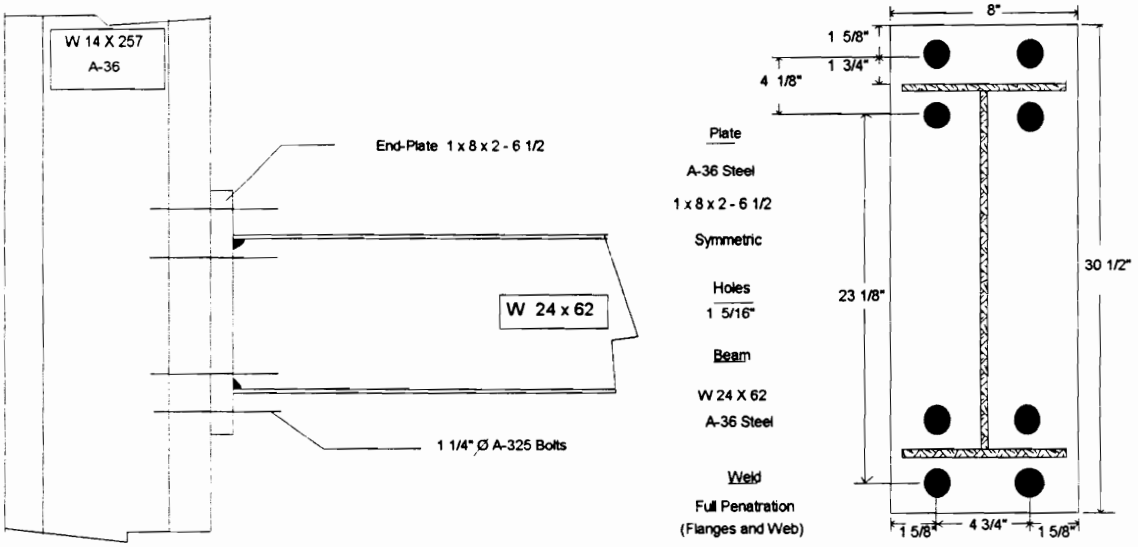

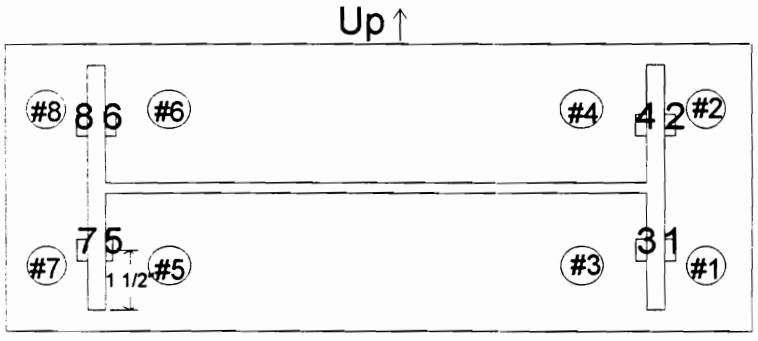

Strain Gauge and Bolt Location

Loading History for TEST RH - 2A

Load (kips) => Deflection (in.) =>

Cycle 1	Cycle 2	Cycle 3	Cycle 4	Cycle 5	Cycle 6	Cycle 7	Cycle 8	Cycle 9	Cycle 10	Cycle 11	Cycle 12	Cycle 13	Cycle 14	Cycle 15	Cycle 16	Cycle 17	Cycle 18	Cycle 19
0	0	0	0	0	0	0	0	0	0	0	0	0	0	0	0	0	0	0
6	6	6	9	9	9	0.180	0.180	0.180	0.450	0.450	0.450	0.450	0.450	0.450	0.899	0.899	0.899	0.899
12	12	12	18	18	18	0.360	0.360	0.360	0.675	0.675	0.675	0.899	0.899	0.899	1.349	1.349	1.349	1.799
18	18	18	27	27	27	0.540	0.540	0.540	0.899	0.899	0.899	1.349	1.349	1.349	1.799	1.799	1.799	2.248
24	24	24	36	36	36	0.719	0.719	0.719	1.199	1.199	1.199	1.799	1.799	1.799	2.248	2.248	2.248	2.698
28	28	28	42	42	42	0.899	0.899	0.899	1.499	1.499	1.499	2.098	2.098	2.098	2.698	2.698	2.698	3.148
24	24	24	36	36	36	0.719	0.719	0.719	1.799	1.799	1.799	2.398	2.398	2.398	2.998	2.998	2.998	3.597
18	18	18	27	27	27	0.540	0.540	0.540	1.499	1.499	1.499	2.698	2.698	2.698	3.298	3.298	3.298	3.897
12	12	12	18	18	18	0.360	0.360	0.360	1.199	1.199	1.199	2.398	2.398	2.398	3.597	3.597	3.597	4.197
6	6	6	9	9	9	0.180	0.180	0.180	0.899	0.899	0.899	2.098	2.098	2.098	3.298	3.298	3.298	4.497
0	0	0	0	0	0	0	0	0	0.675	0.675	0.675	1.799	1.799	1.799	2.998	2.998	2.998	4.197
									0.450	0.450	0.450	1.349	1.349	1.349	2.698	2.698	2.698	3.897
									0	0	0	0.899	0.899	0.899	2.248	2.248	2.248	3.597
												0.450	0.450	0.450	1.799	1.799	1.799	3.148
												0	0	0	1.349	1.349	1.349	2.698
															0.899	0.899	0.899	2.248
															0	0	0	1.799
																		0.899
																		0

delta = $\pm$ 0.899 in.

Note: For more efficient use of space, only positive load and deflection values are tabulated.
A complete cycle included both positive and negative (load or deflection) excursions of equal magnitude.

TEST RH - 2A
W 24 x 62
1 in. End-plate

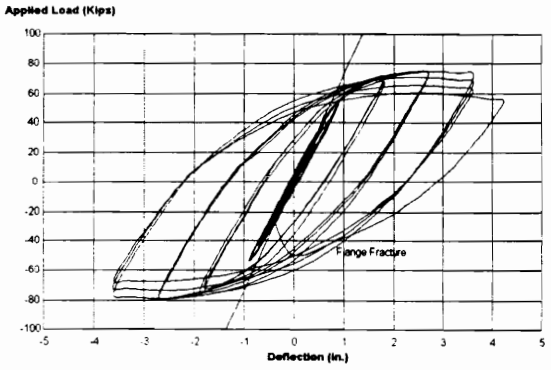

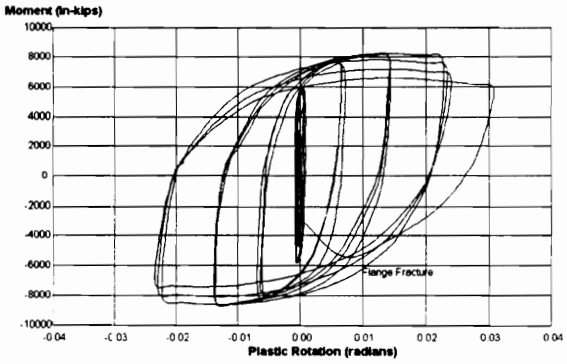

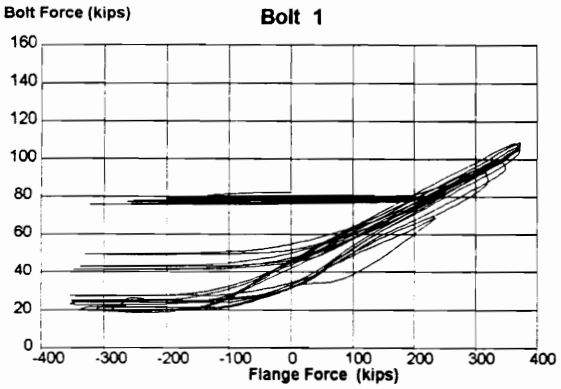

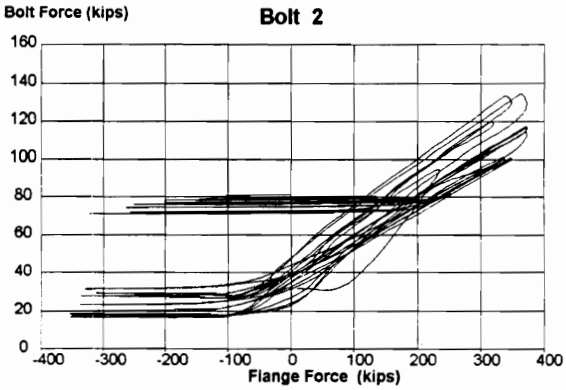

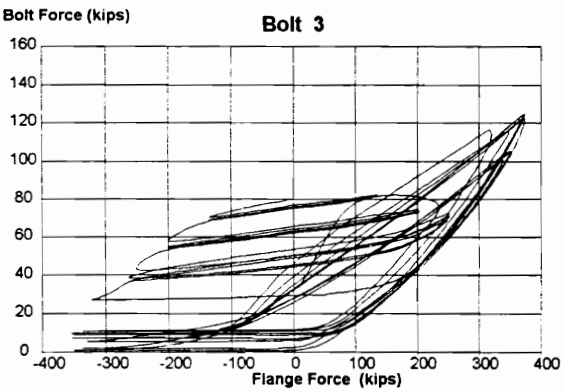

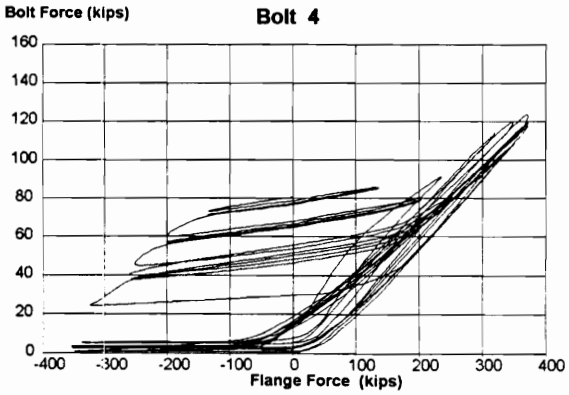

TEST RH - 2A
W 24 x 62
1 in. End-plate

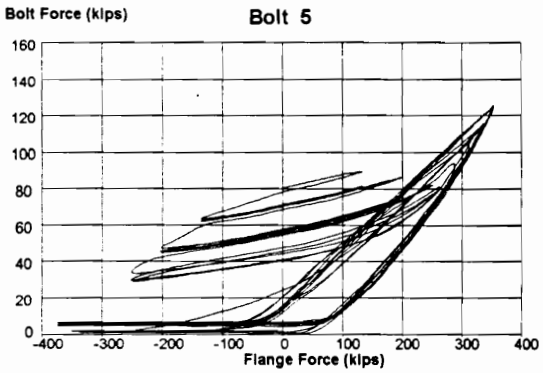

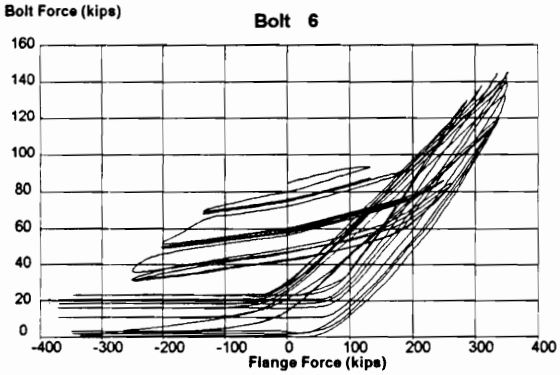

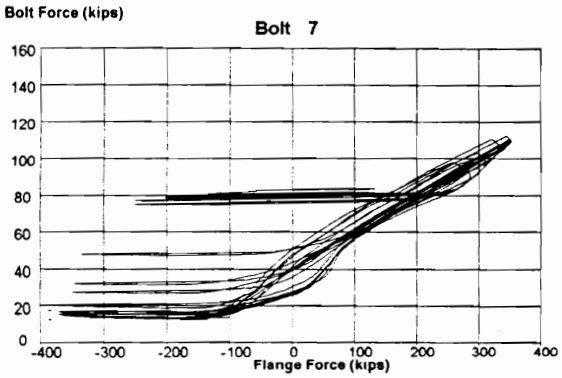

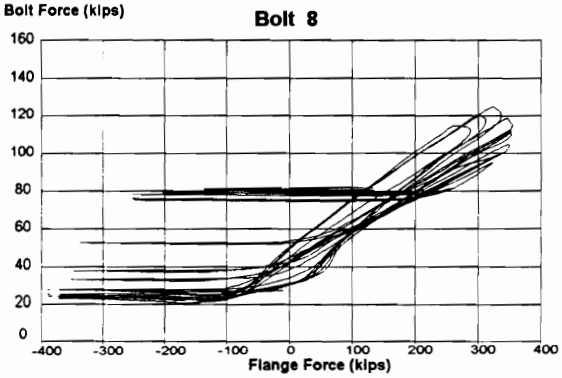

TEST RH - 3

Connection End-Plate: Extended Four-Bolt, 1 in. Thick

Cycles Completed: 15

Failure Mode: Beam Flange Fracture

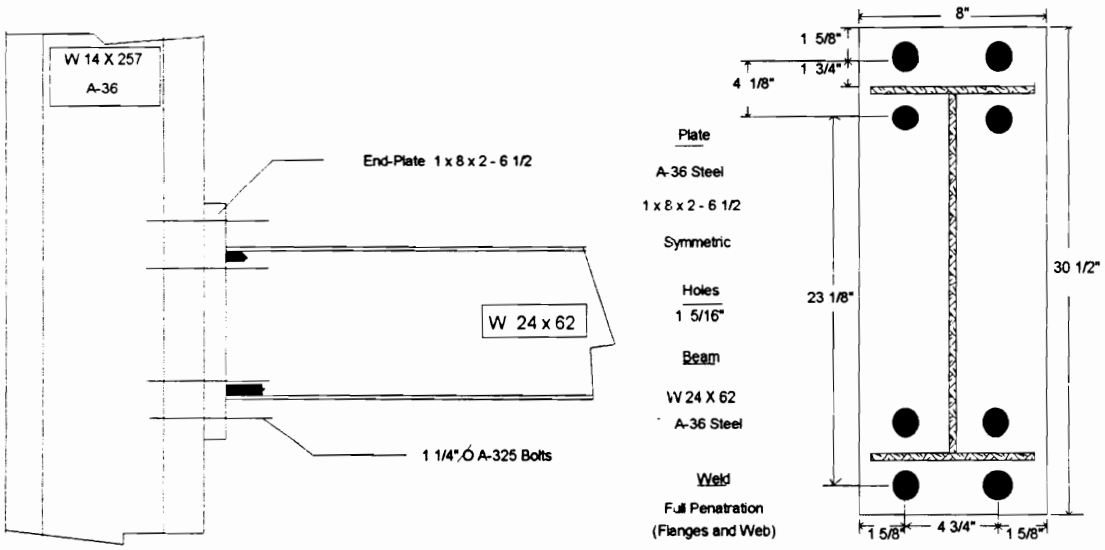

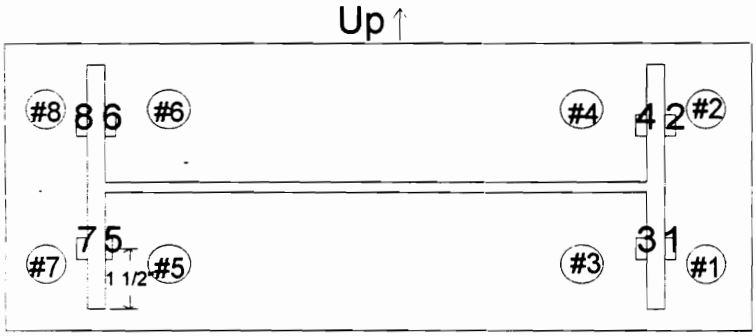

Strain Gauge and Bolt Location

Loading History for TEST RH - 3

Load (kips)	=>					Deflection	(in.)		=>					
Cycle 1	Cycle 2	Cycle 3	Cycle 4	Cycle 5	Cycle 6	Cycle 7	Cycle 8	Cycle 9	Cycle 10	Cycle 11	Cycle 12	Cycle 13	Cycle 14	Cycle 15
0	0	0	0	0	0	0	0	0	0	0	0	0	0	0
6	6	6	9	9	9	0.180	0.180	0.180	0.450	0.450	0.450	0.450	0.450	0.450
12	12	12	18	18	18	0.360	0.360	0.360	0.675	0.675	0.675	0.900	0.900	0.900
18	18	18	27	27	27	0.540	0.540	0.540	0.900	0.900	0.900	1.350	1.350	1.350
24	24	24	36	36	36	0.720	0.720	0.720	1.200	1.200	1.200	1.800	1.800	1.800
28	28	28	42	42	42	0.900	0.900	0.900	1.500	1.500	1.500	2.101	2.101	2.101
24	24	24	36	36	36	0.720	0.720	02019	1.800	1.800	1.800	2.401	2.401	2.401
18	18	18	27	27	27	0.540	0.540	0.540	1.500	1.500	1.500	2.701	2.701	2.701
12	12	12	18	18	18	0.360	0.360	0.360	1.200	1.200	1.200	2.401	2.401	2.401
6	6	6	9	9	9	0.180	0.180	0.180	0.900	0.900	0.900	2.101	2.101	2.101
0	0	0	0	0	0	0	0	0	0.675	0.675	0.675	1.800	1.800	1.800
									0.450	0.450	0.450	1.350	1.350	1.350
									0	0	0	0.900	0.900	0.900
												0.450	0.450	0.450
												0	0	0

delta = $\pm$ 0.900 in.

Note: For more efficient use of space, only positive load and deflection values are tabulated.
A complete cycle included both positive and negative (load or deflection) excursions of equal magnitude.

TEST RH - 3
W 24 x 62
1 in. End-Plate

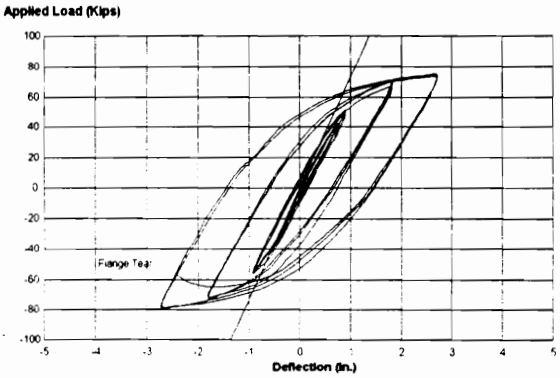

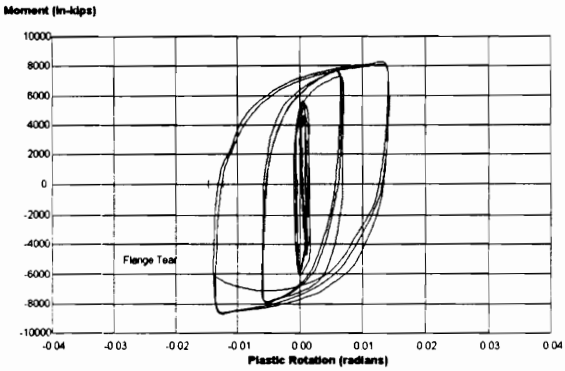

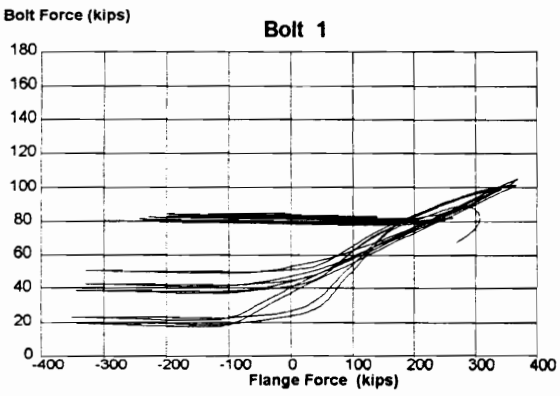

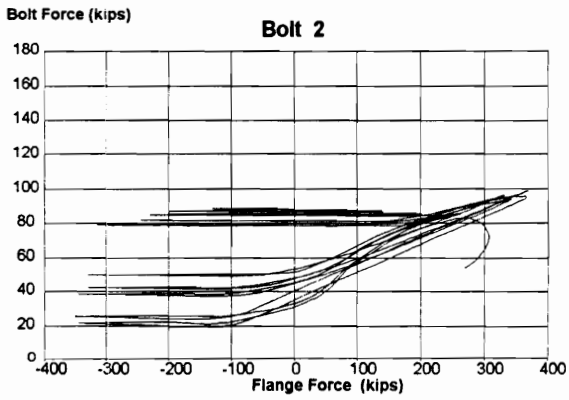

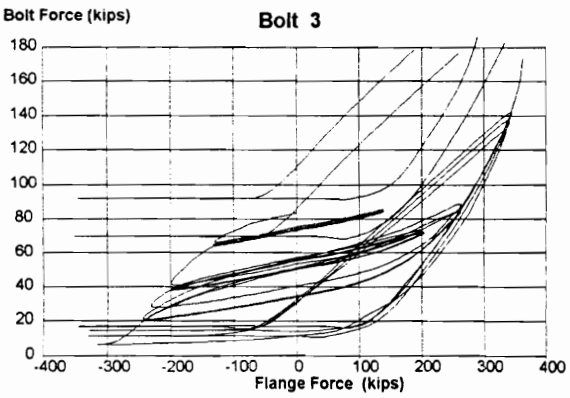

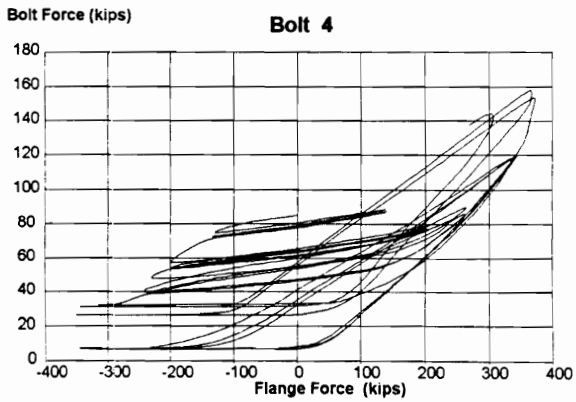

TEST RH - 3
W 24 x 62
1 in. End-Plate

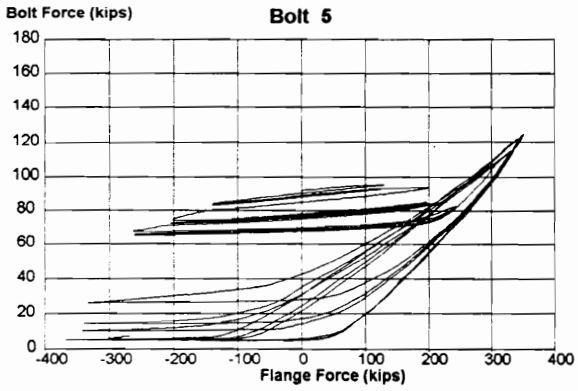

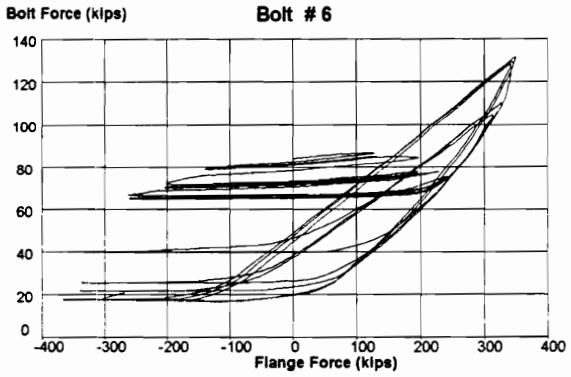

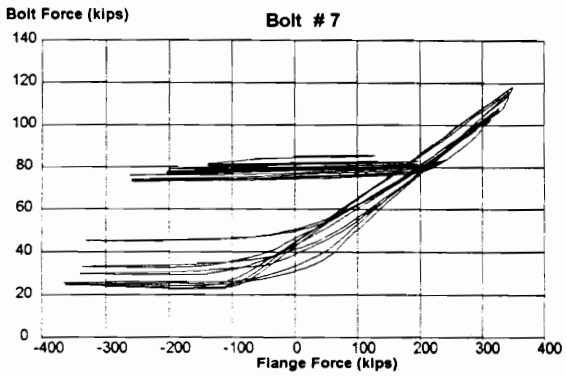

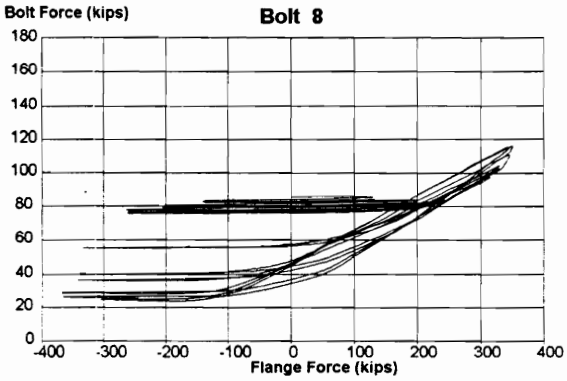

APPENDIX E

W 24 X 76 BEAM TEST RESULTS AND DATA

TESTS RH - 1, RH - 1A, RH - 1B & 8 / 95 - 9 / 95

Beam Section W 24 x 76, A-36 Steel

$d = 23.92$ in. $t_w = 0.44$ in. $t_f = 0.68$ in $b_f = 8.99$ in.

$S_x = 176$ in^4. $Z_x = 200$ in^3.

Specimen Preparation and Welding Technique

End-Plates were flame cut to length and ground if required to smooth rough edges. Preheating of end-plate and/or beam was conducted as required by AWS. Connection was welded via flux core technique utilizing 5/64 in. E70 electrode Lincoln wire.

Beam Coupon tests of 08/22/95

Web # 1 (#1176)

.461 x 1.504 = area of 0.6933

Lower Yield Stress - 66,000 psi.
Tensile Strength - 77,560 psi.
Elongation (8 in. base) - 25%

Web # 2 (#1177)

.459 x 1.504 = area of 0.6903

Lower Yield Stress - 64,530 psi.
Tensile Strength - 77,290 psi.
Elongation (8 in. base) - 25%

Web # 3 (#1179)

.456 x 1.500 = area of 0.6840

Lower Yield Stress - 64,000 psi.
Tensile Strength - 79,190 psi.
Elongation (8 in. base) - 25.8%

Flange # 1 (#1187) (top)

.618 x 1.502 = area of 0.9282

Lower Yield Stress - 58,500 psi.
Tensile Strength - 73,990 psi.
Elongation (8 in. base) - 28.1%

Flange # 2 (#1188) (top)

.685 x 1.503 = area of 1.0296

Lower Yield Stress - 57,500 psi.
Tensile Strength - 73,990 psi.
Elongation (8 in. base) - 28.1%

Flange # 3 (#1189) (bottom)

.600 x 1.503 = area of 0.9018

Lower Yield Stress - 60,100 psi.
Tensile Strength - 74,890 psi.
Elongation (8 in. base) - 27.3%

Flange # 4 (#1190) (bottom)

.685 x 1.503 = area of 1.0296

Lower Yield Stress - 58,000 psi.
Tensile Strength - 74,000 psi.
Elongation (8 in. base) - 25 %

Web Strengths:	**64,840 psi (yield)**	**78,000 psi (ultimate)**
Flange Strengths:	**58,520 psi (yield)**	**74,220 psi (ultimate)**

TESTS RH - 1, RH - 1A & RH - 1B

The same connection was used for all three tests.
RH - 1 and RH -1A were not tested to failure. (See Chapter IV for further details.)

Connection End-Plate: Extended Four-Bolt, 1 1/4 in. Thick

Cycles Completed: 16 (Test RH - 1B)

Failure Mode: Beam Flange Fracture (Test RH - 1B)

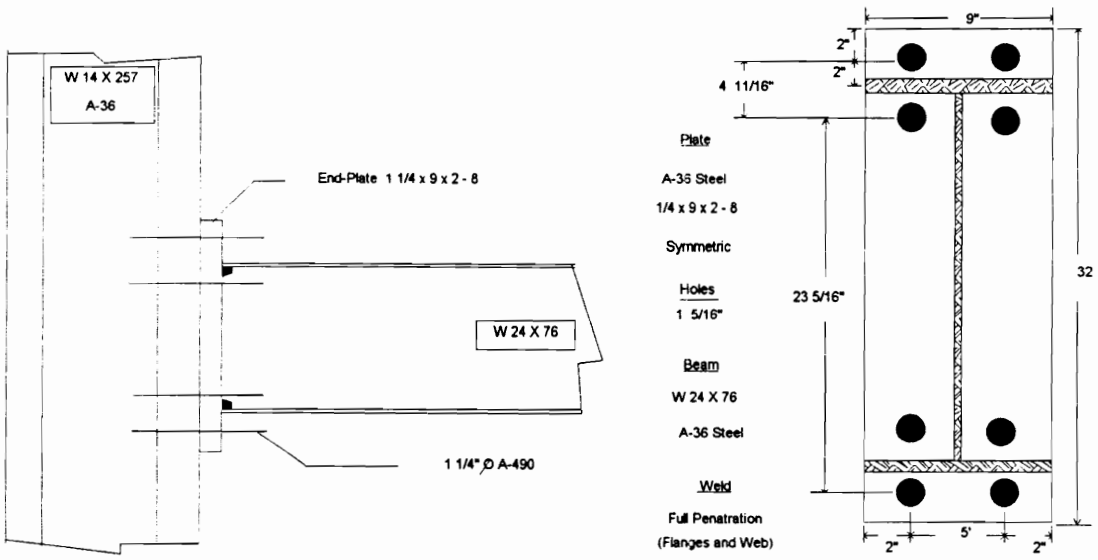

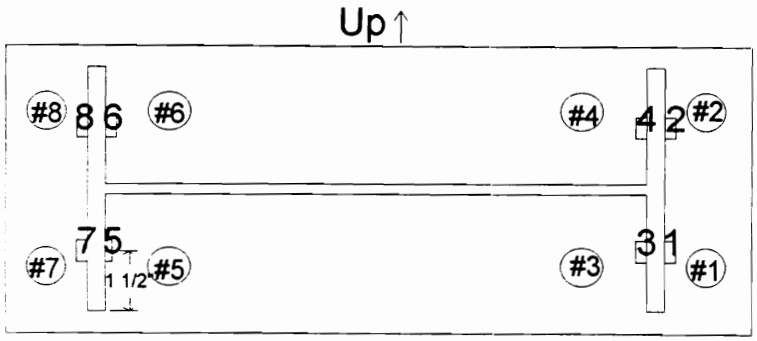

Strain Gauge and Bolt Location

Loading History for TEST RH - 1B

Load (kips) =>						Deflection (in.) =>									
Cycle 1	Cycle 1	Cycle 3	Cycle 4	Cycle 5	Cycle 6	Cycle 7	Cycle 8	Cycle 9	Cycle 10	Cycle 11	Cycle 12	Cycle 13	Cycle 14	Cycle 15	Cycle 16
0	0	0	0	0	0	0	0	0	0	0	0	0	0	0	0
10	10	10	22	22	22	.0228	.0228	.0228	0.571	0.571	0.571	0.571	0.571	0.571	1.142
20	20	20	33	33	33	0.457	0.457	0.457	0.857	0.857	0.857	1.142	1.142	1.142	1.713
30	30	30	44	44	44	0.685	0.685	0.685	1.142	1.142	1.142	1.713	1.713	1.713	2.284
40	40	40	55	55	55	0.914	0.914	0.914	1.523	1.523	1.523	2.284	2.284	2.284	2.855
44	44	44	66	66	66	1.142	1.142	1.142	1.903	1.903	1.903	2.665	2.665	2.665	3.426
40	40	40	55	55	55	0.914	0.914	0.914	2.284	2.284	2.284	3.045	3.045	3.045	3.807
30	30	30	44	44	44	0.685	0.685	0.685	1.903	1.903	1.903	3.426	3.426	3.426	4.187
20	20	20	33	33	33	0.457	0.457	0.457	1.523	1.523	1.523	3.045	3.045	3.045	4.568
10	10	10	22	22	22	0.228	0.228	0.228	1.142	1.142	1.142	2.665	2.665	2.665	4.187
0	0	0	0	0	0	0	0	0	0.857	0.857	0.857	2.284	2.284	2.284	3.807
									0.571	0.571	0.571	1.712	1.712	1.712	3.426
									0	0	0	1.142	1.142	1.142	2.855
												0.571	0.571	0.571	2.284
												0	0	0	1.713
															1.142
															0

delta = $\pm$ 1.1420 in.

Note: For more efficient use of space, only positive load and deflection values are tabulated.
A complete cycle included both positive and negative (load or deflection) excursions of equal magnitude.

TEST RH - 1B
W 24 x 76
1 1/4 in. End-Plate

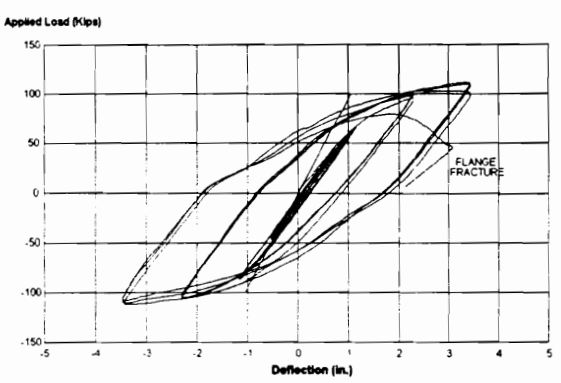

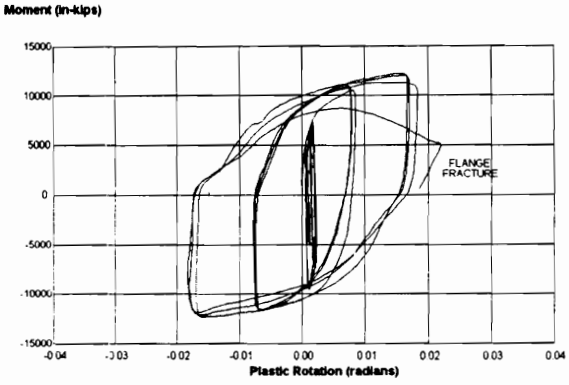

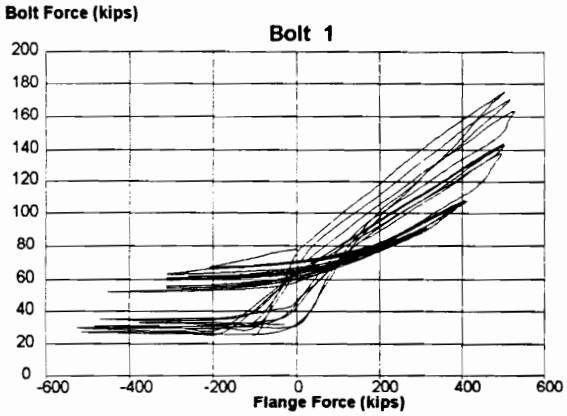

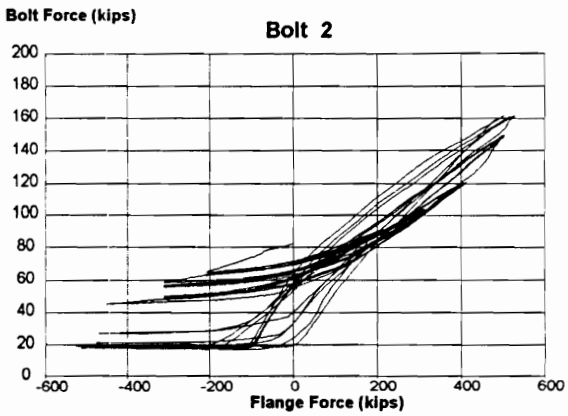

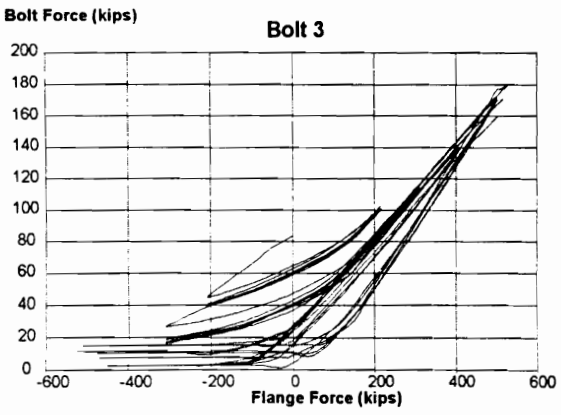

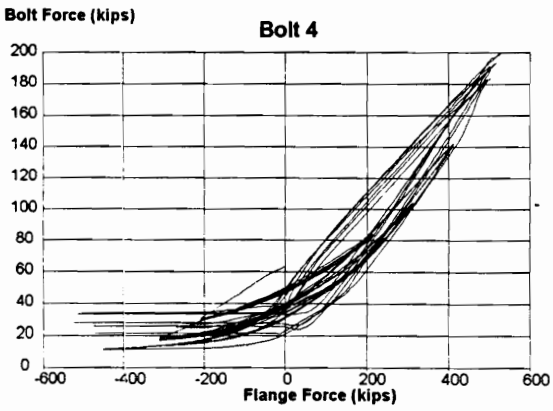

TEST RH - 1B
W 24 x 76
1 1/4 in. End-Plate

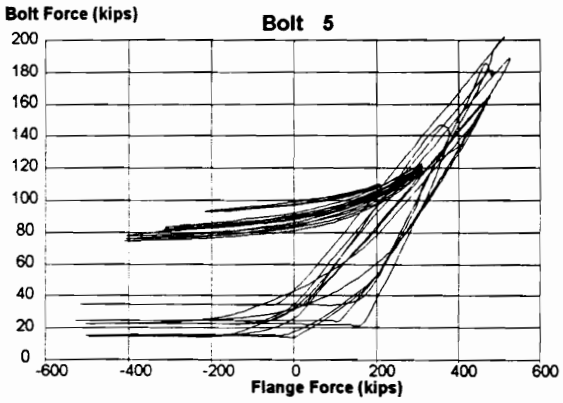

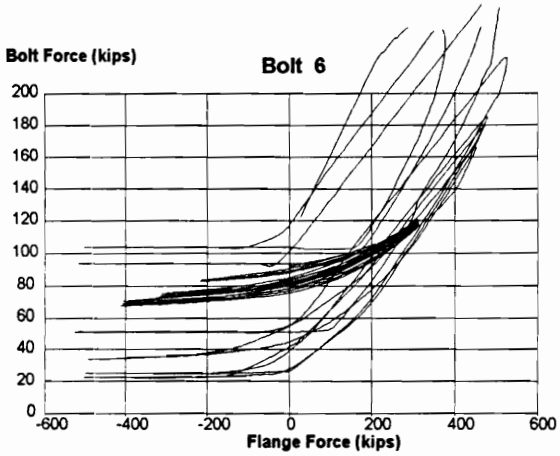

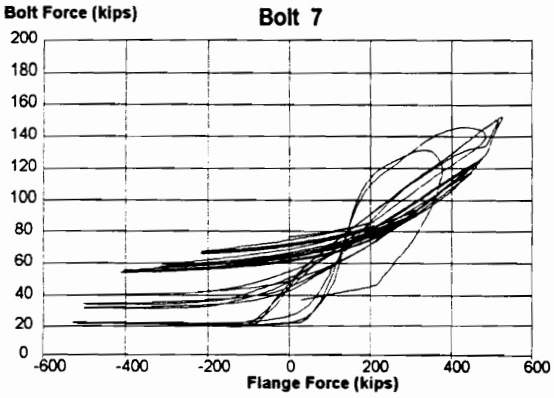

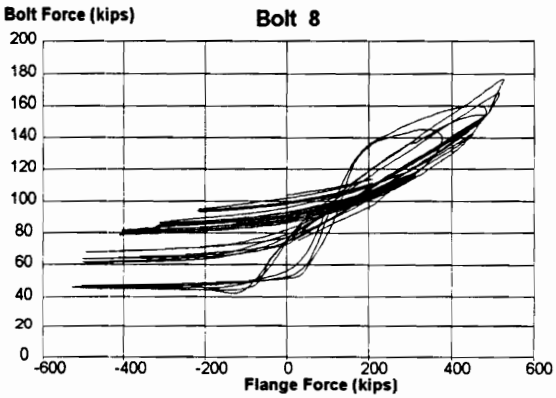

TEST 8 / 95

Connection End-Plate: Extended Four-Bolt, 1 1/4 in. Thick

Cycles Completed: 14

Failure Mode: Beam Flange Fracture

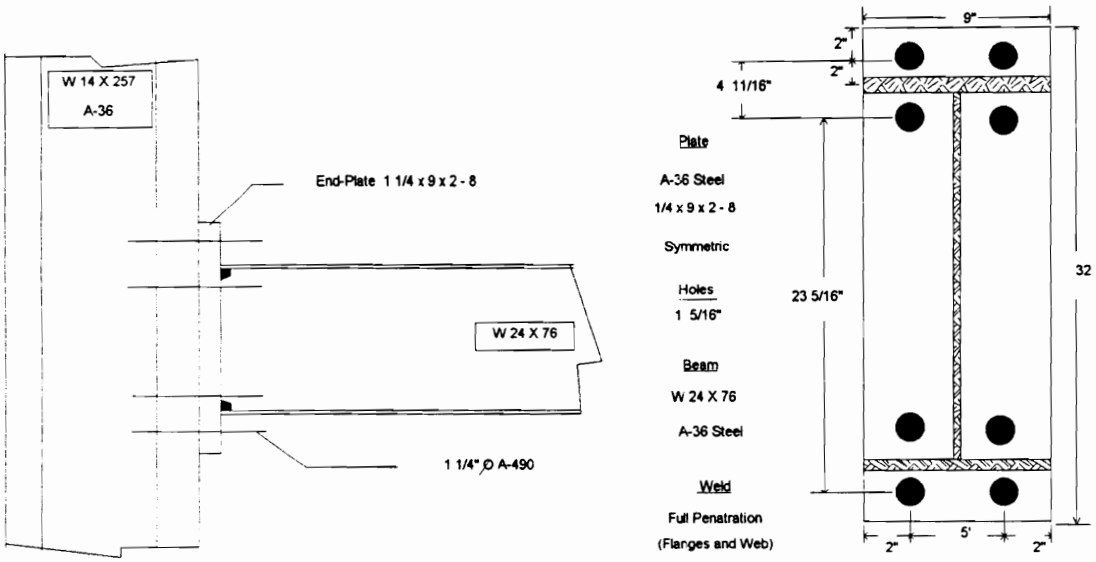

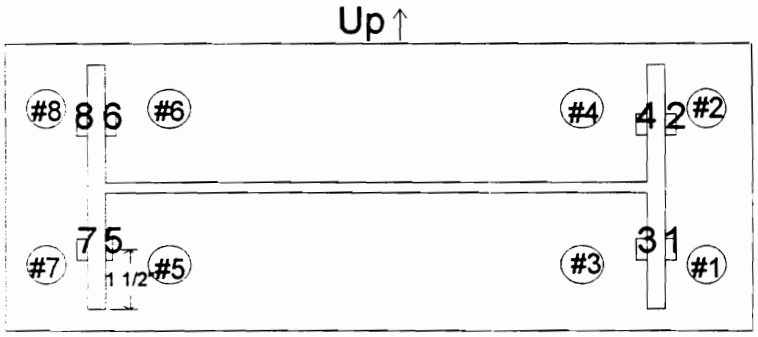

Strain Gauge and Bolt Location

Loading History for TEST 8 / 95

Load (kips) =>						Deflection (in.) =>							
Cycle 1	Cycle 1	Cycle 3	Cycle 4	Cycle 5	Cycle 6	Cycle 7	Cycle 8	Cycle 9	Cycle 10	Cycle 11	Cycle 12	Cycle 13	Cycle 14
0	0	0	0	0	0	0	0	0	0	0	0	0	0
10	10	10	22	22	22	0.264	0.264	0.264	0.661	0.661	0.661	0.661	0.661
20	20	20	33	33	33	0.529	0.529	0.529	0.991	0.991	0.991	1.321	1.321
30	30	30	44	44	44	0.793	0.793	0.793	1.321	1.321	1.321	1.982	1.982
40	40	40	55	55	55	1.057	1.057	1.057	1.762	1.762	1.762	2.643	2.643
44	44	44	66	66	66	1.321	1.321	1.321	2.202	2.202	2.202	30.83	30.83
40	40	40	55	55	55	1.057	1.057	1.057	2.643	2.643	2.643	3.524	3.524
30	30	30	44	44	44	0.793	0.793	0.793	2.202	2.202	2.202	3.964	3.964
20	20	20	33	33	33	0.529	0.529	0.529	1.762	1.762	1.762	3.524	3.524
10	10	10	22	22	22	0.264	0.264	0.264	1.321	1.321	1.321	3.083	3.083
0	0	0	0	0	0	0	0	0	0.991	0.991	0.991	2.643	2.643
									0.661	0.661	0.661	1.982	1.982
									0	0	0	1.321	1.321
												0.661	0.661
												0	0

delta = $\pm$ 1.3213 in.

Note: For more efficient use of space, only positive load and deflection values are tabulated.
A complete cycle included both positive and negative (load or deflection) excursions of equal magnitude.

TEST 8/95
W 24 x 76
1 1/4 in. End-Plate

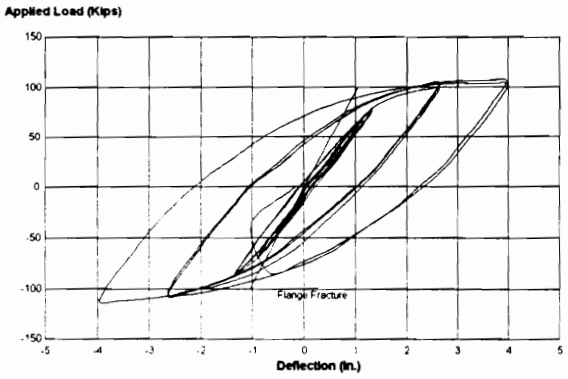

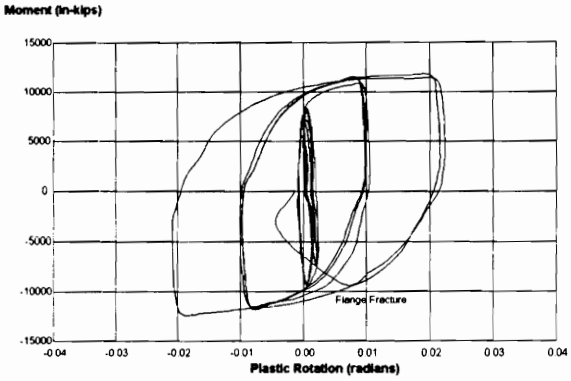

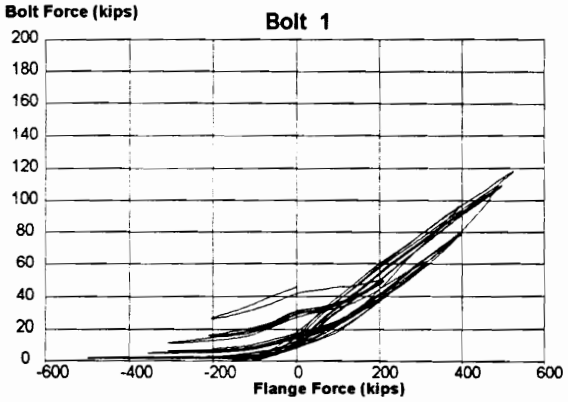

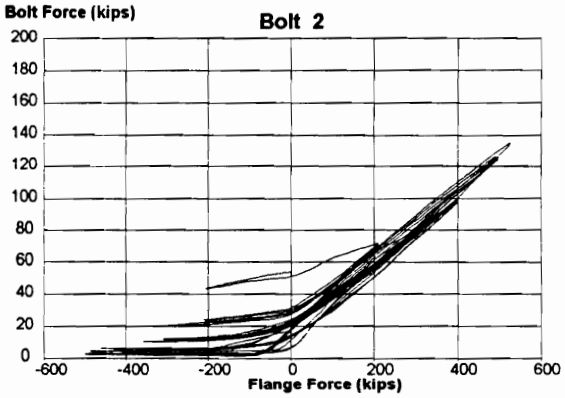

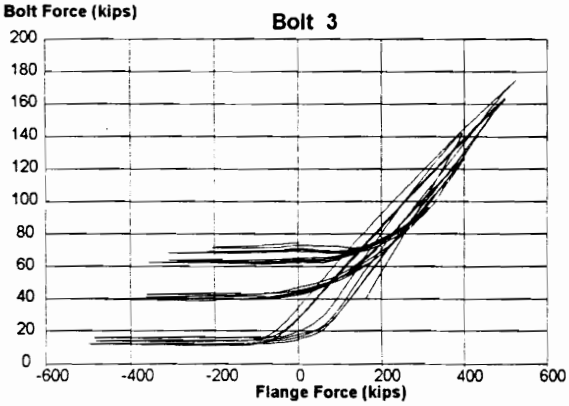

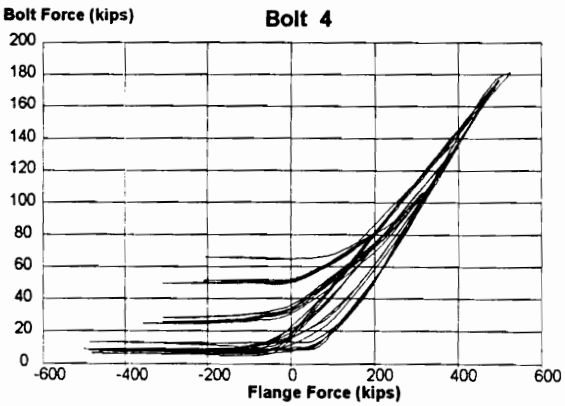

TEST 8/95
W 24 x 76
1 1/4 in. End-Plate

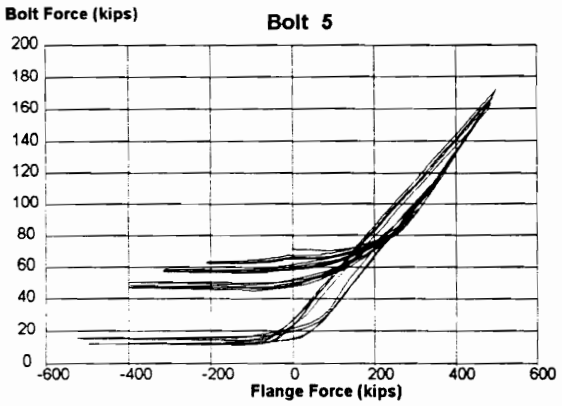

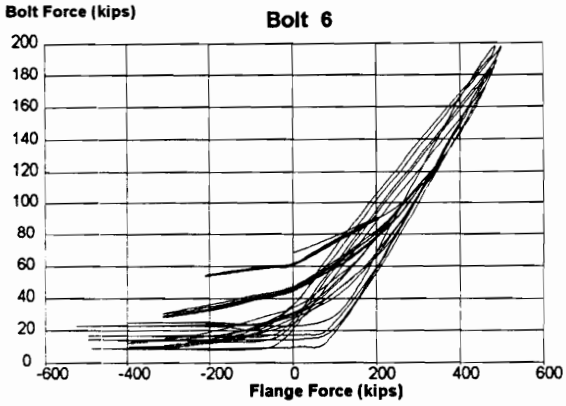

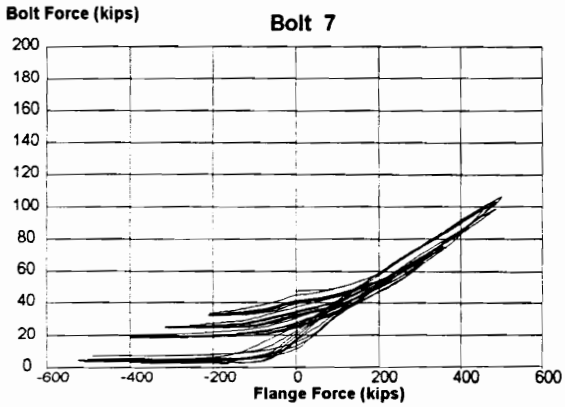

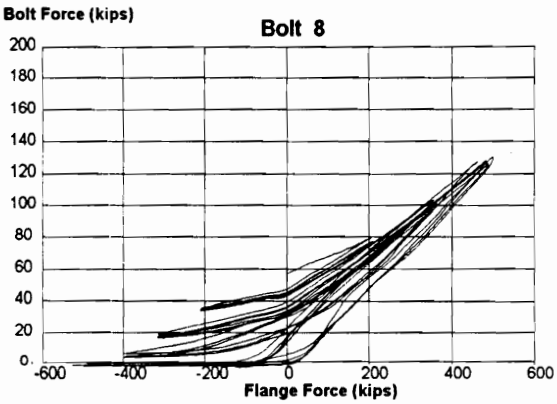

TEST 9 / 95

Connection End-Plate: Extended Four-Bolt, 2 1/4 in. Thick

Cycles Completed: 21

Failure Mode: Local Beam Flange Buckling

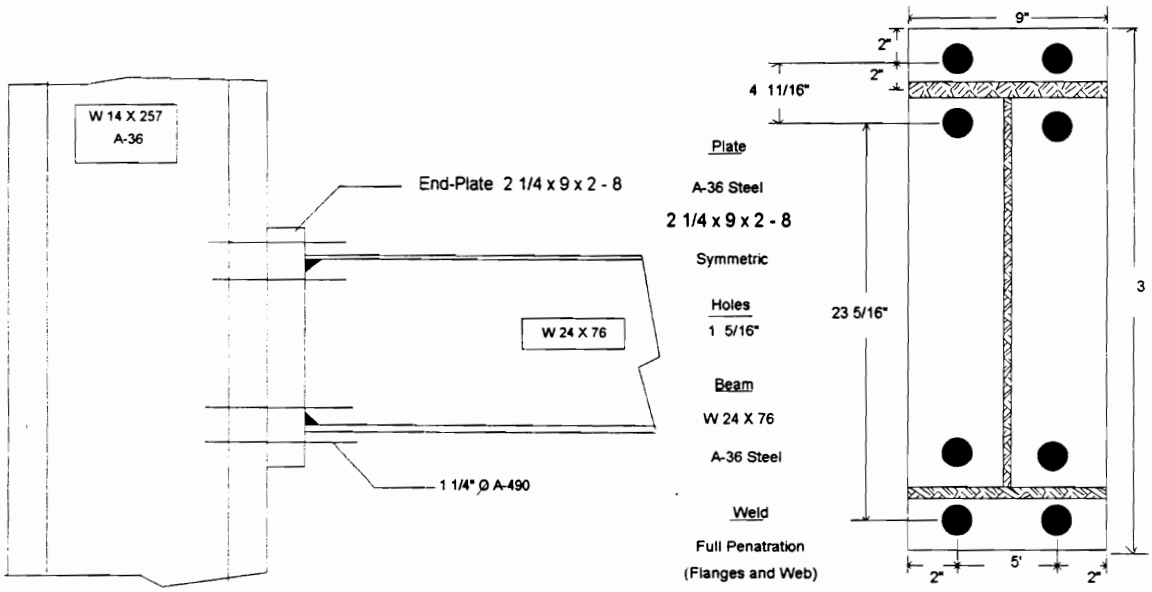

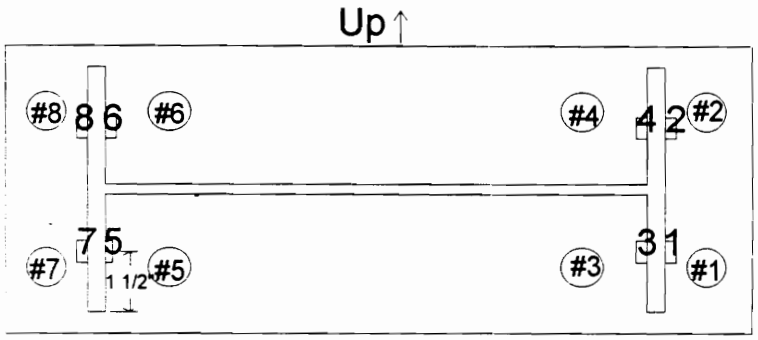

Strain Gauge and Bolt Location

Loading History for TEST 9/95

Load (kips) => Deflection (in.) =>

Cycle 1 & 2	Cycle 3	Cycle 4	Cycle 5	Cycle 6	Cycle 7	Cycle 8	Cycle 9	Cycle 10	Cycle 11	Cycle 12	Cycle 13	Cycle 14	Cycle 15	Cycle 16	Cycle 17	Cycle 18	Cycle 19	Cycle 20	Cycle 21
0	0	0	0	0	0	0	0	0	0	0	0	0	0	0	0	0	0	0	0
7	7	11	11	11	0.192	0.192	0.192	0.480	0.480	0.480	0.480	0.480	0.480	0.960	0.960	0.960	0.960	0.960	0.960
14	14	22	22	22	0.384	0.384	0.384	0.720	0.720	0.720	0.960	0.960	0.960	1.439	1.439	1.439	1.919	1.919	1.919
21	21	33	33	33	0.576	0.576	0.576	0.960	0.960	0.960	1.439	1.439	1.439	1.919	1.919	1.919	2.399	2.399	2.399
28	28	44	44	44	0.768	0.768	0.768	1.279	1.279	1.279	1.919	1.919	1.919	2.399	2.399	2.399	2.879	2.879	2.879
37	37	55	55	55	0.960	0.960	0.960	1.599	1.599	1.599	2.239	2.239	2.239	2.879	2.879	2.879	3.358	3.358	3.358
28	28	44	44	44	0.768	0.768	0.768	1.919	1.919	1.919	2.559	2.559	2.559	3.199	3.199	3.199	3.838	3.838	3.838
21	21	33	33	33	0.576	0.576	0.576	1.599	1.599	1.599	2.879	2.879	2.879	3.518	3.518	3.518	4.158	4.158	4.158
14	14	22	22	22	0.384	0.384	0.384	1.279	1.279	1.279	2.559	2.559	2.559	3.838	3.838	3.838	4.478	4.478	4.478
7	7	11	11	11	0.192	0.192	0.192	0.960	0.960	0.960	2.239	2.239	2.239	3.518	3.518	3.518	4.798	4.798	4.798
0	0	0	0	0	0	0	0	0.720	0.720	0.720	1.919	1.919	1.919	3.199	3.199	3.199	4.478	4.478	4.478
								0.480	0.480	0.480	1.439	1.439	1.439	2.879	2.879	2.879	4.158	4.158	4.158
								0	0	0	0.960	0.960	0.960	2.399	2.399	2.399	3.838	3.838	3.838
											0.480	0.480	0.480	1.919	1.919	1.919	3.358	3.358	3.358
											0	0	0	1.439	1.439	1.439	2.879	2.879	2.879
														0.960	0.960	0.960	2.399	2.399	2.399
														0	0	0	1.919	1.919	1.919
																	0.960	0.960	0.960
																	0	0	0

delta = $\pm$ 0.960 in.

Note: For more efficient use of space, only positive load and deflection values are tabulated.
A complete cycle included both positive and negative (load or deflection) excursions of equal magnitude.

TEST 9/95
W 24 x 76
2 1/4 in. End-Plate

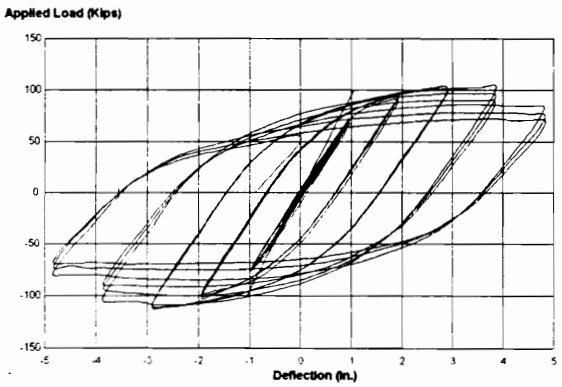

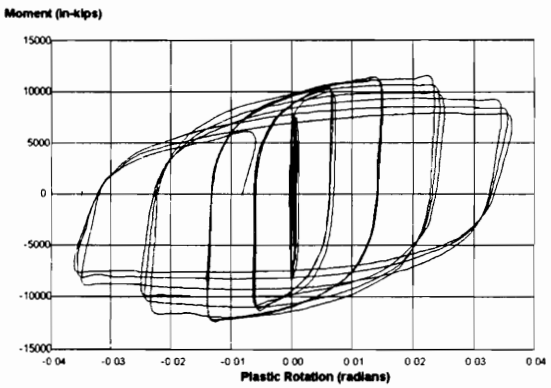

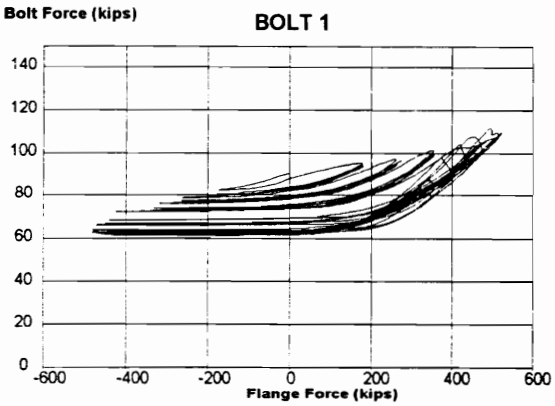

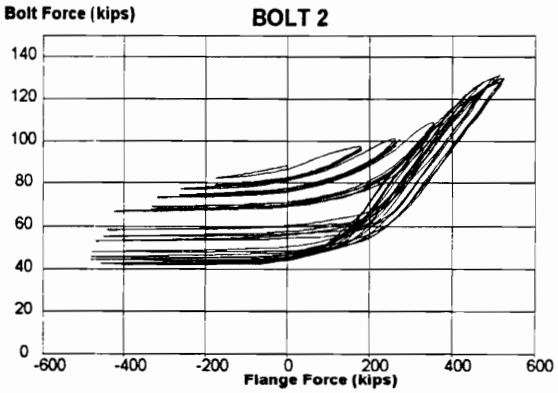

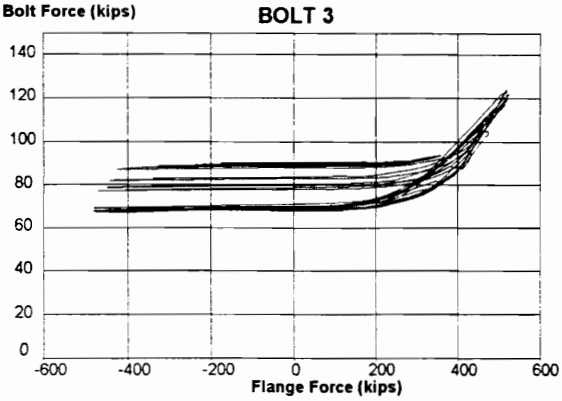

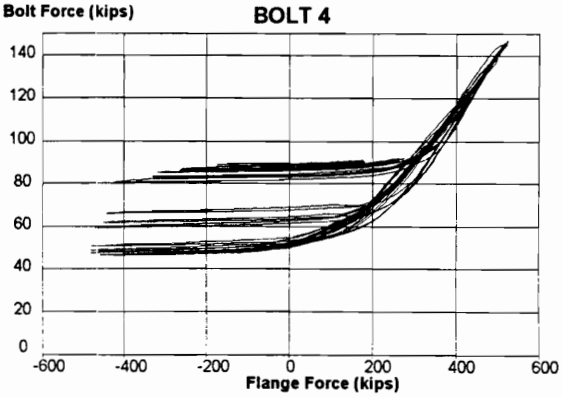

TEST 9/95
W 24 x 76
2 1/4 in. End-Plate

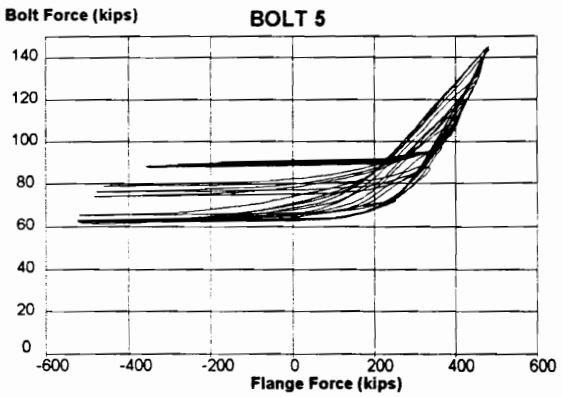

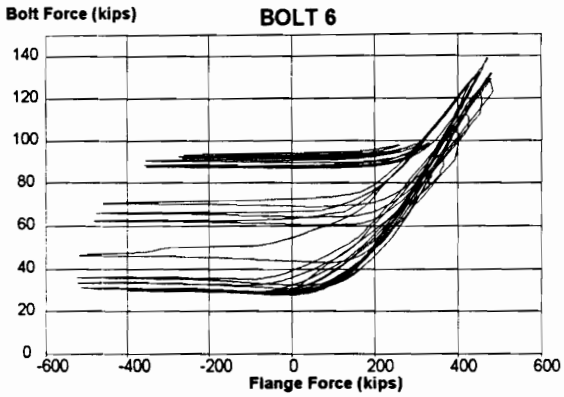

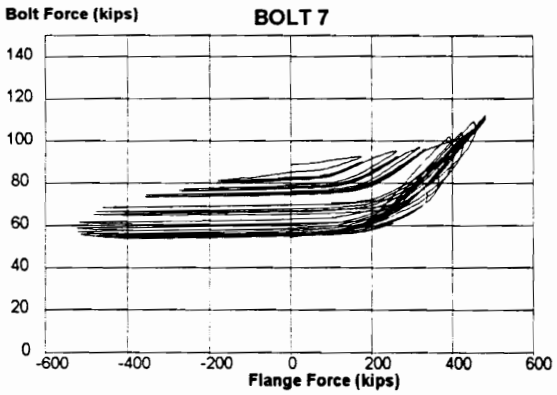

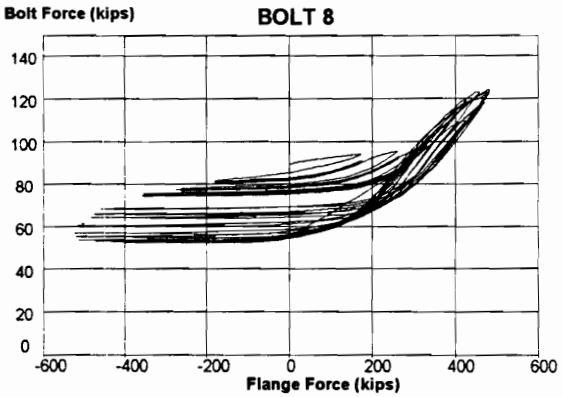

APPENDIX F

W 36 X 135 BEAM TEST RESULTS AND DATA

TESTS 10 /95 & 12 / 95

Beam Section W 36 x 135, A-36 Steel

$d = 35.55$ in. $t_w = 0.60$ in. $t_f = 0.79$ in $b_f = 11.95$ in.

$S_x = 439$ in^4. $Z_x = 509$ in^3.

Specimen Preparation and Welding Technique

End-Plates were flame cut to length and ground if required to smooth rough edges. Preheating of end-plate and/or beam was conducted as required by AWS. Connection was welded via flux core technique utilizing 5/64 in. E70 electrode Lincoln wire.

Beam Coupon tests of 08/22/95 (completed 01/22/96)

Flange # 1 (#86)

.725 x 1.500 = area of 1.0875

Lower Yield Stress - 43,600 psi.
Tensile Strength - 61,233 psi.
Elongation (8 in. base) - 26.6%

Flange # 2 (#87)

.721 x 1.500 = area of 1.0815

Lower Yield Stress - 43,510 psi.
Tensile Strength - 61,447 psi.
Elongation (8 in. base) - 25 %

Web # 1 (#1181)

.613 x 1.503 = area of 0.9213

Lower Yield Stress - 45,360 psi.
Tensile Strength - 59,990 psi.
Elongation (8 in. base) - 27.3%

Web # 2 (#85)

.607 x 1.499 = area of 0.9099

Lower Yield Stress - 42,600 psi.
Tensile Strength - 60,940 psi.
Elongation (8 in. base) - 30.5 %

Web Strengths:	**43,980 psi (yield)**	**60,465 psi (ultimate)**
Flange Strengths:	**43,555 psi (yield)**	**61,340 psi (ultimate)**

TEST 10 / 95

Connection End-Plate: Extended Four Bolt Wide, 1 1/2 in. Thick

Cycles Completed: 13

Failure Mode: Flange Fracture

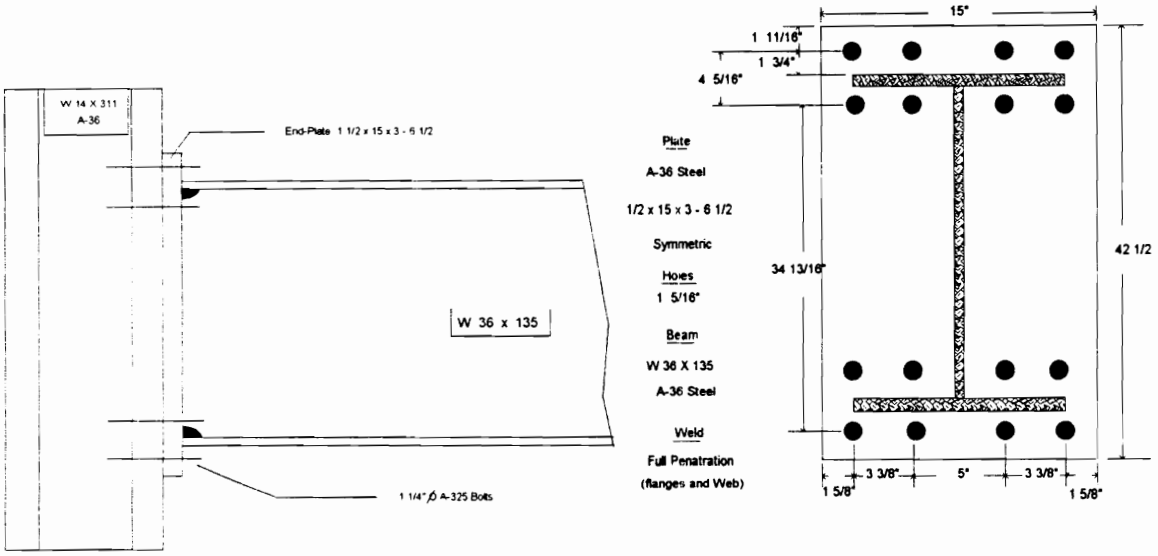

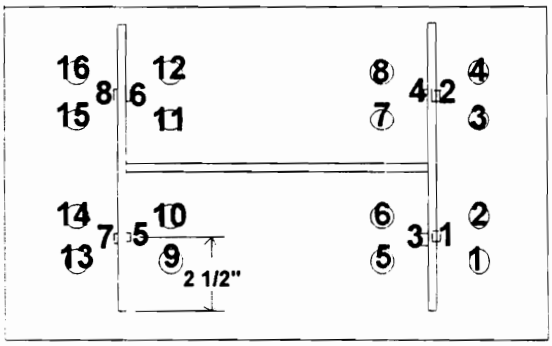

Strain Gauges 1 1/2 inch from End-Plate

Strain Gauge and Bolt Location

Loading History for TEST 10 / 95

		Load	(kips)		<= =>			Deflection	(in.)			
Cycle 1	Cycle 2	Cycle 3	Cycle 4	Cycle 5	Cycle 6	Cycle 7	Cycle 8	Cycle 9	Cycle 10	Cycle 11	Cycle 12	Cycle 13
0	0	0	0	0	0	0	0	0	0	0	0	0
15	15	15	20	20	20	0.227	0.227	0.227	0.568	0.568	0.568	0.586
30	30	30	45	45	45	0.455	0.455	0.455	0.853	0.853	0.853	1.137
45	45	45	70	70	70	0.682	0.682	0.682	1.137	1.137	1.137	1.705
60	60	60	90	90	90	0.910	0.910	0.910	1.516	1.516	1.516	2.274
74	74	74	111	111	111	1.137	1.137	1.137	1.895	1.895	1.895	2.653
60	60	60	90	90	90	0.910	0.910	0.910	2.274	2.274	2.274	3.032
45	45	45	70	70	70	0.682	0.682	0.682	1.895	1.895	1.895	3.411
30	30	30	45	45	45	0.455	0.455	0.455	1.516	1.516	1.516	3.032
15	15	15	20	20	20	0.227	0.227	0.227	1.137	1.137	1.137	2.653
0	0	0	0	0	0	0	0	0	0.853	0.853	0.853	2.274
									0.566	0.566	0.566	1.705
									0	0	0	1.137
												0.586
												0

delta = $\pm$ 1.137 in.

Note: For more efficient use of space, only positive load and deflection values are tabulated.
A complete cycle included both positive and negative (load or deflection) excursions of equal magnitude

TEST 10 / 95
W 36 x 135
1 1/2 in. End-Plate

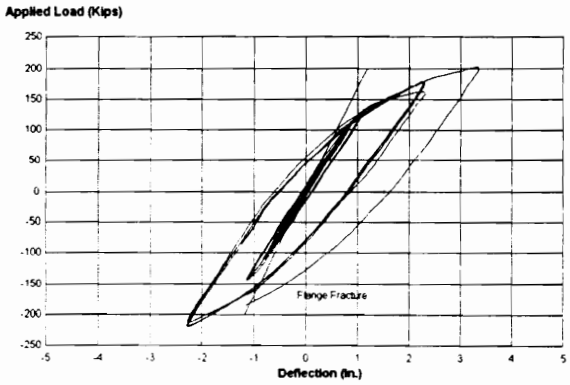

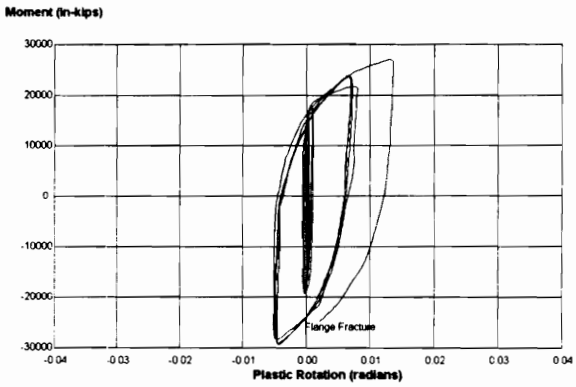

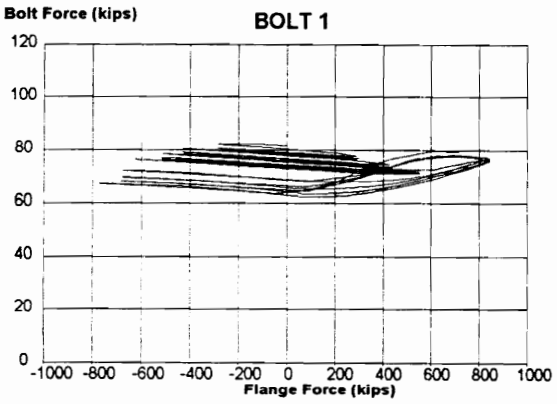

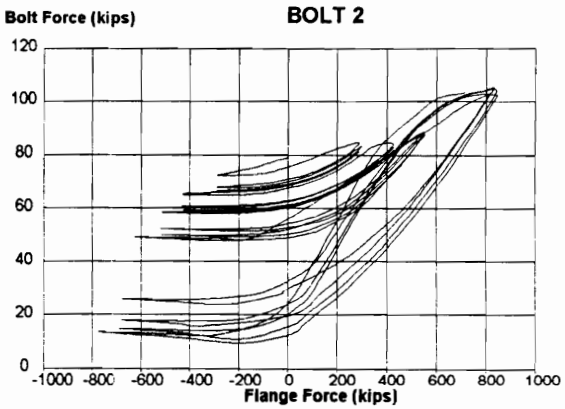

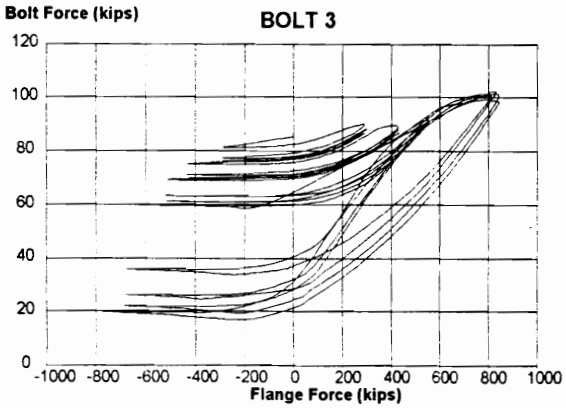

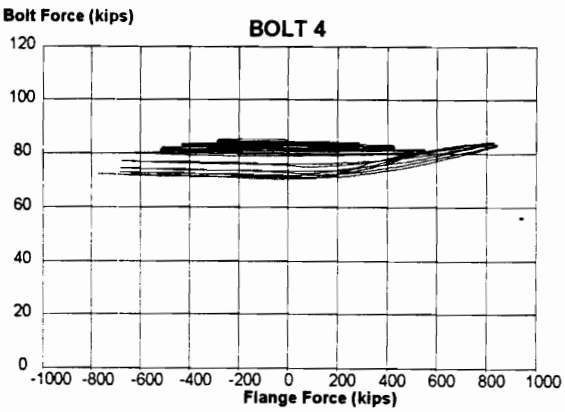

TEST 10 / 95
W 36 x 135
1 1/2 in. End-Plate

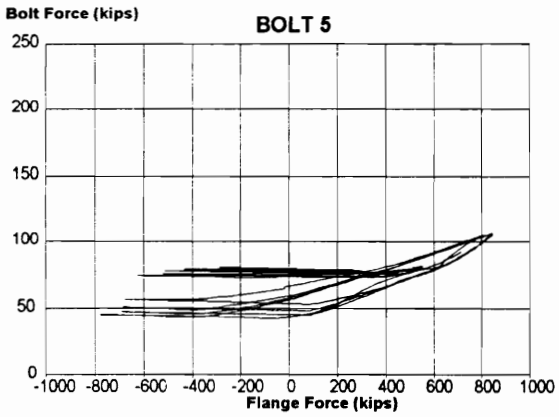

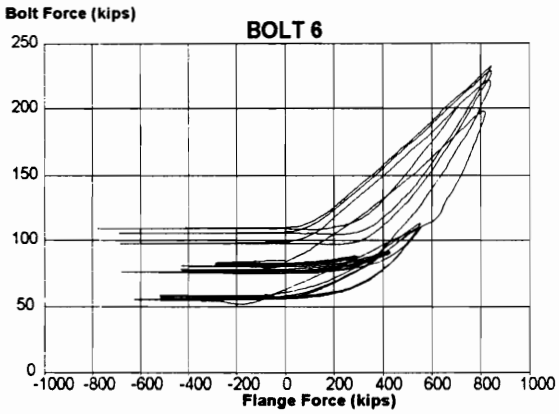

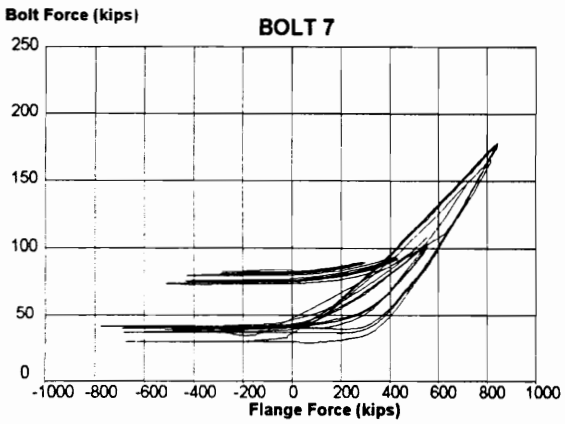

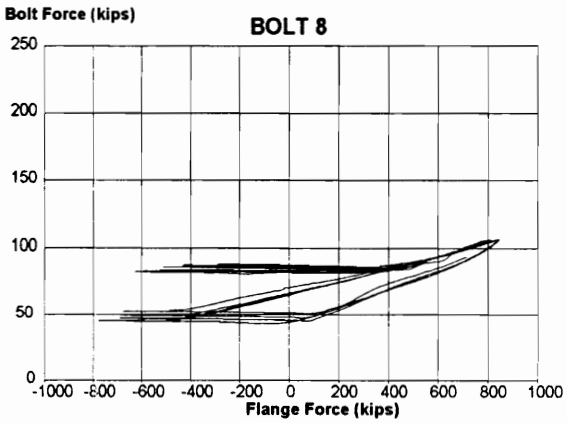

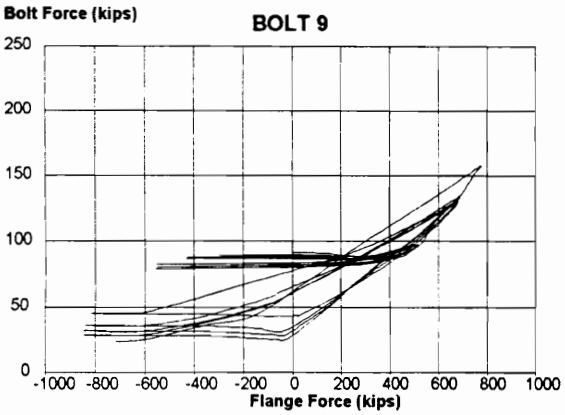

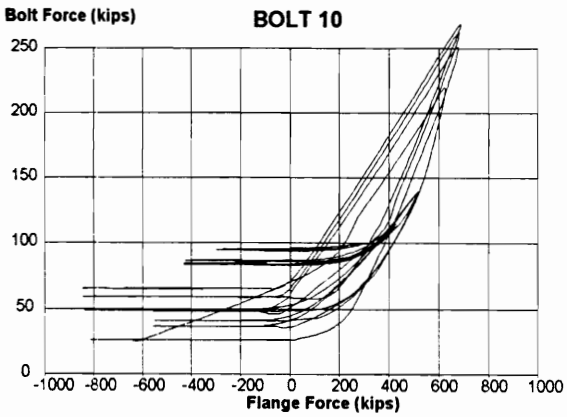

TEST 10 / 95
W 36 x 135
1 1/2 in. End-Plate

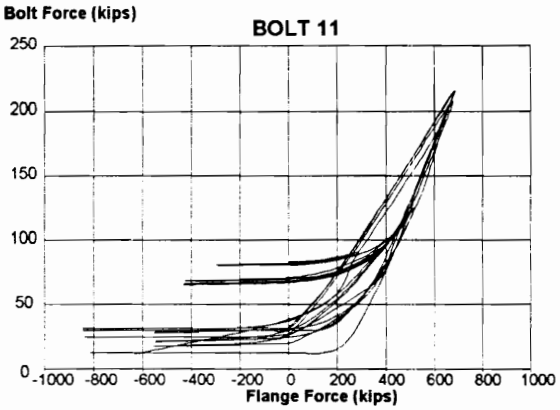

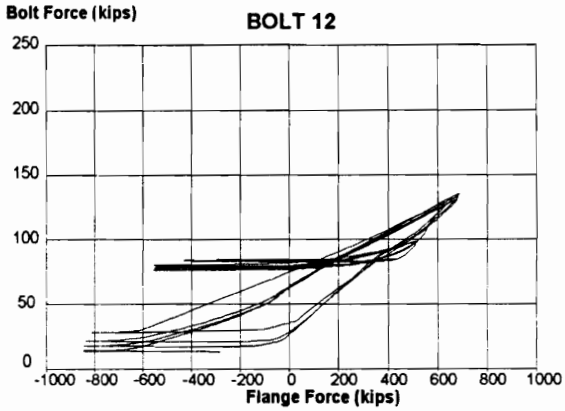

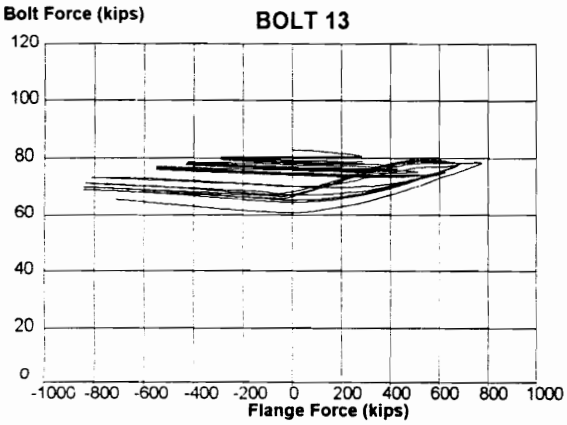

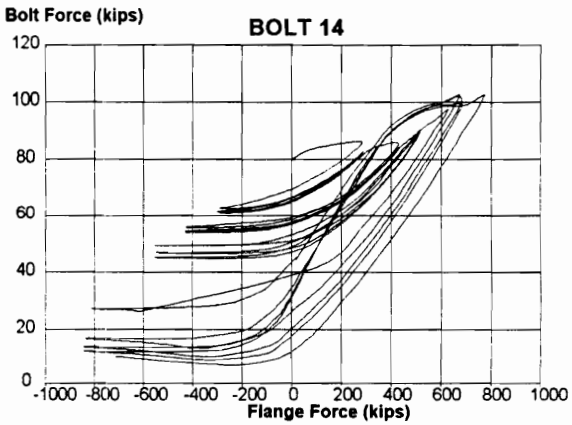

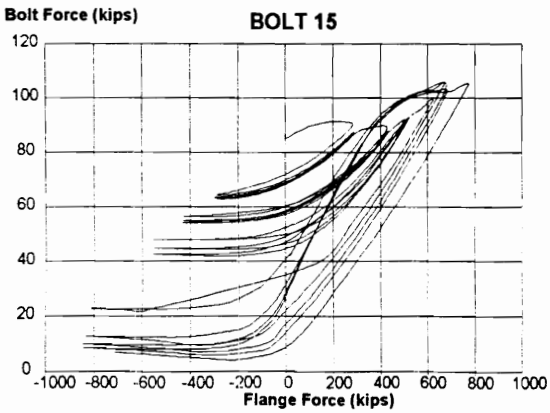

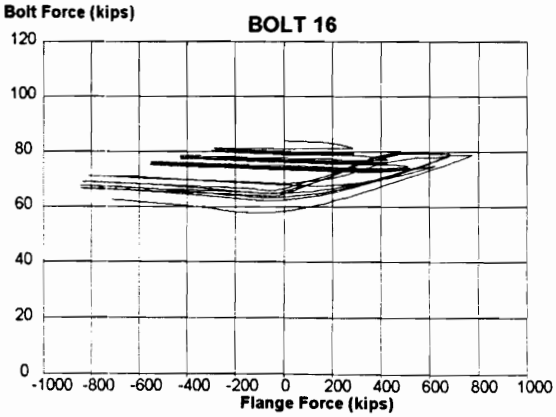

TEST 12 / 95

Connection End-Plate: Extended, Stiffened Four Bolt Wide, 1 1/2 in. Thick

Cycles Completed: 19

Failure Mode: Local Flange Buckling

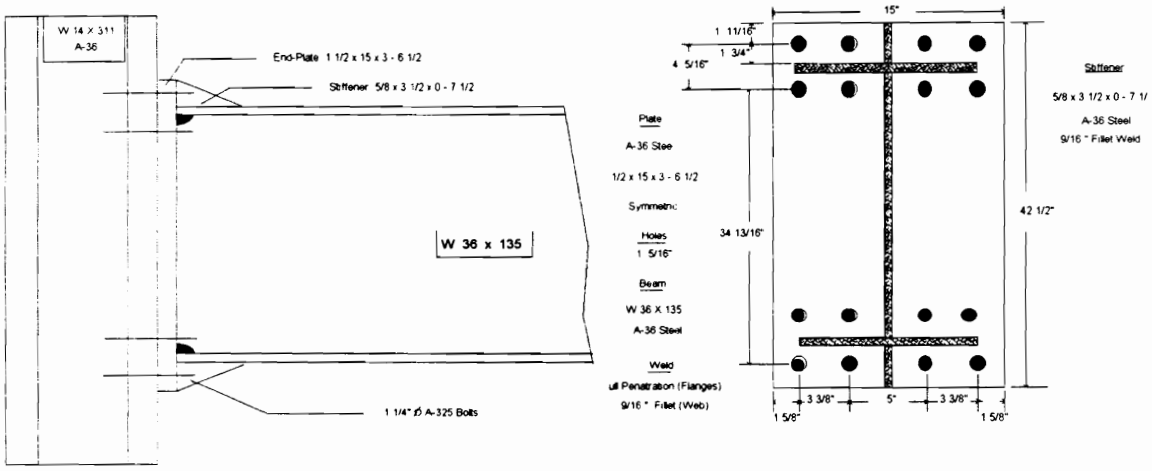

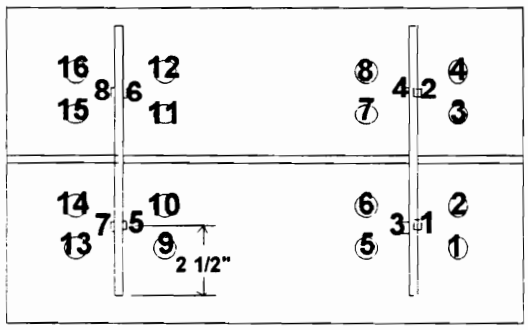

Strain Gauges 1 1/2 inch from End-Plate

Strain Gauge and Bolt Location

Loading History for TEST 12 / 95

Load (kips) <= => Deflection (in.)

Cycle 1	Cycle 2	Cycle 3	Cycle 4	Cycle 5	Cycle 6	Cycle 7	Cycle 8	Cycle 9	Cycle 10	Cycle 11	Cycle 12	Cycle 13	Cycle 14	Cycle 15	Cycle 16	Cycle 17	Cycle 18	Cycle 19
0	0	0	0	0	0	0	0	0	0	0	0	0	0	0	0	0	0	0
15	15	15	20	20	20	0.228	0.228	0.228	0.569	0.569	0.569	0.569	0.569	0.569	1.139	1.139	1.139	1.139
30	30	30	45	45	45	0.455	0.455	0.455	0.854	0.854	0.854	1.139	1.139	1.139	1.708	1.708	1.708	1.708
45	45	45	70	70	70	0.683	0.683	0.683	1.139	1.139	1.139	1.708	1.708	1.708	2.277	2.277	2.277	2.277
60	60	60	90	90	90	0.911	0.911	0.911	1.518	1.518	1.518	2.277	2.277	2.277	2.847	2.847	2.847	2.847
74	74	74	111	111	111	1.139	1.139	1.139	1.898	1.898	1.898	2.657	2.657	2.657	3.416	3.416	3.416	3.416
60	60	60	90	90	90	0.911	0.911	0.911	2.277	2.277	2.277	3.036	3.036	3.036	3.796	3.796	3.796	3.796
45	45	45	70	70	70	0.683	0.683	0.683	1.898	1.898	1.898	3.416	3.416	3.416	3.416	3.416	3.416	3.416
30	30	30	45	45	45	0.455	0.455	0.455	1.518	1.518	1.518	3.036	3.036	3.036	2.847	2.847	2.847	2.847
15	15	15	20	20	20	0.228	0.228	0.228	1.139	1.139	1.139	2.657	2.657	2.657	2.277	2.277	2.277	2.277
0	0	0	0	0	0	0	0	0	0.854	0.854	0.854	2.277	2.277	2.277	1.708	1.708	1.708	1.708
									0.569	0.569	0.569	1.708	1.708	1.708	1.139	1.139	1.139	1.139
									0	0	0	1.139	1.139	1.139	0	0	0	0
												0.569	0.569	0.569				
												0	0	0				

delta = $\pm$ 1.139 in.

Note: For more efficient use of space, only positive load and deflection values are tabulated.
A complete cycle included both positive and negative (load or deflection) excursions of equal magnitude

TEST 12/95
W 36 x 135
1 1/2 in. Stiffened, End-Plate

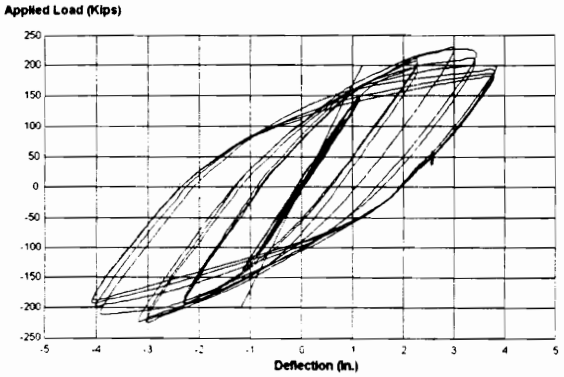

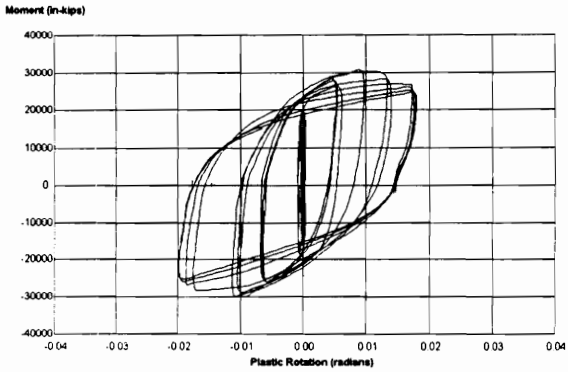

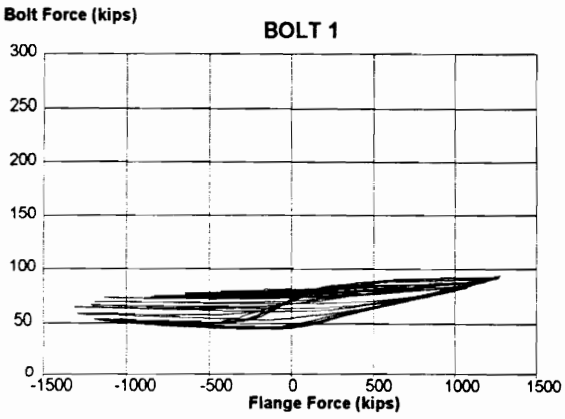

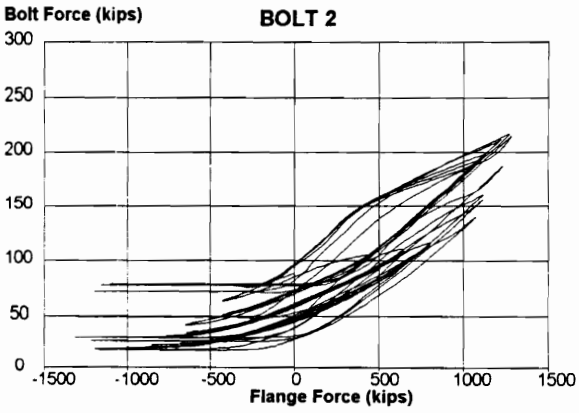

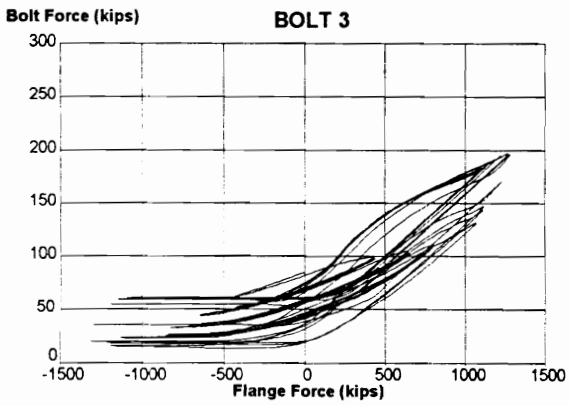

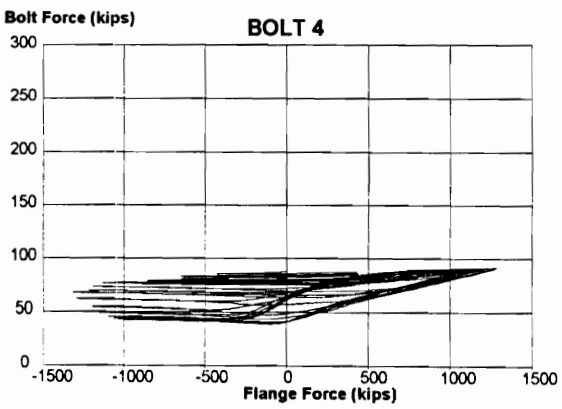

TEST 12/95
W 36 x 135
1 1/2 in. Stiffened, End-Plate

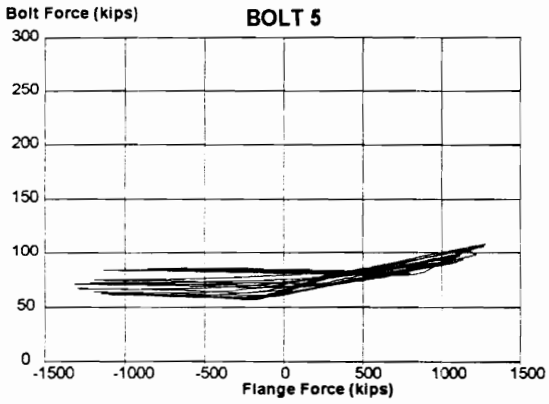

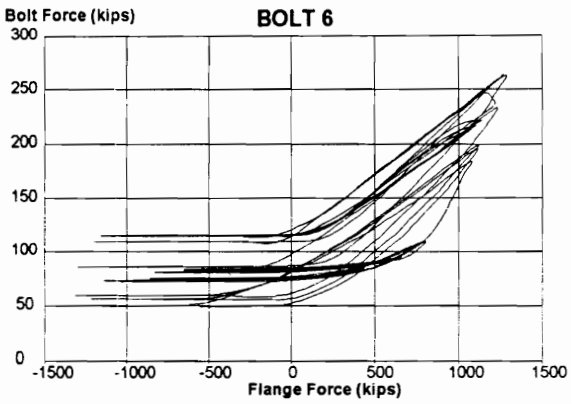

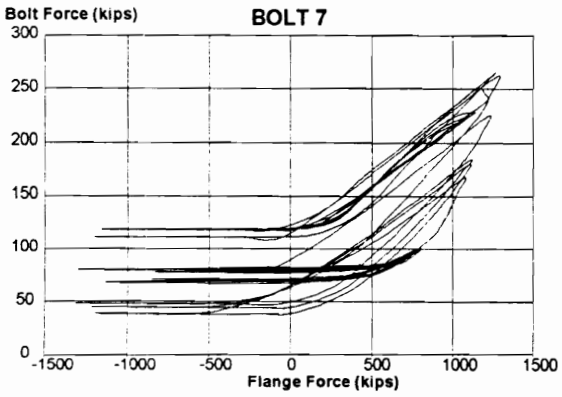

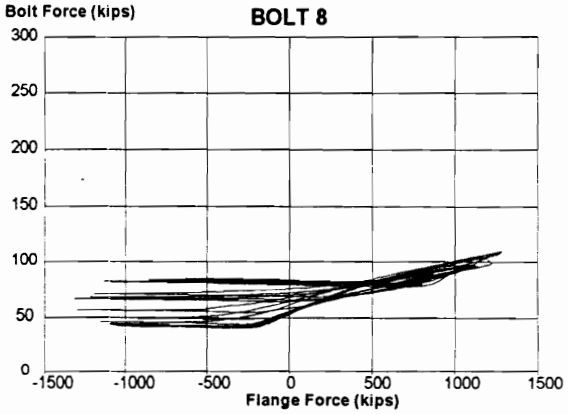

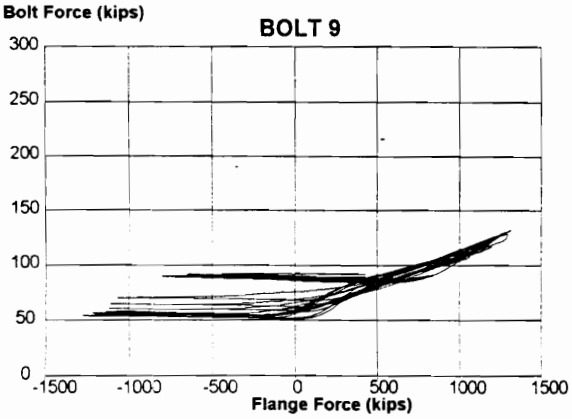

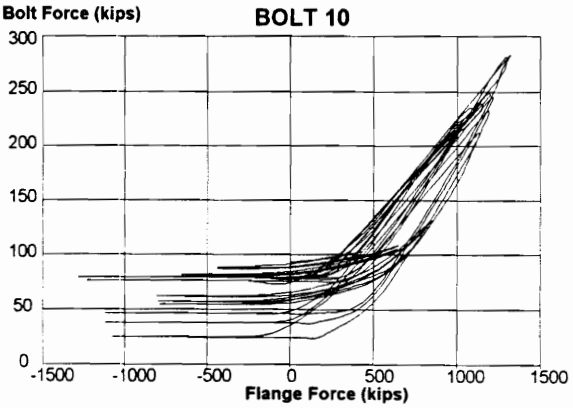

TEST 12/95
W 36 x 135
1 1/2 in. Stiffened, End-Plate

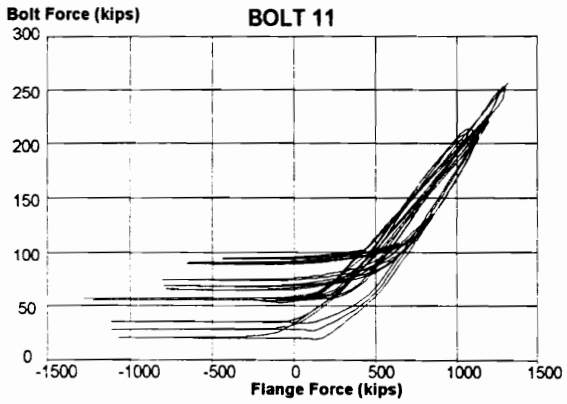

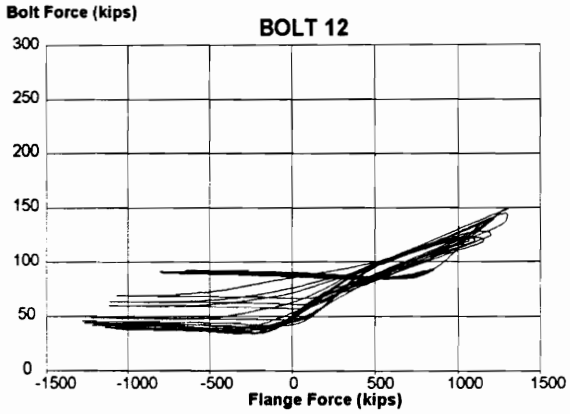

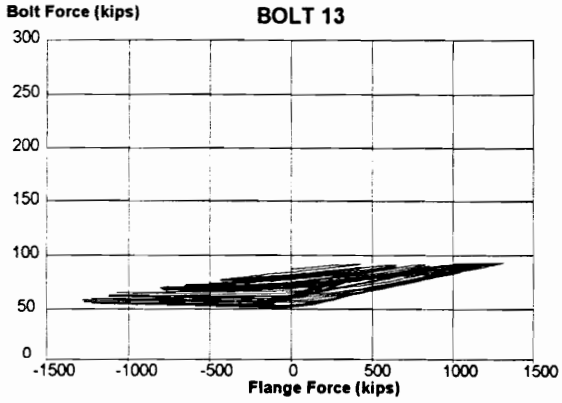

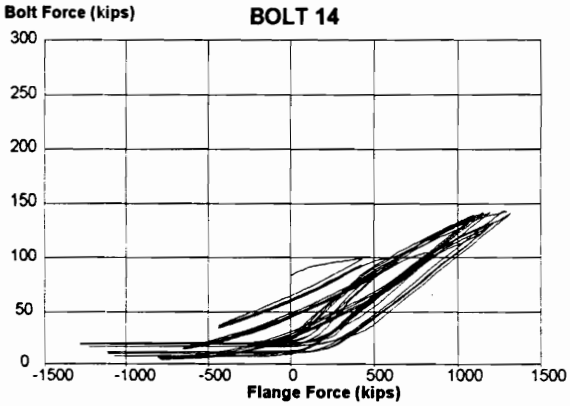

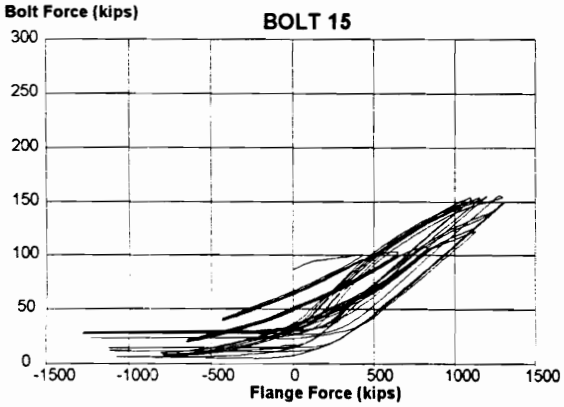

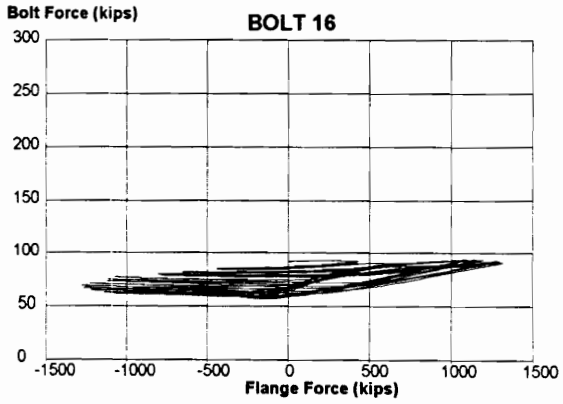

APPENDIX G

BUILT-UP SECTIONS

Grade 50 Steel

TESTS BuS 1 & BuS 2

Beam Section Built-up, Gr 50 Steel

d = 23.50 in. t_w = 0.375 in. t_f = 0.50 in b_f =8.00 in.

S_x = 120 in^4. Z_x = 139.5 in^3.

Beam Coupon tests of 09/18/95

Web # 1 (#10)

.376 x 1.496 = area of 0.5625

Lower Yield Stress - 62,773 psi.
Tensile Strength - 81,093 psi.
Elongation (8 in. base) - 22.66%

Web # 2 (#11)

.380 x 1.500 = area of 0.5700

Lower Yield Stress - 62,272 psi.
Tensile Strength - 80,848 psi.
Elongation (8 in. base) - 23.44%

Flange # 1 (#1205)

..496 x 1.500 = area of 0.7440

Lower Yield Stress - 65,000 psi.
Tensile Strength - 89,000 psi.
Elongation (8 in. base) - 21.9%

Flange # 2 (#1206)

.497 x 1.500 = area of 0.7455

Lower Yield Stress - 65,000 psi.
Tensile Strength - 90,930 psi.
Elongation (8 in. base) - 24.2%

Web Strengths:	**62,522 psi (yield)**	**80,970 psi (ultimate)**
Flange Strengths:	**65,000 psi (yield)**	**89,965 psi (ultimate)**

Column Section W 14 x 257, A-36 Steel

d = 16.38 in. t_w = 1.175 in. t_f = 1.89 in b_f = 15.995 in.

S_x = 415 in^4. Z_x = 487 in^3.

TEST BuS 1

Connection End-Plate: Extended Four-Bolt, 1 in. Thick

Cycles Completed: 18

Failure Mode: Web-to-Flange Weld Fracture

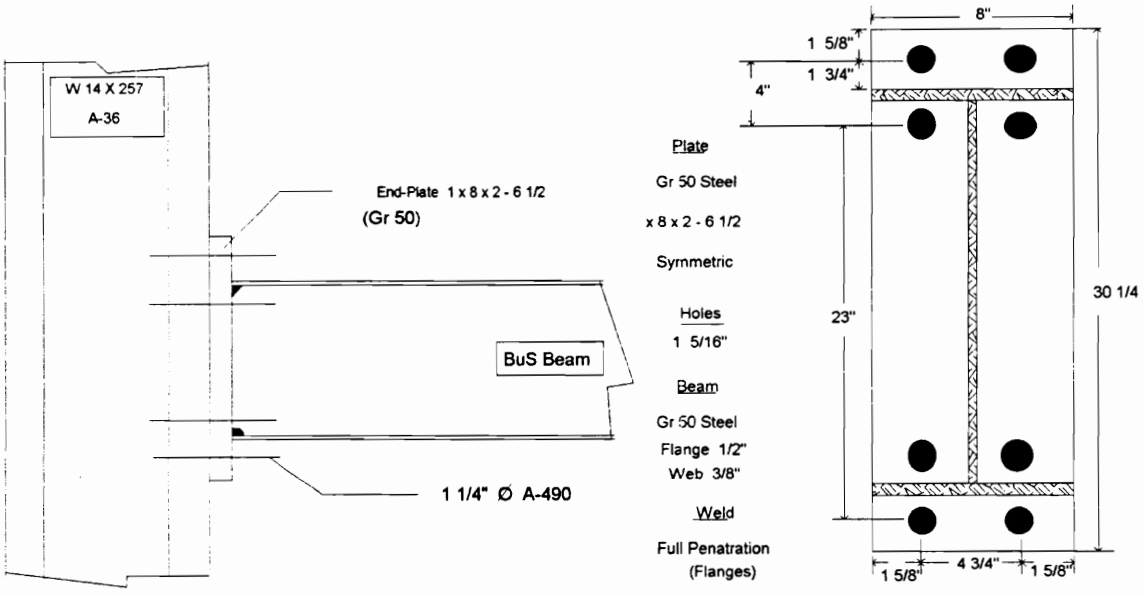

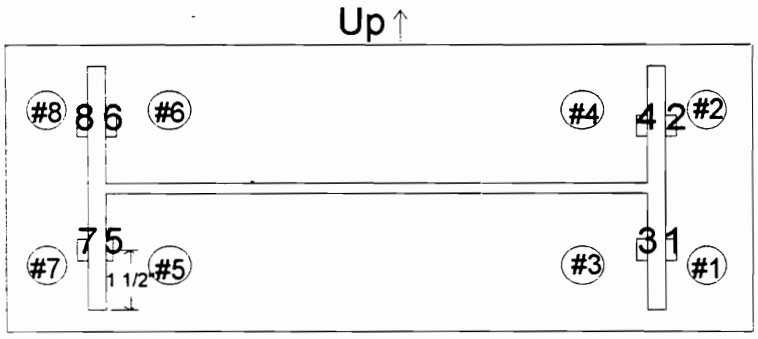

Strain Gauge and Bolt Location

Loading History for TEST BuS 1

Load (kips) =>						Deflection (in.) =>											
Cycle 1	Cycle 2	Cycle 3	Cycle 4	Cycle 5	Cycle 6	Cycle 7	Cycle 8	Cycle 9	Cycle 10	Cycle 11	Cycle 12	Cycle 13	Cycle 14	Cycle 15	Cycle 16	Cycle 17	Cycle 18
0	0	0	0	0	0	0	0	0	0	0	0	0	0	0	0	0	0
10	10	10	9	9	9	0.197	0.197	0.197	0.492	0.492	0.492	0.492	0.492	0.492	0.984	0.984	0.984
15	15	15	18	18	18	0.393	0.393	0.393	0.738	0.738	0.738	0.984	0.984	0.984	1.475	1.475	1.475
20	20	20	27	27	27	0.590	0.590	0.590	0.984	0.984	0.984	1.475	1.475	1.475	1.967	1.967	1.967
25	25	25	36	36	36	0.787	0.787	0.787	1.311	1.311	1.311	1.967	1.967	1.967	2.459	2.459	2.459
30	30	30	45	45	45	0.984	0.984	0.984	1.639	1.639	1.639	2.295	2.295	2.295	2.951	2.951	2.951
25	25	25	36	36	36	0.787	0.787	0.787	1.967	1.967	1.967	2.623	2.623	2.623	3.279	3.279	3.279
20	20	20	27	27	27	0.590	0.590	0.590	1.639	1.639	1.639	2.951	2.951	2.951	3.606	3.606	3.606
15	15	15	18	18	18	0.393	0.393	0.393	1.311	1.311	1.311	2.623	2.623	2.623	3.934	3.934	3.934
10	10	10	9	9	9	0.197	0.197	0.197	0.984	0.984	0.984	2.295	2.295	2.295	3.606	3.606	3.606
0	0	0	0	0	0	0	0	0	0.738	0.738	0.738	1.967	1.967	1.967	3.279	3.279	3.279
									0.492	0.492	0.492	1.475	1.475	1.475	2.951	2.951	2.951
									0	0	0	0.984	0.984	0.984	2.459	2.459	2.459
												0.492	0.492	0.492	1.967	1.967	1.967
												0	0	0	1.475	1.475	1.475
															0.984	0.984	0.984
															0	0	0

delta = $\pm$ 0.984 in.

Note: For more efficient use of space, only positive load and deflection values are tabulated.
A complete cycle included both positive and negative (load or deflection) excursions of equal magnitude.

TEST BuS 1
Built-Up Section
1 in. End-Plate

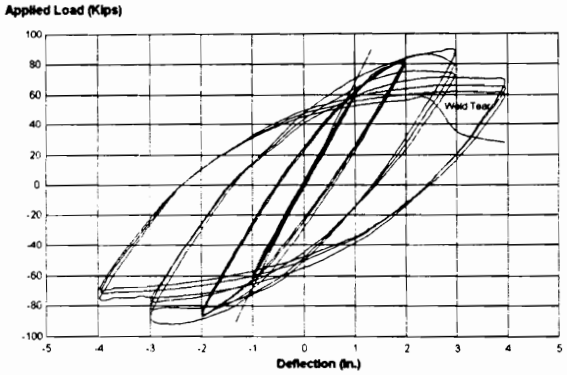

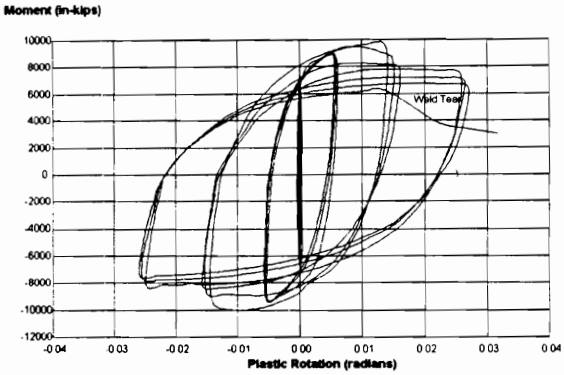

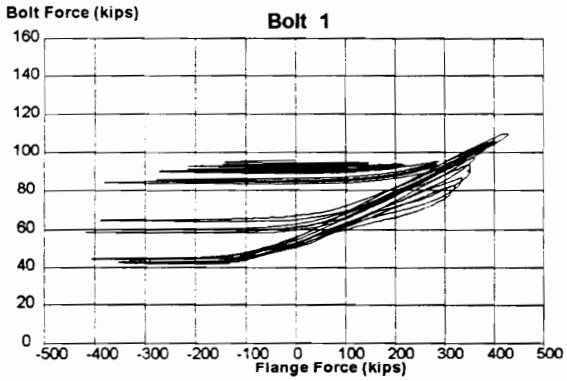

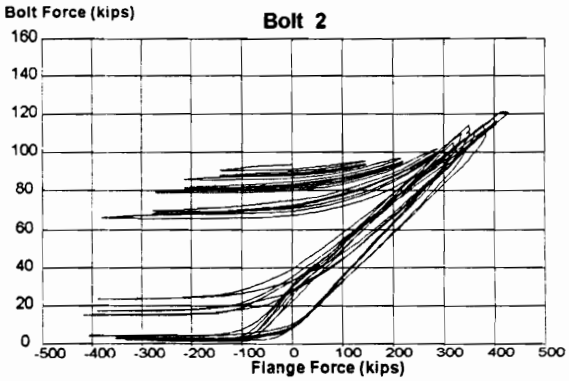

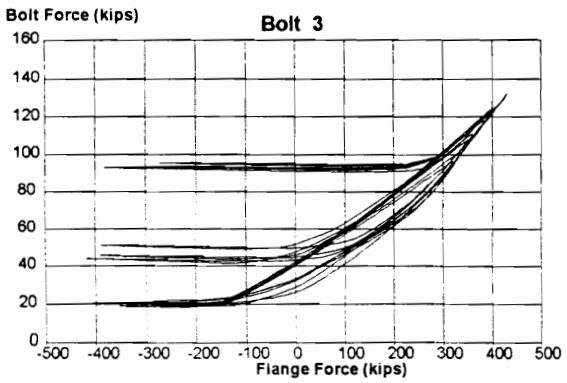

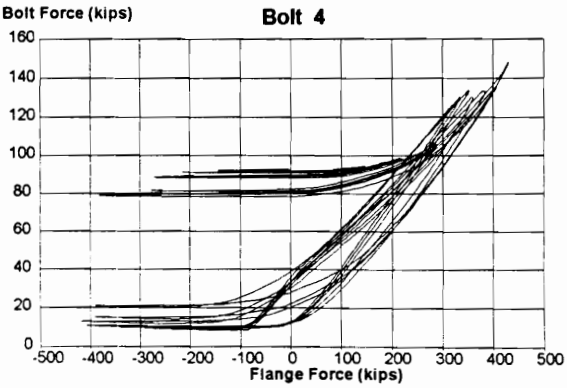

TEST BuS 1
Built-Up Section
1 in. End-Plate

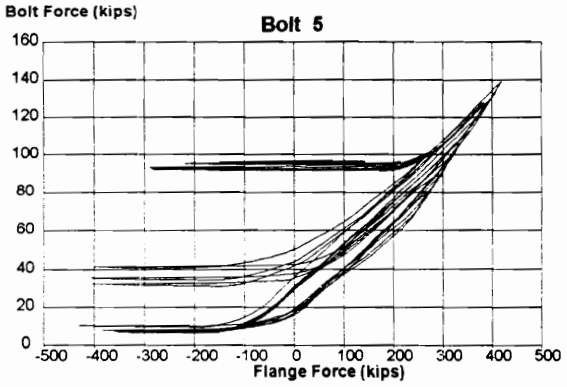

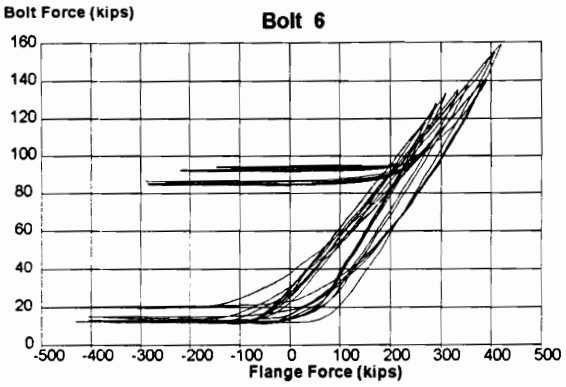

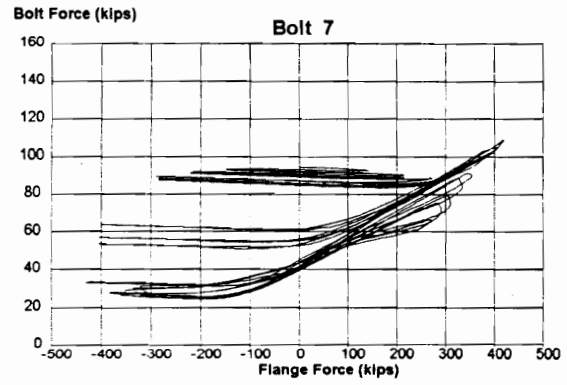

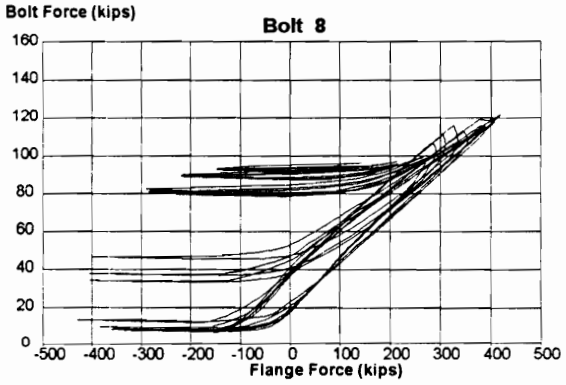

TEST BuS 2

Connection End-Plate: Extended Four-Bolt, 1 in. Thick

Cycles Completed: 16

Failure Mode: Web-to-Flange Weld Fracture

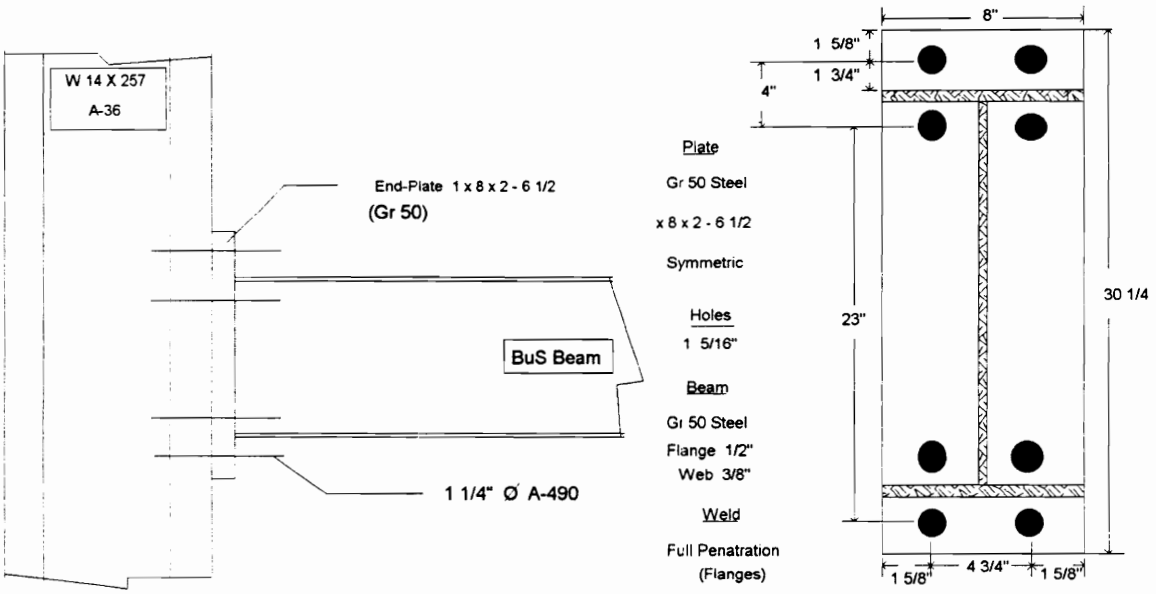

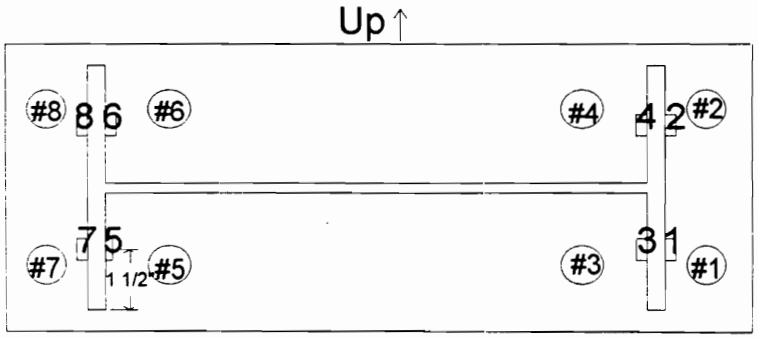

Strain Gauge and Bolt Location

Loading History for TEST BuS 2

Load (kips) =>						Deflection (in.) =>									
Cycle 1	Cycle 2	Cycle 3	Cycle 4	Cycle 5	Cycle 6	Cycle 7	Cycle 8	Cycle 9	Cycle 10	Cycle 11	Cycle 12	Cycle 13	Cycle 14	Cycle 15	Cycle 16
0	0	0	0	0	0	0	0	0	0	0	0	0	0	0	0
10	10	10	9	9	9	0.196	0.196	0.196	0.490	0.490	0.490	0.490	0.490	0.490	0.979
15	15	15	18	18	18	0.392	0.392	0.392	0.735	0.735	0.735	0.979	0.979	0.979	1.469
20	20	20	27	27	27	0.588	0.588	0.588	0.979	0.979	0.979	1.469	1.469	1.469	1.959
25	25	25	36	36	36	0.783	0.783	0.783	1.306	1.306	1.306	1.959	1.959	1.959	2.448
30	30	30	45	45	45	0.979	0.979	0.979	1.632	1.632	1.632	2.285	2.285	2.285	2.938
25	25	25	36	36	36	0.782	0.782	0.782	1.959	1.959	1.959	2.612	2.612	2.612	3.264
20	20	20	27	27	27	0.588	0.588	0.588	1.632	1.632	1.632	2.938	2.938	2.938	3.591
15	15	15	18	18	18	0.392	0.392	0.392	1.306	1.306	1.306	2.612	2.612	2.612	3.917
10	10	10	9	9	9	0.196	0.196	0.196	0.979	0.979	0.979	2.285	2.285	2.285	3.591
0	0	0	0	0	0	0	0	0	0.735	0.735	0.735	1.959	1.959	1.959	3.264
									0.490	0.490	0.490	1.469	1.469	1.469	2.938
									0	0	0	0.979	0.979	0.979	2.448
												0.490	0.490	0.490	1.959
												0	0	0	1.469
															0.979
															0

delta = $\pm$ 0.979 in.

Note: For more efficient use of space, only positive load and deflection values are tabulated.
A complete cycle included both positive and negative (load or deflection) excursions of equal magnitude.

TEST BuS 2
Built-Up Section
1 in. End-Plate

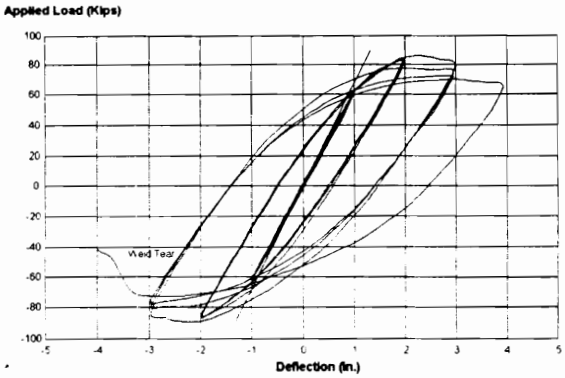

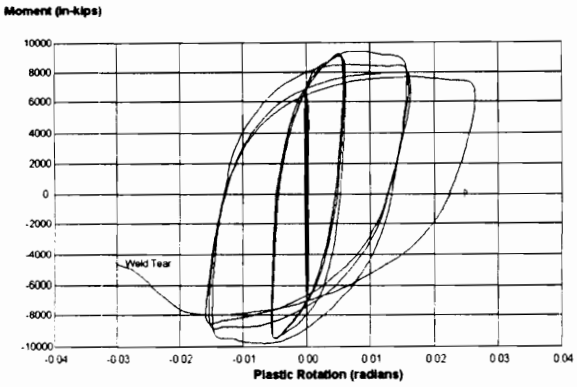

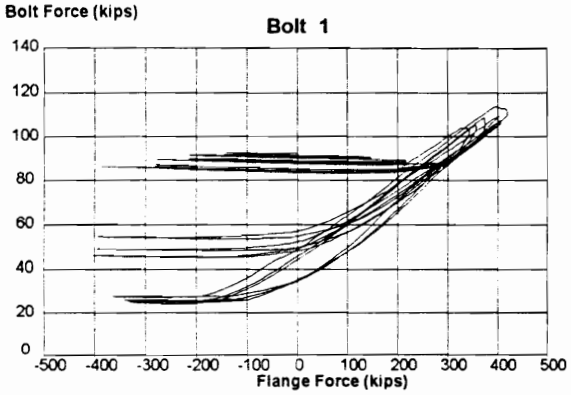

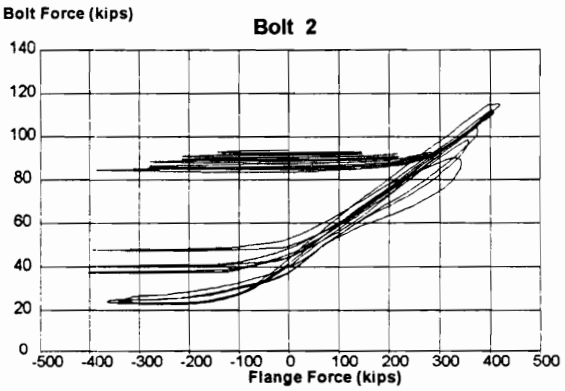

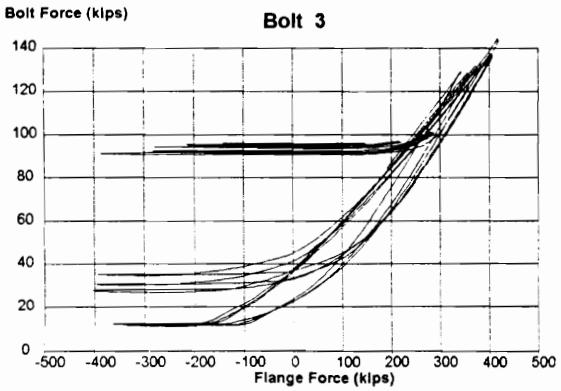

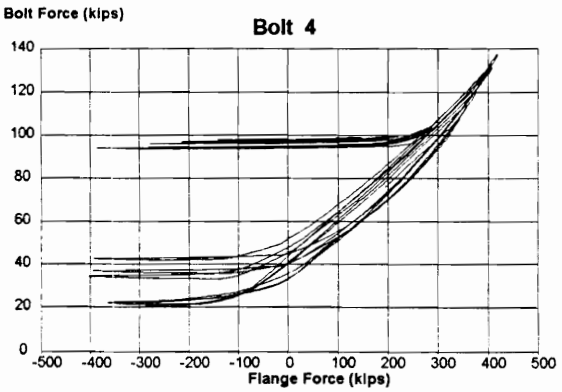

TEST BuS 2
Built-Up Section
1 in. End-Plate

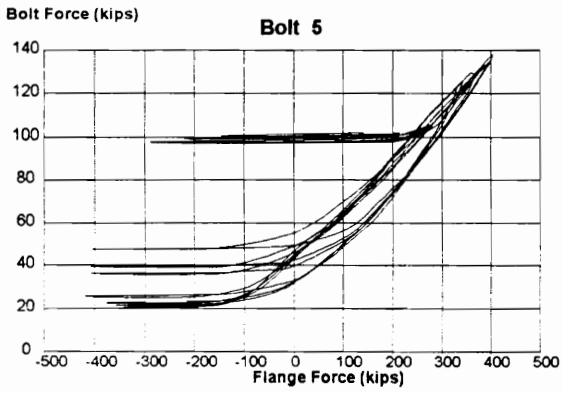

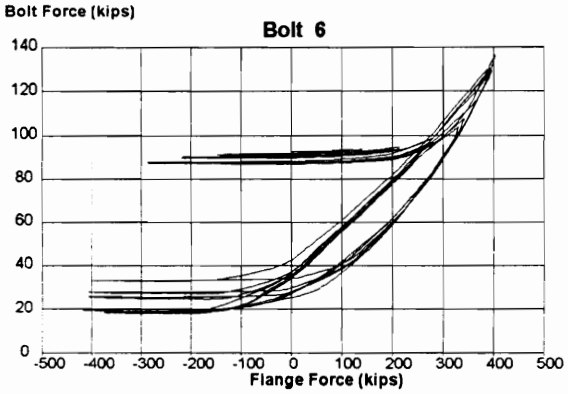

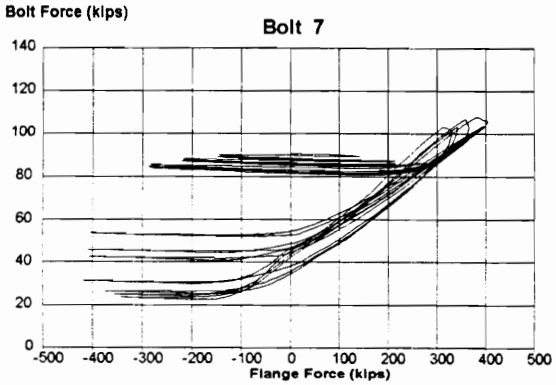

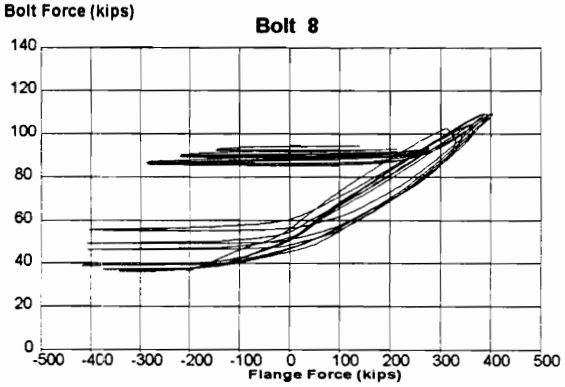

TESTS BuS 1A & BuS 2A

Beam Section Built-up, Gr 50 Steel

d = 23.50 in. t_w = 0.375 in. t_f = 0.50 in b_f =8.00 in.

S_x = 120 in^4. Z_x = 139.5 in^3.

Beam Coupon tests of 01/22/96

Flange # 1 (#80) RH2B

..495 x 1.496 = area of 0.7405

Lower Yield Stress -63,320 psi.
Tensile Strength - 90,042 psi.
Elongation (8 in. base) - 25%

Flange # 2 (#81) RH2AT

.495 x 1.498 = area of 0.7415

Lower Yield Stress - 63,260 psi.
Tensile Strength - 91,512 psi.
Elongation (8 in. base) - 22.7%

Flange # 3 (#82) RH2F

..498 x 1.500 = area of 0.7470

Lower Yield Stress - 63,380 psi.
Tensile Strength - 89,513 psi.
Elongation (8 in. base) - 24.2%

Web # 1 (#83)

.376 x 1.498 = area of 0.5632

Lower Yield Stress - 58,110 psi.
Tensile Strength - 78,289 psi.
Elongation (8 in. base) - 22.7%

Web # 2 (#84)

.376 x 1.499 = area of 0.5636

Lower Yield Stress - 58,200 psi.
Tensile Strength - 78,162 psi.
Elongation (8 in. base) - 23.4%

Web Strengths:	**58,155 psi (yield)**	**78,225 psi (ultimate)**
Flange Strengths:	**63,320 psi (yield)**	**90,355 psi (ultimate)**

Column Section W 14 x 257, A-36 Steel

d = 16.38 in. t_w = 1.175 in. t_f = 1.89 in b_f = 15.995 in.

S_x = 415 in^4. Z_x = 487 in^3.

TEST BuS 1A

Connection End-Plate: Extended Four-Bolt, 1 in. Thick

Cycles Completed: 19

Failure Mode: Beam Flange Fracture

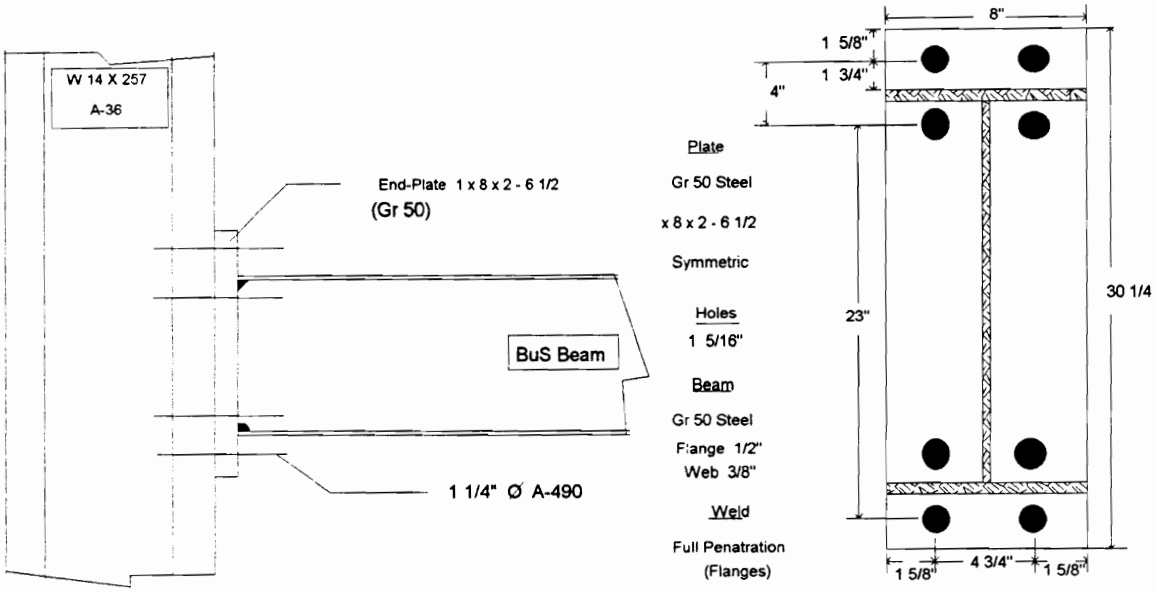

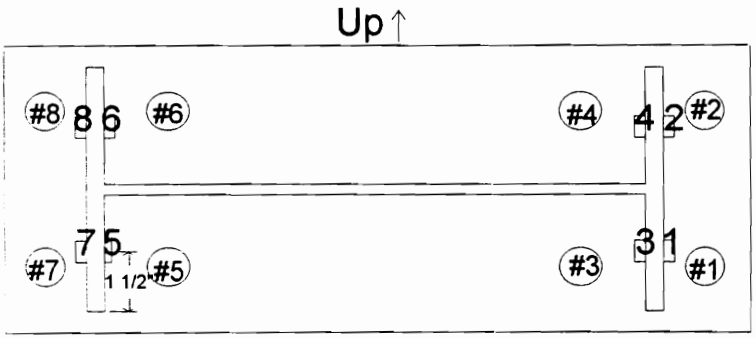

Strain Gauge and Bolt Location

Loading History for TEST BuS 1A

Load (kips) =>						Deflection (in.) =>												
Cycle 1	Cycle 2	Cycle 3	Cycle 4	Cycle 5	Cycle 6	Cycle 7	Cycle 8	Cycle 9	Cycle 10	Cycle 11	Cycle 12	Cycle 13	Cycle 14	Cycle 15	Cycle 16	Cycle 17	Cycle 18	Cycle 19
0	0	0	0	0	0	0	0	0	0	0	0	0	0	0	0	0	0	0
10	10	10	9	9	9	0.193	0.193	0.193	0.484	0.484	0.484	0.484	0.484	0.484	0.967	0.967	0.967	0.967
15	15	15	18	18	18	0.387	0.387	0.387	0.725	0.725	0.725	0.967	0.967	0.967	1.451	1.451	1.451	1.934
20	20	20	27	27	27	0.580	0.580	0.580	0.967	0.967	0.967	1.451	1.451	1.451	1.934	1.934	1.934	2.418
25	25	25	36	36	36	0.774	0.774	0.774	1.289	1.289	1.289	1.934	1.934	1.934	2.418	2.418	2.418	2.901
30	30	30	45	45	45	0.967	0.967	0.967	1.612	1.612	1.612	2.257	2.257	2.257	2.901	2.901	2.901	3.385
25	25	25	36	36	36	0.774	0.774	0.774	1.934	1.934	1.934	2.579	2.579	2.579	3.224	3.224	3.224	3.868
20	20	20	27	27	27	0.580	0.580	0.580	1.612	1.612	1.612	2.901	2.901	2.901	3.546	3.546	3.546	4.191
15	15	15	18	18	18	0.387	0.387	0.387	1.289	1.289	1.289	2.579	2.579	2.579	3.868	3.868	3.868	4.513
10	10	10	9	9	9	0.193	0.193	0.193	0.967	0.967	0.967	2.257	2.257	2.257	3.546	3.546	3.546	4.836
0	0	0	0	0	0	0	0	0	0.725	0.725	0.725	1.934	1.934	1.934	3.224	3.224	3.224	4.513
									0.484	0.484	0.484	1.451	1.451	1.451	2.901	2.901	2.901	4.191
									0	0	0	0.967	0.967	0.967	2.418	2.418	2.418	3.868
												0.484	0.484	0.484	1.934	1.934	1.934	3.385
												0	0	0	1.451	1.451	1.451	2.901
															0.967	0.967	0.967	2.418
															0	0	0	1.934
																		0.967
																		0

delta = $\pm$ 0.967 in.

Note: For more efficient use of space, only positive load and deflection values are tabulated.
A complete cycle included both positive and negative (load or deflection) excursions of equal magnitude.

TEST BuS 1A
Built-up Section
1 in. End-Plate

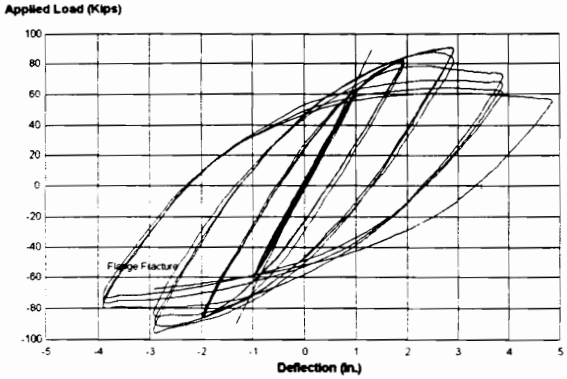

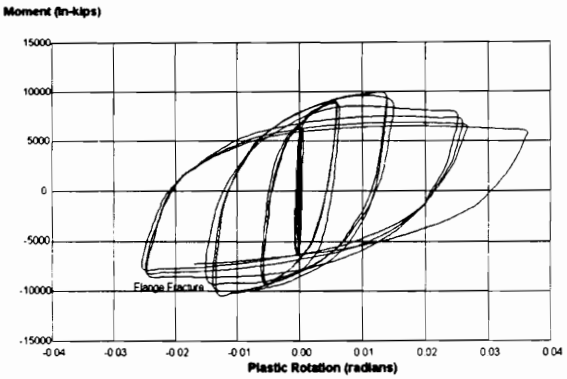

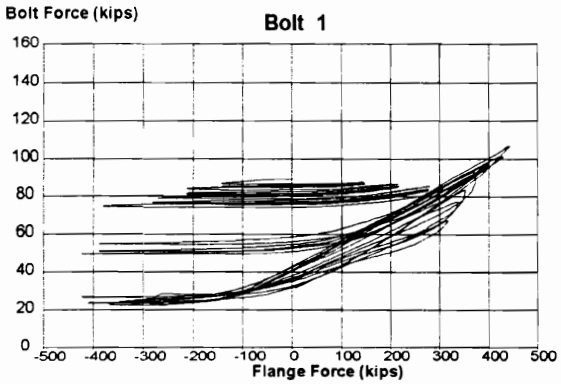

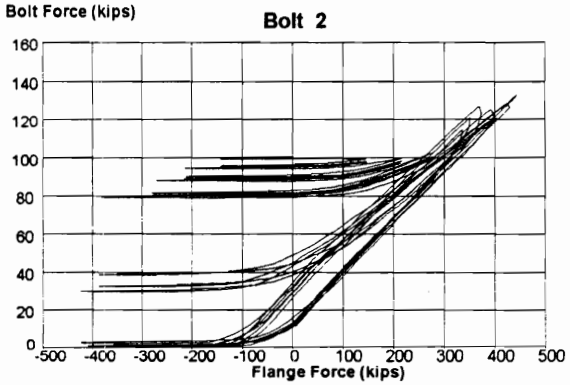

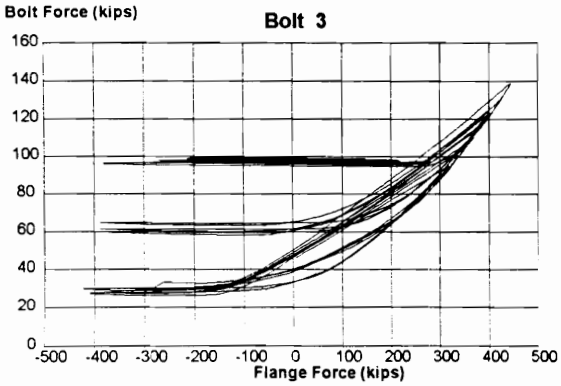

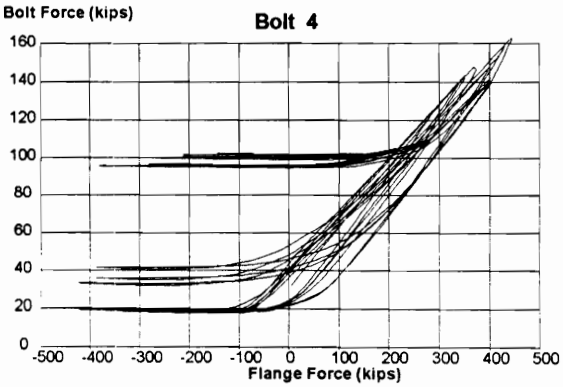

TEST BuS 1A
Built-up Section
1 in. End-Plate

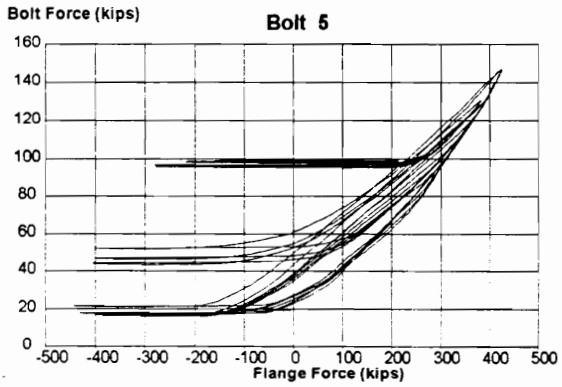

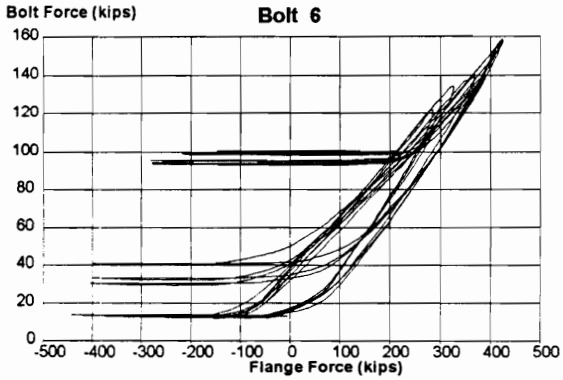

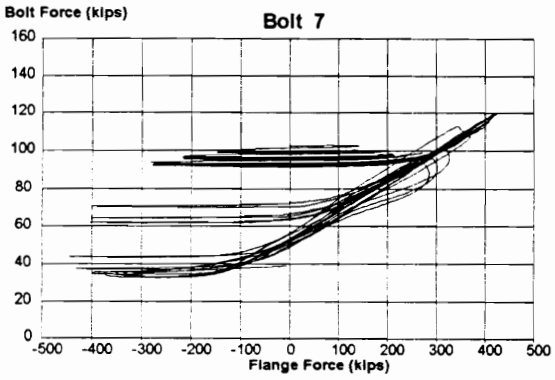

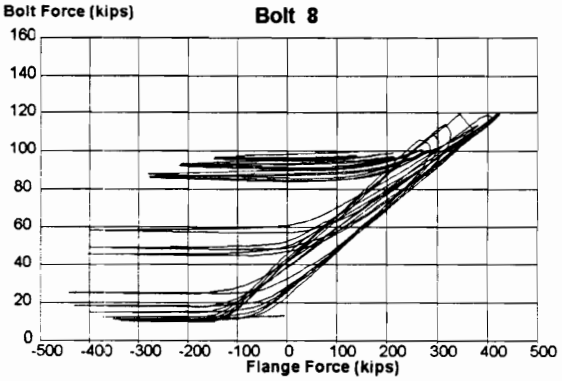

TEST BuS 2A

Connection End-Plate: Extended Four-Bolt, 1 in. Thick

Cycles Completed: 20

Failure Mode: Web-to-Flange Weld Fracture

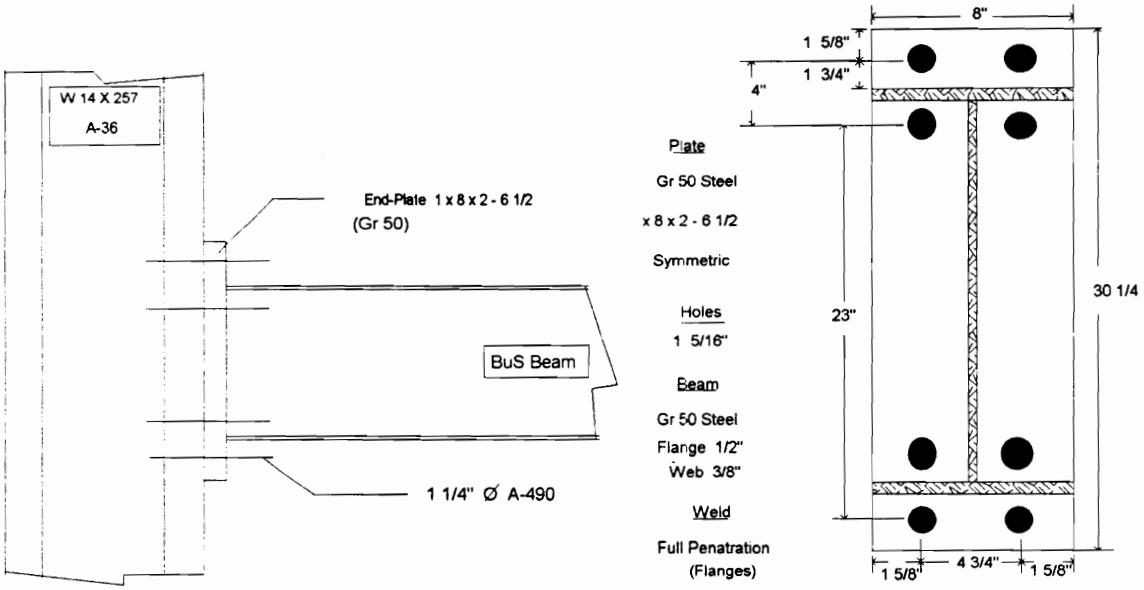

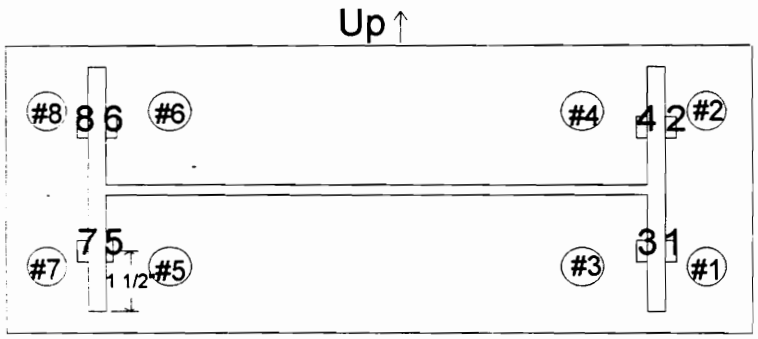

Strain Gauge and Bolt Location

Loading History for TEST BuS 2A

Load (kips) =>						Deflection (in.) =>													
Cycle 1	Cycle 2	Cycle 3	Cycle 4	Cycle 5	Cycle 6	Cycle 7	Cycle 8	Cycle 9	Cycle 10	Cycle 11	Cycle 12	Cycle 13	Cycle 14	Cycle 15	Cycle 16	Cycle 17	Cycle 18	Cycle 19	Cycle 20
0	0	0	0	0	0	0	0	0	0	0	0	0	0	0	0	0	0	0	0
10	10	10	9	9	9	0.194	0.194	0.194	0.485	0.485	0.485	0.485	0.485	0.485	0.969	0.969	0.969	0.969	0.969
15	15	15	18	18	18	0.388	0.388	0.388	0.727	0.727	0.727	0.969	0.969	0.969	1.454	1.454	1.454	1.939	1.939
20	20	20	27	27	27	0.582	0.582	0.582	0.969	0.969	0.969	1.454	1.454	1.454	1.939	1.939	1.939	2.423	2.423
25	25	25	36	36	36	0.775	0.775	0.775	1.292	1.292	1.292	1.939	1.939	1.939	2.423	2.423	2.423	2.908	2.908
30	30	30	45	45	45	0.969	0.969	0.969	1.616	1.616	1.616	2.262	2.262	2.262	2.908	2.908	2.908	3.393	3.393
25	25	25	36	36	36	0.775	0.775	0.775	1.939	1.939	1.939	2.585	2.585	2.585	3.231	3.231	3.231	3.877	3.877
20	20	20	27	27	27	0.582	0.582	0.582	1.616	1.616	1.616	2.908	2.908	2.908	3.554	3.554	3.554	4.200	4.200
15	15	15	18	18	18	0.388	0.388	0.388	1.292	1.292	1.292	2.585	2.585	2.585	3.877	3.877	3.877	4.524	4.524
10	10	10	9	9	9	0.194	0.194	0.194	0.969	0.969	0.969	2.262	2.262	2.262	3.554	3.554	3.554	4.847	4.847
0	0	0	0	0	0	0	0	0	0.72	0.72	0.72	1.939	1.939	1.939	3.231	3.231	3.231	4.524	4.524
									0.485	0.485	0.485	1.454	1.454	1.454	2.908	2.908	2.908	4.200	4.200
									0	0	0	0.969	0.969	0.969	2.423	2.423	2.423	3.877	3.877
												0.485	0.485	0.485	1.939	1.939	1.939	3.393	3.393
												0	0	0	1.454	1.454	1.454	2.908	2.908
															0.969	0.969	0.969	2.423	2.423
															0	0	0	1.939	1.939
																		0.969	0.969
																		0	0

delta = $\pm$ 0.969 in.

Note: For more efficient use of space, only positive load and deflection values are tabulated.
A complete cycle included both positive and negative (load or deflection) excursions of equal magnitude.

TEST BuS 2A
Built-Up Section
1 in. End-Plate

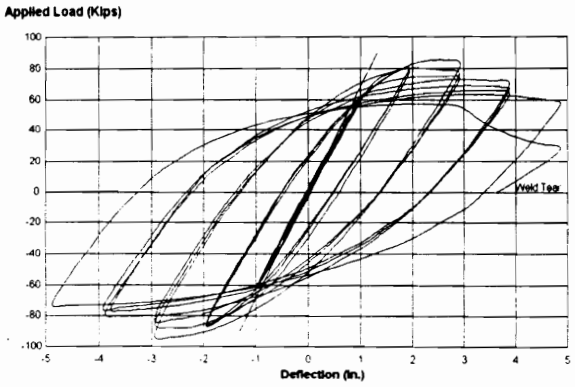

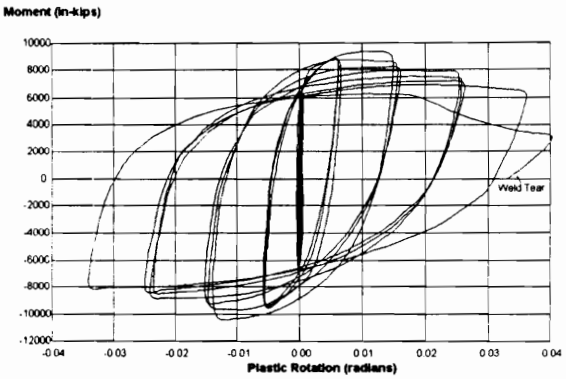

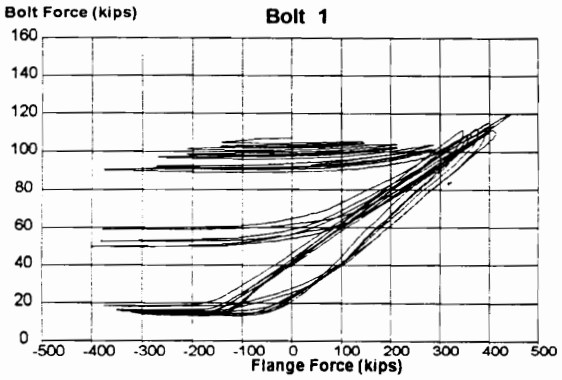

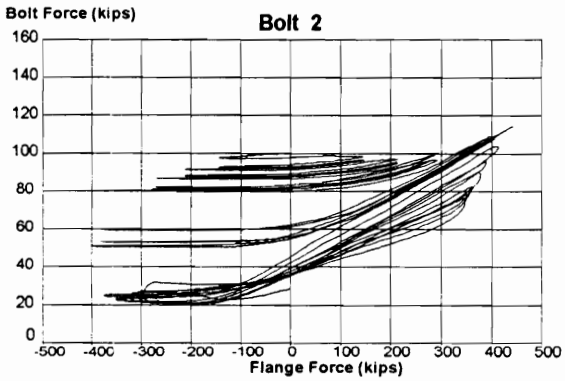

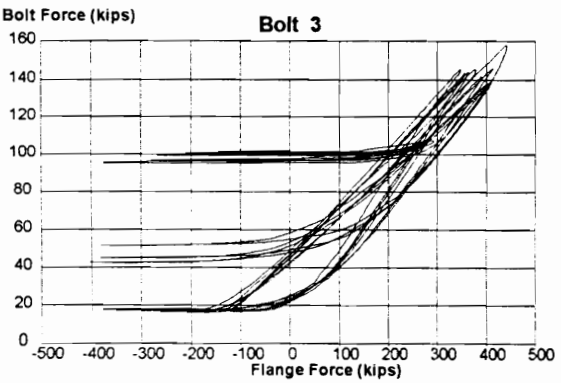

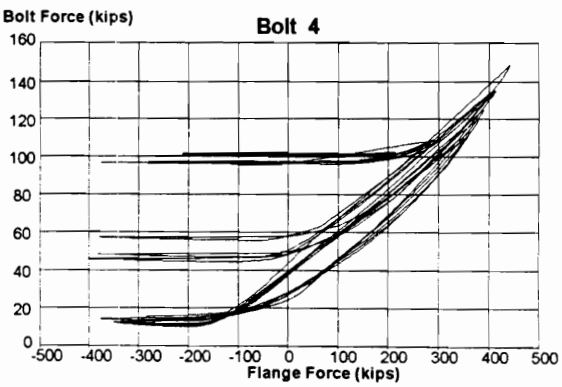

TEST BuS 2A
Built-Up Section
1 in. End-Plate

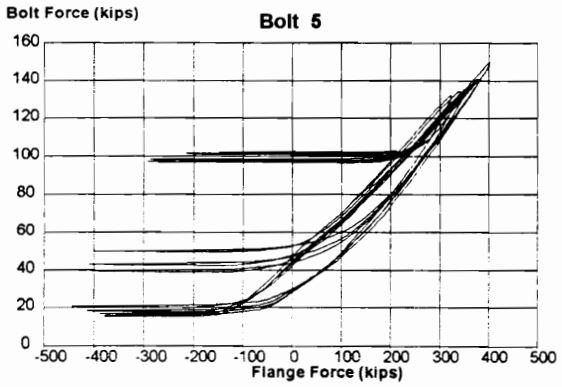

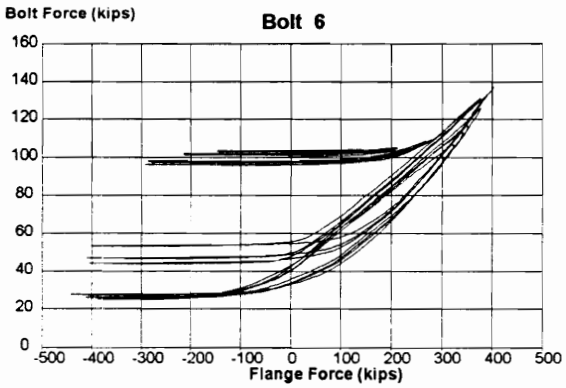

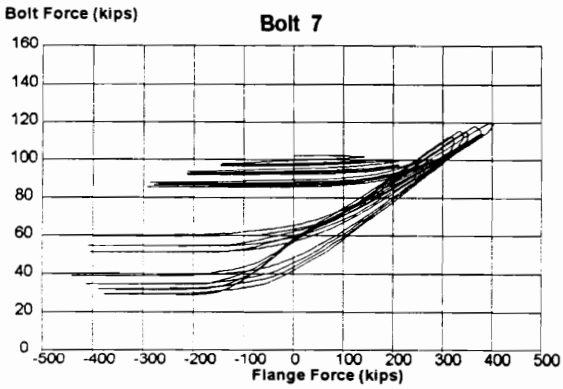

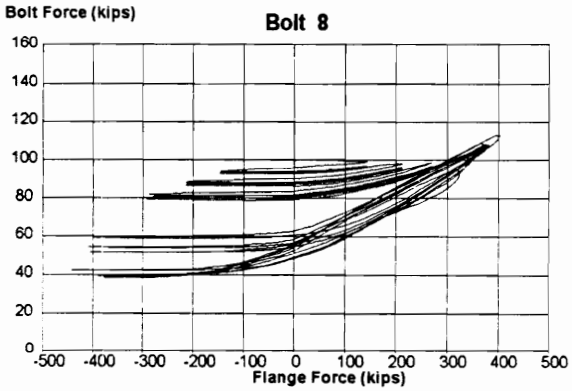

APPENDIX H

FINITE ELEMENT MODELS

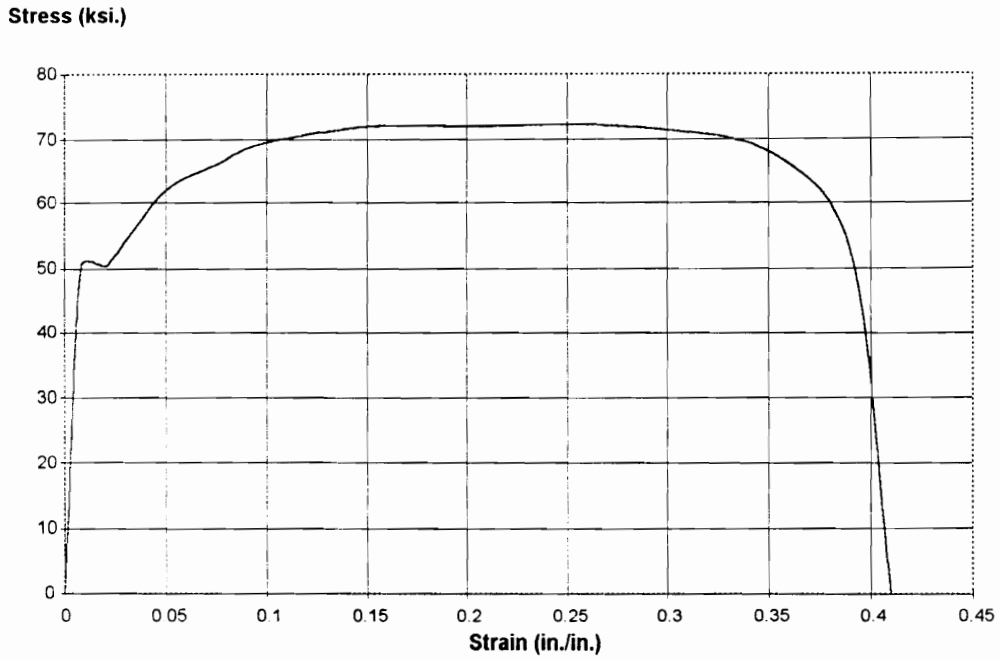

Figure H.1 W18x35 Beam Material Strength

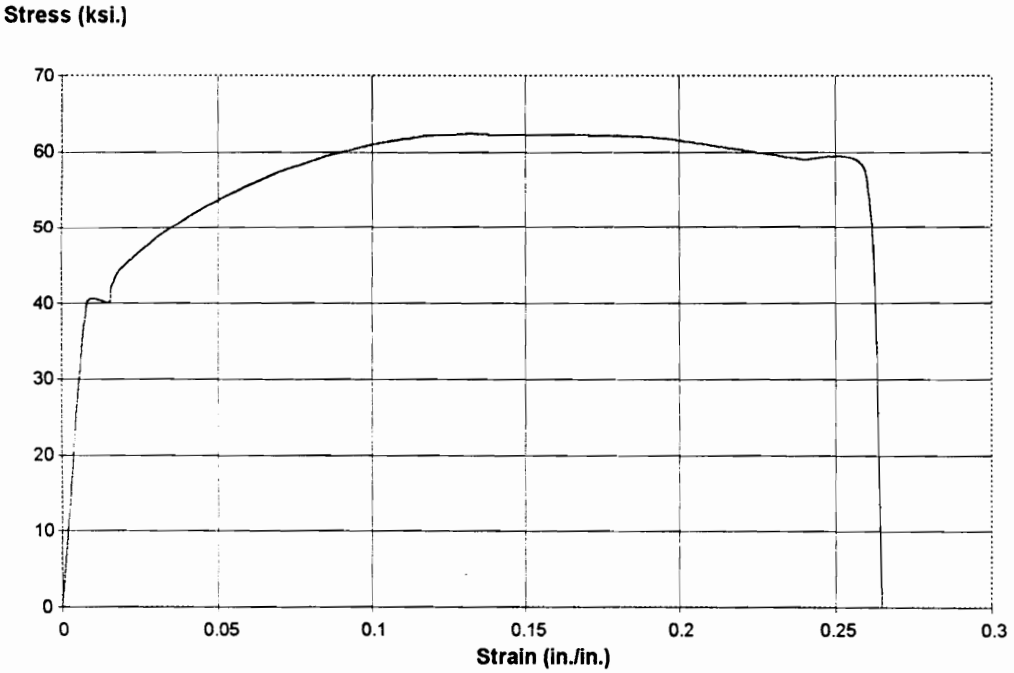

Figure H.2 W18x35, End-Plate Material Strength

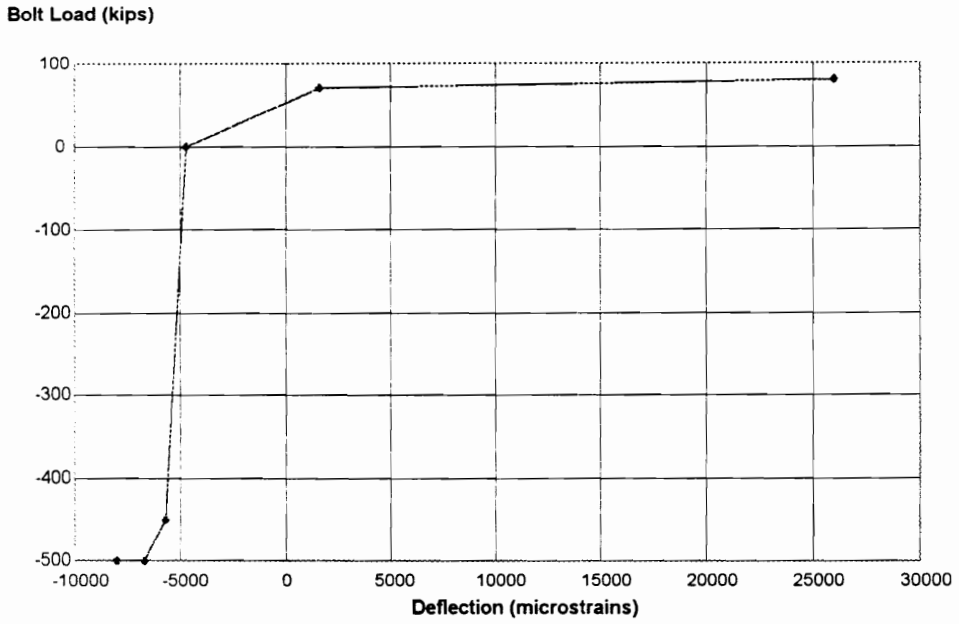

Figure H.3 1 in. Diameter A325 Bolt Model

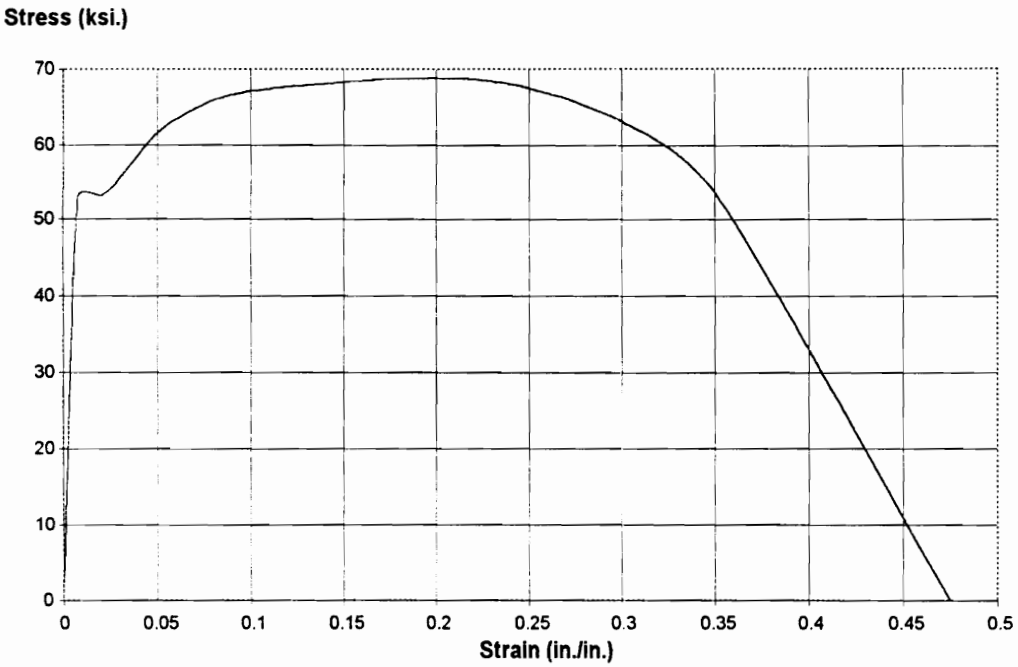

Figure H.4 W24x62 Beam Material Strength

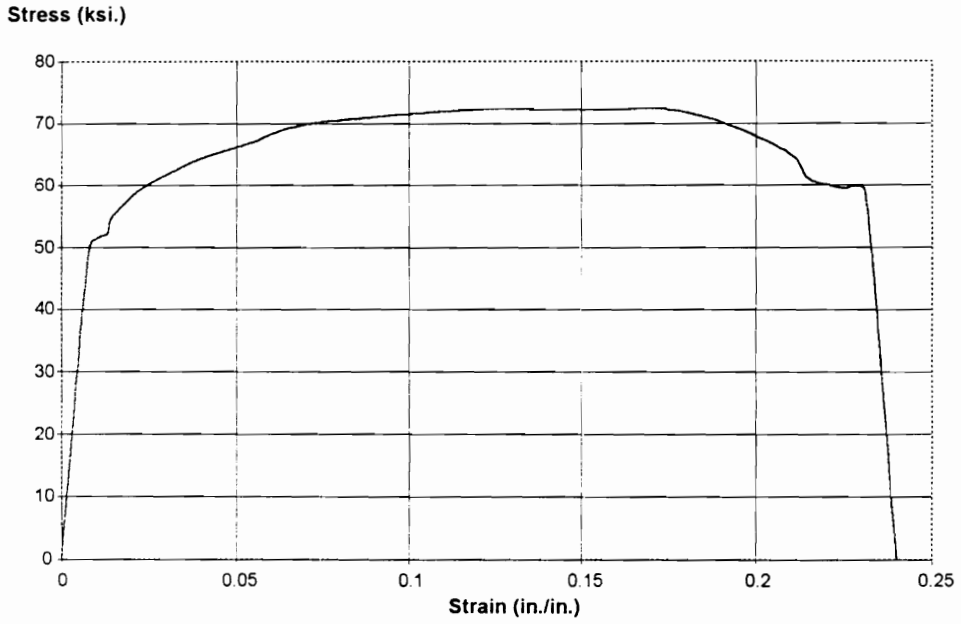

Figure H.5 W24x62, End-Plate Material Strength

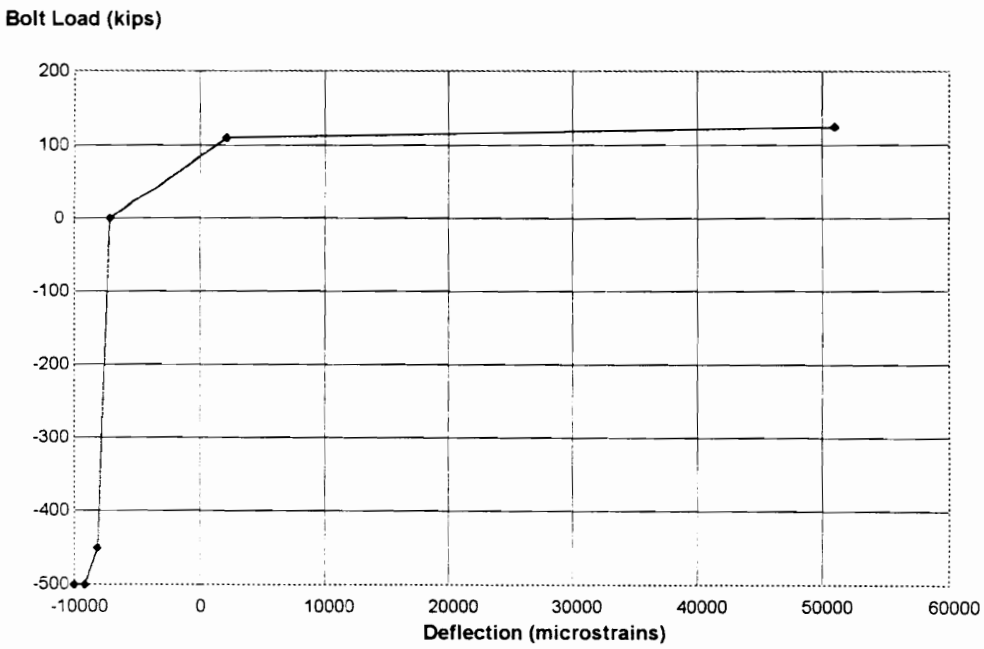

Figure H.6 1 1/4 in. Diameter A325 Bolt Model

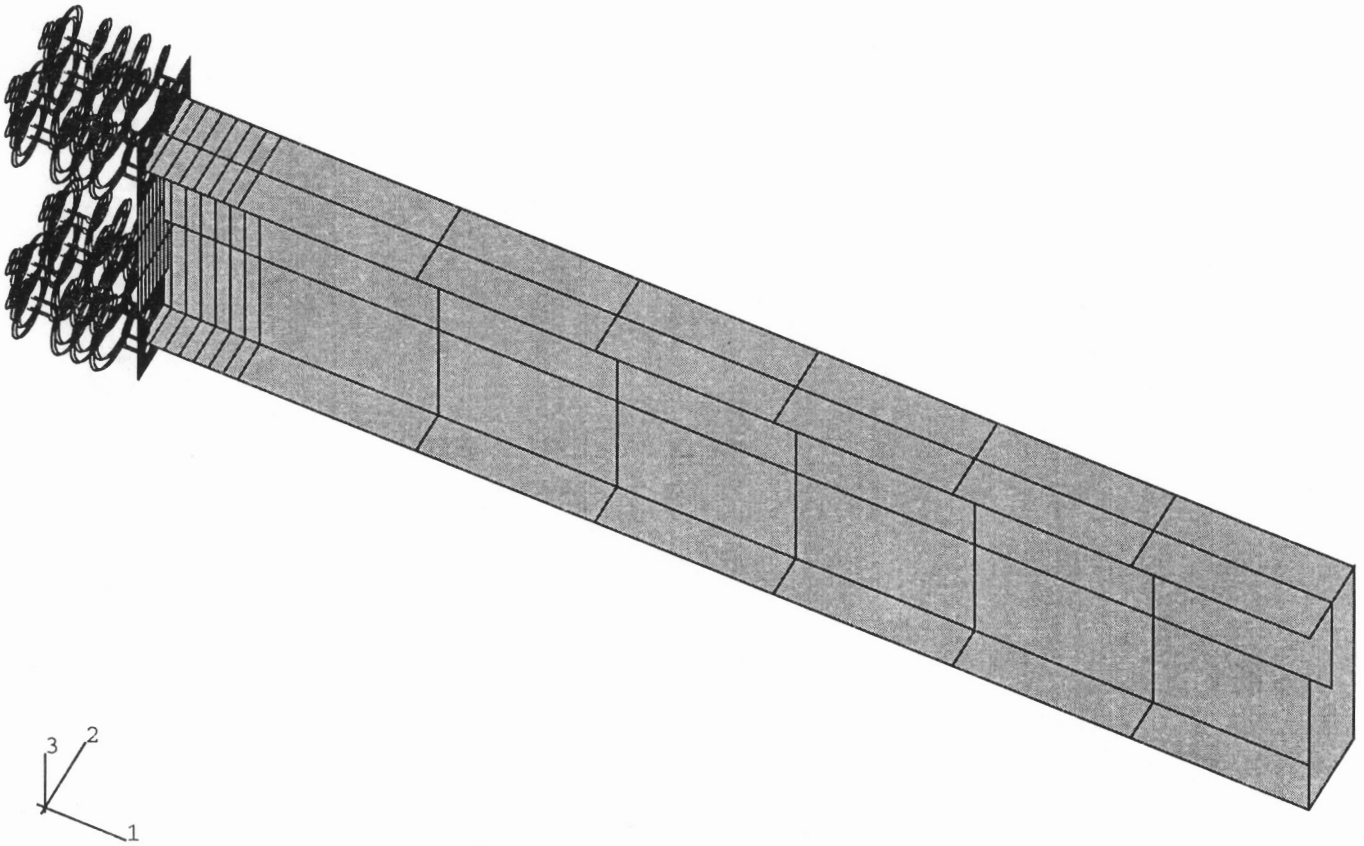

Figure H.7 Finite Element Model of W18x35 Beam Connection

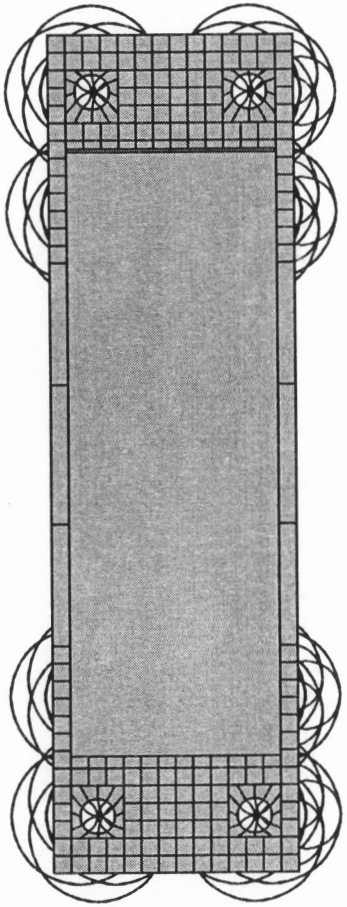

Figure H.8 Finite Element Model,
W18x35 Beam Connection (End View)

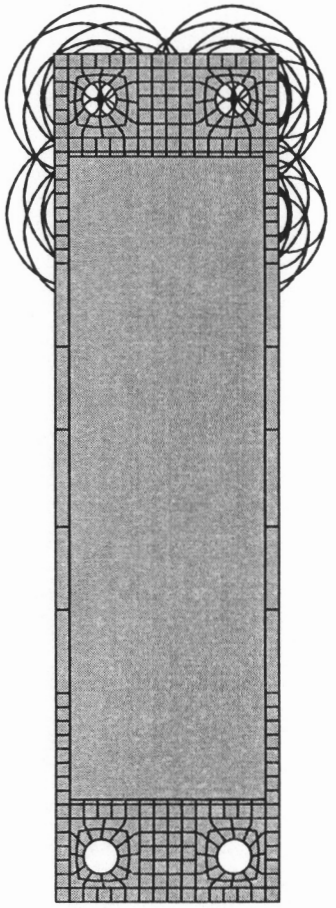

Figure H.9 Finite Element Model,
W24x62 Beam Connection (End View)

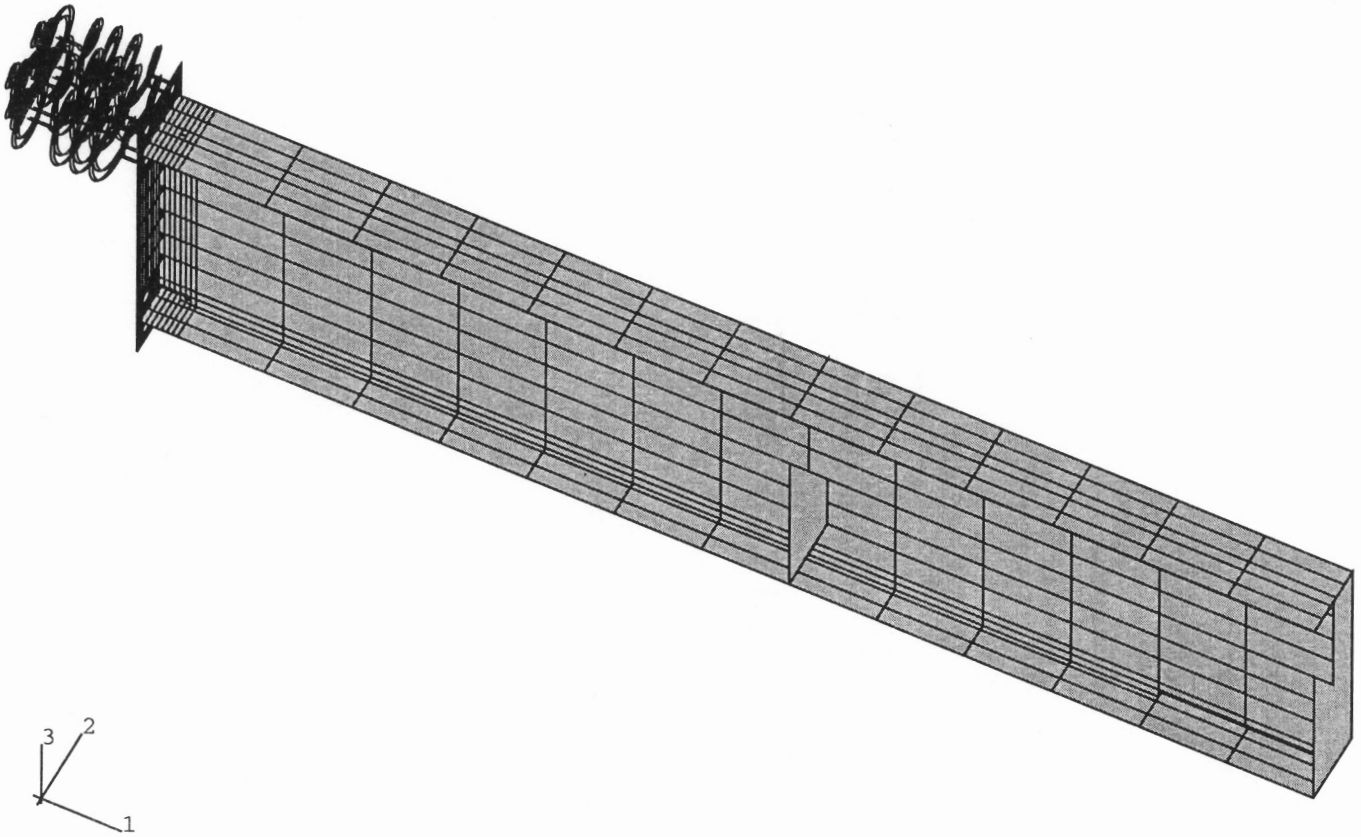

Figure H.10 Finite Element Model of W24x62 Beam Connection

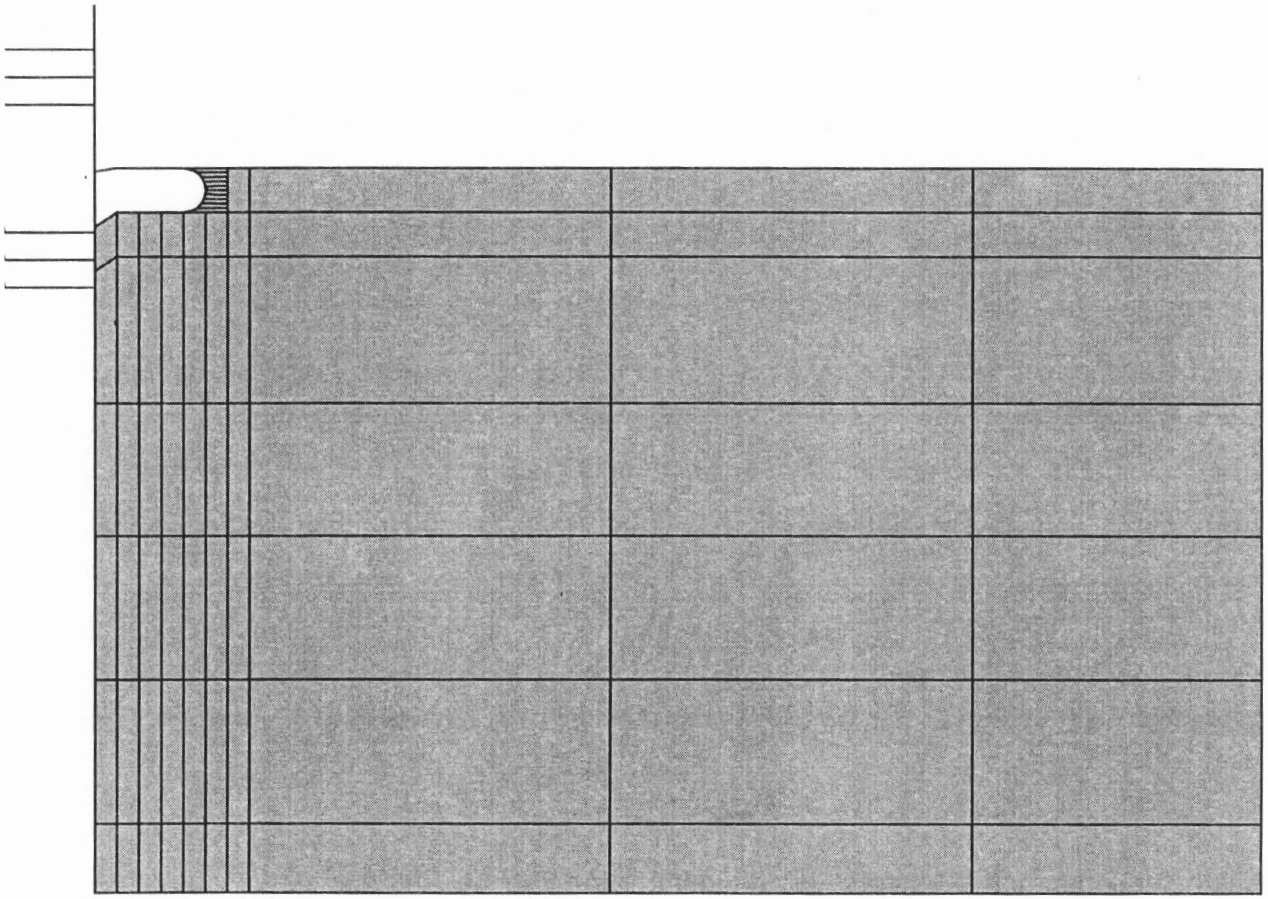

Figure H.11 Weld Access Hole Model (W24x62 Beam Section)

VITA

Ronald L. Meng was born in Sellersville, Pennsylvania, on April 16, 1949. On May 16, 1971, he graduated from Virginia Military Institute with a Bachelor of Science Degree in Civil Engineering and a commission as a Second Lieutenant in the United States Marine Corps. During twenty-two years in the Marine Corps, he served primarily as a helicopter pilot and saw service around the globe. He received a Master of Science Degree in Aeronautical Engineering in April 1984 from the Naval Postgraduate School, and for the next three years saw duty as a Senior Lecturer in Aerospace Engineering at the United States Naval Academy. During his career Lieutenant Colonel Meng commanded a Marine Helicopter Squadron and during his last tour of duty was Test Director, Light Armored Vehicles for the Marine Corps. In January 1993, he enrolled at Virginia Polytechnic Institute and State University to pursue a doctoral degree in Civil Engineering, Structures.

Ronald L. Meng